LOCAL, INTRA-ARTICULAR DELIVERY OF ZOLEDRONIC ACID AS A DISEASE-MODIFYING THERAPEUTIC FOR POST-TRAUMATIC OSTEOARTHRITIS

by

Michael Aaron David

A dissertation submitted to the Faculty of the University of Delaware in partial fulfillment of the requirements for the degree of Doctor of Philosophy in Biomedical Engineering

Spring 2019

LOCAL, INTRA-ARTICULAR DELIVERY OF ZOLEDRONIC ACID AS A DISEASE-MODIFYING THERAPEUTIC FOR POST-TRAUMATIC OSTEOARTHRITIS

by

Michael Aaron David

Approved: _____
Dawn M. Elliott, Ph.D.
Chair of the Department of Biomedical Engineering

Approved: _____
Levi T. Thompson, Ph.D.
Dean of the College of College Engineering

Approved: _____
Douglas J. Doren, Ph.D.
Interim Vice Provost for Graduate and Professional Education

I certify that I have read this dissertation and that in my opinion it meets the academic and professional standard required by the University as a dissertation for the degree of Doctor of Philosophy.

Signed: _____

Christopher Price, Ph.D.
Professor in charge of dissertation

I certify that I have read this dissertation and that in my opinion it meets the academic and professional standard required by the University as a dissertation for the degree of Doctor of Philosophy.

Signed: _____

Dawn M. Elliott, Ph.D.
Member of dissertation committee

I certify that I have read this dissertation and that in my opinion it meets the academic and professional standard required by the University as a dissertation for the degree of Doctor of Philosophy.

Signed: _____

Randall L. Duncan, Ph.D.
Member of dissertation committee

I certify that I have read this dissertation and that in my opinion it meets the academic and professional standard required by the University as a dissertation for the degree of Doctor of Philosophy.

Signed: _____

Jason P. Gleghorn, Ph.D.
Member of dissertation committee

ACKNOWLEDGMENTS

While this dissertation and the experience that has come along with it certainly had its up and downs, if it were not for the tremendous support network in my life, none of this would have been possible. It has been an opportunity of a lifetime to work on this dissertation, and for that, I am forever grateful. Most importantly, I am thankful to the countless individuals that have helped me along the way, shaping me into the researcher and person I am today. To those who have encouraged, mentored, and helped me, particularly concerning the completion of this dissertation, I am indebted to you. Unfortunately, there is not enough space to acknowledge everyone, so I would like to bring the most influential people to light.

I would first like to thank one of the most impactful individuals on my dissertation journey, my advisor, Dr. Christopher Price. I have learned so much from you, both in and out of the lab. Joining your lab from the beginning has been a once in a lifetime experience; seeing the trials and tribulations, and the dedication and work ethic needed to start a lab in a new department will be something I will carry with me for the rest of my career. Thank you for taking a chance with me, constantly attempting to teach me how to be a better scientist and communicator, and dealing with my stubbornness, love for music, and constant desire to chase down scientific rabbit holes. I would also like to thank the countless undergraduates, as well as the high school and graduate students from the Price Lab that throughout the years helped to make this dissertation come to fruition. I am also extremely grateful for the

financial support from Dr. Price and the University of Delaware's (UD) internal fellowships enabling me to carry out the work in this dissertation.

Secondly, I would like to acknowledge my committee members: Drs. Dawn Elliott, Randall Duncan, and Jason Gleghorn. Each of you has had an incredible impact on me, and I am grateful for the critical scientific and professional advice that you had provided me when I needed it the most.

Friends inside and outside of the academic community have been pivotal to my ability to complete this dissertation. I could not have done it without the constant support and advice from a network of friends from UD, the University of Rochester (especially my fellow Dekes), and high school. Special thanks to Melanie Smith, Brian Graham, Janty Shoga, Omar Banda, Axel Moore, John Delucca, LaMont Cannon, Jilian Melemad, Rachel Riley, Aditya Jagarapu, Nicholas Trompeter, Dylan Bochicchio, Nicolas Negron, Ryan Locke, and Ian Marozas for helping me throughout this dissertation, either in the lab or simply as someone to hear me rant about science. I would also like to thank the band Lotus and all the associated experiences and friends, especially my closest group of friends, the 'Vibin Disco Babes'. If it were not for countless shows and experiences from Lotus over the years, I doubt I would have achieved what I have today in this dissertation.

Lastly, I am forever thankful for the unconditional love and support from my family, especially my parents and brother. A final special thanks to my grandparents who have always inspired, loved, and helped me throughout life; you will always be in my heart.

TABLE OF CONTENTS

LIST OF TABLES

LIST OF FIGURES

ABSTRACT

Post-traumatic osteoarthritis (PTOA) is an accelerated form of osteoarthritis (OA) resulting from traumatic joint injury, e.g. meniscus or ligament tears. Presently, PTOA is incurable, and the prognosis for patients suffering from PTOA is poor; approximately 50% of patients suffering joint injuries experience cartilage degeneration, pain, and loss of joint immobility within as little as 10-15 years post-injury. Existing PTOA treatment strategies only address secondary symptoms, such as pain and inflammation, and fail to address the aberrant biology that underpins PTOA initiation and progression. Therefore, there exists an unmet need to find disease-modifying therapies that can prevent or delay PTOA initiation and progression, particularly ones aimed at early disease-stage biology. Overall, this dissertation sought to uncover potentially-druggable biological targets at immediate-to-early timepoints post-injury, and to evaluate the efficacy a novel therapeutic strategy (intra-articular injection of the bisphosphonate zoledronic acid) to mitigate deleterious aspects of cartilage/chondrocyte biology that precipitate PTOA disease initiation and progression.

Despite an extensive body of literature regarding cartilage biology and injury-induced PTOA, the early cellular mechanisms that occur within injured cartilage leading to long-term tissue degeneration and disease remain unclear. To shed insight onto the immediate-early cartilage biology changes that precipitate PTOA it was essential to study the spatiotemporal progression of cartilage structure and cellularity that occurred in the immediate aftermath of the joint injury. Chapter 2 of this

dissertation employed a well-established murine model of PTOA, the destabilization of the medial meniscus (DMM), to evaluate the spatial evolution of changes to cartilage's cellular and structural properties following injury. We revealed that DMM-injury induced a rapid and focally-distinct loss of chondrocyte presence in articular cartilage of the medial tibial plateau and femoral condyle. This cell loss appears to be the precipitator of the long-term focal cartilage erosions that accompany DMM-injury. Importantly, this focal loss of chondrocyte cellularity and subsequent development of focal cartilage erosions was intimately linked to regions of the cartilage that experienced acute alterations in medial meniscus coverage (i.e. uncovering) due to DMM-injury. The findings from Chapter 2 enhanced our understanding of the spatiotemporal changes that accompany cartilage injury and degeneration and identified a potentially-druggable and focal population of chondrocytes as targets for PTOA prevention. Ultimately, the findings from Chapter 2 were leveraged in Chapters 3 and 4 to evaluate the preclinical efficacy of a locally-delivered, intra-articular bisphosphonate for the prophylactic treatment of PTOA.

Bisphosphonates (BPs) are an FDA-approved class of drugs historically used to treat bone-related diseases because of their ability to inhibit bone resorption and bone remodeling. Given these properties and the observation that aberrant subchondral bone remodeling is a hallmark of arthritis, BPs had been suggested, and recently shown, to have disease-modifying capabilities in preclinical PTOA studies. Specifically, the newest and most potent nitrogen-containing BP, zoledronic acid (ZA), prevented subchondral bone remodeling and cartilage degeneration in several animal models of PTOA. Unfortunately, such studies utilized high-dose, continuous, and systemic ZA administration strategies that increase the risk of severe skeletal side

effects, e.g. osteonecrosis of the jaw and atypical fractures, hindering its potential adoption as a clinical PTOA treatment. However, local ZA administration may offer an alternative ZA administration approach, which, if efficacious, would represent a potentially more acceptable and clinically translatable disease-modifying strategy for PTOA.

Supporting the potential of locally-delivered, i.e. intra-articularly injected, ZA as a PTOA therapeutic was work by our collaborators and others demonstrating that ZA could directly modulate chondrocyte biology and cartilage health *in situ*. However, translation of intra-articular injection of ZA into preclinical models of PTOA had not been investigated before this dissertation. In Chapters 3 and 4 of this dissertation, we employed the murine DMM model of PTOA to evaluate the disease-modifying potential of repeated vs. single (immediate vs. delayed) intra-articular injection of ZA in injured joints. In Chapter 3, we found that no intra-articular injection strategy was able to mitigate the superficial cartilage damage that accumulated shortly after DMM-injury. However, we found that four, weekly-repeated intra-articular injections of ZA could suppress the development of subsequent long-term cartilage erosions: neither single (immediate or delayed) intra-articular injection strategies protected against injury-induced cartilage erosions. Upon further investigation, we identified that the prevention of cartilage erosions by repeated intra-articular ZA treatment appeared to involve the spatiotemporal modulation of chondrocyte proliferation, proteoglycan production, and death. In Chapter 4, we focused our attention on repeated intra-articular ZA administration because it was the only strategy that provided meaningful cartilage protection following DMM-injury. We found that repeated intra-articular injection did not appreciably alter DMM-induced joint synovitis, meniscal

hypertrophy, or ectopic bone formation, aside from promoting a moderate increase in meniscal proteoglycan content and bone volume fraction. In addition, repeated intra-articular injection of ZA did not alter osteophyte size but did delay the transition of osteophytes from their cartilaginous templates to boney tissue following DMM-injury. Lastly, repeated intra-articular injection of ZA did not appear to influence the structure of the subchondral bone underlying the joint, nor bone compartments distant from the intra-articularly treated joint, namely the epiphyseal and metaphyseal bone of the ipsilateral tibia. Collectively, the findings from Chapter 3 and 4 support the notion that four, weekly-repeated intra-articular injection of ZA may represent a simple and efficacious PTOA disease-modifying strategy, one that can minimize the potential for adverse side effects that are associated with systemic administration of BPs.

While prior work conducted by our collaborators and others provided preliminary evidence to support the studies in Chapters 3 and 4, our knowledge of ZA's direct effects and modes of action on chondrocytes remained largely incomplete. In Chapter 5, we explored the potential modes of ZA action on chondrocytes *in vitro* using ATDC5 cells, a well-accepted chondrocyte-like cell line. ATDC5 cells allowed us to evaluate ZA's effects on both undifferentiated (higher proliferative capacity) and differentiated (lower proliferative capacity) chondrocytes, mimicking proliferative and quiescent chondrocytes, respectively, that may be seen *in vivo* following injury. We found that ZA exerts pleiotropic effects on ATDC5 cells that are concentration-, exposure-, and differentiation-stage dependent. In undifferentiated ATDC5 cells (mitotic), increasing ZA concentration and exposure time resulted in decreased cell proliferation, viability, and metabolism, as well as depolarization of mitochondria, cell-cycle progression arrest, and disruption of cytoskeletal architecture. However, in

differentiated ATDC5 cells (post-mitotic), ZA only drove decreases in cell proliferation, metabolism, and viability at the highest ZA concentrations. Collectively, the findings from Chapter 5 confirm ZA's ability to directly modulate chondrocyte behavior *in vitro* and establishes critical ZA concentrations and exposure times that drive significant alterations in chondrocyte health.

Overall, this dissertation shines a light on the early cartilage and non-cartilaginous changes that accompany traumatic joint injury and demonstrates the initial efficacy of intra-articular injection of ZA for PTOA prevention in a preclinical mouse model. Additionally, this work establishes a framework for future studies *in vitro*, *in situ*, and *in vivo* to optimize intra-articular administration of ZA as a prophylactic PTOA disease-modifying strategy. Most importantly, this work supports the potential translation of intra-articular injection of ZA as a novel, safe, simple, cheap, and clinically-feasible PTOA therapy.

Chapter 1

INTRODUCTION

1.1 Osteoarthritis and Risk Factors

1.1.1 Epidemiology and Cost of Osteoarthritis

Osteoarthritis (OA) is the most common chronic joint disorder afflicting approximately 52 million Americans in 2012[1,2], a patient population that is expected to increase to more than 67 million by 2030[3]. The World Health Organization estimates that 10% of the world's population over 50 years of age suffers from OA[4], and the disease affects both men and women and is prevalent across all ethnicities and geographical regions[2,5–13]. Once OA develops, individuals experience worsening joint pain and disability[12,14,15]. Of patients that are affected by OA, nearly 80% have limited range of movement and approximately 25% are unable to perform many daily activities[2,4,9]. In addition, OA tends to increase the risk of other chronic diseases, including heart disease, diabetes, obesity, sleep disturbance, depression, and anxiety[2,3,7,12,14,16]. OA ranks high among health-related drivers of economic loss worldwide. For instance, OA costs the United States' economy more than $100 billion per year[7,17]; in Europe, OA is the 5th highest health care expenditure[7].

OA has been historically characterized as a degenerative disease of the articular cartilage; however, it is now understood that OA affects other joint tissues as well[18–23]. For example, in the knee, the synovium, ligaments, menisci, subchondral bone, and osteophytes are all impacted by OA as illustrated in Figure 1.1. Thus, OA is

best-described as a whole-joint disease[18–23] where various joint tissues may contribute to OA initiation and progression. Despite our extensive knowledge of tissues and cells involved with OA, the underpinning mechanisms of OA initiation and progression remain largely unknown[7,23–25].

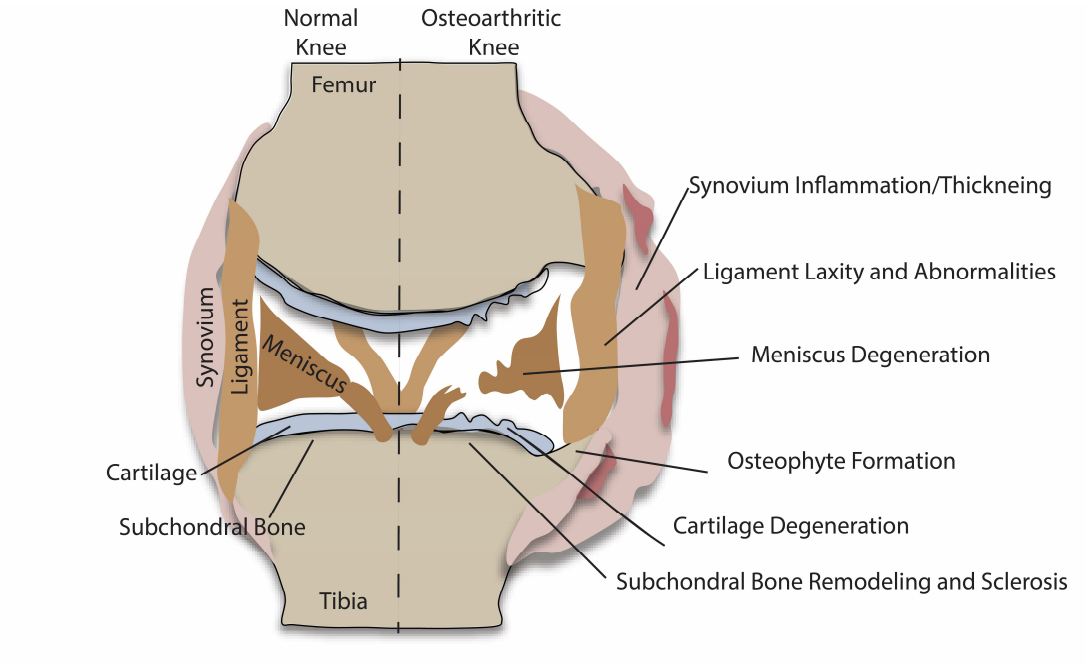

Figure 1.1: Osteoarthritis is a Whole-Joint Disease. In osteoarthritis (OA) various tissues of the knee joint are affected and thought to contribute to disease initiations and progression. As a result, OA is now appreciated as a whole-joint disease. (Adapted from Hunter et al. 2011[23]).

1.1.2 Risk Factors for Osteoarthritis

Although the mechanisms driving idiopathic OA are not understood fully, there are various risk factors that increase the risk of developing OA[4,7,11–14,26–28]. Historically, OA is considered an age-related disease; however, other risks for OA

have been implicated including genetic and gender, joint abnormalities (dysplasia), occupation, excessive weight bearing (obesity), sustained joint unloading (disuse), and traumatic joint injury[11–14,26–28]. In this dissertation, a focus is placed on the mechanistic understanding of traumatic joint injury as a risk factor, which is referred to as post-traumatic OA (PTOA).

1.2 Epidemiology and Costs of Post-Traumatic Osteoarthritis

In post-traumatic osteoarthritis (PTOA), a traumatic joint injury (e.g., ligament and meniscal tears, intraarticular fractures, and joint sprains) directly drives an accelerated form of OA-like cartilage degeneration[17,29–33]. PTOA can occur in almost any joint of the body but is predominately found in the ankle, hip, and knee. Individuals, often younger athletes[34–43] and uniformed service members[44–53], have a 20-50% chance of developing cartilage degeneration within 10-15 years of joint injury[32,33,54–58]; this likelihood of developing cartilage denegation is greater than a 3-fold increase compared to uninjured, age-matched counterparts[59]. It has been estimated that PTOA afflicts 5.6 million individuals (representing ~12% of all OA cases) and drives approximately $3 billion in healthcare costs annually in the United States[17]. These costs will continue to grow, especially given increases in high-risk activity participation in our society[60–62].

1.3 Post-Traumatic Osteoarthritis Pathophysiology

1.3.1 Articular Cartilage Structure, Composition, and Function

Articular cartilage is an avascular, specialized connective tissue that lines the ends of bones in diarthrodial joints[63,64]. Its unique composition and architecture enables pain-free, frictionless motion while supporting physiological joint loading for

decades[65]. The extracellular matrix (ECM) of articular cartilage, which is 2 to 4-mm thick in humans and 50 to 100-μm in mice[64,66], is comprised of macromolecules such as collagen and proteoglycans and resident cells called chondrocytes (Figure 1.2).

Articular cartilage has a hierarchical and bi-phasic structure that gives rise to its unique biomechanical, and tribological (friction) properties[63,65,67,68]. Overall, articular cartilage consists of 60-80% water by weight, the remainder consisting of collagen and proteoglycan of the ECM, and sparse chondrocytes contributing approximately 2% of the articular cartilage volume. Structurally, cartilage has three distinct zones, each exhibiting different ratios, distributions, and orientations of ECM macromolecules and chondrocytes (Figure 1.2). The uppermost cartilage zone, known as the superficial or tangential zone, makes up approximately 10-20% of the articular cartilage volume. In this zone, both chondrocytes and collagen are aligned parallel to the articular surface and serve as a sliding surface bathed in synovial fluid. In this zone, one finds the highest density of chondrocytes, high collagen fiber and water content with low proteoglycan content. Immediately beneath this zone is the middle zone (40-60% of tissue volume), also known as the transitional zone. The transitional zone exhibits a more random organization of collagen fibers, a reduction in chondrocyte number and collagen content, and an increase in proteoglycans and water content. The deep zone (30-40% of tissue volume), which anchors the articular cartilage to the underlying calcified cartilage and subchondral bone, contains collagen fibers that are oriented perpendicular to the cartilage surface and direction of sliding, and exhibit high proteoglycan content with low collagen and water content.

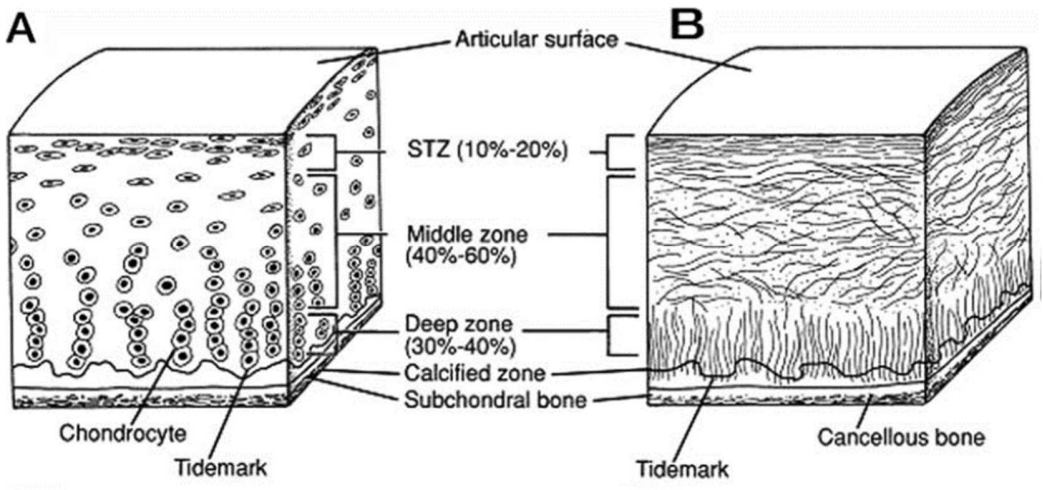

Figure 1.2: Schematic of Articular Cartilage. (A.) Organization of chondrocytes in the various zones of the articular cartilage. Note the morphology differences between each zone. (B.) Alignment of the collagen and proteoglycan in the different zones, which resembles the alignment of the chondrocytes (Excerpt from Buckwalter et al. 1994[69]).

Chondrocytes play a unique role in the development, maintenance, and repair of the articular cartilage cartilage's ECM[63], which is influenced by daily physiolocial loading and resulting mechanical forces. Mechanical forces, caused by loading associated with walking, running, jumping, etc., are converted into biochemical signals that affect chondrocyte metabolism and the production of ECM macromolecules, a process known as mechanotransduction[70–72]. Specifically, loading induces mechanical stimuli, e.g. tensile strains, compressive forces, shear forces, hydrostatic pressure, and interstitial fluid flow, within articular cartilage that regulate chondrocyte mechanotransduction. The survival of chondrocytes relies on the presence of appropriate mechanical and biochemical stimuli. When the balance of these stimuli is altered, chondrocytes can respond in deleterious ways, diminishing

articular cartilage integrity and its ability to support physiological loading. This can lead to tissue wear and arthritis (i.e., OA and PTOA)[73].

1.3.2 Current Understanding of Post-Traumatic Osteoarthritis Disease Initiation and Progression

Our understanding of PTOA disease progression is predominately based upon studies of late-stage osteoarthritic tissue, often following the accumulation of irreversible damage. This is because in classic idiopathic OA the precise mechanical and/or biological changes that precipitate the initiation of OA are unknown. However, unlike in idiopathic OA, the precipitating event driving PTOA is a known injury. As a result, there exists a unique, early window of opportunity to study cartilage and/or other joint tissue changes that may contribute to a loss of cartilage and joint function post-injury[55,74,75]. In recent years, clinical studies looking at the early-to-mid disease stages following joint injury have found that patients experience altered joint loading and kinematics following injury[31,76]. These changes lead to similar outcomes as seen in idiopathic OA, such as pain, joint inflammation[77–79], osteophyte formation[80–82], subchondral bone remodeling/sclerosis[74,81,83,84], and cartilage damage. Recently, injury-mediated meniscal extrusion has also been shown to correlate with disease severity and cartilage damage[84–88]. Despite our general understanding of the tissues and cells involved with OA, a mechanistic understanding of how acute joint injury leads to the initiation and progressive loss of cartilage and joint function in PTOA clinically remains unclear.

Determining the mechanisms involved in PTOA disease initiation and progression on a tissue and cellular level in humans has been difficult to study. This is partly due to: i) limited availability of human cartilage from early disease stage, ii)

limited *in vivo* cartilage assessment techniques, and iii) the long period required for disease progression clinically. To overcome these limitations, researchers have turned to various *in vitro, in vivo,* and *in situ* models of PTOA using animal species including horses, dogs, rabbits, rats, and mice[55,89,98,90–97]. One commonly used model that was employed in this dissertation is the murine destabilization of the medial meniscus (DMM) model of PTOA[99]. This model is commonly used because of its ease of implementation, high reproducibility, and pattern of disease progression thought to closely recapitulate human PTOA. In the murine DMM model, the anterior region of the medial meniscotibial ligament is transected, causing a medial extrusion of the medial meniscus within the joint space and subsequent joint instability leading to loss of cartilage and joint function. From countless preclinical studies utilizing the DMM and other models of PTOA, the field has generated a generalized paradigm of the mechanisms and timings underpinning PTOA initiation and progression (Figure 1.3). It is believed that altered joint mechanical environment/stimuli drive progressive cartilage loss likely due to acute chondrocyte injury responses[55,76,79,100–106]; including imbalances in catabolic (matrix degrading) and anabolic (matrix forming) processes, cell death, proliferation, and inflammation responses (increased pro-inflammatory cytokine production).

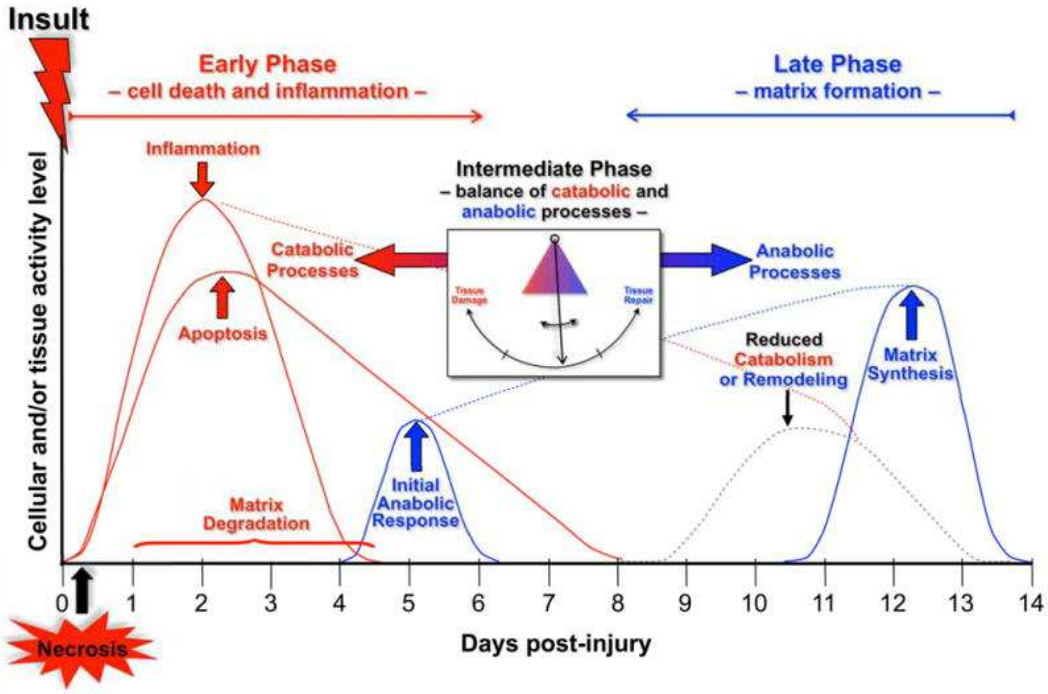

Figure 1.3: Conceptual Paradigm of Cellular and Tissue-Level Activity Underpinning PTOA Initiation and Progression. Following a traumatic joint injury, it is believed that cartilage undergoes significant changes at the tissue and cellular-level; these include, initial catabolic (red) processes followed by an overlap of anabolic (blue) processes in attempts to repair the tissue over time. Irrespective of these overlapping responses, the integrity and function of cartilage ultimately deteriorates leading to a complete loss of cartilage and joint function. Unfortunately, the underlying mechanisms driving these changes and the spatial evolution of such changes is largely unknown (Excerpt from Anderson et al. 2011[55]).

While tremendous effort has been undertaken to help establish the generalized paradigm of PTOA initiation and progression, understanding the spatial evolution of the cellular and structural changes has been underappreciated and understudied. Knowledge regarding the spatial progression of cartilage degeneration may help to link together injury-specific changes in joint biomechanics to cartilage-level

mechanobiology and allow the identification of specific populations of chondrocytes that drive the initiation and propagation of injury-mediated cartilage damage. Chapter 2 of this dissertation uses the murine DMM-model to evaluate the spatiotemporal evolution of tissue- and cellular-level processes associated with cartilage damage initiation and progression.

1.4 Current Post-Traumatic Osteoarthritis Treatment Strategies/Limitations

Unfortunately, no preventative therapies exist that can ameliorate the development of PTOA (or OA)[79,104]. Current palliative treatments and life-style changes[7,107] only address secondary symptoms of the disease, such as joint pain and immobility, and patients typically require invasive and expensive joint repair/replacement surgeries (e.g. total knee arthroplasty) when joint dysfunction and pain becomes unbearable[51,74,75,104,108–110]. Given that many patients in the PTOA cohort are younger adults[32,33,35,59,104] due their having experienced joint injuries in adolescence or young adulthood, joint arthroplasty is typically not recommended due to the finite life-spans of artificial joints and the inevitable need for knee arthroplasty revision as the patients and implants age[14,111–115]. The lack of preventative PTOA treatments is concerning given the increasing numbers of individuals (including children) participating in sports with high injury-risk and the huge socioeconomic burden that PTOA places on patients, caregivers, and the medical establishment. The present lack of PTOA preventative therapies is partially due to a limited knowledge of how early acute joint injury lead to loss of cartilage and joint function[55,104]. Further, when and how clinical therapies should be implemented following joint injury remains unclear. However, preclinical studies suggest that the most successful PTOA

treatments are those administered prophylactically as preventative treatments immediately upon the occurrence of acute joint injury[55,79,104].

Preventing cartilage degeneration following a traumatic joint injury is the primary goal of PTOA treatment; the ability to develop such therapies requires understanding the early pathological changes that precipitate long-term cartilage damage. Therapeutics that can directly influence injury-mediated changes to chondrocyte biology *in vivo* would represent ideal disease-modifying leads. For instance, preclinical studies suggest that early modulation of chondrocyte proliferation, death, and matrix metabolism following injury can mitigate the course of cartilage degeneration *in situ* and *in vivo*[55,104]. While cartilage protection is undoubtedly critical in PTOA prevention, PTOA (like OA) is a whole-joint disease; thus, therapeutic leads that target the articular cartilage, as well as other joint tissues of disease importance, could provide additional, multi-functional benefits in PTOA modification. For instance, preclinical and clinical PTOA studies have used, with promising multi-functional outcomes, a wide variety of therapeutic leads mitigating joint inflammation following joint injuries, such as interleukin-1 receptor antagonists or targets of other cytokines implicated in joint inflammation[78,116–119]. However, while a number of these anti-inflammatory therapeutic leads have demonstrated efficacy in preclinical models of PTOA, none have received FDA-approved for human PTOA.

Beyond joint inflammation, therapeutic leads targeting the subchondral bone of the joint are gaining significant attention due to the general belief that aberrant subchondral bone remodeling plays a role in cartilage degneration[120–125]. Studies have demonstrated changes in subchondral bone structure and cellularity[120–125], as well as elevated cross-talk between the cartilage and subchondral bone via fluid flow through

small canals and vessels post-injury[126]. Thus, therapies that can influence subchondral bone remodeling may hold promise for preventing or delaying PTOA development. Recently, one FDA-approved class of therapeutics has gained significant interest as a drug that can positively influence subchondral bone remodeling and cartilage degeneration post-injury, the bisphosphonates. This dissertation is dedicated to exploring the potential clinical use of locally targeted bisphosphonate administration for PTOA disease modification.

1.5 Bisphosphonates

1.5.1 A Brief History of Bisphosphonates and Mechanisms of Action

Bisphosphonates (BPs) are a class of FDA-approved drugs historically used to treat bone-related diseases because of their anti-resorptive and anti-remodeling capabilities. Prior to their application biologically, BPs, which were first synthesized in the late 1800s, were used industrially as water-softeners to inhibit calcium carbonate precipitation[127,128]. BPs were originally referred to as inorganic diphosphates because these molecules contain an inorganic phosphate-oxygen-phosphate, or pyrophosphate linkage, which inhibit hydroxyapatite crystal formation and calcification[127–129]. Upon the discovery that pyrophosphates bound selectively to hydroxyapatite crystals in the body, especially bone, and prevent their dissolution, the study of BPs transitioned into the biological realm. Since the first published use for their biological application in 1969[127,128], the evolution of BPs has been astonishing (Figure 1.4). Thousands of BPs have been synthesized and tested, but only about a dozen have received FDA-approval for use as therapeutics[127,128]. As a result, decades

of research inform our current understanding of how BPs affect mammalian cells; particularly in osteoclasts, their canonical cellular target in the body.

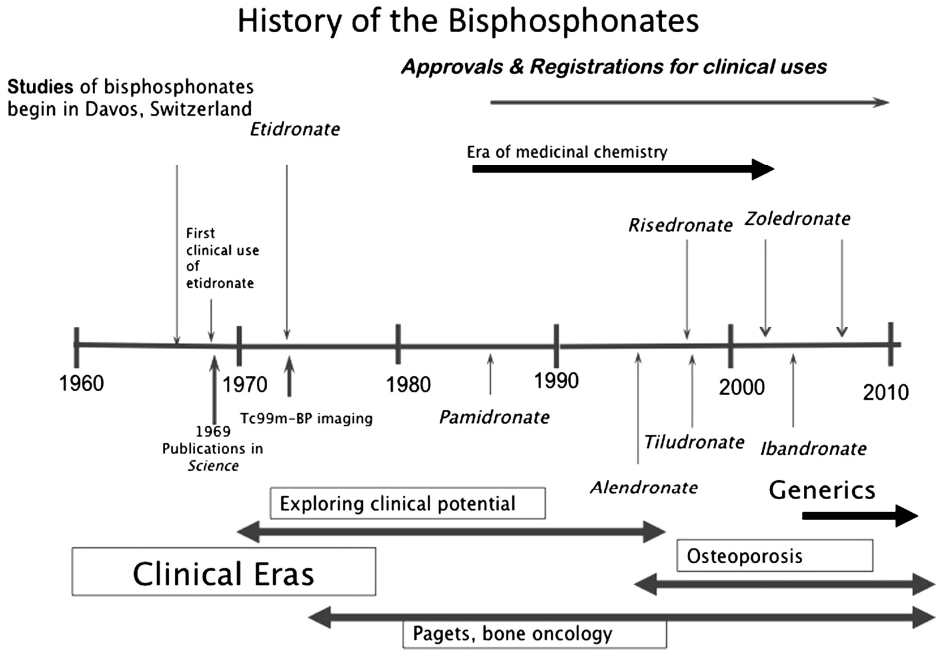

Figure 1.4: History of Bisphosphonates. Over the years, bisphosphonates have been synthesized and tested as therapies for bone-related diseases, such as Paget's disease of bone and osteoporosis. The bisphosphonates indicated on the timeline have received FDA-approval, with Zoledronate (or zoledronic acid) being the most recent and potent one. (Excerpt from Russell 2011[128]).

The evolution of BPs from the first-generation (e.g. clodronate) to third-generation derivatives (e.g. alendronate and zoledronate) led to an increase in affinity for bone and anti-resorptive potency. The increased bone affinity and anti-resorptive potency are due to the modification of their molecular structure that has resulted in increased hydroxyapatite binding and alteration in the cellular mechanisms of BP

action[130,131,140–142,132–139]. In Figure 1.5A, the molecular structure for each generation of BPs are shown. The first-generation bisphosphonates do not contain nitrogen atoms and are metabolized into toxic ATP analogs, which causes osteoclasts dysfunction and apoptosis, resulting in the classically understood anti-resorptive properties of BPs *in vivo*. The newer generations (2nd and 3rd) contain nitrogen atoms in their side chain and are referred to as nitrogen-containing BPs (nBPs). The addition of the nitrogen atom (either as cyclic or non-cyclic structure) increased their affinity for bone, as well as their anti-resorptive potency; the newest and most potent nBP, zoledronate (commercial names: Zometa, Aclasta, and Reclast) and herein referred to as zoledronic acid (ZA), is the focus in this dissertation. Mechanistically, nBPs inhibit the mevalonate biosynthetic pathway in osteoclasts (as well as all eukaryotic cells) by inhibiting the enzyme farnesyl pyrophosphate synthase, driving inhibition of osteoclasts bone resorption and induction of osteoclast apoptosis[134,143–147] (Figure 1.5B). The mevalonate, or isoprenoid, pathway is critical for cellular function and is ubiquitous in mammalian cells[136,148–151]. This pathway is responsible for the biosynthesis of cholesterol and the prenylation of various small GTPases, such as Rho, Ras, and Rac, which are critical for the regulation of the cytoskeleton structure and function, proliferation, migration, mechanosensation, and cell health[151–155]. Thus, mammalian cells that possess the mevalonate pathway should be susceptible to the effects of nBPs. Consequentially, targeting this pathway may provide benefits for diseases that include multiple joint tissues and cells, such as OA or PTOA.

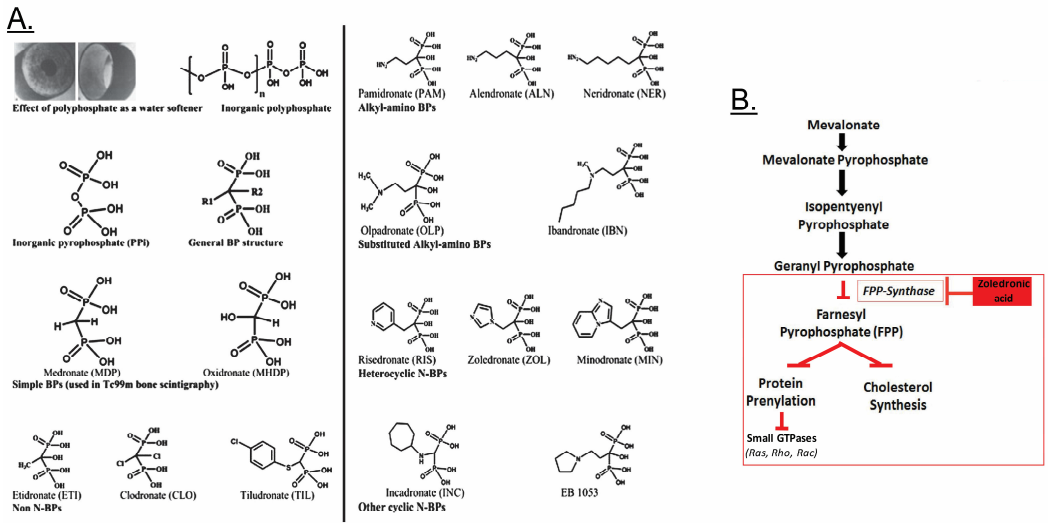

Figure 1.5: Bisphosphonates Structure and the Mevalonate Pathway. (A.) Structures of older, first-generation bisphosphonates (left of solid line) and newer generations of nitrogen-containing bisphosphonates (Excerpt from Russell 2011[128]). (B.) Simplified schematic of the mevalonate pathway indicating that nitrogen-containing bisphosphonates, like zoledronic acid, selectively targeted inhibit farnesyl pyrophosphate (FFP) synthase, inhibiting cholesterol production and prenylation of small GTPase (Adapted from Rogers 2011[156]).

1.5.2 Bisphosphonates for Osteoarthritis

Aside from their well-accepted influence on osteoclasts, nBPs, by targeting the ubiquitous mevalonate pathway, can influence cell growth/differentiation, gene expression, metabolism, cytoskeletal assembly, and cell survival[136] in almost all mammalian cells; including osteoblasts[128,144,157–163], osteocytes[128,159], vascular smooth muscle cells[164,165], vascular endothelial cells[166–169], epithelia cells[170–173], kidney cells[174], stromal cells[175], fibroblasts[172,173,176,177], regulatory T-cells[178], monocytes[179–181], macropages[156,181–186], and even chondrocytes[187]. Because of this, ZA use has extended beyond bone-related diseases for uses in cancer and arthritis chemotherapy[188,189]. In chemotherapy-directed treatment, ZA prevents proliferation

and induces apoptosis in cancerous cells[131,162,196–205,188,206–208,189–195]. In treating arthritis, administration of ZA reduces cartilage damage, bone remodeling, and pain in a variety of preclinical models of inflammatory arthritis (rheumatoid arthritis)[209–216] and OA[217–219]. While demonstrating efficacy in preclinical models, translation of ZA[220,221] and other BPs (e.g., clodronate[222,223], neidronate[224], alendronate[225,226], and risedronate[227–231]) into the clinic for idiopathic OA has been somewhat limited. Findings from such studies have produced mixed results; some show benefits in term of pain reduction and improved gait and mobility, whereas others demonstrate equivocal results. While the cause of these discrepancies is unknown, differences in patient populations and timing of administration provide the most likely explanations[232–237]; many of the OA patients enrolled in these studies already had irreversible cartilage damage. Consequentially, a patient's disease state likely limits the ability of BPs to delay or reverse OA progression. However, this interpretation does not exclude the possibility that nBPs could be leveraged for joint disease modification if their use were targeted toward more appropriate patient cohorts and if their timing and doses were more properly titrated. Because of this, patients that experience a known joint injury and likely develop PTOA could be ideal candidates for nBPs therapy as opposed to late-stage idiopathic OA patients. Thus, the primary goal of this dissertation was to establish the disease-modifying potential of nBPs, specifically ZA, for PTOA using a preclinical model of PTOA.

1.6 Intra-Articular Injection of Zoledronic Acid Therapy for Post-Traumatic Osteoarthritis

1.6.1 Bisphosphonates for Post-Traumatic Osteoarthritis and Current Limitations/Opportunities

Given the anti-resorptive properties of BPs, particularly ZA, and the belief that subchondral bone remodeling may play a role in PTOA initiation and progression, nBPs have been thought to be an ideal disease-modifying therapeutic for PTOA. To this end, numerous researchers have demonstrated that ZA provides cartilage protection and anti-inflammatory benefits when systemically and continuously administered at high-doses in animal models of PTOA[238–241]. However, this systemic, high-dose strategy carries increased risk of adverse side effects for both the skeleton (e.g., systemic inhibition of bone remodeling, osteonecrosis of the jaw, and atypical bone fractures[242–244]) and non-skeletal systems (e.g., renal and cardiovascular[245]). Thus, despite promising preclinical findings, clinical acceptance of systemic, high-dose administration of ZA for the treatment of PTOA, especially in the often younger PTOA patient populations, may face substantial hurdles. Furthermore, it is unclear if the PTOA disease-modifying abilities of ZA are attributed to more direct 'chondro-modulatory' mechanisms or require systemic dosing to be efficacious. Since systemically-administered ZA may face insurmountable challenges towards clinical acceptance for PTOA therapy, the study of alternative, locally targeted routes of ZA administration, such as intra-articular (i.a.) injections[246–252], are warranted.

1.6.2 Evidence Supporting the Use of Intra-Articular Injection of Zoledronic Acid for Post-Traumatic Osteoarthritis Treatment

Support for the use of intra-articular injection of ZA as a PTOA therapy comes from the knowledge that many tissues and cells in the joint that are implicated in

arthritis[78,253] can directly be affected by ZA. In general, aside from its classical understood inhibition of bone resorption, ZA is known to modulate inflammatory cytokine production, and cell maturation, proliferation, and death in monocytes[181], monocyte-derived dendritic cells[179–181], macrophages[181–186], and endothelial cells[170,171], which all reside in the synovium. Mesenchymal-derived cells, including chondrocytes, are thus susceptible to bisphosphonates. Studies have demonstrated the ability of nBPs to regulate chondrocyte proliferation, viability, and death *in vitro*[187,254]. Furthermore, work from our collaborators has suggested that ZA can directly benefit chondrocyte health and cartilage biomechanical properties *in situ* under experimental conditions that mimic aspects of PTOA[255–258]. Preclinical translation of these findings has been limited to a single research group that explored the use of intra-articularly injected ZA within the context of PTOA. In two reports published after the initiation of this dissertation[259,260], this team demonstrated that repeated i.a. injection of ZA appeared to reduce joint inflammation, cartilage damage, and chondrocyte apoptosis in the rat anterior cruciate ligament model of PTOA[259,260]. Collectively, these studies demonstrated preliminary evidence that intra-articular injection of ZA (i.a.ZA) could provide cartilage protection following injury. However, the following questions remained: i) could i.a.ZA modulate cartilage damage and other non-cartilaginous tissues in different species and injury model; ii) is repeated versus single i.a.ZA required for disease-modifying efficacy; iii) what are i.a.ZA mode(s) of action in mitigating PTOA; and iv) can ZA directly modulate chondrocytes and cartilage health.

1.7 Structure of Dissertation

1.7.1 Overview

PTOA is incurable and represents a growing socioeconomic burden. Unfortunately, current clinical treatments have limited therapeutic efficacy and still require joint repair surgeries and joint replacement to relieve the pain and loss of mobility accompanying PTOA. This lack of therapeutic success is derived partly from a lack of understanding regarding the underlying mechanisms that initiate and drive the loss of cartilage and joint function following acute joint injury. Shedding insights into the early changes of cartilage and non-cartilaginous joint tissues following an acute injury may help guide the development of successful therapies for PTOA prevention. Despite the promising results associated with the systemic administration of ZA for PTOA (and OA), this strategy will likely face considerable, if not insurmountable hurdles to clinical adoption. Thus, targeted ZA delivery mechanisms, like intra-articular injection, represent a logical strategy for PTOA disease-modification. However, the use of intra-articular injection of ZA for PTOA prevention *in vivo* has received minimal investigation and knowledge ZA's mode(s) of action in chondrocytes and cartilage is largely unknown.

Overall, we believe that injurious insult to the joint initiates early and focal chondrocyte dysfunction and cartilage damage that can be targeted to modify PTOA progression. Furthermore, we believe that intra-articular injection of ZA can modulate the response of chondrocytes to these perturbations, suppressing the development of cartilage erosions, and alter the response of non-cartilaginous joint tissues following injury. Therefore, this dissertation investigated the following three aims: i) to characterize the early, spatiotemporal progression of cartilage's cellular and tissue

level changes post-injury *in vivo*; ii) to determine the disease-modifying benefits of early, intra-articular injection of ZA post-injury for PTOA prevention *in vivo*; and iii) to determine the concentration and exposure-dependent pleiotropic effects of ZA on chondrocyte health and function *in vitro*.

1.7.2 Aim #1: Characterize the early, spatiotemporal progression of cartilage's cellular and tissue level changes post-injury *in vivo*. (Chapter 2)

To better understand the pathophysiology of PTOA and to identify druggable mechanistic targets for PTOA prevention and disease-modification, we evaluated the temporal and spatial evolution of cartilage degeneration following injury-induced changes in joint stability (Chapter 2). We used a well-established surgically induced murine model of PTOA, the destabilization of the medial meniscus (DMM)[99], to induce cartilage degeneration. We placed emphasis on histological and immunohistochemical analysis of the spatiotemporal evolution of cartilage damage and chondrocyte presence resulting from injury-induced meniscal extrusion. Findings from Chapter 2 established a foundation of knowledge that was leveraged in Chapters 3 and 4 to test the efficacy of locally-delivered ZA into the injured knee to protect chondrocytes and cartilage from degeneration and its influence other non-cartilaginous joint tissues' responses.

1.7.3 Aim #2: Determine the disease-modifying benefits of early, intra-articular injection of zoledronic acid post-injury *in vivo*. (Chapters 3 and 4)

Given the whole-joint nature of PTOA disease, a therapeutic drug that could be locally-delivered to prevent cartilage degeneration while also possessing anti-resorptive and anti-inflammatory properties would be ideal. In Chapters 3 and 4, one such promising therapeutic was investigated. We investigated the disease-modifying

potential of repeated versus single intra-articular injection of ZA on cartilaginous and non-cartilaginous tissues following injury in the murine DMM model using histological, immunohistochemical, and micro-computed tomography analyses. In Chapter 3, we focused on the influence of intra-articularly injected ZA on cartilage structure, composition, and cellularity following injury. In Chapter 4, we evaluated ZA's influence on injury-induced evolution of osteophyte formation, meniscus response, inflammation, and subchondral bone remodeling, as well as on the structure of skeletal compartments distant from the injured joint. Collectively, the goal of both chapters was to demonstrate if intra-articular ZA can drive disease-modifying outcomes in injured joints and if local intra-articular injections of ZA could minimize the adverse skeletal side effects typically associated with systemically administered ZA. The knowledge gained from this aim demonstrated the *in vivo* efficacy of intra-articular injection of ZA in modifying PTOA initiation and progression and shined light on possible modes of ZA action on chondrocytes further explored in Chapter 5.

1.7.4 Aim #3: Determine the concentration and exposure-dependent pleiotropic effects of ZA on chondrocyte health and function *in vitro*. (Chapter 5)

While it is critical to establish proof-of-concept for locally delivered ZA as a PTOA treatment *in vivo*, the use of *in vivo* studies limits our ability to ask detailed mechanistic questions regarding ZA and chondrocytes, e.g. what is the effect of ZA concentration and exposure on chondrocyte health and homeostasis in isolation from other joint tissues? In Chapter 5 we explored potential cellular modes of action of ZA in chondrocytes *in vitro* using an immortalized chondrocyte-like cell line culture in the absence of other joint tissues/cells. Knowledge gained from Chapter 5 will help to inform the potential modes of action of ZA in the joint *in vivo* and establishes a

baseline of concentrations and exposure times for studying the effect of ZA on chondrocyte and cartilage health *in vivo* and *in situ*.

Chapter 2

EARLY, FOCAL CHANGES IN CARTILAGE CELLULARITY AND STRUCTURE FOLLOWING SURGICALLY INDUCED MENISCAL DESTABILIZATION IN THE MOUSE

(MA David, MK Smith, RN Pilachowski, AT White, RC Locke, C Price, *Published 2017*)

2.1 Abstract

Post-traumatic osteoarthritis (PTOA) is an accelerated form of osteoarthritic cartilage degeneration affecting approximately 20-50% of patients experiencing joint injury. Currently, PTOA is incurable; to better understand the etiology of PTOA and to develop rational anti-osteoarthritic therapies, it is critical to understand the spatiotemporal initiation and the progression of PTOA. In this study, we employed semi-quantitative histological scoring and quantitative damage analysis to examine disease progression in the murine destabilization of the medial meniscus (DMM) model of PTOA from early- (3-days) through late- (112-days) disease timepoints. We observed significant, progressive articular cartilage (AC) cellular and structural changes in the medial compartments of injured joints as early as 3-days. Spatially within the joint, cartilage damage (erosions) were observed anteriorly at 84-days. Furthermore, a drastic loss in chondrocyte number (by 3-days), surface damage (at 7-days), and cartilage erosion (at 84-days) was found to co-localize to the specific region of the medial tibial plateau AC that experienced a change in meniscal coverage due to meniscal extrusion following DMM. Taken together, these results suggest that DMM-mediated extrusion of the medial meniscus leads to rapid, spatially-dependent changes

in AC cellularity and structure, and precipitates the focal degeneration of cartilage associated with PTOA. Importantly, this study suggests that joint instability injuries may trigger immediate (<3 days) processes within a small population of chondrocytes that directs the initiation and progression of PTOA, and that development of chondroprotective strategies for preventing and/or delaying PTOA-related cartilage degeneration are best targeted toward these immediately-early processes following joint injury.

2.2 Introduction

Approximately 20-50% of patients suffering traumatic joint injury, e.g., anterior cruciate ligament tears, articular fracture, meniscal tears, or meniscectomies, will develop post-traumatic osteoarthritis (PTOA) within 10-15 years of injury[54,55]. Currently, PTOA is not preventable and the precise mechanisms by which acute joint injury leads to long-term cartilage degeneration remains unknown[55] partly due to: i) limited availability of early disease stage human cartilage, ii) limited in vivo cartilage assessment techniques, and iii) the long timespan of clinical disease progression. To overcome these limitations and to define the mechanisms underpinning PTOA initiation and progression, cartilage degeneration has been studied in numerous pre-clinical small-animal models of joint injury.

The destabilization of the medial meniscus (DMM), a surgically-induced joint instability model, is a commonly used murine model of PTOA due to its ease of implementation, high reproducibility, and pattern of disease progression thought to closely recapitulate human osteoarthritis[99]. Collectively, murine DMM studies have identified mild cartilage damage in early-disease (7- and 14-days)[261–266] and mild-to-severe cartilage loss/erosion at mid-to-late stage disease (28 through 112-days)

[126,261,270–279,262,280,281,263–269]. Typically, cartilage damage severity and progression has been evaluated using whole-joint level semi-quantitative histological scoring systems[277,282–284]. However, such systems have limited ability to fully characterize early changes in articular cartilage (AC) degeneration because they rely on: i) binary metrics of superficial tissue damage (fibrillations and clefts), which only indicate the presence of these changes not their spatial extent, and ii) metrics of cartilage erosion that simultaneously incorporate width-wise (across the surface) and depth-wise (into the tissue) damage components in their analysis. Furthermore, scores are oftentimes presented as a single aggregated damage metric derived from the maximal extent of damage within a section or across a joint compartment, or summed/averaged across the joint. Thus, while semi-quantitative scoring systems have helped to define the time-course of whole-joint level cartilage damage post-DMM, they can inadvertently mask key aspects of the spatial initiation and progression of cartilage degradation.

Defining the anterior-to-posterior and medial-to-lateral distribution of cartilage damage may provide critical insight into the mechanisms by which PTOA initiates and progresses. In the pioneering DMM study by Glasson et al.[99], qualitative observations of cartilage erosions being preferentially localized to anterior-to-central regions of the medial tibial plateau (MTP) of DMM joints were made. Furthermore, while not addressed in prior studies, our qualitative impressions of the murine DMM literature suggests a co-localization of cartilage damage to medial regions of the MTP that were previously covered by the medial meniscus (MM)[126,264,266,271–273,277–280]. Supporting these impressions, studies utilizing DMM within various species have indicated increased joint laxity and anterior translation (mice)[285], altered medial compartment contact stresses (mice and rabbit)[267,286], and cartilage damage to the middle and outer

MTP (rat)[287]. Furthermore, non-invasive murine models of PTOA support the co-localization of applied load, cartilage damage, and chondrocyte apotosis[288]. While a few murine studies have identified increased chondrocyte death post-DMM[261,263,280,283,289], the details regarding the spatial distribution of chondrocyte loss across the AC and their relationship to meniscal extrusion have yet to be investigated.

Taken together, we believe that meniscal extrusion post-DMM plays an important role in the rapid, focal initiation and progression of cartilage damage. We hypothesized that chondrocyte loss and cartilage structural damage would rapidly (≤7-days) and preferentially localize to cartilage regions where DMM-induced MM extrusion results in altered femur-on-meniscus-on-tibia contact. However, the use of conventional semi-quantitative scoring alone would likely be unable to address such relationships. Therefore, we utilized a set of spatiotemporal scoring and evaluation methods to address this hypothesis and to elucidate the relationship between meniscal extrusion and changes in cartilage cellularity and structure from early- (3-day) through late-stage (112-days) disease in the murine DMM model of PTOA.

2.3 Methods

2.3.1 Animals and Surgeries

Male C57BL/6 mice (n = 83) were purchased from the Jackson Laboratory at 9-weeks of age and housed in standard cages (≤5 mice/cage). Mice were maintained on a 12-hour light-dark cycle in a climate controlled vivarium with access to food (Prolab RMH 3000) and water *ad libitum*. Mice were randomly assigned to one of three groups: DMM, sham, or baseline/age-matched controls

At 12-weeks of age, right knees of mice in the DMM group (n = 5-10 mice/group) underwent the DMM surgery[99,126]; contralateral limbs served as un-operated internal controls. Briefly, mice were anesthetized using inhaled isoflurane and prophylactically administered antibiotic and analgesic. Using aseptic techniques, the medial meniscotibial ligament (MMTL) was exposed and transected to release the anterior horn of the MM from the tibia and surgical incisions were subsequently closed. A subset of mice underwent sham surgery, identical to the DMM surgery, except transection of the MMTL was omitted. Following surgery, mice recovered quickly to full ambulation and unrestricted cage activity. Collection of tibiofemoral joints occurred upon euthanasia (CO^2 exposure and cervical dislocation) at either 3-, 7-, 14-, 56-, 84- or 112-days post-injury, or 0-days for non-surgical baseline controls. All animal procedures were approved by the University of Delaware's Institutional Animal Care and Use Committee (Protocol Number 1252).

2.3.2 Histological Processing and Staining

Following tissue collection, joints were processed for paraffin embedding, sectioning, and histological staining using standard techniques[284]. Briefly, all joints were placed within tissue cassettes at a flexion angle of ~80º, approximating the joint's natural flexed position. Specimens were then fixed in 4% paraformaldehyde for 48-hours at 4ºC, decalcified in 14% EDTA (pH 7.4) over 15-days at 4ºC, and processed for paraffin embedding. Joints were serially cut into 5-µm thick coronal sections and placed on charged slides (two sections/slide). Starting at the front of the joint (anterior), every tenth slide (every ~100-µm) was stained with 1% Safranin-O, 0.02% fast green, and Weigert's iron hematoxylin. From these, a subset of five slides spanning ~500-µm of the joint and centered about the tibial plateau and femoral

condyle cartilage contact region were selected for damage analysis (Figure 2.1A). These slides were labeled (1-5), from the anterior to the posterior level of the joint.

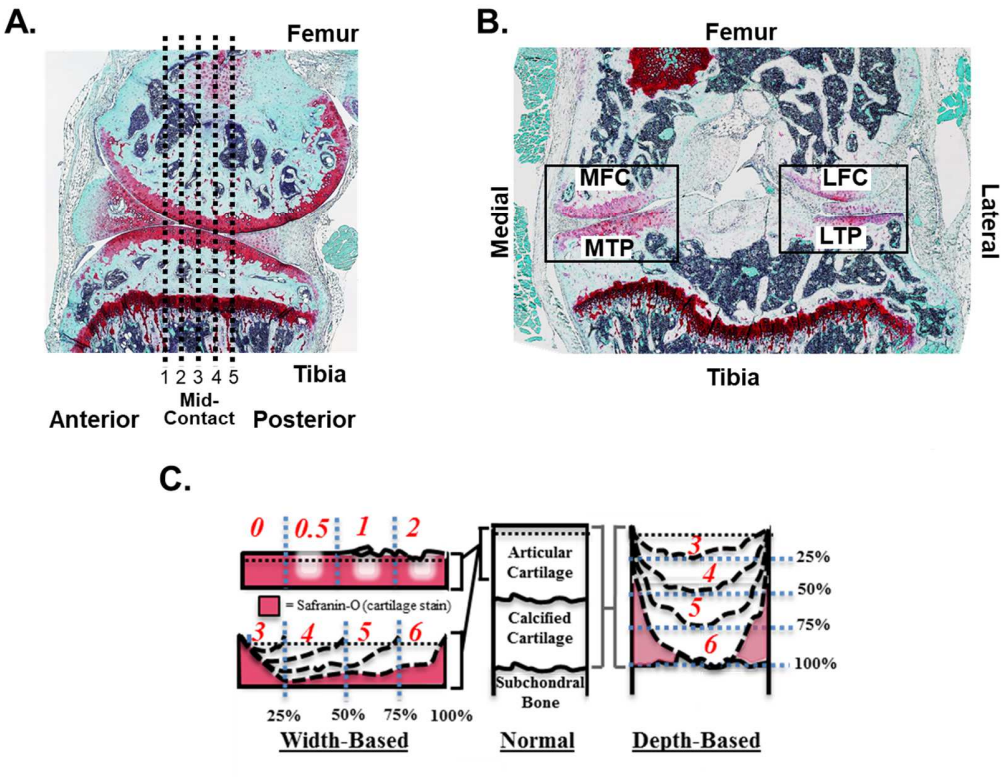

Figure 2.1: Histological analysis of cartilage structural damage. Representative safranin-O/fast green stained sagittal (A.) section demonstrating the region of interest and slide positions selected for analysis, and (B.) a coronal section used for semi-quantitative histological analysis of the medial femoral condyle (MFC), medial tibial plateau (MTP), lateral femoral condyle (LFC), lateral tibial plateau (LTP). Images were captured at 5x magnification. Independent width- and depth-based scoring systems (C.) were utilized in this study. Damage values of 0-2 were identical in both scoring systems, while scores of 3 and higher allowed differentiation of width- vs. depth-based erosions extending beyond the superficial layer. A complete description of the scoring system can be found in Table 2.1.

2.3.3 Spatiotemporal Scoring of Width- and Depth-Based Cartilage Damage

Semi-quantitative scoring of cartilage damage was performed across all stages of disease development (3- to 112-days). Three blinded scorers (MAD, MKS, and ATW or RNP) scored the degree of cartilage damage present in each slide using two separate semi-quantitative scoring metrics to evaluate the extent of width- vs. depth-wise cartilage damage. Width-wise damage across the articular surface was assessed (Figure 2.1C, Table 2.1) using a modified version of the OARSI scoring system[284]. Depth-wise cartilage damage, relative to the calcified cartilage (CC)/subchondral bone interface (Figure 2.1C, Table 2.1), was assessed using an adapted version of Chambers' et al.[282] scoring system. For each metric, cartilage damage was assessed on a 0-6 scale. Scores of 0-2 were applied identically within both scoring systems, while scores of 3-6 differed. This allowed for classification of cartilage erosion based on its width-wise extent independent of depth-wise extent, and vice versa. Scoring was performed and aggregated separately for each of the four compartments of the joint: the MTP, the medial femoral condyle (MFC), the lateral tibial plateau (LTP), and the lateral femoral condyle (LFC) (Figure 2.1B). At each level, scores (anterior [1] to posterior [5]) were aggregated across observers within an individual joint. For overall temporal analysis, scores from each level were averaged to generate a whole-joint damage score used to calculate group means. For spatial analysis of anterior-to-posterior damage, the average individual specimen score at each level was used to calculate a group mean for each level and timepoint.

Table 2.1: Description of the semi-quantitative width- and depth-based histological scoring systems utilized in the present study.

Score	Width-Based	Depth-Based
0	Normal	
0.5	Loss of Safranin-O without structural changes*	
1	Fibrillations/discontinuities and/or roughened superficial surface*	
2	Erosion to the layer immediately below the superficial layer and some loss of surface lamina*	
3	Erosion[#] extending <25% of AC width	Erosion[#] extending for <25% of total cartilage depth[‡]
4	Erosion[#] extending 25-50% of AC width	Erosion[#] extending for 25-50% of total cartilage depth[‡]
5	Erosion[#] extending 50-75% of AC width	Erosion[#] extending for 50-75% of total cartilage depth[‡]
6	Erosion[#] extending >75% of AC width	Erosion[#] extending for >75% of total cartilage depth[‡]

[*] indicates damage can extend across any percentage (%) of the articular cartilage surface width
[#] indicates erosion must extend beyond the layer immediately below the superficial layer/lamina
[‡] indicates depth measured relative to total cartilage (AC + CC) thickness

2.3.4 Quantification of Meniscal Coverage of the Cartilage Surface, Cartilage Damage, and Chondrocyte Cellularity

To establish spatial (medial-to-lateral) and temporal relationships between meniscal extrusion and changes in chondrocyte cellularity and cartilage damage within the medial joint compartment, sections from joints 3- to 84-days post-DMM were stained immunohistochemically (IHC) for type II collagen and DAPI-positive cells (n = 5-mice/group), and quantified via custom semi-automated image processing. Briefly, IHC staining was performed on slides adjacent to the Safranin-O sections, and surrounding the center of cartilage contact (levels 2-4). Sections from DMM and contralateral (control) joints were stained immunohistochemically for type II collagen and the presence of cells (DAPI counterstain for nuclei). Type II collagen was used as a structural indicator to assist in distinguishing between the articular and calcified

cartilages within each section and DAPI counterstain was used to differentiate the presence of chondrocytes in each tissue. Briefly, antigen retrieval was performed on the sections using pepsin (0.4% w/v; Sigma) in 0.01N hydrochloric acid for 15 minutes at 37°C. Sections were then blocked with 5% normal donkey serum (Sigma) in phosphate-buffered saline with 0.1% Tween-20 (Fisher Scientific) for one-hour at room temperature (RT), and incubated with a rabbit anti-mouse type II collagen primary antibody (1:200 dilution, ThermoFisher) overnight at 4°C. Sections were then incubated with an AlexaFluor-555 donkey anti-rabbit secondary antibody (1:400, ThermoFisher) for 1 hour at RT in the dark, treated with 0.1% w/v Sudan black (FisherBioReagents™) in 70% ethanol for 30 minutes at RT to reduce autofluorescence, and then mounted with a DAPI-containing mounting medium (ThermoFisher) for the detection of cell nuclei. Fluorescent images of the collagen type II and DAPI stained sections were obtained within 72-hours of completing the immunohistochemical staining procedure to limit fluorescent signal loss. Following staining, overlapping images of the sections were captured at 20x magnification using an epifluorescent microscope (Axio.Observer.Z1, Carl Zeiss) and a digital camera (AxioCam MrC, Zeiss) and combined (tiled) using Zen software (Zeiss). A custom semi-automated MATLAB (MathWorks) algorithm was used to: i) define the MTP region of interest (ROI) in each image, ii) manually trace the AC, CC, and MM, and iii) count DAPI-positive cells within the AC and CC (Appendix A Figure A.1). Traces were automatically segmented width-wise into four regions (quadrants 1-4; Appendix A Figure A.1) and cartilage structural (i.e., AC and CC thickness) and cellular (i.e., number of DAPI-positive cells) parameters were quantified within each quadrant. Quadrant 1 represents the innermost region of the joint while quadrant 4 was nearest

the joint margin. Additionally, the degree of meniscal extrusion was calculated as the extent of cartilage surface covered by the meniscus (length of meniscus covering AC/total AC width; herein referred to as 'meniscal coverage'), and the linear extent of width-wise cartilage surface damage, including fibrillations, clefting, and erosions (length of AC damage/total AC width), were traced[281], and quantified.

2.3.5 Statistical Analysis

All data is presented as mean ± standard deviation. Statistical analyses were performed using GraphPad Prism 6.0. Paired t-tests were used to establish differences in cartilage outcomes between DMM and contralateral joints at each timepoint. One-way ANOVAs with Tukey's post-hoc tests were used to determine differences in cartilage outcomes i) between contralateral, sham, and age-matched joints at a given timepoint; and ii) over time for either DMM or control joints. Linear regression was performed to identify i) spatial patterns (among levels 1-5) within DMM or contralateral joints, and ii) the relationship between whole-joint depth- versus width-wise damage. Pearson correlation coefficients were calculated to establish relationships between meniscal extrusion/coverage, chondrocyte loss, and cartilage damage. Statistical significance and trends were set at $p<0.05$ and $p<0.10$, respectively.

2.4 Results

2.4.1 Whole-Joint Temporal Changes in AC Structure Post-DMM

Early and progressive changes in AC structure at the whole-joint level were confirmed within the medial compartments of DMM joints (Figure 2 and Appendix A Table A.1). Within the MFC, DMM joints exhibited a trend towards increased whole-

joint cartilage damage (i.e., loss of proteoglycan staining and the presence of fibrillations/clefting) relative to contralateral limbs as early as 7-days (Figure 2.2A and B), and significant damage accumulation beyond 56-days. In the MTP, similar damage progression was observed in the DMM joints; however, this damage was statistically significant as early as 3-days (score = 0.7; $p<.05$; Figure 2.2C and D). In both the MFC and MTP of DMM joints, damage appeared to stabilize (scores of ~1-2) between 7- and 56-days before increasing again at 84-days and beyond (scores ≥ 3; $p<.001$). At 112-days, damage scores highlighted a moderate degree of width- and depth-wise cartilage erosion (~25-50% of the MTP width involved and ~50% of the AC depth; scores = 3.3 and 3.4, respectively). No significant cartilage damage was observed within the lateral compartments of DMM compared to contralateral joints or within contralateral joints compared to sham, age-matched, and non-surgical controls (Appendix A Table A.1)

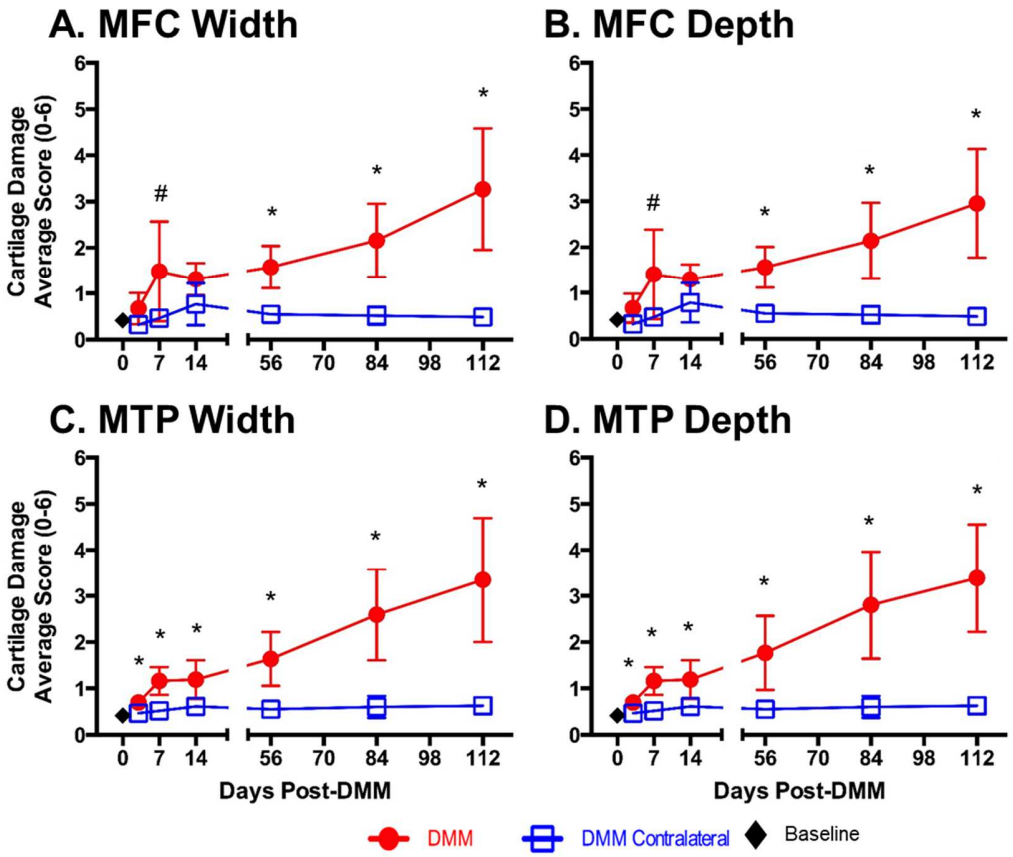

Figure 2.2: Progression of whole-joint cartilage damage post-DMM. Semi-quantitative histological scoring of width- (A.) and depth-wise (B.) MFC damage, and width- (C.) and depth-wise (D.) MTP damage across the joint demonstrated an early accumulation of proteoglycan loss and surface fibrillations [scores = .5-1] post-DMM (by 3-days), which preceded surface clefting [scores = 1-2] (7- to 56-days) and overt cartilage erosions [scores ≥3] (84+ days). Results are presented as mean ± STD (n = 5-10/timepoint/group) where * = $p<0.05$, # = $p<0.10$ (trend) for paired t-test between DMM and DMM contralateral.

We also investigated whether the use of semi-quantitative scoring of width- or depth-wise erosion resulted in different interpretations of AC damage progression by plotting MFC and MTP width-wise scores against their paired depth-wise scores and

performing linear regression (Appendix A Figure A.2). Damage scores ≤2 are classified identically in both schemes, and thus exhibit an expected one-to-one relationship (MFC [slope = .98; r^2 = .99] and MTP [slope = 1.0; r^2 = .99]). However, for scores >2 the slope of the linear regression differed significantly from 1.0 in the MTP (slope = .75; r^2 = .79), indicating a slight, albeit significant preference for higher width-wise damage scores. A trend towards significance was observed in scores >2 in the MFC (slope = .83; r^2 = .86). However, the overall interpretation of damage progression remained similar (Figure 2.2).

2.4.2 Anterior-to-Posterior Distribution of Cartilage Damage Post-DMM

To determine the anterior-to-posterior progression of cartilage damage within the joint, we investigated the distribution of semi-quantitative histological scores across the medial compartment from level 1 (anterior) to level 5 (posterior) over time. Our qualitative impression of preferential, anteriorly-localized damage (Figure 2.3) was confirmed by semi-quantitative analysis of damage distribution among Safranin-O stained sections (Figure 2.4). In the MFC of DMM joints, no significant spatial preference was observed at any timepoint (width-wise Figure 2.4A; depth-wise Appendix A Figure A.3). In contrast, anteriorly-localized damage was observed in the MTP at later-stage disease (width-wise damage p=0.02 & 0.08 at 84- and 112-days, respectively, Figure 4B; depth-wise Appendix A Figure A.3).

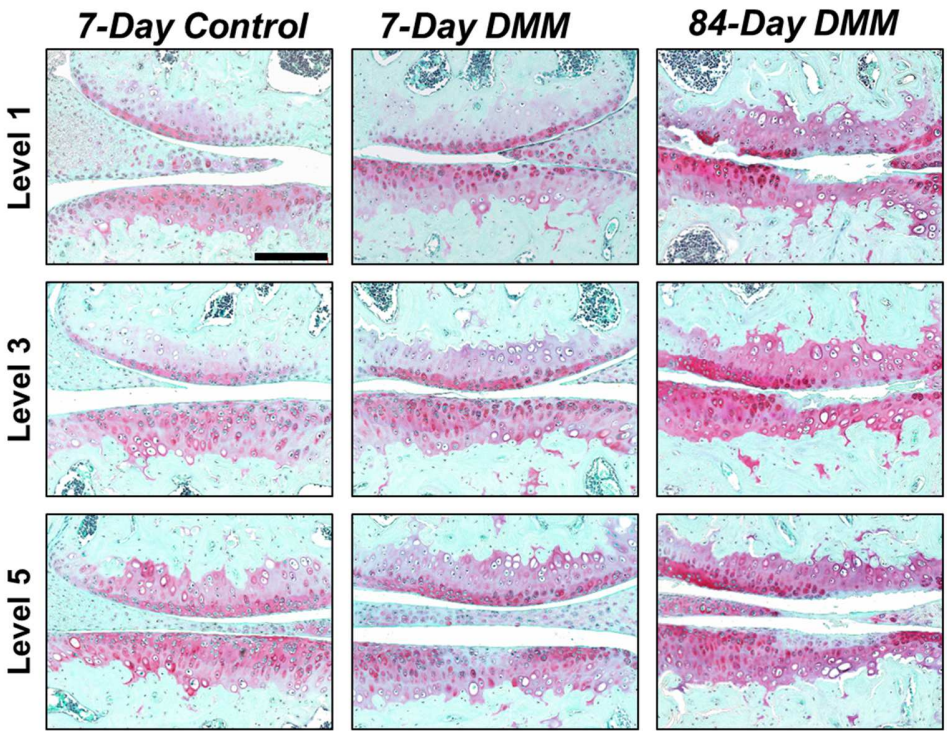

Figure 2.3: Spatiotemporal progression of cartilage damage in medial knee compartments post-DMM. Representative safranin-O/fast green stained sections highlight the changes in medial meniscus (MM) location and the distribution of cartilage damage from the anterior (level 1) to posterior (level 5) of DMM and contralateral (control) joints. Anteriorly-localized cartilage damage was qualitatively observed in the MTP of DMM joints at later timepoints. Images were acquired at 20x magnification, scale bar (200-µm) applies to all images.

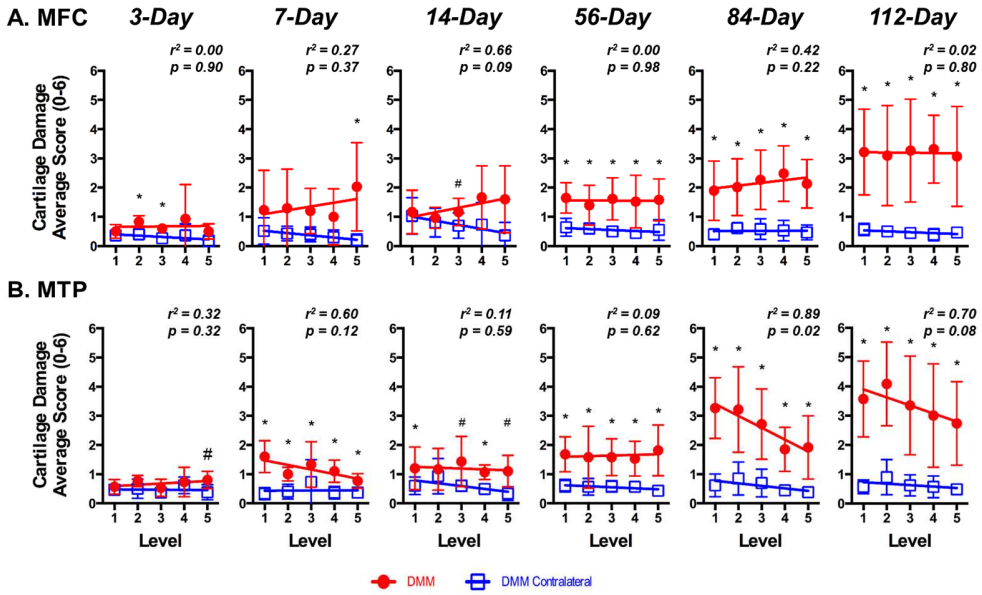

Figure 2.4: Anterior-to-posterior distribution of width-wise cartilage damage within the medial knee compartments post-DMM. Semi-quantitative width-wise scoring of cartilage damage in the MFC (A.) and MTP (B.), from anterior (level 1) to posterior (level 5) of the joint. The appearance of spatially-dependent damage was only observed in the MTP of DMM joints at late timepoints (84- and 112-days), i.e. increased damage anteriorly compared to posteriorly. Results are presented as mean ± STD (n = 5-10/timepoint/group) where * = $p<0.05$ and # = $p<0.10$ (trend) for paired t-test between DMM and contralateral joints at a given level. Linear regression r2- and p-values are shown for DMM joints only.

2.4.3 Meniscal Coverage of the AC Surface Post-DMM

Qualitative observations in both Safranin-O and IHC stained sections (Figure 2.5) reinforced our impressions of a spatial relationship between AC damage in the joint and meniscal extrusion post-DMM. IHC sections (type II collagen) were used to measure the extent of the central MTP (levels 2-4) covered by the MM. In non-surgical controls and contralateral limbs, ~50% of the MTP was covered by the MM throughout the study (Figure 2.6). In contrast, an immediate ~30-40% reduction in

meniscal coverage of the MTP was seen at 3- and 7-days (p=0.16 and 0.05, respectively). MTP coverage stabilized at ~20% coverage (60% reduction compared to contralateral joints; p=0.001) by 56-days. As a result of meniscal extrusion, a full quarter of the central contact region of the MTP (and MFC), largely consisting of quadrant 3 [Q3], experienced an acute and persistent change in meniscal coverage.

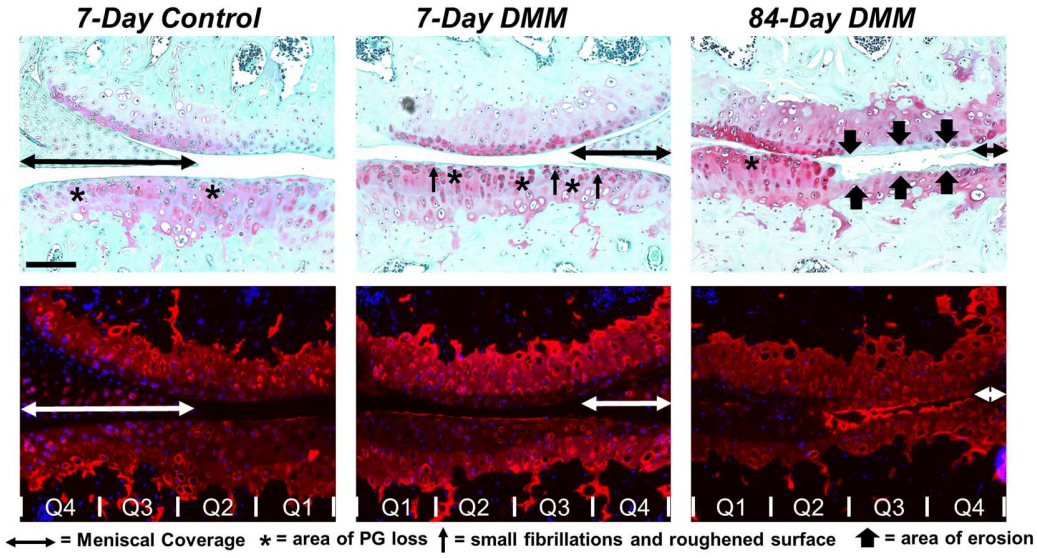

Figure 2.5: Histological and immunohistochemical demonstration of the spatial distribution (medial-to-lateral) of cartilage damage, meniscal coverage, and the presence of chondrocytes post-DMM. Adjacent histological (Safranin-O/fast green [upper panel]) and immunohistochemical (type II collagen and DAPI [lower panel]) images at 7- and 84-days post-DMM. A distinct loss of proteoglycan staining and chondrocyte presence, as well as increased type II collagen staining was observed to co-localize to MTP cartilage regions that experienced a loss of meniscal coverage at 7- and 84-days (Quadrant 3 [Q3]). All sections depict images take from anterior-posterior level 2 (anterior-to-mid-contact) and acquired at 20x magnification, scale bar (100-µm) applies to all images.

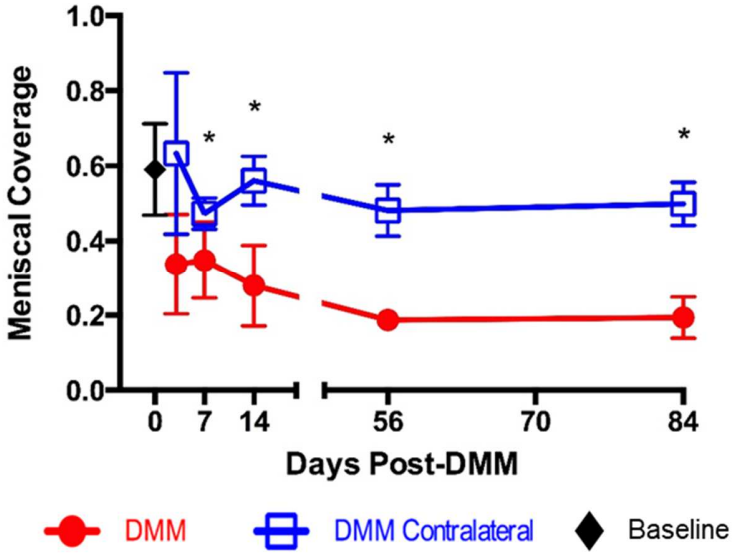

Figure 2.6: Changes in the degree of the articular cartilage covered by the medial meniscus (meniscal coverage) following DMM. The MTP AC in DMM joints experienced a significant loss of meniscal coverage as early as 7-days following injury; coverage stabilized at ~20-40% of the AC over time. Results are presented as mean ± STD (n = 5/timepoint/group) where * = $p<0.05$ for paired t-test between DMM and contralateral joints.

2.4.4 Distribution of Width-Wise MTP AC Damage Post-DMM

To assess the width-wise extent of surface damage and erosions not captured by our semi-quantitative scoring system, we quantitated the linear width-wise surface damage, which included fibrillations (score of 1), clefting (2), and erosions (≥3), across the MTP in IHC stained sections. We observed that the extent of damaged surface increased from ~0 to 35% of the MTP cartilage width between 0- and 7-days (Figure 2.7A), then stabilized at ~35-40% for the remainder of the study. We also observed that the extent of compromised cartilage surface was inversely correlated with the extent of meniscal coverage ($R^2 = .40$ and $p < .001$; Figure 2.7B) and that the spatial location of this damage was typically centered about the newly exposed Q3 of

the MTP (data not shown). In the same sections, we measured the average thickness of the AC and CC within each quadrant (Q1-4). Interestingly, a statistically significant reduction in AC thickness was only observed within Q3 at 84-days (Appendix A Figure A.4). No change in CC thickness was observed in DMM or contralateral joints (data not shown). We also qualitatively observed that the linear extent of width-wise surface damage coincided with an increase in type II collagen staining in DMM and contralateral joints (Figure 2.5). Collagen staining intensity appeared greater at all timepoints in DMM joints, while also appearing to co-localize to AC regions demonstrating a loss of Safranin-O staining, and later overt damage.

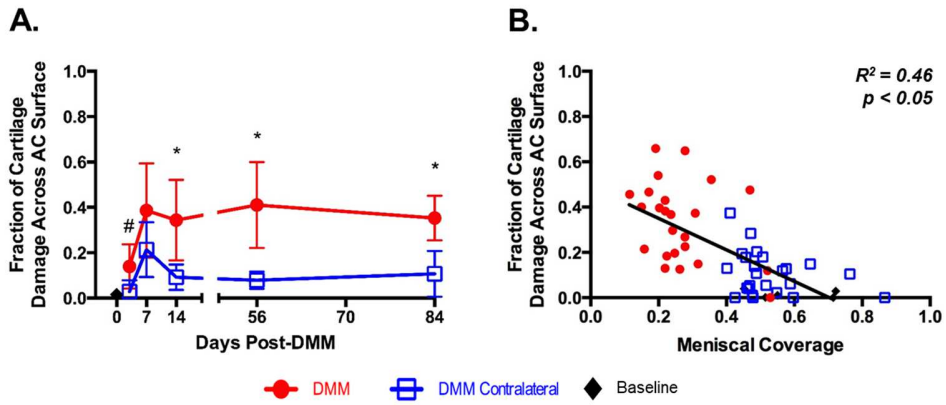

Figure 2.7: Progression of the degree of surface damage across the width of the MTP post-DMM and its relationship to meniscal coverage. In DMM joints, damage across the width of the MTP surface appeared rapidly following DMM, ultimately stabilizing at ~35-40% involvement of the MTP width over time (A.). Results are presented as mean ± STD (n = 5), where * = $p<0.05$ and # = $p<0.10$ (trend) for paired t-test between DMM and contralateral joints. The extent of damage across the width of the MTP was inversely related to the degree of meniscal coverage (B.). Pearson correlation coefficients (R2)- and p-value indicated.

2.4.5 Spatiotemporal Changes in MTP Chondrocyte Cellularity Post-DMM

Lastly, in analyzing IHC stained sections we observed alterations in the spatial distributions of chondrocytes (DAPI-positive cells) within the AC post-DMM (Figure 2.5). As early as 3-days, a significant loss of chondrocytes was seen in Q3 of the AC of DMM joints (~60% reduction compared to contralateral joints, p=0.005; Figure 2.8), which progressed until that quadrant was effectively devoid of chondrocytes by 84-days. In Q1, chondrocyte number remained unchanged, while Q2 and Q4 exhibited less substantial chondrocyte losses (Figure 2.8A). In contralateral joints, no significant changes in chondrocyte number were observed. Furthermore, we observed that the number of AC chondrocytes in quadrants 2, 3, and 4 were linearly correlated to the degree of meniscal coverage (Figure 2.8B). No significant correlation between meniscal coverage and chondrocyte number was observed in Q1. The number of chondrocyte in MTP CC remained unaltered (data not shown).

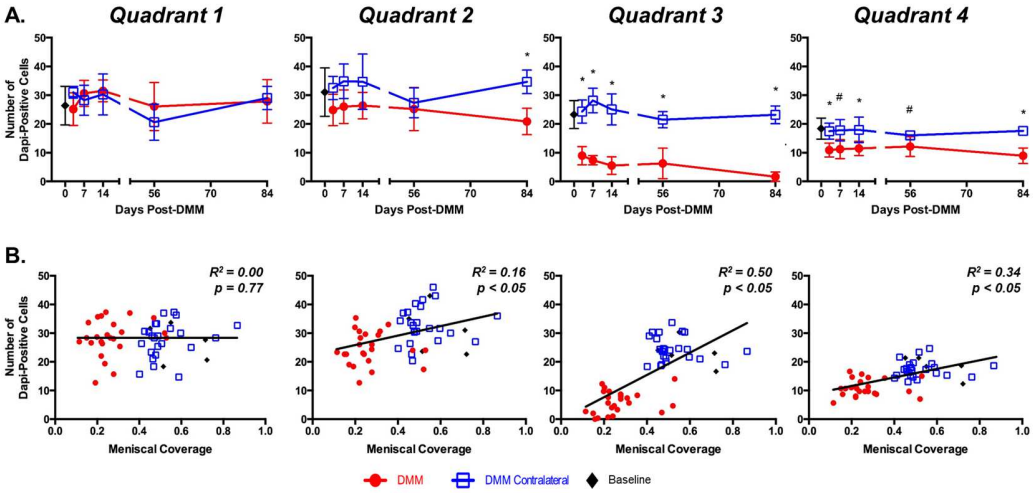

Figure 2.8: Spatiotemporal quantification of chondrocyte presence across the MTP of articular cartilage post-DMM and their relationship to meniscal coverage. The MTP demonstrated a significant loss of chondrocytes that localized to specific MTP quadrants (Q2-4) (A.) that also experienced alterations in meniscal coverage. In these quadrants, chondrocytes loss was linearly related to degree of meniscal coverage (B.). Results are presented as mean ± STD (n = 5/timepoint/group) where * = $p<0.05$ and # = $p<0.1$ (trend) for paired t-test between DMM and DMM contralateral. Pearson correlation coefficients (R2)- and p-value indicated.

2.5 Discussion

In the present study, we identified early, localized chondrocyte loss and cartilage damage in the murine DMM model of PTOA using semi-quantitative histological scoring and quantitative analysis. The findings of immediate cellular, compositional, and structural changes to cartilage highlighted the rapidity of the post-DMM injury response in male C57BL/6 mice and refined the timeline of damage initiation following meniscal destabilization. While our findings were consistent with previous semi-quantitative studies of DMM in the mouse[126,261,270–278,280,262,285,263–269], rat[287], and rabbit[286], and with early clinical changes seen in human cartilage following ACL tears[290], we also observed that semi-quantitative cartilage scoring schemes,

whether based upon width- or depth-wise classifications, did not provide a complete picture of the progression of cartilage degeneration. Instead, through implementation of detailed spatial analysis of cartilage damage progression, we uncovered additional aspects of the post-DMM cartilage injury response. Specifically, a strong relationship between meniscal extrusion/coverage and the location/progression of AC cellularity and structural changes.

Under physiological conditions, the meniscus stabilizes the joint and transmits load during articulation[291]. After meniscal detachment from the tibia, either from natural root tears or surgical procedures (like DMM), the meniscus' stabilizing function is lost as wedging effects[291] between the femoral condyle and meniscus causes its extrusion into the joint space. As a result of this alteration, several joint-level changes occur, including increased joint laxity and anterior motion[285], and increased tibial plateau contact stresses[267,286]. Clinically, increased meniscal extrusion has been related to increased cartilage damage[85–87]. Our findings in the murine DMM model are consistent with these observations. We observed that DMM-induced meniscal extrusion led to an immediate alteration in meniscal coverage of the MTP AC surface, and the co-localization of cartilage changes (e.g. loss of chondrocytes and proteoglycan content, surface damage, and overt erosions) to the uncovered regions. These findings confirmed the outward extrusion of the MM within the joint post-DMM, and identified the specific regions of the AC that are exposed to potentially altered contacts and mechanics due to changes in meniscal coverage.

Through the detailed spatiotemporal analysis of cartilage damage, the present study provides insight into the anterior-to-posterior and medial-to-lateral progression of cartilage damage post-DMM. While the present analysis, demonstrating a

progressive increase in anteriorly-localized MTP damage, was limited to coronal sections spanning the central-cartilage-contact-region of each joint, and thus may exclude damage more anteriorly or posteriorly, our results were consistent with similar observations made by Glasson et al., in the initial murine DMM study[99]. Analysis of a small set of sagittally-sectioned joints also confirmed our findings across the full MTP, while also suggesting an increase damage in the MFC anteriorly (Appendix A Figure. A.5). This was not evident in the semi-quantitative analysis, potentially due to increased variability within femoral cartilage scoring[284]. Additionally, the sagittal sections from joints 3-days post-DMM demonstrated, similar to the Glasson study[99], no signs of the DMM procedure inducing inadvertent cartilage damage. Interpreting these results in light of established joint-level biomechanical changes[267,285,286] supports the hypothesis that DMM-mediated meniscal extrusion causes altered anterior-to-posterior loading of the knee joint and subsequent anteriorly-to-centrally localized cartilage damage.

A distinct and informative pattern of medial-to-lateral damage progression in the medial joint post-DMM was also observed. Damage across the width of the MTP surface accumulated rapidly and then stabilized, resulting in the presence of increased type II collagen staining and extensive fibrillation and clefting across ~20-40% of the MTP surface by 7-days, with this damage being localized to MTP regions experiencing alterations in meniscal coverage due to meniscal extrusion. Interestingly, as time progressed (84+-days) cartilage erosions and a decrease in AC thickness also co-localized to the same MTP regions. Similar findings were observed for the MFC (data not shown). The highly focal nature of this damage highlights the important role of meniscal extrusion/coverage in establishing the location of damage initiation and

progression in the DMM model. While this study was not designed to establish the cause of this focal damage progression, several mechanisms could be involved including: i) alterations in cartilage-on-cartilage and cartilage-on-meniscus contact mechanics[285,286] following extrusion, ii) differences in the mechanical properties of cartilage tissues previously covered by the meniscus [292–294], and/or iii) changes in the accessibility of inflammatory[295] and pro-catabolic mediators to the local cartilage regions post-injury. Determining if these, or other, mechanisms are involved in the observed phenomena requires further investigation. The apparent stabilization of AC surface fibrillation and clefting between 7- and 56-days post-DMM was interesting and consistent with previous studies[261]. This may reflect a natural ability of the cartilage extracellular matrix to withstand alterations in the tissue's mechanical environment and even loss of resident chondrocytes, temporarily, before developing into larger erosions at later disease stages.

A potentially more significant finding with regards to understanding PTOA initiation was the identification of a striking, immediate, and highly focal loss of chondrocytes within the AC of injured joints post-DMM. As early as 3-days, a drastic decrease in chondrocyte number was observed within the regions of the MTP that experienced changes in meniscal coverage (Q3). Over time, chondrocyte number continued to decrease in DMM joints compared to their contralateral joints until there was a complete loss of cells in Q3, and a moderate loss of chondrocytes in adjacent quadrants. Given the critical role that chondrocytes play in the maintenance, repair, and regeneration of AC[63], this rapid and focal loss of chondrocytes may constitute the precipitating biological event leading to the initiation and progression of PTOA. This idea is supported by two observations: i) that cartilage erosions predominately localize

to areas of earlier chondrocyte loss within and surrounding the 'uncovered' quadrant (Q3), and ii) that the innermost MTP quadrant (Q1) appeared more resistant to both chondrocyte loss and cartilage damage. Together, this data suggest that rapid chondrocyte loss post-DMM co-localized to AC quadrants experiencing an immediate loss of meniscal coverage (Q3). Subsequently, progression of cartilage damage (fibrillations, clefts, and erosions) may also be driven by this focal loss of meniscal coverage and chondrocytes.

While the rapid and localized loss of chondrocytes within the AC of DMM joints in the present study was remarkable, the biological mechanisms underlying this pattern of cell loss remains unknown. Numerous studies implicate chondrocyte necrosis and apoptosis in the initiation and progression of cartilage degeneration following severe, acute cartilage injury in vitro[295,296], and in murine DMM models of PTOA[261,263,280,283,289]. In a non-invasive murine cartilage injury study, co-localization of chondrocyte apoptosis to specific regions of injurious load application was identified 5-days post-injury[288] and a loss of DAPI-positive cells was observed at 14-days, consistent with the present study. The early and rapid loss of chondrocytes in our study also indicate that significant changes in chondrocyte health occur very quickly, prior to 3-days, post-DMM. In this regard, a recent study by Burleigh et al.[268] identified changes in gene expressions within murine cartilage as early as 6 hours post-DMM, supporting rapid changes in chondrocyte health/metabolism. Further studies are required to establish: i) whether the observed loss of chondrocytes in DMM joints is attributable to apoptotic or necrotic events; ii) when, relative to the timing of injury, such critical biological changes are initiated; and iii) the molecular and cellular mechanisms that precipitate these changes.

Of important note is that the present study focused on the role of DMM-induced meniscal extrusion on the spatiotemporal of cartilage changes in male C57BL/6 mice due to the pervasive use of the DMM model[126,261,270–279,262,280,281,285,297,298,263–269] and the increased susceptibility of these mice to develop cartilage damage in this model[279]. Whether similar outcomes would be observable in female C57BL/6 mice[279] or in other mouse strains[99], species[286,287], destabilizing injury models[288,299,300], or clinical injuries requires further investigation. However, given the similarities in the progression of cartilage damage among the murine DMM and other injury models, we suspect that the observed relationships may be a general feature of PTOA initiation and progression. Although this response pertains to the murine DMM model, we believe these data support the expanded study of immediate restoration of meniscal function for providing chondroprotective benefit post-injury, both pre-clinically and clinically.

It is important to acknowledge a few limitations of this study. Firstly, histological-based approaches may introduce artifacts in the analysis of meniscal extrusion due to variability in knee joint positioning during fixation (we attempted to place joints in same naturally flexed position), embedding, and sectioning (some section orientation variability was observed). However, given the small deviations in meniscal positioning that we observed, as well as the robust correlations between damage degree, location, and meniscal position, we are confident that our data reflect a strong relationship between meniscal extrusion/coverage and AC changes. Secondly, our analysis does not provide insight into the spatial evolution of proteoglycan loss, which may have significant impact on the early cartilage biomechanical functionality. While we qualitatively noted early proteoglycan loss in Q3 of the MTP, the

relationship between proteoglycan depletion and chondrocyte loss remains unknown. Lastly, while this study incorporated independent mechanisms for width- and depth-wise semi-quantitative scoring of cartilage erosions, we found depth-wise scoring harder to evaluate due to the variability in the position of the CC/subchondral bone interface across the MTP, as well as the fact that erosion of the AC made determination of relative depth-wise damage increasingly difficult. However, given the general similarities in width-wise and depth-wise damage progression, we suggest, for the sake of simplicity and unambiguity, using width-wise scoring for evaluating mouse cartilage damage.

Finally, the present findings have several implications regarding the study of PTOA prevention and treatment in the DMM model and translational studies. The focal population of cells identified represent an ideal target to investigate the chondroprotective effects of various pre-clinical therapies, including joint unloading/rehabilitation[268] and pharmacological interventions[269,271,274,277,278]. However, it appears that such interventions may need to be initiated immediately/shortly post-injury to have the greatest anti-osteoarthritic potential, an observation that may explain the equivocal findings of chondroprotective drugs within clinical trials[301]. Alternatively, the presence of an apparent plateau in the progression of cartilage damage, between ~7-56-days post-DMM, supports the possibility of the DMM-model as a platform to test alternative treatment targets based on cartilage regeneration[110].

In conclusion, the approaches described here present a benchmark for the detailed study of cartilage damage progression within murine models of surgery-/injury-induced PTOA while providing detailed analyses of the spatiotemporal progression and relationships between cartilage damage, changes in chondrocyte

cellularity, and meniscal extrusion within the murine DMM model. This study also provides a comprehensive baseline for ongoing assessment of the cellular and molecular pathoetiology of PTOA, as well as the study of its prevention and treatment.

2.6 Acknowledgments

The authors would like to thank Mr. Frank Warren and Dr. Gwen Talham, DVM for oversight of animal care, Brianna Gietter, Olivia Laxton, and Fiona Flowerhill for assistance in preparing histological samples, and Brian Graham for assisting with MATLAB programming. This study was supported by a grant from the US DOD CDMRP PRMRP W81XWH-13-1-0147.

Chapter 3

REPEATED INTRA-ARTICULAR INJECTION OF ZOLEDRONIC ACID SUPPRESSES CARTILAGE EROSIONS IN A MURINE MODEL OF POST-TRAUMATIC OSTEOARTHRITIS

(MA David, MK Smith, S Shah, B Hulbert, A Merritt, RN Pilachowski, RC Locke, XL Lu, C Price, *In Preparation 2019a*)

3.1 Abstract

Clinical therapies that hinder and/or prevent the development of cartilage degeneration following joint-injury are required to reduce the burdens of injury-induced post-traumatic osteoarthritis (PTOA). Recently, researchers have looked to the anti-resorptive bisphosphonates, including zoledronic acid (ZA), as potential PTOA-modifying therapeutics. Promising preclinical studies have shown that high-dose, systemic ZA administration could suppress cartilage damage in animal models of PTOA. However, translation of this strategy to the clinic faces significant hurdles due to risks of severe skeletal side-effects associated with systemic suppression of bone remodeling. Fortunately, studies indicate that ZA can directly modulate chondrocytes and cartilage health *in vitro* and *ex vivo*, suggesting that locally administered ZA (i.e. intra-articularly injected) could represent an effective and more clinically-acceptable PTOA-modifying strategy. The purpose of this study was to investigate the ability of four, repeated-weekly (4.q7d) intra-articular injections of ZA (i.a.ZA) starting at 0-days post-injury vs. single i.a.ZA (either 0 or 7-days post-injury) to prophylactically prevent short- and long-term cartilage damage in the murine destabilization of the medial meniscus (DMM) model of PTOA. Using histology and

immunohistochemistry, this study demonstrated that i.a.ZA administration was unable to mitigate the development of superficial cartilage damage (fibrillations and clefts in cartilage) in the immediate aftermath of DMM-injury. However, repeated i.a.ZA, but not single injections, could suppress the development of long-term cartilage erosions post-DMM. Furthermore, repeated i.a.ZA's ability to suppress cartilage erosions appeared to be linked to ZA's ability to modulate proteoglycan metabolism, and chondrocyte proliferation and death in a spatiotemporally-dependent manner; specifically, in regions adjacent to those experiencing cell loss and matrix damage immediately following DMM-injury. Collectively, this study supports the potential of local, i.a.ZA as a prophylactic PTOA-modifying therapeutic and highlights the need for directed studies into i.a.ZA's mode of action in injured cartilage.

3.2 Introduction

No clinical therapies exist to ameliorate the initiation and development of post-traumatic osteoarthritis (PTOA) that often accompanies traumatic joint injury, e.g. ligamentous tears and intra-articular fractures[79,104]. Unfortunately, the prognosis for patients suffering from PTOA is poor: these individuals have an approximately 50% chance of experiencing joint degeneration, immobility, and pain within 10-15 years after injury[17,29,303–305,30–33,54,55,104,302]. In order to alleviate pain and improve the mobility of these diseased joints, clinicians may employ palliative, reparative (e.g. microfracture, autologous chondrocyte implantation, or osteochondral grafting)[306] or replacement (joint arthroplasty)[51,74,75,104,108–110] approaches. However, these strategies only address symptoms of PTOA, instead of the aberrant biology processes underpinning disease initiation and progression. Therefore, an unmet need exists to identify and implement disease-modifying therapies that can prevent (or delay) PTOA

initiation and progression following injury; thereby lessening the socioeconomic burden of PTOA[17,303].

Recently, bisphosphonates (BPs), a class of FDA-approved drugs, have shown promise as disease-modifying therapeutics for PTOA. Clinically, BPs have been used to treat bone disease and cancer-related skeletal fragility[245,307] because of their anti-resorptive properties. Since their first introduction in 1969[128], the potency of BPs against osteoclasts has steadily increased as the molecular structure of these compounds has evolved; with the most recent generation of nitrogen-containing BPs (nBPs) exhibiting the highest potencies[128,245,307,308]. Given the anti-resorptive properties of nBPs and the identification of associations between cartilage degeneration, PTOA, and aberrant subchondral bone remodeling[120,126,233,234], nBPs were seen as potential PTOA disease-modifying drugs. To this end, numerous preclinical studies have demonstrated the ability of nBPs, including zoledronic acid (ZA; the most recent and most potent nBP to receive FDA-approval), to prevent cartilage degeneration, bone loss, and pain in arthritic diseases, such as rheumatoid arthritis[209–216], osteoarthritis[217–219], and PTOA[238–241,309]. Unfortunately, these studies utilized systemic and repeated high-dose administration of ZA; where ZA doses (equivalent of ~1-20 mg/kg/year) far exceeded those utilized for osteoporosis (~0.04-0.05 mg/kg/yr[245,307]) and cancer (~0.5-0.9mg/kg/yr[189]) therapy. Furthermore, recent evidence suggests that use of high-dose nBP strategies for PTOA prevention would be accompanied by substantial risk for serious skeletal side effects, including osteonecrosis of the jaw and atypical bone fractures[134,242–245], as well as cardiovascular and renal complications[245]. Therefore, systemic, high-dose administration of ZA for the treatment of PTOA may face substantial, if not insurmountable, hurdles to clinical

implementation. Alternatively, if local delivery of ZA directly into the injured joint, via intra-articular (i.a.) injection, could be leveraged for PTOA prevention, it would potentially overcome the hurdles associated with systemic delivery by reducing overall nBP burden and minimizing the risk of adverse side effects associated high-dose ZA administration.

Support for the potential of locally-delivered, intra-articular injection of ZA as a PTOA therapeutic comes from evidence provided by several *in vitro* and *in situ* studies of ZAs ability to directly modulate chondrocyte and cartilage health. *In vitro* studies have demonstrated that nBPs can directly regulate chondrocyte proliferation, viability, and death[187,254]. Furthermore, work from our collaborators has suggested that nBPs can also improve chondrocyte health and cartilage biomechanical outcomes *in situ* under experimental conditions that mimic aspects of PTOA[255–258]. Thus, we hypothesize that intra-articular injection of nBPs into the injured knee can be leveraged to prophylactically protect chondrocytes and cartilage against injury-induced degeneration. However, prior to the present work, the effect of intra-articular injection of ZA on cartilage-injury outcomes had been limited to a single study demonstrating the ability of repeated intra-articular injection of ZA (equivalent of ~2.0 mg/kg/yr) to reduce chondrocyte apoptosis and prevent cartilage degeneration in the rat anterior cruciate ligament transection (ACLT) model of PTOA[260]. Despite the promise of these preclinical findings, the following questions remained: i) could intra-articular injection of ZA (i.a.ZA) modulate cartilage damage following injury in a different species and injury model); ii) is repeated versus single i.a.ZA required for disease-modifying efficacy; and iii) what are i.a.ZA's mode(s) of action in mitigating PTOA.

The objective of this study was to establish if single versus repeated i.a.ZA could prevent cartilage degeneration post-injury in the murine destabilization of the medial meniscus (DMM) model of PTOA. We evaluated tissue- and cellular-level changes to articular cartilage following DMM at early- (7-days) to late-stage (84-days) disease with either a single immediate (0-days), single delayed (7-days), or four repeated weekly (4q7) i.a.ZA. We observed that only repeated, not single immediate or delayed, i.a.ZA could suppress the development of long-term cartilage erosions (84 days) post-DMM. Furthermore, we identified that the suppression of cartilage erosions was associated with the ability of i.a.ZA to modulate proteoglycan metabolism and chondrocyte presence, through influences on death and proliferation post-DMM. These results suggest that i.a.ZA, when delivered immediately and repeatedly post-DMM, can provide a degree of protection against DMM-mediated cartilage degeneration in the mouse knee. Ultimately, this study can help to guide future studies of ZA's mode and mechanism of action in chondrocytes and cartilage, and pre-clinical studies aiming at translating i.a.ZA for modify cartilage degeneration and PTOA following joint injury.

3.3 Methods

3.3.1 Animals and Surgeries

Adult, male C57BL/6 mice (n = 110; Jackson Labs) underwent DMM surgery[99,310] in their right hind limbs at 12-wks of age; contralateral limbs served as internal, uninjured controls. Mice receiving intra-articular (i.a.) injection of ZA (i.a.ZA; Sigma-Aldrich) were randomly assigned to three different treatment strategies post-DMM: i) repeated i.a.ZA injections at 0-, 7-, 14-, and 21-days (repeated-i.a.ZA);

ii) single i.a.ZA at 0 day (single-i.a.ZA_{0d}); and, iii) single i.a.ZA at 7 days (single-i.a.ZA_{7d}). For all i.a. injections: i) an incision in the skin of the frontal medial aspect of the joint was made; ii) 6µL of sterile saline containing ZA was injected into the joint capsule (via an anteromedial approach) using a 36-gauge needle (NanoFil; World Precision Instruments); and iii) the skin incision was closed with tissue adhesive (GLUture, Abbott Labs). For 0-day injections, the joint capsule was sutured immediately post-DMM, ZA was then injected intra-articularly, and the skin incision was closed. ZA was administered intra-articularly at a dose of ~650ng/kg per injection (based upon preliminary work by our collaborators[255–258]). All mice were housed in standard cages (≤5 mice/cage) and maintained on a 12-hour light–dark cycle in a climate-controlled vivarium with access to food (Prolab RMH 3000) and water *ad libitum*. The University of Delaware's Institutional Animal Care and Use Committee approved all animal handling and procedures. For all surgical procedures, mice were anesthetized using inhaled isoflurane, antibiotics and analgesics were administered prophylactically, and mice were allowed unrestricted cage access following surgery. No adverse effects or differences in weight gain were observed among mice during the study. Following approved euthanasia protocols, intact tibiofemoral joints were collected at 7-, 14-, 56-, or 84-days post-DMM.

3.3.2 Histological Processing and Staining

Tibiofemoral joints (n=5-10 mice/group/time point) were harvested, processed for paraffin-embedded histology, and cut serially into 5-µm thick coronal sections (collected 2 sections/slide) as previously described[310]. Starting from the front of the joint (anterior), every tenth slide (~100-µm apart) was selected and stained with Safranin-O, fast green, and Wiegerts hematoxylin, hereon referred to as Saf-O. From

these slides, a subset of five stained-slides (spanning ~500-μm) centered about the medial compartment tibial plateau and femoral condyle mid-contact regions were selected and labeled levels 1-5, anteriorly to posteriorly[310]. Three immediately adjacent slides were selected from the central-contact region (levels 2-4) for H&E staining (Mayer's hematoxylin and 0.25% eosin). After staining, mounted slides were imaged at 5x magnification on a standard upright microscope (Axio.Imager.A2, Carl Zeiss) using a color digital camera (AxioCam MRc5, Carl Zeiss) and consistent illumination and exposure settings.

3.3.3 Semi-Quantitative Scoring and Quantitative Analysis of Cartilage Damage

Semi-quantitative scoring of cartilage damage, on a 0-6 scale (Table 3.1)[310], was performed on Saf-O stained slides by three individuals (MAD, MKS, and RCP) blinded to specimen identity. Damage values, from joint levels 1-5, were aggregated separately for the medial tibial plateau and the medial femoral condyle. Of note, semi-quantitative cartilage damage scores for the untreated DMM and their contralateral controls (uninjured) have been previously published[310], and are reproduced here (with permission) as the comparative controls for the i.a.ZA treated DMM-joints. To provide quantitative measures of cartilage damage, the width-wise extent of cartilage damage and overt cartilage erosions (i.e. fraction of damaged and eroded surface, respectively) were quantified in Saf-O stained slides from joint levels 2-4, while articular and calcified cartilage were traced separately in H&E stained slides and cartilage areas and thicknesses (using a Euclidian distance transform) were extracted, on a quadrant-by-quadrant basis (see below), as described previously[310].

Table 3.1: Semi-quantitative histological scoring used to assess the width-wise extent of cartilage damage.

Score	Width-Based Scoring Evaluation
0	Normal
0.5	Loss of Safranin-O but no structural damage
1	Fibrillations and/or roughened superficial surface
2	Damage to the layer immediately below the superficial layer and some loss of surface lamina
3	Erosion <25% of AC width
4	Erosion 25-50% of AC width
5	Erosion 50-75% of AC width
6	Erosion >75% of AC width

3.3.4 Quantification of Articular Cartilage Proteoglycan Content and Proteoglycan-Rich Chondrons

To evaluate changes to articular cartilage proteoglycan content, the proteoglycan-rich (Saf-O positive; Saf-O^+) tissue area, the proteoglycan composition (Saf-O^+ tissue staining intensity), and the number of Saf-O^+ chondrons were quantified on a quadrant-by-quadrant basis across the medial tibial plateau using a custom image analysis algorithm (MATLAB R2015a, The MathWorks, Natick, MA). Briefly, the articular cartilage of the medial tibial plateau was manually traced in Saf-O stained slides from joint levels 2-4. These traces were segmented into four equal-width quadrants (quadrants 1-4), from the innermost region of the tibial plateau (Q1; nearest the intercondylar eminence) to the region nearest the medial joint margin (Q4). Within these quadrants, we assessed the amount (area) of proteoglycan-rich tissue (Saf-O^+), proteoglycan composition (as defined by Saf-O^+ staining intensity relative to the

growth plate staining intensity; see Supplementary Methods in Appendix B) and the number of proteoglycan-rich chondrons (chondrons exhibiting halo-like, pericellular Saf-O^+ staining that is more intense than the local interterritorial matrix).

3.3.5 Histological and Immunohistochemical Analysis of Chondrocyte Presence, Death, and Proliferation

To provide insights into chondrocyte dysfunction, we investigated chondrocyte presence, proliferation, and death using histology and immunohistochemistry. Chondrocyte presence in the articular and calcified cartilage was quantified on a quadrant-by-quadrant basis by counting the number of hematoxylin-positive chondrocytes in H&E stained slides from joint levels 2-4. Chondrocyte health was assessed qualitatively through evaluation of nuclear staining and morphology; where chondrocytes were defined as having normal, pyknotic (condensed), karyolitic (faded), or karyorrhectic (fragmented) nuclei, eosinophilic nuclei, or as empty chondrons. Chondrocyte death/apoptosis were qualitatively assessed in slides from joint level 2 immunohistochemically stained with the Click-iT® Plus TUNEL Assay and DAPI (Molecular Probes). Chondrocyte proliferation was assessed by staining slides from joint level 2 with an anti-Ki-67 antibody (SC-7846; Santa Cruz Biotechnology); Ki-67 is a marker for cells that are in the G1/S/G2- or mitotic-phases of the cell cycle, while it is absent in quiescent cells (G0 phase)[311]. Specifics regarding immunohistochemical staining procedures can be found in the Supplementary Material (Appendix B). Fluorescent images were captured at 20x magnification on an epifluorescent microscope (Axio.Observer.Z1, Carl Zeiss) using a digital camera (AxioCam MrC, Carl Zeiss) and consistent illumination and exposure settings.

3.3.6 Statistical Analysis

Statistical analyses were performed using GraphPad Prism 6.0 for Mac (GraphPad Software, La Jolla, CA). One-way ANOVA's with Dunnett post-hoc comparisons were conducted at each time point to identify differences between individual treatment groups (uninjured, single-i.a.ZA_{0d}, single-i.a.ZA_{7d}, repeated-i.a.ZA) and the untreated DMM joints. The threshold for statistically significant relationships was defined as a $p < 0.05$. All data are presented as mean ± standard deviation.

3.4 Results

3.4.1 Repeated-i.a.ZA Administration Suppressed Cartilage Erosions Post-DMM

Histological assessment of cartilage damage demonstrated that surface fibrillations and clefting (semi-quantitative scores of 1 and 2, respectively) accumulated rapidly following DMM-injury, being present as early as 7-days post-DMM (Figure 3.1A and B). Of special note, this damage appeared largely confined to quadrants 2 and 3 (Q2 & Q3) of the medial tibial plateau and medial femoral condyle, tissue regions that experienced the most dramatic changes in cartilage-on-meniscus-on-cartilage contact post-DMM[310]. As time progressed, this surface damage evolved into overt cartilage erosions (average damage score = 2.6), which again localized predominately to Q3. However, in DMM-joints treated with four, repeated weekly (4.q7d) intra-articular injections of ZA (repeated-i.a.ZA), this superficial cartilage damage did not progress into overt cartilage erosions long-term (average damage score of 1.6 at 84-days; $p = 0.02$). Conversely, neither of the single intra-articular injection strategies, whether administered immediately (single-i.a.ZA_{0d}) or 7-days (single-

i.a.ZA_{7d}) following DMM-injury, we able to suppress the development of cartilage erosions (Figure 3.1A and 3.1B). In fact, single-i.a.ZA_{0d} treated DMM-joints experienced worsening of cartilage erosions (average score of 3.5 at 84-days; $p = .02$); damage in the single-i.a.ZA_{7d} treated DMM-joints was no different than untreated DMM-joints (average score of 2.3 at 84-days; $p = 0.7$). Quantitative assessment of damage accumulation across the width of the cartilage supported these semi-quantitative findings (Appendix B Figure B.1). Since only repeated-i.a.ZA administration demonstrated the ability to suppress the development of cartilage erosions, we have limited the presentation of our results hereon to those from the repeated-i.a.ZA joints; data for the single-i.a.ZA treatment groups are presented in the Supplementary Materials (Appendix B).

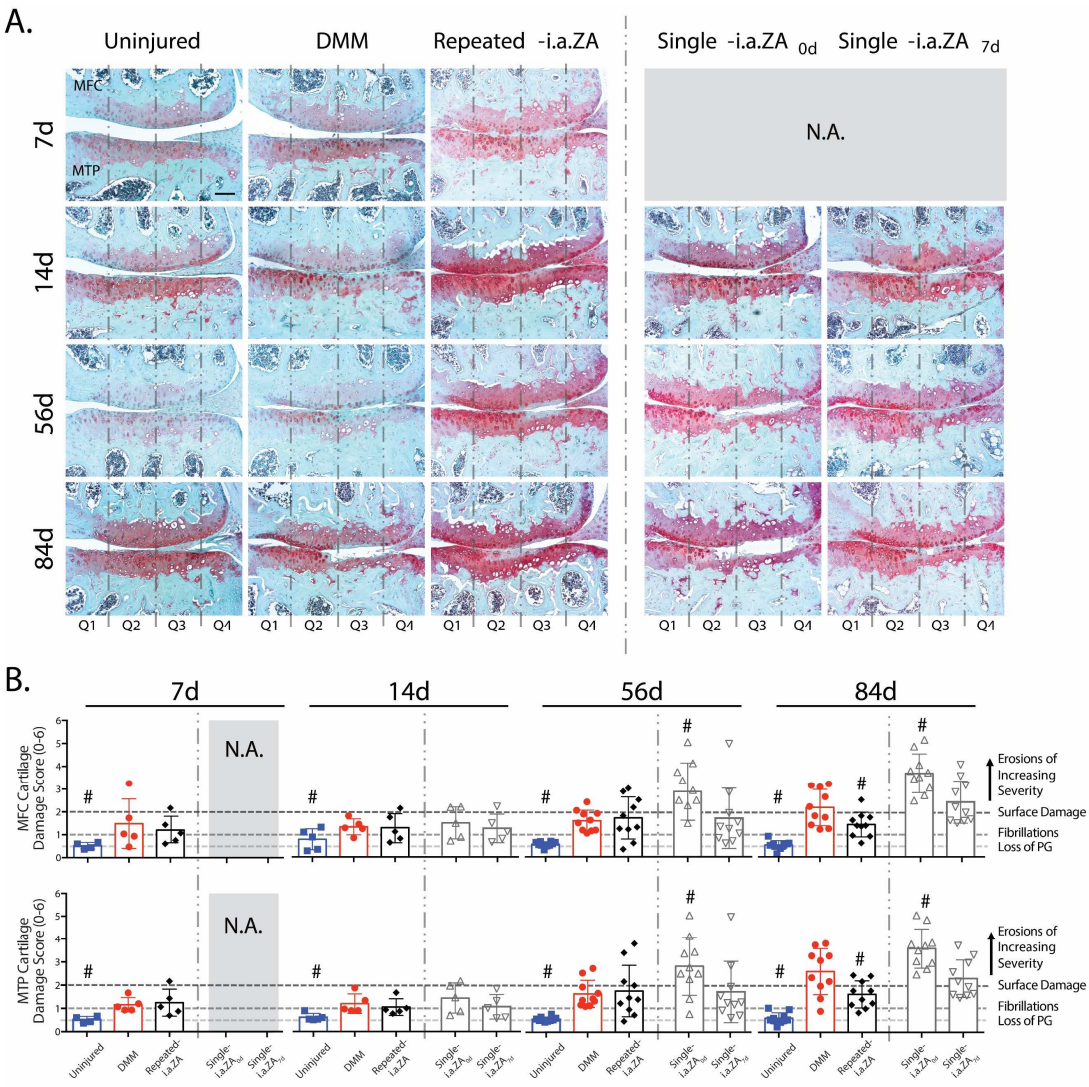
A.
Uninjured
DMM
Repeated -i.a.ZA
Single -i.a.ZA 0d
Single -i.a.ZA 7d
MFC
MTP
7d
14d
56d
84d
N.A.
Q1 Q2 Q3 Q4
B.
7d
14d
56d
84d
MFC Cartilage Damage Score (0-6)
MTP Cartilage Damage Score (0-6)
N.A.
Erosions of Increasing Severity
Surface Damage
Fibrillations
Loss of PG
Uninjured
DMM
Repeated-i.a.ZA
Single-i.a.ZA0d
Single-i.a.ZA7d

Figure 3.1: Repeated Intra-Articular Administration of ZA to DMM-injured Joints Suppressed the Development of Cartilage Erosions. (A.) Safranin-O stained sections highlight the DMM-induced meniscus extrusion that drives the long-term development (by 84d) of cartilage erosions in the medial compartment of tibiofemoral joints (see quadrant 3 [Q3] in the DMM joints). Repeated-i.a.ZA administration, but not single injections (single-i.a.ZA_{0d} and single-i.a.ZA_{7d}), appeared to suppress the development of these cartilage erosions. These representative images were acquired from the anterior region (level 2) of the joint at 10x magnification (scale bar = 100µm); images from uninjured joints are reoriented for anatomical comparison. (B.) Semi-quantitative scoring of cartilage damage indicated a significant reduction in cartilage damage scores in joints treated with repeated-i.a.ZA injections at 84d post-DMM (repeated-i.a.ZA scores = 1.6 vs 2.6 for DMM-alone). Unexpectedly, single-i.a.ZA_{0d} injection caused the appearance of worse cartilage erosions, while single-i.a.ZA_{7d} injection provided no benefit compared to untreated DMM-joints. None of the i.a.ZA treatments could mitigate early (by 7d) DMM-mediated superficial tissue damage, i.e. fibrillations and clefts (see Q2 and Q3 at 7 & 14d). Results are presented as mean ± STD (n=5-10/timepoint/group), # indicates $p < 0.05$ between the denoted group and the untreated DMM group at the respective timepoint.

3.4.2 Repeated-i.a.ZA Administration Caused Articular Cartilage Thinning Post-DMM

To quantitatively assess changes to cartilage structural following injury and i.a.ZA-treatment, we evaluated articular and calcified cartilage area and thickness in H&E stained slides (Figure 3.2A). In untreated DMM-joints, loss or thinning of the articular cartilage only occurred in Q3 at the latest disease stages (area change shown in Figure 3.2A; thickness data not shown); no change in cartilage area or thickness was observed at earlier timepoints or in other quadrants compared to uninjured controls. Intriguingly, in DMM-joints treated with repeated-i.a.ZA, articular cartilage thinning was observed in Q3, as well as in Q1 and Q2; however, this thinning could not be explained by erosional loss, per our semi-quantitative scoring, but rather by an overall decrease in articular cartilage height (Figure 3.2A). In DMM-joints receiving

single-i.a.ZA therapies, the loss of articular cartilage thickness was similar to that of the repeated-i.a.ZA joints (Appendix B Figure B.2A); however, this thinning could be explainable by both reduction in cartilage height and erosional loss. No appreciable changes in the area or thickness of the underlying calcified cartilage were observed among any group (data not shown).

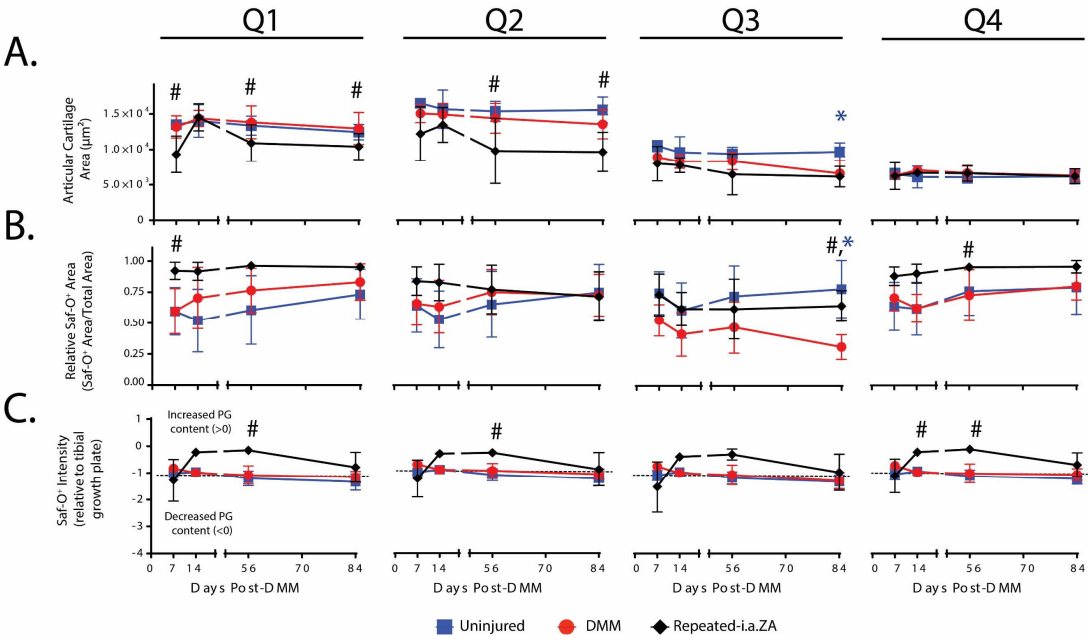

Figure 3.2: Repeated-i.a.ZA Administration Following DMM Resulted in Location-Specific Modulation of Articular Cartilage Area and Proteoglycan Content**.** (A.) DMM-injury drove a long-term reduction in the area of articular cartilage tissue present in Q3 of the medial tibial plateau. Repeated-i.a.ZA treatment caused similar reduction in tissue area in Q3, however, additional areal decrease was also observed in Q1 & Q2. Unlike in the untreated DMM-joints, cartilage thinning in repeated-i.a.ZA joints were attributable to loss of articular cartilage height, not the development of erosions. (B.) Quantitative assessment of the relative area of proteoglycan-rich, Safranin-O positive (Saf-O^+) articular cartilage demonstrates decrease in proteoglycan (PG)-rich matrix in Q3 following DMM-injury. Repeated-i.a.ZA treatment could prevent this loss of PG-rich in Q3, however, it also markedly enhanced the fraction of PG-rich cartilage found in Q1 and Q4. (C.) Furthermore, within these PG-containing areas, PG composition (defined as Saf-O^+ cartilage intensity relative to the tibial growth plate Saf-O^+ intensity) did not change within or among the DMM and control joints; on the contrary, repeated-i.a.ZA led to cartilage that generally exhibited enhanced PG-rich staining intensity, and thus PG composition. Results are presented as mean ± STD (n=5-10/timepoint/group); where # indicates $p< 0.05$ for the difference between repeated-i.a.ZA and untreated DMM-joints at that timepoint, * indicates $p< 0.05$ between the untreated DMM and uninjured joints at that timepoint.

3.4.3 Repeated-i.a.ZA Administration Enhanced Articular Cartilage Proteoglycan Composition Post-DMM

In untreated DMM-joints, only articular cartilage in Q3 experienced significant changes in the presence of proteoglycan-rich tissue (i.e. a rapid and consistent loss Saf-O^+ cartilage area fraction; Figure 3.2B). Furthermore, the tissue-level proteoglycan composition of the tibial articular cartilage in both the uninjured and untreated DMM-joint remained relatively unchanged over time, as assessed by Saf-O^+ (proteoglycan) staining intensity of the articular cartilage relative change to the growth plate (Figure 3.2C). Conversely, in DMM-joints administered repeated-i.a.ZA, the loss of proteoglycan-rich tissue seen in Q3 was largely mitigated (Figure 3.2B) and the proteoglycan composition of the articular cartilage was markedly increased, especially in the peripheral quadrants (i.e. Q1 and Q4, and to a lesser extent Q2; Figure 3.2C). In the single-i.a.ZA treated DMM-joints, no long-term changes in the relative amount of proteoglycan-rich tissue compared to untreated DMM-joints were observed (Appendix B Figure B.2B); however, the proteoglycan composition (relative Saf-O^+ staining intensity) in these joints was consistently reduced compared to untreated DMM-joints (Appendix B Figure B.2C). Together, these data indicate that while cartilage thinning occurred in the DMM-joints treated following repeated-i.a.ZA, the tissue that was present possessed a relatively greater fraction of proteoglycan-rich tissue and increased proteoglycan composition.

3.4.4 Repeated-i.a.ZA Administration Altered Chondrocyte Presence, Proteoglycan Production, Death, and Proliferation Post-DMM

To evaluate changes in chondrocyte health and dysfunction, we first assessed the presence of articular cartilage chondrocytes across the medial tibial plateau articular using H&E staining. In untreated DMM-joints, we observed a clear loss of

chondrocytes (decreased hematoxylin-positive nuclei) in Q3 of the articular cartilage when compared to uninjured joints (Figure 3.3A). As seen in Figure 3.3A, this loss of chondrocytes was also accompanied by increases in empty chondrons (no nuclei), eosinophilic nucleoli presence, and the following abnormal nuclear staining: pyknotic (condensed), karyolitic (faded), and karyorrhectic (fragmented) chondrocyte nuclei on the margins and periphery of Q3. To provided quantitative measures for chondrocyte loss, we counted the number of chondrocytes with hematoxylin-positive nuclei across the articular cartilage of the medial tibial plateau on a quadrant by quadrant basis (Figure 3.3B). These counts confirmed a drastic reduction in chondrocyte number in Q3 as early as 7 days post-DMM, which then spread to Q2 and Q4; chondrocyte presence in Q1 was unaffected. In DMM-joints treated with repeated-i.a.ZA, we observed similar quadrant-specific patterns of chondrocyte loss and the appearance of empty lacunae and abnormally stained chondrocyte nuclei as in the untreated DMM-joints (Figure 3.3A and 3.3B). However, from a quantitative perspective, repeated-i.a.ZA treatment appeared to drive an accelerated loss of chondrocyte number in Q2 (seen by 56-day data in Figure 3.3B). In DMM-joints receiving single-i.a.ZA administrations, chondrocyte presence in the articular cartilage followed a similar pattern as repeated-i.a.ZA treated and untreated DMM-injured joints (Appendix B Figure B.3A); however, the loss of chondrocytes in Q3 again occurred more rapidly and was accompanied by reductions in Q1 as well. Chondrocyte presence throughout the calcified cartilage of the medial tibial plateau was similar among all groups (data not shown). Together, this suggests that ZA can modulate chondrocyte loss in the medial tibial plateau articular cartilage in a location-dependent manner.

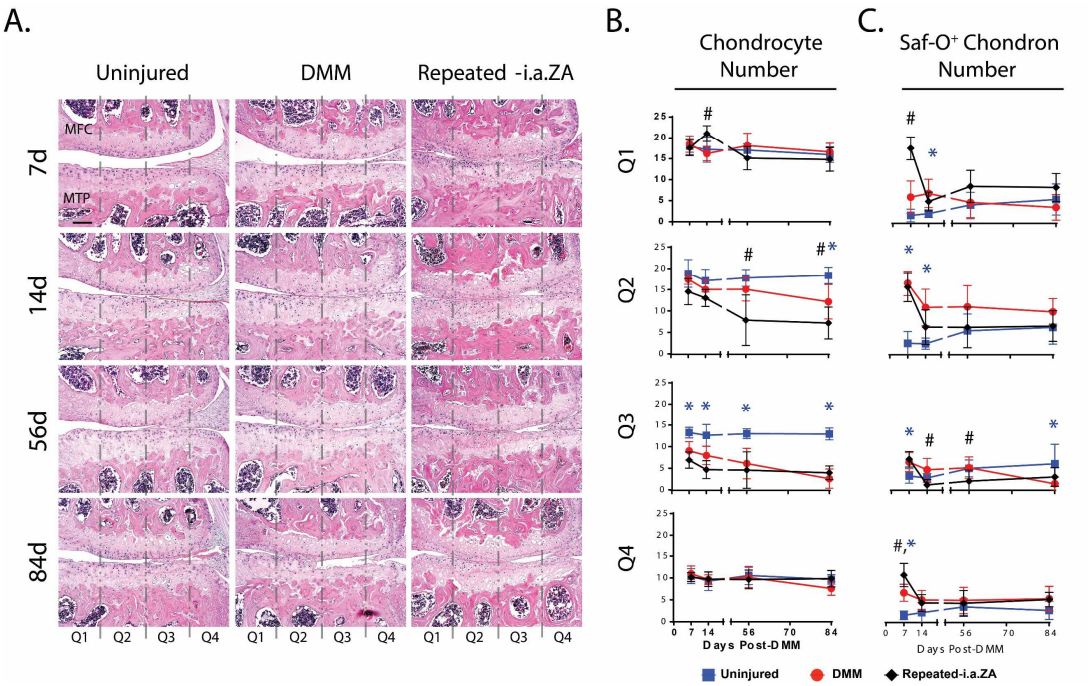
A.
Uninjured
DMM
Repeated -i.a.ZA
MFC
MTP
7d
14d
56d
84d
Q1
Q2
Q3
Q4
B.
Chondrocyte Number
C.
Saf-O+ Chondron Number
Q1
Q2
Q3
Q4
Days Post-DMM
Uninjured
DMM
Repeated-i.a.ZA

Figure 3.3: Repeated-i.a.ZA Administration Following DMM Drove Location-Dependent Changes in Chondrocyte Loss and PG-Rich Chondron Presence. (A.) H&E stained sections highlight the initial focal presence and then spreading of chondrocyte dysfunction and loss, especially in Q3, following DMM. Accompanying this loss were the appearance of empty chondrons and pyknotic (condensed), karyolitic (faded), and karyorrhectic (fragmented) chondrocyte nuclei, as well as eosinophilic nucleoli (possibly indicating proliferative cells); which are especially apparent at 7- and 14-d onward. While H&E staining confirmed a reduction in DMM-driven cartilage erosions following repeated-i.a.ZA treatment, visual improvement in articular cartilage cellularity was not obvious. Representative images were acquired from the anterior region (level 2) of the joint at 10x magnification (scale bar = 100µm). (B.) Counting, on a quadrant-by-quadrant basis, the number of hematoxylin-positive chondrocytes within the medial tibial plateau's articular cartilage identified a drastic loss of chondrocyte cellularity in Q3 immediately following DMM-injury (by 7d); where the development of overt tissue erosion co-localized at later disease stages (84d). The number of chondrocytes present in the other three quadrants of the tibial plateau over time appeared largely unaffected by DMM-injury. In DMM-joints receiving repeated-i.a.ZA, a similar, if not accelerated, loss of chondrocyte number in Q3 was observed, a change that was also accompanied by a significant increase (acceleration) in chondrocyte loss in Q2, while Q1 and Q4 remained relatively unchanged. (C.) In untreated DMM-joints, the number of proteoglycan-rich (Saf-O^+) chondrons increased across the tibial plateau early on (7 and 14d); repeated-i.a.ZA injection further enhanced the presence of these proteoglycan-rich chondrons in all quadrants except Q3. Results are presented as mean ± STD (n=5-10/timepoint/group); where # indicates $p< 0.05$ for the difference between repeated-i.a.ZA and untreated DMM-joints at that timepoint, * indicates $p< 0.05$ between the untreated DMM and uninjured-joints.

Histologically, we also observed changes in the presence of chondrons that exhibited intense 'peri-cellular' proteoglycan staining (i.e. more intense Saf-O^+ staining than observed within the local interterritorial matrix) in the medial tibial plateau articular cartilage (Figure 3.1A). Counting, on a quadrant-by-quadrant basis, we observed a rapid (7-14 days) increase in the number of chondrons exhibiting

intense peri-cellular Saf-O$^+$ staining in untreated DMM-injured joints that returned to levels of the uninjured joints at later disease stages (Figure 3.3C). In DMM-joints treated with repeated-i.a.ZA, similar, and in some cases even greater, quadrant-specific increases in the presence of intense Saf-O$^+$ chondrons were observed (Figure 3.3C). One exception to this was the observation of a slight, but significant decrease in Saf-O$^+$ chondrons in Q3 at mid-disease timepoints (14 through 56-days). In single-i.a.ZA treated DMM-joints a different pattern of Saf-O$^+$ chondron presence was observed: a marked increase in Saf-O$^+$ chondrons in Q1 and Q4 throughout the study, but no changes in Q2 and Q3 (Appendix B Figure B.3B).

Finally, we used immunohistochemistry to study two cellular processes, chondrocyte death/apoptosis and proliferation, that may underpin the aforementioned tissue- and cellular-level changes. TUNEL staining for cell death/apoptosis confirmed that DMM-injury could drive rapid focal chondrocyte cell death (TUNEL$^+$ cells) in Q2 and Q3 of the medial tibial plateau articular cartilage (seen at 7-and 14-days timepoints post-DMM; Figure 3.4A). Furthermore, increased staining for chondrocyte death (TUNEL$^+$) spatially localized with the presence of cells exhibiting a lack of DAPI$^+$ nuclear staining and with the pattern of abnormal nuclear staining and empty chondrons seen via H&E staining (Figure 3.3A). However, in DMM-joints treated with repeated-i.a.ZA, chondrocyte death (TUNEL$^+$) was only observed in Q2 at 7 days and largely absent at the other timepoints or in the other quadrants (Figure 3.4A). Staining for the presence of Ki-67 indicated that DMM-injury drove a consistent increase in chondrocyte proliferation in Q1 and Q2 of the medial tibial plateau articular cartilage; Ki-67$^+$ cells were apparent as early as 7-days post-DMM (Figure 3.4B) and maintained through 14-days post-injury. It is noteworthy that proliferative

(Ki-67^{+}) chondrocytes were generally found immediately adjacent to regions exhibiting visible chondrocyte loss and death. While the articular cartilage was typically devoid of Ki-67^{+} chondrocytes in Q3, presumably do to extensive cell death in that quadrant, we did observe the presence of eosinophilic nucleoli at the borders of Q3 and its adjacent quadrants (Q2 and Q4) in Figure 3.3A, which has been suggested as an indicator of cell proliferation[312]. In DMM-joints treated with repeated-i.a.ZA, chondrocyte proliferation was consistently reduced at 7-days and largely absent from 14-days and onward. The pattern of chondrocyte death and proliferation seen in the repeated-i.a.ZA treated joints was also observed in DMM- joints treated with single-i.a.ZA (data not shown).

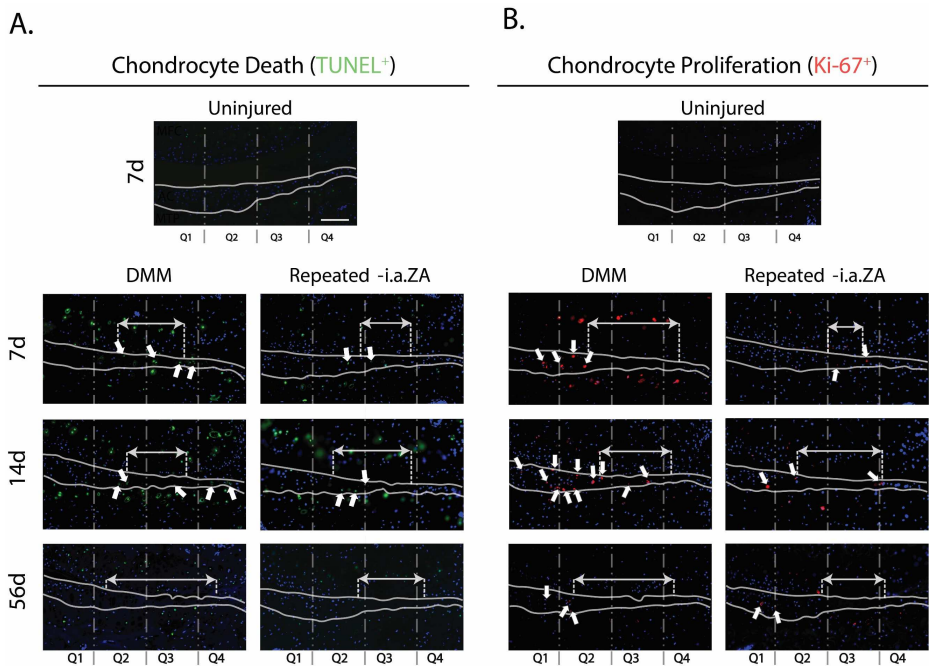

Figure 3.4: Repeated-i.a.ZA Treatment Modulated Chondrocyte Apoptosis and Proliferation Following DMM. (A.) TUNEL staining indicated a general absence of dead/apoptotic cells in the medial tibial plateau cartilage (between the gray traces) and the medial femoral condyle cartilage in uninjured joints; a small number of TUNEL$^+$ cells were found in the calcified cartilage. However, following DMM-injury chondrocyte death/apoptosis (white block arrows) was prevalent in Q2 & Q3 of DMM-joints, TUNEL$^+$ staining was seen as early as 7d post-injury and diminishing by 56d. TUNEL$^+$ staining also coincided spatially with the regions of articular cartilage that exhibited a loss of DAPI staining (width of these regions denoted by the gray double arrows). Following DMM, an increase in the number of TUNEL$^+$ cells in the calcified cartilage of the medial tibial plateau and medial femoral condyle was also observed. After repeated-i.a.ZA treatment, fewer TUNEL$^+$ chondrocytes were seen at 7d post-DMM and they were largely absent from 14d onwards. These representative images were acquired from the anterior region (level 2) of the joint at 20x magnification (scale bar = 100µm). (B.) Ki-67 staining, indicating cells in the cell cycle, highlighted a general absence of proliferative chondrocytes in uninjured joints. Following DMM-injury, robust cell proliferation was observed in Q1 and Q2 of the articular cartilage as early as 7 and 14d, which diminishes by 56d; some proliferative cells are found in the calcified cartilage. In joints receiving repeated-i.a.ZA injections, cell proliferation was either absent or greatly diminished in both the articular and calcified cartilages at all timepoints.

3.5 Discussion

In this study, we utilized the murine destabilization of the medial meniscus (DMM) model of PTOA to establish intra-articular (i.a.) injection of zoledronic acid (i.a.ZA) as a prophylactic therapeutic for post-traumatic osteoarthritis (PTOA). At the tissue-level, we showed that four repeated weekly i.a.ZA (4.q7d; administered at 0-, 7-, 14-, & 21-days post-DMM), but not single i.a.ZA (administered at 0 or 7-days post-DMM), could suppress long-term articular cartilage erosions (at 84-days) post-DMM. At the cellular-level, we identified that repeated i.a.ZA (repeated-i.a.ZA) could modulate chondrocyte proteoglycan production, proliferation, and death in a spatiotemporal dependent manner. Our findings agree with recent work that observed a similar prevention of articular cartilage erosions following repeated-.i.a.ZA in a rat model of PTOA, albeit at much higher i.a.ZA doses[260]. This study provided new insight into i.a.ZA's modes of action in cartilage and the spatiotemporally-dependent effects it has on cell- and tissue-health, and PTOA initiation and progression.

While the administration of four weekly-repeated i.a. injections of ZA provided meaningful long-term protection against the development cartilage erosions in the DMM-joint, none of the i.a.ZA strategies could prevent the development of superficial cartilage damage (fibrillations and clefting) in the immediate aftermath of DMM-injury (7-14-days). Instead, surface-based damage evolved similarly and rapidly among all DMM-joints; appearing predominately in regions of the medial tibial plateau and femoral condyle that experienced immediate changes in cartilage-on-meniscus-on-cartilage contact and loading post-DMM (predominately Q3)[285,286,310]. Such surface damage might be a function of differences in the mechanical properties of cartilage among regions normally covered by the meniscus and those in direct contact with opposing cartilage[292–294]. However, since repeated-i.a.ZA could suppress

the later evolution of superficial damage into overt cartilage erosions it suggests that long-term PTOA progression is more likely driven by cell-mediated processes than by simple mechanical wear and tear, and that prophylactically-administered repeated-i.a.ZA can modulate these cell-mediated processes for beneficial tissue-level outcomes.

At the tissue-level, we observed unique changes in both cartilage structure and composition when injured joints were treated with repeated-i.a.ZA. Structurally, we saw an unexpected thinning of the articular cartilage in the repeated-i.a.ZA group. However, this thinning appeared to be due to a loss in the 'height' of intact cartilage, as opposed to cartilage erosion; possibly due to a global 'wearing-away' of the superficial layer and/or a transition of articular cartilage into calcified cartilage by endochondral ossification[313,314]. Nevertheless, no changes in the integrity of the lamina splendens nor meaningful differences in the structure or cellularity of the calcified cartilage among the treated and untreated DMM-joints were observed. Instead, our results suggest that the presence of thinned cartilage that nonetheless resisted cartilage erosions following repeated-i.a.ZA treatment could have resulted from other cartilage 'adaptations', particularly the regulation of proteoglycan composition.

Compositionally, in untreated DMM-joints, we noted a rapid and focal loss of proteoglycan rich-tissue in the regions of the medial joint articular cartilage that experienced acute changes in cartilage-on-meniscus-on-cartilage contact (Q3); which aligns with the notion that changes in proteoglycan composition is a hallmark of early cartilage dysfunction in PTOA[65,280,288,310,315–318]. However, in DMM-joints receiving repeated-i.a.ZA, this focal loss of proteoglycan rich-tissue was suppressed. In addition, repeated-i.a.ZA treatment enhanced the proportion of proteoglycan rich-tissue and

tissue-level proteoglycan composition (Saf-O^+ staining intensity) found across the remainder of the articular cartilage. Given that cartilage proteoglycan composition and tissue mechanical properties are intrinsically linked[65,319], our results suggest that repeated-i.a.ZA might well protect, or possibly enhance, the tissue-level properties of murine articular cartilage following DMM-injury. While such findings are supported by investigations of cartilage explants mechanically-stimulated in the presence of ZA[256,257], further investigations will be required to establish if i.a.ZA treatment can indeed regulate the tissue-level mechanical properties and composition of articular cartilage *in vivo*.

The ability of repeated-i.a.ZA to regulate tissue-level changes/adaptations in cartilage following traumatic injury is likely rooted in the response of chondrocytes to locally-delivered ZA. Traditionally, the health and longevity of articular cartilage is thought to depend on the presence of healthy chondrocytes and their ability to maintain their extracellular matrix[73,320]. However, the role of chondrocytes in regulating cartilage homeostasis following acute injury appears more complicated. Traumatic injury can trigger rapid changes in cell viability (potentially due to both necrosis and cell-mediated death), as well as modulate chondrocyte injury responses (e.g. anabolic, catabolic, and inflammatory programming)[55,79,104–106]. Nonetheless, how and when such changes, which often occur simultaneously and in spatially-distinct manners, contribute to PTOA progression remains unclear.

In this study, we observed clear differences in chondrocyte biology (i.e. death, proliferation, and proteoglycan production) among untreated DMM-joints and those treated with repeated-i.a.ZA. Specifically, we found that DMM-injury induced a rapid and focal loss of chondrocytes in the region of articular cartilage that experienced

acutely altered meniscal coverage and later developed cartilage erosions (Q3). This cell loss was spatially coincident with the presence of empty chondrons, chondrocytes with abnormal nuclei (pyknotic, karyolitic, and karyorrhectic), and TUNEL-positive chondrocytes, which collectively suggest the presence of chondrocyte necrosis, apoptosis/chondroptosis[321], and cellular dysfunction. Furthermore, our findings also indicate an intimate relationship between this focal population of dead and dying chondrocytes (in Q3) and the temporal response of viable cells in adjacent regions of cartilage (Q1, Q2, and Q4); suggesting that this population of dead and dying chondrocytes may be critical to the initiation and propagation of cartilage degeneration following DMM. For instance, Ki-67^{+} chondrocytes, which are indicative of cells in G_1, S, G_2, or M-phase[311], rapidly appeared at the immediately periphery of the region of chondrocyte death/loss (Q3); whereas Ki-67^{+} cells were effectively absent in uninjured cartilage. These data suggest that in healthy cartilage chondrocytes are largely quiescence (in G_0-phase), and injury induces the activation of chondrocyte proliferation in a spatially-dependent manner. Activation of chondrocyte proliferation is a necessary pre-requisite for the chondrocyte-cloning associated with arthritic diseases and is reminiscent of the mitotic processes accompanying post-natal cartilage morphogenesis[73,313,320,322,323]. However, if activation of chondrocyte proliferation represents an innate injury-/repair-response, it seems unlikely that it would be beneficial to the adult joint, as proliferation requires local matrix remodeling, which could drive a vicious-cycle of cell-mediated catabolic and proliferative responses. Another injury-mediated adaptation that was observed was an increase in the number of chondrocytes that exhibited intense, halo-like Saf-O^{+} staining of their peri-cellular matrix compared to uninjured joints. This matrix response suggests an enhanced

production/deposition of proteoglycan in the local vicinity of viable chondrocytes following injury, particularly in the innermost region of the medial tibial plateau (Q1 and Q2). Our findings of increased chondrocyte proliferation and proteoglycan deposition align well with prior studies of PTOA (chondrocyte proliferation[299,324–331] and proteoglycan production[290,332–340]) and suggest that chondrocyte death, proliferation, and proteoglycan deposition might represent druggable targets for ameliorating cell-mediated cartilage degeneration following joint injury.

The capability of repeated-i.a.ZA treatment to prevent DMM-induced cartilage erosions permitted an ability to assess whether prophylactic i.a.ZA could modify chondrocyte death, proliferation, and proteoglycan production in a manner consistent with the observed PTOA mitigation. Our data suggested that repeated-i.a.ZA administration was unable to mitigate the focal loss of chondrocytes associated with DMM-injury in Q3, but instead drove a further, and unexpected, increase/'acceleration' of chondrocyte loss in Q2. In repeated-i.a.ZA DMM cartilage we saw a slightly reduced presence of $TUNEL^+$ cells; which was consistent with the reduction in $TUNEL^+$ chondrocyte staining observed following repeated-i.a.ZA therapy in a rat anterior cruciate ligament transection injury model[260]. While modulation of chondrocyte loss/death by repeated-i.a.ZA treatment appeared equivocal, the treatments ability to influence chondrocyte proliferation and local peri-cellular production of proteoglycan was far more striking. Repeated-i.a.ZA administration appeared to completely suppress ('rescue') the chondrocyte proliferation phenotype associated with DMM-injury and moderately enhanced the presence of chondrons exhibiting proteoglycan-enriched peri-cellular halos. Taken together, these results suggest that repeated-i.a.ZA can modulate chondrocyte death,

proliferation, and local proteoglycan metabolism following DMM-injury, providing the necessary recipe to enhance tissue-level proteoglycan content and suppress cartilage erosions long-term.

While the canonical target of nBPs *in vivo* are traditionally appreciated to be osteoclasts[128], the mevalonate (or isoprenoid) biosynthetic pathway, which nBPs inhibit, is ubiquitous among mammalian cells[136,150]. The mevalonate pathway is responsible for the synthesis of cholesterol and the process of protein prenylation. Prenylation is a form of post-translational modification, and inhibition the mevalonate pathway results in a suppression of the prenylation of small-GTPases. Small-GTPases are G-proteins critical to the regulation of numerous cellular process, including proliferation, differentiation, and cell-survival; cytoskeletal dynamics; vesicular transport; and cell movement. Indeed, it is now well-established that nBPs can directly mediate the inhibition of proliferation and the induction of apoptosis in inflammatory cells[181,182] as well as neoplasms and cancerous cells[188,204] through the inhibition of the mevalonate pathway. Furthermore, *in vitro*[187,254] and *in situ*[255–258,341] studies have demonstrated that ZA, and other nBPs, can directly modulate chondrocyte homeostasis, matrix metabolism, and cartilage health. The ability of repeated-i.a.ZA to modulate death, proliferation, and proteoglycan metabolism in chondrocytes demonstrated herein is entirely in line with known mechanisms of nBP action in the vast majority of mammalian cells.

Together, our tissue- and cellular-level findings establish a pattern of spatiotemporally-dependent cartilage changes following DMM-injury that provide insights into the mechanical and cellular basis of PTOA initiation and progression, and how intra-articularly injected ZA may modify these processes. Joint injury appears to

drive the rapid development of superficial cartilage damage and focal chondrocyte necrosis/apoptosis[55,75,79,104]. Rapid and focal chondrocyte necrosis in the face of acute changes in joint loading/stability would contribute to cell-loss, but it is unclear how (or even if) cell necrosis would influence tissue function[55,75,79,104]. We suspect that a far more important regulator of PTOA initiation is the presence of the focal population of chondrocytes undergoing the slower process of cell-mediated death (apoptosis/chondroptosis) following joint-destabilization. These dying cells could represent a nexus of mechanically- and biochemically-derived signals[55,75,79,104] driving an ever-expanding region of cartilage 'adaptation' and degeneration across the medial joint. For example, after DMM-injury, the focal population of dying cells appears to be surrounded by an annulus of chondrocytes in which i) nearby cells re-enter the cell-cycle (activate cell division) and ii) more distance cells deposit ECM with enhanced proteoglycan composition. Such a behavior can be interpreted as an innate, adaptive- or reparative-response. However, it must be recognized that proliferation of cells entombed in a dense ECM requires local tissue remodeling and catabolism[73,313,320,322,323], which could act as a further activator of cell death and injury response; initiating a vicious cycle of cellular dysfunction and cell-mediated cartilage degeneration[55,75,79,104]. Such a process appears evident in our observation of a lock-step progression of cell proliferation, apoptosis, and cartilage degeneration across the medial tibial plateau over time post-DMM.

Eliminating dying cells, and their injury-alarm signals, from injured cartilage, and/or preventing the proliferative and adaptive responses driven in neighboring 'activated' cells could represent a key to suppressing cell-mediated processes that drive PTOA. We speculate that just such a modulation of injury-response processes,

i.e. the enhancement of cell death, suppression of cell proliferation, and promotion of cell- and tissue-level proteoglycan content, underlie the ability of repeated-i.a.ZA to prevent cartilage erosions in the murine DMM model; a hypothesis supported by the recent demonstration that induction of chondrocyte death in cartilage's superficial layer prevents erosions in the murine DMM model[329]. However, the inability for single-i.a.ZA administrations to promote similar degrees of beneficial cell- and tissue-level outcomes suggests that a sustained/repeated presence of ZA within the joint may be required for PTOA disease-modifying efficacy. Future *in vitro* and *in situ* work are needed to confirm the role of chondrocyte death/apoptosis and cell-cycle re-entry, and their modulation by ZA, in the initiation and progression of cartilage degeneration.

While this study provides compelling evidence supporting the efficacy of repeated intra-articular administration of ZA to suppressing the progression of cartilage damage following joint injury in the mouse, several limitations should be noted. While four, weekly-repeated i.a.ZA injections over the course of the first 3-weeks of injury could provide a meaningful degree of cartilage protection at 12-weeks following DMM-injury, whether continued weekly i.a.ZA administration over longer timescales, or with different delivery schedules (e.g. delayed, reduced, or alternatively-spaced injections) or dosages would improve cartilage outcomes at and beyond 12-weeks is unknown and a focus of future work. Similarly, given that the earliest evaluations occurred at 1-week post-injury/post-treatment, we can only speculate on i.a.ZA-driven changes to cartilage and chondrocyte-biology at earlier timepoint based upon outcomes observed at 1-week post-injury/treatment. The present study also restricted itself to histological and immunohistochemical assessments of *in vivo* cartilage outcomes; the use of multi-scale approaches investigating molecular- to

organismal-physiology outcomes in injured and repeatedly treated joints will be necessary to advance this work towards clinical translation. Furthermore, while the murine DMM PTOA model is well characterized, the ability to generalize our present findings to more clinically-representative joint injuries are limited by the invasive, surgically-driven nature of the DMM injury. To the best of our knowledge, no studies of i.a.ZA treatment following non-invasive joint injuries exist; thus, it is unclear if the choice of injury model might influence therapeutic efficacy. Future studies are necessary to establish the efficacy of i.a.ZA in preventing cartilage damage in more clinically representative joint injury situations and other large pre-clinical animal models. Lastly, PTOA is a whole-joint disease[19], with injury-associated changes to other tissues in the knee known to influence PTOA progression; the effect of i.a.-ZA administration on the response of other tissues in the knee joint to DMM-injury is presented in an accompanying companion paper (Chapter 4).

In conclusion, the present study provides compelling evidence supporting the ability of intra-articularly administered ZA to prophylactically modulate cartilage damage progression following joint injury. Specifically, four, weekly i.a.ZA injections (4.q7d), initiated immediately following DMM-injury, could suppress the development of overt, long-term articular cartilage erosions through the modulation cartilage composition (proteoglycan content) and chondrocyte homeostasis (proliferation, death/apoptosis, and proteoglycan metabolism). However, i.a.ZA treatment was unable to prevent the development of damage to cartilage's superficial surface following-DMM. These findings suggest that superficial damage to articular cartilage following injury is likely a mechanically-driven process and unlikely to be modifiable by ZA or other cell-modulating therapeutics. However, longer-term

development of focal cartilage erosions appears to be cell-mediated, and dependent upon processes that repeated-i.a.ZA administration can influence. Together, this and our companion study (Chapter 4) provide new knowledge to guide the continued study of ZA's modes and mechanisms of action in chondrocytes and to drive pre-clinical studies investigating the translatability of prophylactically-administered intra-articular ZA for modifying and treating PTOA.

3.6 Acknowledgments

The authors would like to give special thanks to Mr. Frank Warren and Dr. Gwen Talham, DVM for oversight of animal care and the following individuals for technical assistance: Avery White, Jon Lowman, Ryan McDonough, Srinivasa Gajjala, Christopher Hernandez, Malhar Sakarwala, Brianna Gietter, Michael Lan, Pooja Kaiji, Oliva Laxton, Fiona Flowerhill. This work was supported by the Office of the Assistant Secretary of Defense for Health Affairs through the (Peer-Reviewed Medical Research Program) under Award No. W81XWH-13-1-0147. Any opinions, interpretations, conclusions, or recommendations expressed in this material are those of the authors and are not necessarily endorsed by the Department of Defense.

Chapter 4

THE INFLUENCE OF REPEATED INTRA-ARTICULAR INJECTION OF ZOLEDRONIC ACID ON NON-CARTILAGINOUS JOINT TISSUES FOLLOWING JOINT DESTABILIZATION IN THE MOUSE

(MA David, MK Smith, BT Graham, RN Pilachowski, AT White, RC Locke, L Wang, C Price, *In Preparation 2019b*)

4.1 Abstract

Post-traumatic osteoarthritis (PTOA) is an incurable, whole-joint disease. In search of disease-modifying PTOA therapeutics, bisphosphonates have gained attention due to their ability to inhibit subchondral bone remodeling and cartilage damage post-injury. In our companion paper, we showed that locally-targeted zoledronic acid (ZA), delivered as four weekly intra-articular (i.a.) injections following injury, could suppress long-term cartilage erosions in the murine destabilization of the medial meniscus (DMM) model of PTOA. Beyond ZA's classically understood ability to inhibit bone remodeling, it can also mediate anti-proliferative and anti-inflammatory activities across numerous mammalian cell types. To evaluate the ability of intra-articular injection of ZA (i.a.ZA) to shape the response of knee joint tissues other than cartilage to DMM-injury, we used microtomography and histological analysis to assess meniscal, osteophyte, and synovial tissue responses, along with subchondral, epiphyseal, and metaphyseal bone structure. Following DMM-injury, repeated-i.a.ZA did not appreciably alter injury-induced meniscal changes or ectopic bone formation, aside from promoting a moderate increase in meniscal proteoglycan content and bone volume fraction. Repeated-i.a.ZA did not

alter osteophyte size but did delay the transition of osteophytes from their cartilaginous templates to boney tissue following DMM-injury. Furthermore, repeated-i.a.ZA did not suppress joint synovitis induced by DMM-injury, nor appreciably affect bone structure in the ipsilateral tibia. These results suggest that, aside from a small anti-resorptive influence on intra-capsular mineralized tissues, repeated-i.a.ZA had limited ability to alter the trajectory of changes to non-cartilaginous tissue following joint-injury and had minimal influence on local or distant skeletal health. Combined with our accompanying paper, our results suggest that prophylactic intra-articular injection of ZA can suppress PTOA progression following joint-injury and in a manner that reduces the risk of adverse skeletal side-effects associated with systemic, high-dose ZA therapies.

4.2 Introduction

Accelerated cartilage degeneration following traumatic joint injury is a hallmark of post-traumatic osteoarthritis (PTOA). Given its incurable nature, and the significant physical and socioeconomic burden the disease presents, the search for PTOA-modifying therapeutics has been on the forefront[342]. A class of FDA-approved drugs receiving attention as potential PTOA disease-modifying therapeutics are the bisphosphonates (BPs) As potent anti-resorptives of bone, BPs are traditionally used to treat osteoporosis and cancer-related bone fragility[245,307]. However, since aberrant subchondral bone remodeling is a hallmark of PTOA initiation and progression[120,126,233,234], BPs have been explored as a means to suppress injury-induced subchondral bone remodeling for cartilage damage prevention. As such, numerous preclinical studies have demonstrated the ability of high-dose, systemic-administration of nitrogen-containing bisphosphonates (nBPs), including zoledronic acid (ZA), to

prophylactically prevent cartilage degeneration, bone remodeling, and pain across several animal models of arthroses including rheumatoid arthritis[209–216], osteoarthritis[217–219], and PTOA[238–241,309]. However, despite these promising strides, PTOA prevention based upon systemic, high-dose ZA administration may face insurmountable challenges to clinical implementation due to significant risk of adverse side effects associated with systemic suppression of bone remodeling, most notably osteonecrosis of the jaw and atypical bone fractures[242–245]. Fortunately, recent *in vitro*[187,254] and *in situ*[255–258] studies indicate that ZA can directly modulate chondrocytes and cartilage health, suggesting that locally-targeted ZA delivery strategies might represent a more clinically-acceptable PTOA-modifying strategy.

In our accompanying paper, our team demonstrated that one such alternative delivery strategy, namely four, weekly-repeated (4.q7d) intra-articular (i.a.) injections of ZA (i.a.ZA) into the knee starting immediately upon injury could suppress cartilage erosions in the murine destabilization of the medial meniscus (DMM) model of PTOA (Chapter 3). This work suggested that repeated i.a.ZA, which should engender far less risk of adverse systemic skeletal complications due to reduced overall ZA dosage, could be leveraged as a prophylactic disease-modifying therapeutic for PTOA. While our accompanying paper focused on changes to cartilage health following injury and i.a.ZA treatment, PTOA is as a whole-joint disease[18–22]. In this regard, numerous injury-induced changes to non-cartilaginous tissues occur within the joint that may contribute to the initiation and progression of cartilage degeneration following injury; these include meniscal changes, osteophyte formation, aberrant subchondral bone remodeling, and joint inflammation[18–22,78,343]. Consequentially, a therapeutic lead for

PTOA prevention that could target multiple joint tissues in the injured joint would be an ideal candidate, and there are reasons to believe that ZA might meet this need.

ZA is well-known for its anti-resorptive in bone[128,245,307,308,344], and has more recently been shown to have anti-immunologic, anti-inflammatory, anti-tumor, and anti-angiogenic properties[131,170,345,179–185,204] because of its ability to inhibit the ubiquitous mevalonate biosynthetic pathway found in all mammalian cells. Thus, it is plausible that i.a.ZA could influence the evolution of injury-induced changes in both mineralized joint tissues, such as those that occur in the subchondral bone, calcified menisci, and osteophytes[18–22,120,343], as well as non-mineralized tissues, such as the synovium[78]. To date, only one study has investigated the ability of repeated i.a.ZA to suppress joint synovitis in a rat ligamentous injury model of PTOA[259]. Yet, it remains unclear: i) how other non-cartilaginous tissues within the joint respond to repeated i.a.ZA treatment following injury; and ii) if repeated i.a.ZA administration can influence extra-capsular skeletal tissue properties and thus global bone health following injury.

In support of our companion paper, demonstrating the ability of four, weekly-repeated (4.q7d) i.a.ZA administration to suppress cartilage erosions in murine DMM-injured knee joints (Chapter 3), this study sought to investigate the influence of repeated i.a.ZA administration on bone remodeling, meniscal injury response, osteophyte formation, and joint synovitis post-DMM. To facilitate this assessment, we performed detailed micro-computed tomography and histological analysis of the DMM-injured and i.a.ZA-treated mouse knees presented in our companion paper. Our findings indicated that four, weekly-repeated (4.q7d) i.a.ZA to the injured joint could mildly influence meniscal injury response and osteophyte development but not joint

synovitis post-DMM. More importantly, the structure properties of the underlying subchondral bone and of more distant (extra-capsular) bone compartments of the ipsilateral of the tibia were largely unaffected by repeated i.a.ZA treatment, suggesting that repeated i.a.ZA administration strategy may represent a safer prophylactic PTOA prevention than systemic treatment with ZA.

4.3 Methods

4.3.1 Animals and Surgeries

Details regarding surgical procedures and sample collection can be found in our accompanying paper (Chapter 3). Briefly, the right tibiofemoral joints of 12-week old male C57BL/6 mice underwent either DMM surgery with no treatment (untreated DMM) or DMM surgery plus repeated intra-articular injection of ZA (i.a.ZA) at 0-, 7-, 14-, and 21-days (repeated-i.a.ZA). For each i.a. injection, 6µL of sterile saline containing ZA at ~615 ng/kg was injected into each knee. Contralateral joints from untreated DMM mice served as uninjured controls. The University of Delaware's Institutional Animal Care and Use Committee approved all animal handling and surgical procedures. Intact tibiofemoral joints were collected at 7-, 14-, 56-, or 84-days post-injury and directed towards either micro-computed tomography (µCT; n=62 joints) or histological analysis (n=110 joints).

4.3.2 µCT Analysis of Intra-capsular and Extra-capsular Calcified Tissue Structures

µCT was used to assess the structural properties of intra-capsular subchondral bone (medial compartment), calcified medial meniscus, and ectopic formed bone in uninjured, untreated DMM, and DMM + repeated-i.a.ZA treated joints (n= 3-

5/group/timepoint), as well as the structure of the extra-capsular ipsilateral tibial subchondral bone and epiphyseal in the medial joint compartment and the metaphyseal trabecular bone. At harvest, tibiofemoral joints were frozen at -80ºC in 1x phosphate-buffered saline supplemented with calcium chloride until scanning. For µCT scanning (Scanco µCT-35; 6µm isotropic voxel size; x-ray voltage and current of 55kVp and 145.5uA, respectively; 500-ms integration time; 500 projections; and 300 images averaged over 2 image each), joints were placed into a custom-built holder that held the joints at ~90° of knee flexion. From 3D reconstructions of these joints, the following were manually traced using CT-Analyser software (CTAn; Bruker-MicroCT): i) the entire calcified anterior medial meniscus and intracapsular ectopic bone; the ii) subchondral bone and iii) underlying epiphyseal bone across a 480µm (80-slice) deep region of the medial tibial plateau and centered about the femur-on-tibia contact; and iv) femur-on-tibia contact region of cancellous bone within the tibial metaphyseal cancellous bone (cuboid ROI of 750µm wide x 1000µm tall). For each region, metrics of tissue volume (TV), bone volume (BV), bone volume fraction (BV/TV), and bone thickness (Th) were quantified via Bruker's CTan software following global segmentation using Otsu's grayscale thresholding technique and despecking[346]. Gross structural changes to mineralized tissues within the joint were visualized using 3D volumetric renderings using ImageJ (National Institute of Health) in combination with Seg3D2.4 (Center for Integrated Biomedical Computer).

4.3.3 Histological Processing and Staining

Intact joints were processed for paraffin-embedded histological staining and assessment as described previously[310] (see also Chapter 3). Briefly, joints (n=5-10/group/timepoint) were fixed, decalcified, processed, embedded, sectioned coronally

at 5-µm, and placed on charged slides (two sections/slide). Five slides, taken at intervals of ~100-µm across the joint and centered about the tibiofemoral cartilage-on-cartilage contact, were selected and labeled levels 1 through 5 from the anterior (level 1) to posterior (level 5) of the joint. These slides were then stained with Safranin-O, fast green, and Wiegert's hematoxylin, hereon referred to as Saf-O, and imaged using a widefield microscope and color digital camera (Axio.Imager.A2 + AxioCam MRc5, Carl Zeiss) under consistent illumination and acquisition settings.

4.3.4 Quantification of Meniscus Coverage, Size, and Proteoglycan Content

To address if i.a.ZA treatment influences medial meniscal extrusion and structure post-DMM, semi-automated histological assessment was performed on Saf-O stained sections from joint levels 2-4. After manually-tracing each medial meniscus, the degree of tibial plateau cartilage covered by the meniscus (the reciprocal of meniscal extrusion)[310], as well as meniscal cross-sectional area was quantified. Additionally, the areal distribution of Saf-O positive (Saf-O^+) tissue within the medial meniscus, as well as the Saf-O^+ staining intensity of the tissue (change relative to the intensity of the tibial growth plate was quantified using a semi-automated color thresholding and analysis algorithm described previously (Chapter 3).

4.3.5 Histological Analysis of Synovitis and Osteophyte Development

To assess whether repeated-i.a. injection of ZA could modify osteophyte formation and joint synovitis post-DMM, osteophyte maturation and extent of joint synovitis (non-native tissue in the joint space exhibiting increased cellularity and/or thickening) within the medial compartment was assessed semi-quantitatively by three blinded individuals (MAD, MKS, AW and/or RNP) within Saf-O stained slides from

joint levels 1-5. Both outcomes were assessed on a 0-3 scale[347]: i) for osteophytes, 0 = no osteophyte, 1 = cartilaginous template, 2 = cartilaginous template with some bone present, 3 = entirely boney osteophyte; and ii) for synovitis, 0 = no synovitis, 1 = mild synovitis, 2 = moderate synovitis, and 3 = severe synovitis. To provided additional insight into osteophyte maturation, several aspects of the forming/formed osteophytes on the medial tibial margin in were assessed quantitatively. Using semi-automatic image process in MATLAB, the osteophyte tissue (in Saf-O stained slides from joint levels 2-4) was traced manually, bone marrow cavities areas were removed from the trace, and the relative areas of the remaining Saf-O^+ and Saf-O negative-fast green positive stained (Saf-O^-) tissues were measured, which allowed for the quantification of the relative amount of cartilaginous and boney osteophyte tissue present, respectively. Finally, the staining intensity of the proteoglycan-rich Saf-O^+ tissue within the osteophyte was determined as described above for the menisci.

4.3.6 Statistical Analysis

Statistical analyses were performed using GraphPad Prism version 6.0 for Mac (GraphPad Software, La Jolla, CA). One-way ANOVAs with Dunnett post-hoc tests (i.e. many-to-one comparisons) were performed to establish differences in parameters between the uninjured and repeated-i.a.ZA treatment groups and those of the untreated DMM-joints at each timepoint. The threshold for defining statistically significant changes was set at $p < 0.05$.

4.4 Results

4.4.1 Meniscal and Intracapsular Ectopic Bone Changes Following Repeated-i.a.ZA Treatment in DMM-Joints

In the healthy adult mouse, both the medial and lateral menisci contain regions of calcified tissue that can be visualized by high-resolution micro-computed tomography (μCT); with the calcified tissue of the anterior menisci being substantially larger than that of the posterior menisci. Visualization of volume rendered μCT scans from joints harvested at 84-days post-DMM demonstrated a clear extrusion of the anterior medial meniscus outwards from the joint space in both untreated DMM-joints and DMM-joints repeatedly administered i.a.ZA, as well as enlargement of the calcified portion of both the anterior and posterior medial menisci (Figure 4.1A). Similar evidence of meniscal extrusion and calcified volume increase were observed in repeated-i.a.ZA treated and untreated DMM-joints at earlier timepoints (data not shown). In both the treated and untreated joints, DMM-injury resulted in similar increases to the total anterior medial meniscal volume (Men.TV; Figure 4.1B). However, repeated i.a.ZA administration resulted in a sustained increase in meniscal bone volume (Men.BV; data not shown) and bone volume fraction (Men.BV/TV; Figure 4.1B) that was seen by 7-days onwards. Volumetric renderings of the joints also revealed a similar appearance and development of ectopically formed bone within both treated and untreated DMM-joints from 56-days and onward post-DMM (Figure 4.1A). This ectopic bone (EcB) formed anteriorly only within DMM-injured joints. While repeated-i.a.ZA administration did not markedly influence the total number (EcB.N; data not shown) or total volume of ectopic bone fragments (EcB.TV; Figure 4.1C) that formed following DMM-injury, it did drive an increase, albeit non-

significant, in the volume of ectopic bone (data not shown) and the bone volume fraction of this tissue at 84-days post-DMM (EcB.BV/TV; Figure 4.1C).

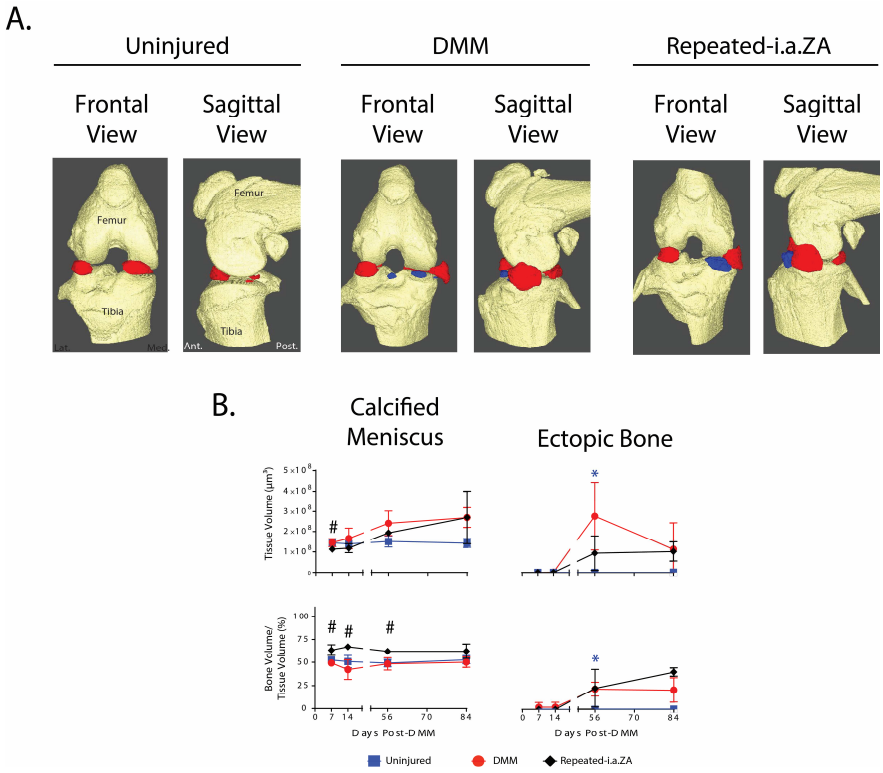

Figure 4.1: Assessment of Periarticular Calcified Tissue Changes in the Tibiofemoral Joint Following DMM and Repeated-i.a.ZA Treatment. (A.) 3D µCT renderings of representative knee joints (at 84 days) following DMM and repeated-i.a.ZA treatment highlight the extrusion and volumetric increase of the medial meniscus (red), and the spontaneous formation of ectopic bone (blue) in all injured joints. (B.) Meniscal tissue volume increased in all DMM-injured joints. Repeated-i.a.ZA treatment did not alter the resultant meniscus size (tissue volume) but did result in increased meniscus bone volume fraction. Periarticular ectopic bone tissue became apparent at 56-days post-DMM injury. Repeated-i.a.ZA treatment did not alter the volume or bone volume fraction of this ectopically formed bone tissue. Results are presented as mean ± STD (n=3-5/timepoint/group); where # indicates $p < 0.05$ for the difference between repeated-i.a.ZA and the untreated DMM-group at that timepoint, * indicates $p < 0.05$ between the untreated DMM and uninjured-joints at that timepoint.

4.4.2 Repeated-i.a.ZA Treatment Post-DMM Did Not Alter Subchondral Bone, Epiphyseal, and Metaphyseal Bone Structure

Quantitative analysis of μCT data indicated that DMM-injury did not alter the structural properties of the medial subchondral bone (SC) compartment when compared to uninjured joints (Figure 4.2A); no change in the total volume (SC.TV), bone volume (SC.BV; data not shown), bone volume fraction (SC.BV/TV), or thickness (SC.Th) was observed post-DMM. Similarly, repeated-i.a.ZA administration to DMM-joints did not significantly alter any these subchondral bone parameters (Figure 4.2A). We also observed that DMM-injury did not result in any measurable changes in the structure of the epiphyseal bone underlying the medial tibial plateau (Figure 4.2B) or the cancellous bone of the tibial metaphysis (Figure 4.2C) when compared to uninjured joints. Similarly, repeated-i.a.ZA administration to DMM-injured joints did not significantly alter bone structure in either of these extra-capsular bone compartments (Figure 4.2B and 4.2C), aside from a moderate increase in epiphyseal bone volume fraction (Epi.BV/TV) and thickness (Epi.Th) at 84-days post-DMM.

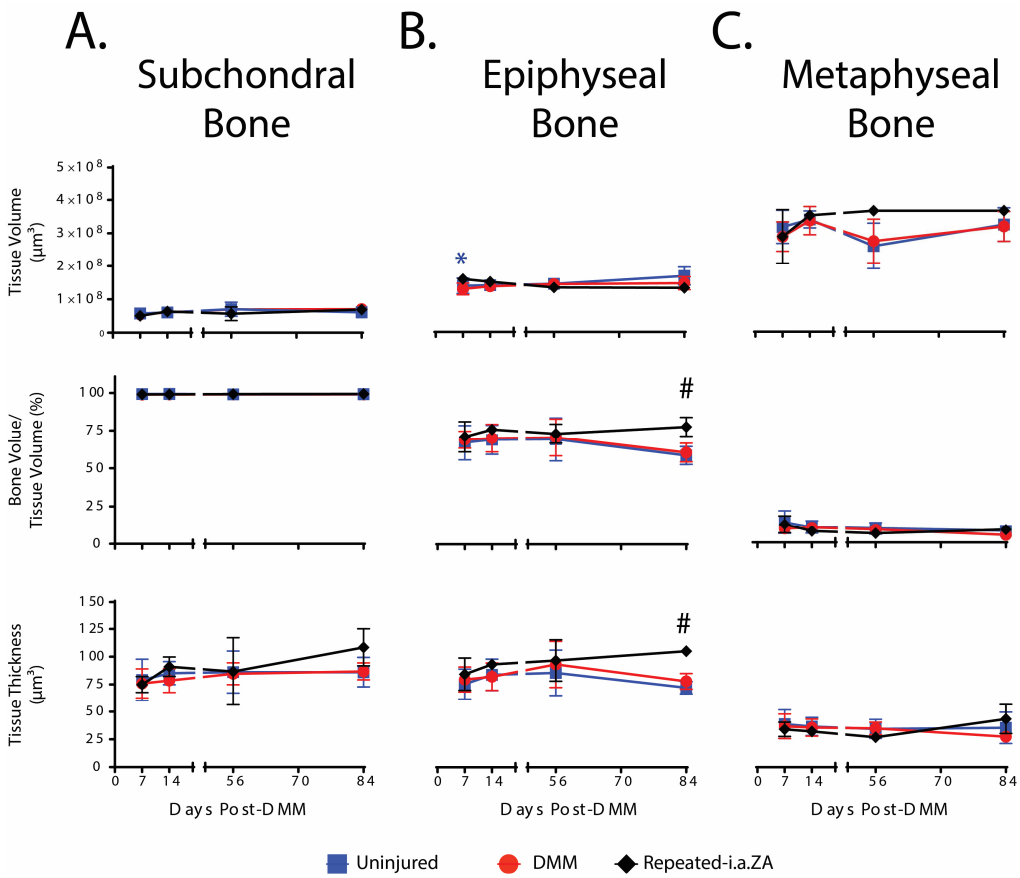

Figure 4.2: Repeated-i.a.ZA Treatment Following DMM Does not Alter Subchondral Bone, Epiphyseal, and Metaphyseal Bone Structure. (A.) µCT analysis indicated that subchondral bone tissue volume, bone volume fraction, and subchondral plat thickness were unaffected by DMM injury or DMM + repeated-i.a.ZA administrations. (B.) Similarly, epiphyseal bone structure (tissue volume, bone volume fraction, and thickness) was largely unaffected by DMM injury or DMM + repeated-i.a.ZA treatment. (C.) The structural of the trabecular bone of the ipsilateral tibial metaphysis was not altered by DMM or DMM+ repeated-i.a.ZA treatment. Results are presented as mean ± STD (n=3-5/timepoint/group); where # indicates $p < 0.05$ for the difference between repeated-i.a.ZA and the untreated DMM-group at that timepoint, * indicates $p < 0.05$ between the untreated DMM and uninjured-joints at that timepoint.

4.4.3 Repeated-i.a.ZA Administration Altered Meniscal Proteoglycan Composition Post-DMM

Histological assessment (Figure 4.3A) confirmed our µCT-based assessments of medial meniscus changes following DMM-injury, and it provided additional insights into DMM-mediated meniscal extrusion (coverage) and changes in meniscal size (area) and proteoglycan composition (Saf-O^+ tissue) in untreated and treated DMM-joints. Medial meniscus coverage (reciprocal of extrusion) was similar among the untreated DMM-joints and those treated with repeated-i.a.ZA (~20-30%), and this coverage was significantly less than that seen in uninjured joints (~45-60%; Figure 4.3B). Additionally, DMM-injury led to a significant increase in medial menisci area compared to uninjured joints, and repeated-i.a.ZA treatment did not influence the trajectory of this injury-induced increase in meniscal area (Figure 4.3C). When evaluating the area of proteoglycan-rich (Saf-O^+) tissue in the medial meniscus, we found no difference in the relative area of Saf-O^+ tissue between the menisci of the uninjured joints and the significantly enlarged menisci of untreated DMM-joints. However, in DMM-joints treated with repeated-i.a.ZA the relative area of this proteoglycan-rich (Saf-O^+) meniscal tissue was significantly increased at early-to-mid timepoints (7 through 56-days). Using changes in Saf-O^+ staining intensity (Figure 4.3C) as a surrogate for changes in tissue proteoglycan composition, we observed that DMM-injury led to a drastic and significant reduction in overall meniscal proteoglycan composition. Repeated-i.a.ZA administration rescued the loss of meniscal proteoglycan composition seen in DMM-joints following a transient/partial decrease in Saf-O^+ tissue staining intensity (at 7-days).

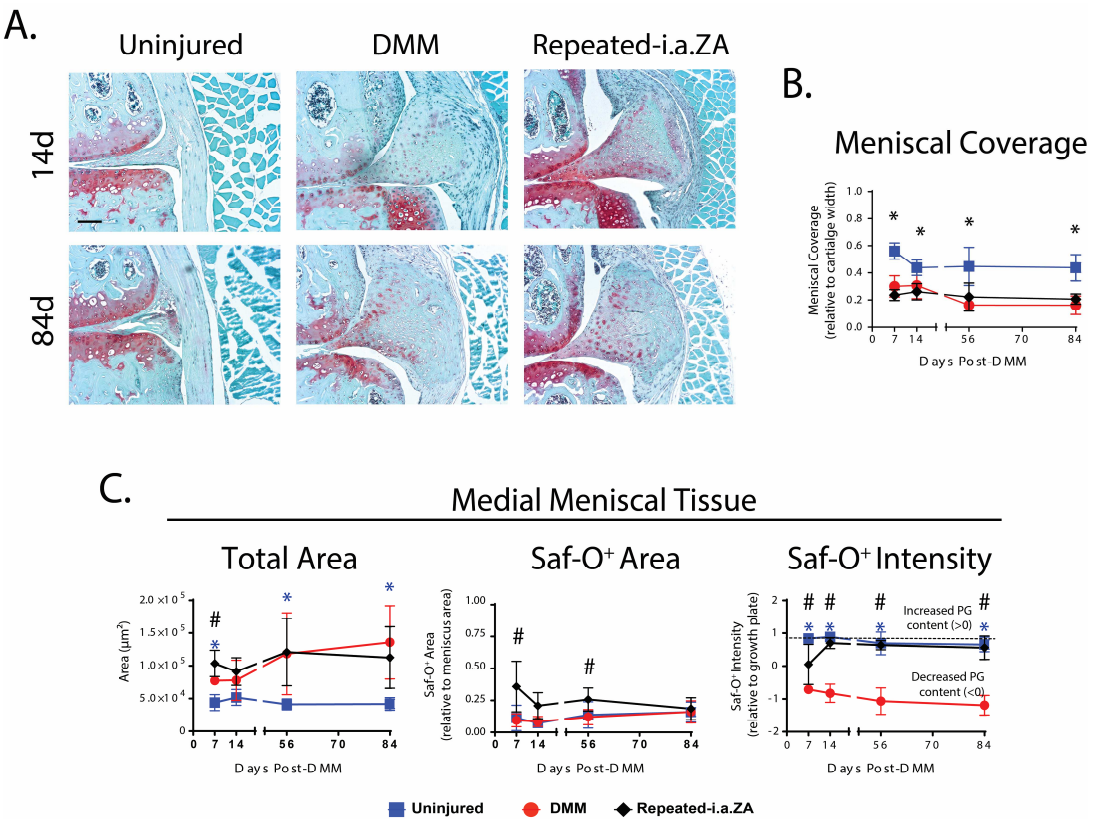

Figure 4.3: Meniscal Changes Associated with Repeated-i.a.ZA Treatment Post-DMM. (A.) Safranin-O stained slides highlighted the medial meniscus extrusion and changes to meniscal size and proteoglycan distribution and intensity following DMM and DMM + repeated-i.a.ZA treatment. These representative images were acquired from the anterior region (level 2) of the joint at 10x magnification (scale bar = 100µm). Histological analyses indicated that following DMM, repeated-i.a.ZA administration did not alter the injury-mediated (B.) uncovering of the medial tibial plateau (i.e. meniscal coverage) or (C.) meniscal growth (Total Area). However, repeated-i.a.ZA treatment did drive increases in the proportion of Saf-O$^+$ (proteoglycan-rich) tissue area and the relative staining intensity of this Saf-O$^+$ area compared to the untreated DMM-joints. Results are presented as mean ± STD (n=3-5/timepoint/group); where # indicates $p< 0.05$ for the difference between repeated-i.a.ZA and the untreated DMM-group at that timepoint, * indicates $p< 0.05$ between the untreated DMM and uninjured-joints at that timepoint.

4.4.4 Repeated-i.a.ZA Administration Delayed Osteophyte Development and Maturation Post-DMM

Using histological assessment, a rapid development of osteophytes at the medial-margins of the tibial plateau (Figure 4.4A) and the femoral condyle (Figure 4.5A) was confirmed in both treated and untreated DMM-joints; uninjured joints did not exhibit osteophytes. Osteophyte development in these locations proceeded from an extensive cartilaginous (Saf-O^+) osteophyte template seen at the earliest timepoint assessed (7-days) post-DMM into boney osteophytes, complete with marrow cavities, present at late stage disease (56 and 84-days). The tempo of osteophyte formation and maturation was assessed via semi-quantitative osteophyte scoring (Figure 4.4B) and quantitative analysis (Figure 4.4C). Osteophytes that formed in response to DMM-injury were similar in size in the repeated-i.a.ZA treated and untreated DMM-joints (Figure 4.4C). However, treatment with repeated-i.a.ZA led to a notable delay in osteophyte maturation. This delay was evident by a lag in the upward trajectory of semi-quantitative osteophyte scores (Figure 4.4B), a prolonged presence of Saf-O^+ tissue area (cartilaginous), and a reduced presence of Saf-O^- tissue area (bone) at earlier timepoints (7 through 56-days) post-DMM (Figure 4.4C). There was no difference in bone marrow cavity area among the repeated-i.a.ZA treated and untreated DMM-joints (data not shown). Additionally, repeated-i.a.ZA treatment of DMM-joints led an increase in the staining intensity of the osteophytes proteoglycan-rich (Saf-O^+) tissue compared to untreated DMM-injured joints (Figure 4.4C).

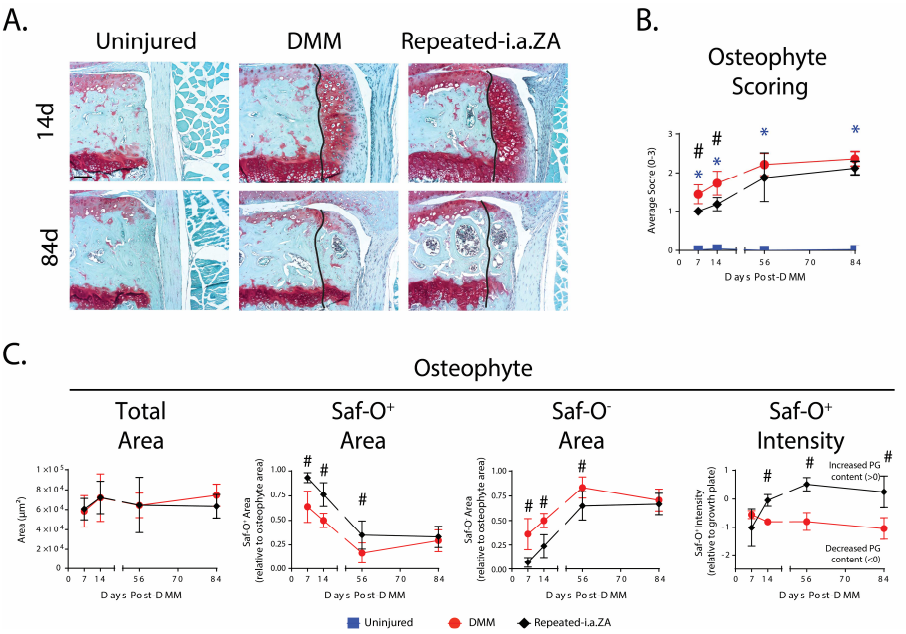

Figure 4.4: Repeated-i.a.ZA Treatment Delayed Osteophyte Maturation Following DMM. (A.) Safranin-O stained slides highlighted the robust formation of osteophytes along the medial tibial plateau joint margin in all DMM-injured joints (tissue to the right of black lines); this process initiated with the formation of a proteoglycan-rich cartilage-like template that subsequently transformed (matured) into fully formed boney osteophyte complete with marrow cavities. These representative images were acquired from the anterior region (level 2) of the joint at 10x magnification (scale bar = 100µm). (B.) Semi-quantitative osteophyte scoring revealed that repeated-i.a.ZA treatment altered the tempo of osteophyte maturation, as indicated by a delay in the conversion of the proteoglycan-rich cartilage-like template (score of 1) into nascent bone (score of 2). (C.) Quantitative analysis indicated that repeated-i.a.ZA treatment did not influence the overall size of the osteophytes that formed following DMM-injury. However, repeated-i.a.ZA treatment resulted in the retention of Saf-O$^+$ relative area (proteoglycan-rich tissue) and a delayed accumulation of Saf-O$^-$ relative area (bone tissue) following-DMM, which confirmed the delay in osteophyte maturation observed via the semi-quantitative osteophyte scoring. Within the Saf-O$^+$ areas of the osteophyte, repeated-i.a.ZA treatment increased the relative staining intensity of this proteoglycan-rich tissue across most of the study. Results are presented as mean ± STD (n=3-5/timepoint/group); where # indicates $p < 0.05$ for the difference between repeated-i.a.ZA and the untreated DMM-groups at that timepoint, * indicates $p < 0.05$ between the untreated DMM and uninjured-joints at that timepoint.

4.4.5 Repeated-i.a.ZA Administration Did Not Mitigate Synovitis Post-DMM

The synovitis-modifying ability of repeated-i.a.ZA treatment in DMM-injured joints was evaluated using semi-quantitative histological analyses of the medial compartment joint synovitis. We observed that DMM-injury led to a rapid (apparent at 7-days) and sustained presence of medial compartment joint synovitis when compared to untreated joints (Figure 4.5). However, repeated-i.a.ZA to DMM-joints did not reduce synovitis at any timepoint post-DMM (Figure 4.5); instead, a small but significant increase in synovitis was observed at 7d post-DMM that returned to the levels of the untreated DMM-joints by 14-days post-DMM.

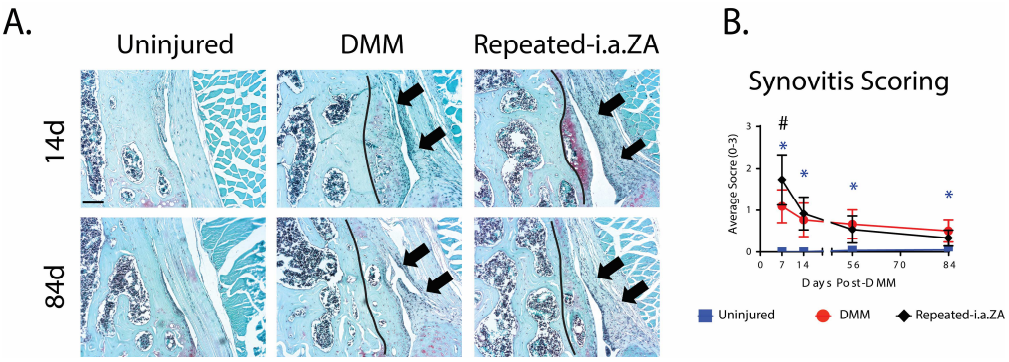

Figure 4.5: Joint Synovitis is Not Altered by Repeated-i.a.ZA Treatment Following DMM-Injury. (A.) Safranin-O stained slides demonstrated the presence of joint synovitis (black arrows) within the medial compartment following DMM, which repeated-i.a.ZA did not appear to suppress. These representative images were acquired from the anterior region (level 2) of the joint at 10x magnification (scale bar = 100µm). The presence of osteophytes along the medial femoral condyle are indicated by the tissue to the right of black lines. (B.) Semi-quantitative synovitis scoring confirmed qualitative impressions regarding joint synovitis, and further indicated a significant increase in synovitis immediately following DMM + repeated-i.a.ZA administration. Results are presented as mean ± STD (n=3-5/timepoint/group); where # indicates $p < 0.05$ for the difference between repeated-i.a.ZA and untreated the DMM-groups at that timepoint, * indicates $p < 0.05$ between the untreated DMM and uninjured-joints at that timepoint.

4.5 Discussion

Bisphosphonates, especially the nitrogen-containing bisphosphonates (nBPs), have gained attention as potential disease-modifying drugs for preventing or delaying PTOA initiation and progression[238–241,259,309,342]. In our accompanying paper (Chapter 3), we demonstrated that four, weekly-repeated (4.q7d), but not single, intra-articular (i.a.) injections of ZA (i.a.ZA) could prevent the development of injury-induced cartilage erosions in the murine DMM model of PTOA. However, PTOA is a disease of the whole-joint[18–22]. Thus, the objective of this study was to investigate how four, weekly-repeated i.a.ZA (repeated-i.a.ZA) administrations influenced the presence of and changes to non-cartilaginous structures (i.e. the meniscus, ectopic bone, osteophytes, and synovium) within the joint following DMM-injury, as well as to changes to bone structure (i.e. subchondral, epiphyseal, and metaphyseal bone properties) outside of the joint. We discovered that repeated-i.a.ZA was unable to suppress the development and increase in size of intracapsular structures that form in response to joint destabilization, including menisci, ectopic bone, and osteophytes. Nevertheless, repeated-i.a.ZA led to moderate delays in the maturation of these mineralized tissues, as well as increases in their bone volume fractions, which are consistent with ZA's resorption suppressing abilities. Despite the anti-inflammatory activities of nBPs in several mammalian cells, repeated-i.a.ZA was unable to suppress joint synovitis in the DMM-model. However, and most importantly, our two studies demonstrated that prophylactic administration of four weekly, intra-articular injections of ZA starting immediately following injury could protect against DMM-mediated cartilage erosion in the absence of appreciable alterations to bone structure, and by extent, bone resorption/remodeling, in more distant bone compartments (the ipsilateral tibial epiphysis and metaphysis).

As a result of the transection of the medial meniscotibial ligament during the DMM-injury, we observed significant outward extrusion and hypertrophy of the medial meniscus, followed by the formation of ectopic bone within the joint capsule. In untreated and repeated-i.a.ZA treated DMM-joints, extrusion of the medial meniscus resulted in a similar uncovering of ~1/3 of the medial tibial plateau cartilage that was previously covered by the meniscus[310]. The inability of repeated-i.a.ZA treatment to alter meniscal extrusion was not unexpected since meniscal extrusion is presumably mediated by geometrical and mechanical considerations within acutely destabilized joints; there is no reason to suspect that ZA would alter such a response. If one uses meniscal extrusion as a surrogate indicator of joint biomechanics, these results would suggest that the post-DMM mechanical environment is similar among untreated and repeated-i.a.ZA treated DMM-joints. Aside from the expected meniscal extrusion, we also noted that the anterior medial meniscus experienced increases in both mineralized and non-mineralized tissue size (volume and area, respectively) in all DMM-injured joints. These data align with preclinical (mouse[348,349] and rabbit[349,350]) and clinical[85–87,349,351–354] studies highlighting increased meniscal extrusion, hypertrophy, and calcification with increasing PTOA and OA disease severity. Increases in meniscal volume and calcification following DMM may very-well represent an adaptation mechanism, possibly to re-stabilize the joint in the face of altered loading and joint stability. Repeated-i.a.ZA treatment was unable to prevent injury-induced increases in meniscus size, seen in both their calcified volumes and non-calcified areas. However, and consistent with the anti-resorptive properties of ZA, repeated-i.a.ZA treatment led to moderate increases in the amount of bone, and thus the bone volume fraction, within these enlarged menisci. Disruption of proteoglycan

(PG) content within the meniscus may constitute another DMM-injury response. To this end, in untreated DMM-joints the hypertrophying menisci exhibited similar proportions of PG-rich (Saf-O$^+$) to those of uninjured-joints; however, the PG composition (Saf-O$^+$ staining intensity) within these PG-rich areas was diminished. On the contrary, repeated-i.a.ZA not only led to a substantial increase in the proportion of PG-rich tissue in the hypertrophying meniscal tissue, but it also rescued the loss in Saf-O$^+$ staining intensity seen in the PG-rich meniscal tissue of untreated DMM-joints. Another response to joint-injury recently appreciated in the rodent[338,355–361] and following orthopaedic trauma[362,363] is the 'spontaneous' development of ectopic bone post-injury. Indeed, we confirmed the development of extensive ectopic bone anteriorly within DMM-injured joints. While the role of ectopically formed bone in PTOA progression remains unclear, we anticipated that ZA could alter its formation because of ZA's anti-resorptive properties. However, we found that ZA was largely unable to alter ectopic bone formation. Collectively, our study suggests that repeated-i.a.ZA treatment was unable to modify DMM-induced meniscus extrusion and hypertrophy, or the formation of ectopic bone, but could moderately alter post-injury meniscal PG-content and the mineralized tissue fraction, thus presumably osteoclast-mediated bone resorption, in these tissues.

Another calcified tissue thought to influence PTOA progression in injured/unstable joints are osteophytes[81,82,364]. In DMM-injured joints, the rapid develop of osteophytes on the medial margins of the tibia and femur were confirmed following injury[263,280,360,365–367]. Initially, these osteophytes appeared as a PG-rich (Saf-O$^+$) cartilaginous templates as early as 7-days post-DMM, and these templates transformed over time, similar to endochondral ossification[82], into a fully-formed

boney-osteophytes complete with marrow cavities (by 84-days). Given the coordinated processes of cartilage formation, cartilage calcification, resorption, and bone remodeling required for osteophyte formation, we anticipated that intra-articular delivery of an anti-resorptive to DMM-joints would influence osteophyte development and maturation. While repeated-i.a.ZA treatment did not alter the overall size of osteophytes that formed in response to DMM-injury, repeated-i.a.ZA did retard their maturation (i.e. the speed of endochondral ossification and bone remodeling). Specifically, in treated joints, a slightly prolonged presence of proteoglycan-rich cartilaginous tissue and delayed appearance of lamellar bone was observed. These findings align with previous studies demonstrating a delay in osteophyte maturation due to alendronate (an older nBP) administration following joint injury[368,369]. Taken together, our data highlight the rapid formation of osteophyte cartilaginous templates post-DMM and the ability of repeated-i.a.ZA to slow the maturation, but not the overall size of forming osteophytes.

Aberrant subchondral bone remodeling and sclerosis is also thought to play a role in PTOA initiation and progression[81,120,126,234,370]. While disagreements exist regarding the precise mechanisms and timing by which changes to subchondral bone and articular cartilage are linked following joint injury[270,285,373–375,287,356–358,365,367,371,372], we found that DMM-injury did not alter subchondral bone remodeling in our male C57BL/6J mouse joints; findings consistent with several murine DMM studies[263,360,366,375]. Furthermore, and unlike studies using systemically administered high-dose nBPs as PTOA therapeutics[309,369,376–382], we found that repeated-i.a.ZA had minimal influence on the subchondral bone structure, and presumably bone remodeling. These findings suggest that ZA's anti-resorptive influences appear to be

largely restricted to calcified tissues within the joint (i.e. the meniscus, ectopic bone, and osteophyte) and do not extend to the calcified cartilage (see Chapter 3) and the subchondral bone.

Since ZA is known to have anti-inflammatory activities on numerous mammalian cells, including those that reside in the synovium, we hoped repeated-i.a.ZA would modulate joint synovitis/inflammation[78,116]. In the present study, we confirmed the rapid appearance (by 7-days) and subsequent persistence of joint synovitis in DMM-injured joints, in agreement with prior murine DMM studies[360,383–385] and PTOA models[338,355–358,386,387]. We are confident that DMM-induced synovitis was predominately an injury-mediated response because sham DMM-surgery induced transient synovitis, which did not persist beyond 7-days (data not shown). Unexpectedly, repeated-i.a.ZA treatment was unable to mitigate DMM-induced joint synovitis; in fact, there was evidence of a transient elevation in synovitis at the earliest timepoint assessed (7-days) following injury and i.a.ZA treatment. This finding conflicts with those of the one other i.a.ZA investigation, which found that repeated-i.a.ZA could suppress joint synovitis in the rat anterior cruciate ligament model of PTOA[259]. The basis of this discrepancy is unclear; however, it is possible that differences in total i.a. dosage (3000 ng/kg per i.a.-injection vs 650 ng/kg presently) or differences in the clearance of the drug from the synovial fluid among differently sized joints could account for this disagreement. It is also possible that our gross-level assessment of synovitis were not refined enough to detect/evaluate the influence of repeated-i.a.ZA on joint inflammation; as we did not investigate changes in resident cell populations and activity, or among fibrotic, angiogenic, or lymphatic responses[388]. Future studies are warranted to identify if i.a.ZA joint synovitis-modifying ability is

subtler in nature or can be improved upon with more frequent injections or at a higher dose. Taken together, our results suggest that the repeated-i.a.ZA strategy is unable to mitigate joint synovitis associated with DMM-injury.

The last goal of this study was to identify if local, i.a.ZA treatment could be leveraged as a PTOA disease-modifying strategy that also minimized the adverse skeletal side-effects (e.g. osteonecrosis of the jaw and atypical femur fracture) that are often associated with high dose, systemic ZA administration[242–245]. In support of this goal, we found that repeated-i.a.ZA administration to DMM-joints had minimal influence on the structure (specifically bone volume and bone volume fraction), and thus remodeling, of bone compartments 'distant' from the joint capsule; including the trabecular bone of the ipsilateral tibial epiphysis and metaphysis. We also confirmed that these bone compartments were unaffected by the DMM-injury alone. Despite detecting no-meaningful influences on the bone structure of trabecular bone in the ipsilateral tibia, future studies are required to identify if ZA cleared from the joint has any impact on the structure and health of skeletal regions known to be sensitive to high-nBPs burden, including the jaw, hip, and vertebrae[242–245,389]. Lastly, it should be noted that our local administration of ZA at a dose of 650 ng/kg per weekly i.a. injection (which equates to an annual dose of ~.032 mg/kg/yr if administered weekly) was drastically reduced when compared to levels demonstrating preclinical efficacy in preventing PTOA when administered systemically (equating to ~5 mg/kg/yr[238–241,309]) and intra-articularly (~2 mg/kg/yr[259]). Together, these data suggest that locally-delivered ZA, when administered weekly over the course of 21-days (4.q7d) following DMM, could prevent the development of cartilage erosions and modify the response

of other joint tissue's in a manner that limits, if not eliminates, concerns over anti-resorptive/anti-remodeling activity of ZA elsewhere in the patient's skeleton.

Similar to our companion paper, the present study is not without its limitations. This work was limited to studying the influence of weekly-repeated i.a.ZA treatment on non-cartilaginous tissues when administered prophylactically over 3-weeks post-DMM. Whether weekly i.a.ZA administration over a longer timescale or with a modified delivery/dosing schedule would lead to different non-cartilaginous tissue responses and/or an increased likelihood of systemic bone-remodeling is unknown and will be the focus of future work. However, to shine a light on this notion, we can turn to our analysis of DMM-joints receiving single individual i.a.ZA treatment, at either 0- or 7-days post-DMM. In DMM-joints receiving single i.a.ZA administration, we saw similar findings in non-cartilaginous tissues compared to those receiving repeated injections (Appendix C Figure C.1-C.5). Given the similarity among these findings, it appears that ZA's influence on non-cartilaginous occurs rapidly upon introduction into the joint space and may only require a single injection to do so. Another limitation that should be considered is that ZA was delivered in the free form, i.e. non-encapsulated, which could alter ZA clearance from the joint space. As a small molecular weight compound (272Da), a substantial portion (~2/3rd's) of each i.a.ZA bolus experienced rapid clearance from the joint (half-life of ~40-minutes for this rapidly cleared component) as determined by *in vivo* imaging of fluorescently-tagged ZA clearance from the naïve, uninjured joint (Appendix C Figure C.6A and C.6B). Such a substantial clearance may appear to represent a limiting factor to therapeutic efficacy. However, and somewhat unexpectedly, the remaining ~1/3rd of the delivered i.a. bolus was retained within the joint over a much-longer timeframe (half-life of ~38-

hours). Furthermore, at 7-days (120-hours) following i.a.ZA injection, macroscopic assessment of dissected joint tissues indicated that fluorescently-tagged ZA could be found within several intracapsular tissues (cartilage, menisci, fat pad, and synovium/capsule; Appendix C Figure C.6C). While these findings were intriguing and the specific location of ZA (i.e whether in tissues extracellular matrix or intracellular) within the joint is unclear, the delivery of ZA encapsulated within controlled/slow-release delivery agents[246,248,249] might represent a way to enhance drug retention and improve the efficacy of i.a.ZA as a PTOA-modifying therapy.

In conclusion, this study demonstrated that repeated-i.a.ZA, while being able to suppress the development of overt, DMM-mediated cartilage erosions following joint injury (see accompanying paper), was unable to prevent the meniscal hypertrophy, ectopic bone formation, osteophyte development, or synovitis associated with joint destabilization injury. However, and consistent with the resorption/remodeling-inhibiting abilities of nBP's, repeated-i.a.ZA administration led to transient delays in the maturation of newly forming meniscal and osteophyte tissues following DMM-injury, as well as driving generalized increases in mineralized tissue/bone volume, and thus bone volume fraction, in the medial meniscus and intracapsular ectopic bone. Furthermore, repeated-i.a.ZA administration was found to exert minimal to no influence on the structure of extra-capsular skeletal tissues (e.g. the subchondral, epiphyseal, and metaphyseal bone of the ipsilateral tibia). This last point is especially important as it suggests that, despite an inability to alter the DMM-mediated changes to non-cartilaginous tissues of the joint, repeated-i.a.ZA was able to prevent the development of overt cartilage erosions in destabilized-joints in a manner that appears to limit systemic inhibition of bone remodeling and minimize the

potential for adverse global skeletal side-effects. Collectively, this investigation and our companion study (Chapter 3) provide compelling data for the continued investigation into i.a ZA's ability to alter the response of joints to injury, and thus prevent PTOA disease initiation and progression.

4.6 Acknowledgments

The authors would like to acknowledge Mr. Frank Warren and Dr. Gwen Talham, DVM for oversight of animal care and the following individuals for technical assistance: Sejal Shah, Brianna Hulbert, Mark Ellsworth, Benedict Maggio, Alexis Merritt, Ryan McDonough, Jon Lowman, Brianna Gietter, Brendan Horne, Srinivasa Gajjala, Christopher Hernandez, Malhar Sakarwala, Pooja Kaiji, Oliva Laxton, Fiona Flowerhill. This work was supported by the Office of the Assistant Secretary of Defense for Health Affairs through the (Peer-Reviewed Medical Research Program) under Award No. W81XWH-13-1-0147. Any opinions, interpretations, conclusions, or recommendations expressed in this material are those of the authors and are not necessarily endorsed by the Department of Defense.

Chapter 5

ZOLEDRONIC ACID'S PLEIOTROPIC EFFECTS ON ATDC5 PROLIFERATION, VIABILITY, MITOCHONDRIA POLARIZATION, CELL CYCLE PROGRESSION, AND CYTOSKELETON ARCHITECTURE IN VITRO

(MA David, B Hulbert, C Price, *In Preparation 2019*)

5.1 Abstract

In search of disease-modifying therapeutics for post-traumatic osteoarthritis (PTOA), our team found that weekly-repeated intra-articular injection of zoledronic acid (ZA) could suppress cartilage erosions in a mouse model of PTOA; via mechanisms that promote chondrocyte proteoglycan production, inhibit chondrocyte proliferation, and modulate chondrocyte death. Despite promising *in vivo* findings, the following critical gaps in our understanding of how ZA interacts with chondrocytes remain: i) whether ZA can directly modulate chondrocyte homeostasis independent of other joint cells/tissues; ii) the mode-of-action of ZA in chondrocytes, and iii) how ZA concentration, timing of exposure, and chondrocyte differentiation status effect ZA-mediated cellular outcomes. Given *a priori* knowledge of the pleiotropic effects of ZA in numerous mammalian cell types, we hypothesized that exposure of ATDC5 cells, a chondrocyte-like cell line, to ZA would modulate proliferation, viability and death, cell-cycle progression, cytoskeleton remodeling, and mitochondria health in a concentration-, exposure-, and differentiation state-dependent manner. Here, we identified that ZA predominately exerted effects on undifferentiated ATDC5 cells. At low ZA concentrations ($\leq 1 \mu M$), ZA did not influence the health of undifferentiated

ATDC5 cells. However, exposure to moderate ZA concentrations (5 and 10µM), ZA i) inhibited cell proliferation (cytostasis) and metabolic activity; ii) caused S-phase cell cycle arrest; iii) depolarized the mitochondria; and iv) altered cell morphology (cell enlargement followed by retraction and rounding) and cytoskeletal architecture (reduced f-actin and microtubule organization). Undifferentiated ATDC5 cells exposed to higher ZA concentrations (50 and 100µM) experienced the same effects, in addition to significate reduction in cell-viability due to caspase 3/7-mediated apoptosis. Lastly, differentiated ATDC5 cells were largely unaffected by low-to-moderate ZA concentrations; however, we observed a slight decrease in cell proliferation, metabolic activity, and viability in these differentiated ATDC5 cells at the highest ZA concentrations. Overall, this study confirmed the ability of ZA to directly influence ATDC5 cell health *in vitro* and supports a continued need to investigate ZA's ability to modulate chondrocytes *in situ* and *in vivo* in the context of cartilage injury and PTOA prevention.

5.2 Introduction

For over two decades, bisphosphonates (BPs), have been used widely to treat bone-related diseases (e.g. osteoporosis and Paget's disease of bone) due to their anti-resorptive and anti-remodeling capabilities[128,245,307]. Since their clinical introduction in the 1970s, bisphosphonates have evolved from initial, low-potency non-nitrogen-containing precursors (e.g. etidronate, clodronate) to the newest generation of nitrogen-containing BPs (nBPs; e.g. alendronate, risedronate, zoledronate), which have increased mineralized matrix binding affinity and potency[128,139,208]. The newer generations of nBPs are classically understood to be potent inhibitors of bone resorption and remodeling because of their high affinity/targeting to the mineralized

skeleton and their ability to mediate osteoclast resorption and apoptosis[128,131,136,139,140,390]. Since aberrant subchondral bone remodeling has also been implicated in the initiation and progression of cartilage degeneration following joint injury[120,126,221,391], preclinical studies have explored the use of third-generation nBPs, like zoledronic acid (ZA), as disease-modifying therapeutics for arthroses, including post-traumatic osteoarthritis (PTOA). Numerous studies have demonstrated that systemically administered ZA can successfully suppress joint inflammation and cartilage damage following joint injury[238–241,309]. However, such studies were performed under conditions of repeated intravenous or subcutaneous, and high concentration ZA administration, therapeutic strategies likely to face significant hurdles to clinical adoption because of increased risks of systemic skeletal and non-skeletal side effects[134,242–245]. Thus, if alternative ZA administration strategies capable of reducing the overall systemic burden of ZA on the skeletal while maintaining PTOA disease-modifying efficacy can be identified, then ZA, and other nBPs, might well represent a step toward the realization of nBPs as an ideal PTOA-modifying therapeutic; one that is cheap, safe, efficacious, and rapidly translatable.

Recently, in studies from our group, and others, utilizing different animal species and PTOA models, a strategy with such promise has been identified: the repeated intra-articular (i.a.) injection of ZA to the joint following injury (Chapter 3 and 4)[259,260]. Collectively, these studies demonstrated that repeated, weekly (q.wk) i.a. injection of ZA into acutely injured knees could suppress the development of injury-mediated articular cartilage erosions, through mechanisms that appeared to involve the ability to modulate of chondrocyte death and proliferation, and that the effects of i.a. injection of ZA were restricted to the intra-capsular tissues of the treated knee and did

not extend to distant skeletal compartments. These studies provided a solid foundation to continue evaluating the potential of i.a. injection of ZA as a disease-modifying therapeutic for PTOA, however the precise mechanisms of action by which local i.a. administration of ZA influenced chondrocyte and cartilage health *in vivo* are unknown.

To unlock ZA's potential mechanisms of action on the cells and tissues implicated in PTOA, particularly chondrocytes, we can turn to the known mechanisms of action of nBPs in other cells of the musculoskeletal system. In its canonical cellular target, osteoclasts, ZA (and all nBPs) inhibits the mevalonate (isoprenoid) biosynthetic pathway resulting in inhibition of bone resorption, reduced osteoclastogenesis, and increased osteoclast apoptosis[134,143–147], which have predictable consequences on skeletal remodeling *in vivo*. More recently, ZA has been shown to have the ability to influence a variety of musculoskeletal cells of mesenchymal origin as well, including osteoblasts[128,144,157–163] and osteocytes[128,159]. Interestingly, the effect of ZA on these cells appears biphasic; lower ZA concentrations (<1µM) promote for cell survival, whereas higher ZA concentrations (≥10uM) tend to be anti-proliferative and induce cell death.

Outside of the musculoskeletal system, ZA has been shown to influence a wide variety of cell/tissue types. For instance, in cancer models, ZA can alter cell-cycle progression, influence mitochondria health and cytoskeleton organization, and drive anti-proliferative and pro-apoptotic activities[131,162,196–205,188,206–208,189–195]. ZA can also modulate the behavior and health of vascular smooth muscle cells[164,165], vascular endothelial cells[166–169], epithelia cells[170–173], kidney cells[174], stromal cells[175], fibroblasts[172,173,176,177], regulatory T-cells[178], monocytes[179–181], and macropages[181–186].

In all of these cells, as in all eukaryotic cells, the effects of ZA, and other nBPs, on cell function are mediated by inhibition of the ubiquitous mevalonate, also known as isoprenoid, biosynthetic pathway[136,344]. This pathway is critical in two specific cellular processes; i) the synthesis of cholesterol, and ii) the post-translation modification of a protein by prenylation, the covalent addition of hydrophobic lipids to protein substrates. More specifically, nBPs inhibit the farnesylation and geranylation of small GTPases; which are essential for regulating numerous cellular activities, including protein targeting, cell function, intercellular signal transduction, cytoskeleton architecture[136]. Given this body of evidence, it is reasonable to posit that ZA could directly influence chondrocytes as well, since they, like all mammalian cells, rely on cell processes downstream from the mevalonate pathway for mechanotransduction[392–395], homeostasis[396], and cell survival[397]. While the limited extent of research investigating the effects of earlier generation non-nBPs and other nBPs on chondrocytes has been conducted[187,254,398–401], our mechanistic understanding of the influence of nBPs, like ZA[254,400], on chondrocyte behavior lags far behind our knowledge of how they influence other cell types of the musculoskeletal system and body.

Therefore, the objective of this study was to determine the concentration- and exposure-dependent effects of ZA on chondrocyte health and function *in vitro*; we focused our attention on ZA's effect on cell proliferation, viability, metabolic activity, cell cycle progression, mode of cell death, mitochondria health, and cytoskeleton architecture. In this study, the well-established ATDC5 chondrogenic murine cell-line was utilized[402–404]; this enabled us to isolate ZA's effect on ATDC5 cells in both undifferentiated and differentiated states, which mimic the different proliferative

capacities and differentiation stages chondrocytes have *in vivo*. The findings presented herein mirror those observed in other cell types demonstrating that ZA has direct, concentration- and exposure-dependent pleiotropic effects on chondrocytes.

5.3 Methods

5.3.1 Cell Culture

Undifferentiated chondrogenic ATDC5 cells (Sigma-Aldrich) were subcultured on standard culture flasks in culture medium (CM) consisting of a 1:1 mixture of high-glucose DMEM and Ham's F12 (CaissonLabs), 5% fetal bovine serum (Fisher Scientific), and 1% Penicillin-Streptomycin (CaissonLabs) at 37°C and 5% CO_2. At passage numbers P12-14, undifferentiated ATDC5 cells were plated into tissue-treated 96-well plates (Greiner CELLSTAR µClear; Greiner Bio-One) at 7,500 cells/cm^2 and cultured for 24hrs before the initiating experiments described below were initiation. To differentiate ATDC5 cells, the CM was supplemented with 1% ITS^+ Premix (Corning) and the cells were cultured for two or three weeks to permit differentiation into a more 'chondrocyte-like' phenotype; differentiation media was changed every other day, and differentiation was confirmed visually with Alcian Blue (Sigma-Aldrich) staining for proteoglycan depositiont[402,403].

Zoledronic acid monohydrate (Sigma-Aldrich) stock solutions were prepared at 3.33 mg/ml in sterile 1x phosphate buffered saline (Fisher Scientific). All subsequent dilutions of ZA were made serially into fresh CM or CM with 1% ITS^+ Premix to final concentrations of 1000, 500, 100, 50, 10, 5, 1, 0.5, and 0.1µM.

5.3.2 Experimental Designs

Experiments utilizing undifferentiated and differentiated (2 and 3wks) ATDC5 cells are summarized in Figure 5.1. Briefly: i) in experiment 1, we sought to identify the concentration-dependent effect of continuous (72-hours) ZA exposure on the proliferation, viability, and metabolic activity; ii) in experiment 2, we investigated the same outcomes at intermediate times, following either 12, 24, 48, and 72-hours of culture in the continuous presence of ZA; iii) in experiment 3 we performed a pulse-chase experiment to define the minimal ZA exposure time (1, 2, 6, 16, 24, 48, 72-hours) required to observe changes in proliferation, viability, and cell cycle progression; iv) in experiment 4, we investigated the effect of continuous vs. pulse-chase exposure of ZA on caspase-3/7-mediated apoptosis; and lastly v) we investigated the influence of ZA concentration and exposure on mitochondria polarization/health and on cytoskeletal architecture/remodeling. For pulse-chase experiments, cells were washed twice with CM following their exposure to ZA and then cultured out to the 72-hour timepoint in fresh CM. We performed experiments 1 through 5 on undifferentiated ATDC5 cells, and subsequently repeated experiments 1 through 3 on differentiated cells (2 and 3wk).

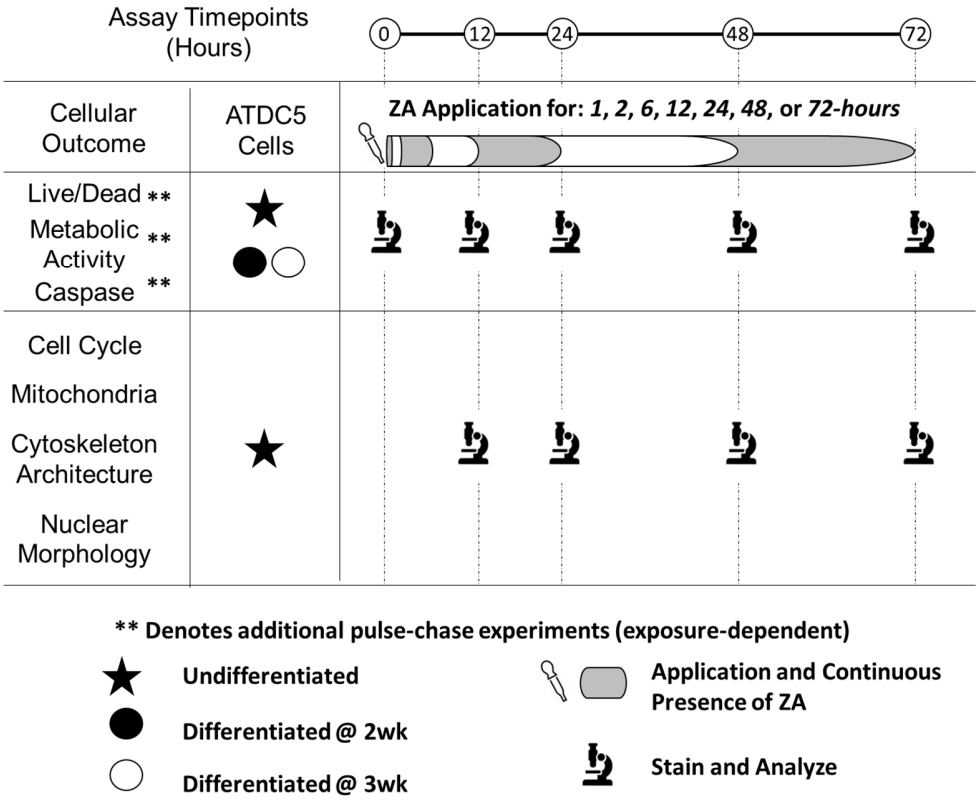

Figure 5.1: General Timeline and Schematic of Cellular Assays and Outcomes Performed. ATDC5 cells were used in an undifferentiated and differentiated (2 and 3wk) state for cellular outcomes at the indicated time points and following various exposure times of ZA.

5.3.3 Assessment of Proliferation and Viability via Live/Dead Assay

Live/dead assessment, in combination with custom image-analysis, was used to evaluate ATDC5 proliferation (via total cell counts) and viability. At indicated time points (Figure 5.1), ATDC5 cells were stained simultaneously with Calcein AM (1µM; ThermoFisher Scientific – eBioscience), propidium iodide (PI; 5µM; Sigma-Aldrich), and Hoechst 34580 (1:2000 dilution of 5 mg/ml; ThermoFisher Scientific) in Opti-MEM (ThermoFisher Scientific) for 1hr at 37°C and 5% CO_2 to identify live

cells, dead/injured cells with compromised cell membranes, and cell nuclei/nuclear morphology, respectively. After staining, each well was immediately imaged at 5- and 10x on a using an epifluorescent microscope (Axio.Observer.Z1, Carl Zeiss, Thornwood, NY) and a digital camera (AxioCam MrC, Zeiss). Images were then exported to MATLAB (MATLAB R2015a, The MathWorks, Natick, MA) for automated image-processing to determine the number of i) total cells present (Hoechst-positive; $Hoechst^{+}$) and ii) dead cells (PI-positive; PI^{+}).

5.3.4 Assessment of Metabolic Activity

The population-level metabolic activity of ATDC5 cells was quantified via an Alamar Blue (resazurin-based) assay (alamarBlue™ Cell Viability Reagent; Thermo Fisher Scientific). In this assay, CM was removed and replaced with 150µL of CM + 1x Alamar Blue solution for 3hrs at 37°C and 5% CO_2. The reaction solution was then removed, placed into an empty 96-well plate (EW-01927-76; Cole-Parmer), and its fluorescence (excitation 560nm; emission 590nm) was immediately measured on a microplate reader (Synergy H1; BioTek).

5.3.5 Analysis of Cell Cycle Progression

Cell cycle progression was quantified in undifferentiated ATDC5 following ZA administration using both flow cytometry and image-based techniques. Cell cycle analysis herein is dependent upon the following assumptions: i) the fluorescent live-cell nuclear stains, i.e. Hoechst and Draq5, bind selectively to A-T grooves in DNA; ii) binding of these nuclear stains, and thus their resultant nuclear fluorescent intensity, is proportional to the amount of DNA present in a cell; iii) cells in G1/G0 have 2N chromosomes (and thus n_{DNA}), those in G2/M have 4N chromosomes ($2n_{DNA}$), while

those in S-phase have between 2N and 4N chromosomes ($n_{DNA} < x < 2n_{DNA}$); and iv) the Watson-Pragmatic model[405] can be used to curve fit DNA intensity histograms resulting from either flow cytometry or cell-based image analysis.

For flow-based analysis, cells were stained with Draq5 (15 µM; Thermo Fisher Scientific) in Opti-MEM for 40 minutes at 37°C and 5% CO_2. Cells were then suspended by trypsination, transferred to an empty 96-well plate on ice and then run through the flow cytometer (NovoCyte Flow Cytometer; ACEA Biosciences). Gating and cell cycle curve fitting was performed using built-in software (NovoExpress Software, ACEA Biosciences). Following cell gating, the nuclear intensity as a function of counts/events were plotted and then fitted using the Watson-Pragmatic curve fitting algorithm to extract the percentages of cells in each cell cycle stage: G1/G0, S, G2/M, subG1, and super-G2. For all curve fitting, the G2/G1 ratio was constrained to 2 (based upon the assumptions described above) while the remaining parameters remained unconstrained for curve fitting optimization (G1 and G2 peaks and width distribution [CV]).

For microscopy-based cell cycle analysis, we implemented in MATLAB a recently developed image-based technique utilizing an object detection and profiling framework to determine cell cycle stage based upon nuclear stain intensity[406–408]. Briefly, in each image, every cell nucleus was detected and the total fluorescent intensity within each nucleus was extracted. Intensity data for all cells in a single image were exported and processed through the flow cytometry curve fitting algorithm to extract the percentages of cells in each cell cycle stage, as described in the description above of flow-based cell cycle analysis. Changes in nuclear morphology in response to ZA were further evaluated using low-(5x magnification) and super-

resolution (63x structured illumination microscopy) images of Hoechst stained cells acquired on an epifluorescent microscope (Carl Zeiss AxioObserver.Z1) equipped with an Apotome.2 structured-illumination microscopy unit.

5.3.6 Apoptosis Detection via Caspase-3/7 Staining

The influence of ZA on the apoptosis of both was assessed using a fluorescent probe for caspase 3/7 activity. Cells were stained in CellEvent Caspase 3/7 reagent (5µM; Thermo Fisher Scientific) + PI (5µM) + Hoechst (1:2000 dilution) in Opti-MEM solution for 1hr at 37°C and 5% CO_2. After staining, images were captured in the center of each well at 10x magnification using the aforementioned epifluorescent microscope. Images were subjected to automated image-processing in MATLAB to determine the number of i) total cells present ($Hoechst^+$), ii) dead cells (PI^+), iii) cells undergoing apoptosis with intact cell membrane ($caspase^+$ only), and iv) cells considered late-stage apoptotic with compromised cell membrane ($caspase^+$ and PI^+).

5.3.7 Mitochondria Polarization/Health

ZA's influences on mitochondria health in undifferentiated ATDC5 cells was assessed using the mitochondrial polarization probe JC-1 (MedChemExpress). The JC-1 dye is unique in that it is fluorescent state can be used to identify the polarization, and thus the health, of mitochondria. JC-1 accumulates in healthy polarized mitochondrial resulting in the presence of punctate, red-fluorescent aggregates due to the fluorescent kinetics of the probe; mitochondrial depolarization leads to the leakage of JC-1 from the mitochondria and a resultant shift in probe distribution (diffuse in cytoplasm) and an increase in green-shifted fluorescent emission. After staining with JC-1 (5µM in phenol-red free DMEM) for 1-hour at 37°C and 5% CO_2, cells were

washed, and then either imaged at 20x magnification on the aforementioned epifluorescent microscope or processed for flow cytometry analysis as described above. Carbonyl cyanide 3-chlorophenylhydrazone (CCCP; Sigma-Aldrich) exposure for 30-minutes or 1-hour at both 10 and 100µM served as a positive control for mitochondria depolarization; CCCP is a mitochondrial protonophore and a known disrupter of the mitochondria membrane potential. Due to spectral discrimination limitations with the JC-1 dye and our flow cytometer[409], we only evaluated the relative shift in JC-1 green monomer intensity, representing an increase in mitochondrial depolarization in cells analyzed by flow cytometry.

5.3.8 Cytoskeleton Staining for Actin (F-Actin) and Microtubule (Alpha-Tubulin)

Immunocytochemistry was utilized to evaluate changes in actin and microtubule organization in undifferentiated ATDC5 following ZA administration (Figure 1). Cells were fixed for 15-minutes in 4% paraformaldehyde (Electron Microscopy;), washed, permeabilized for 5-minutes in 0.1% Triton X-100 (Fisher), then simultaneously stained for 1-hour in 1% bovine serum albumin with an AlexaFluor 555-conjugated phalloidin (5 µg/mL; ThermoFisher Scientific) for F-actin, an Alexa Fluor 488-conjugated alpha-tubulin primary antibody (5 µg/mL; DM1A; ThermoFisher Scientific) for microtubules, and Hoechst (1:2000 dilution) for nuclei detection. Following staining, cells were imaged on the aforementioned super-resolution at 63x magnification.

5.3.9 Statistical Analysis

Data was collated in MATLAB and Microsoft Excel, and statistical analysis was performed using GraphPad Prism 6.0. All assays were repeated on ATDC5 cells

from passages 12, 13, and 14 in triplicates. In order to identify significant differences between untreated and ZA treated cells in each assay, two-way ANOVA with Tukey post-hoc was performed; the threshold for statistically significant differences was set at $p < .05$.

5.4 Results

5.4.1 Effects of ZA Concentration on ATDC5 Cell Number Expansion, Viability, and Metabolic Activity

To establish how continuous ZA administration influence the behavior of undifferentiated and differentiated ATDC5 cells, we first evaluated the effects of 72-hours of continuous ZA exposure on cell proliferation and viability (Figure 5.2). Qualitatively at 72-hours and in the absence of ZA, undifferentiated ATDC5 cells had spread to cover the majority of their wells (~95% confluency) and exhibited very-high viability, whereas differentiated cells were present as a confluent mat that exhibited a basal level of cell viability (Figure 5.2A). In undifferentiated ATDC5 cells, reductions in cell number and viability at 72-hours were observed as ZA concentration increased, and the overall size of the cells enlarged dramatically. In differentiated ATDC5 cells, ZA had far less pronounced effects after 72-hours of exposure with only 100µM being able to (slightly) reduce cell viability. We quantitatively confirmed these observations by demonstrating that undifferentiated ATDC5 cells exhibited significant concentration-dependent reductions in relative cell number (ratio of total cells in an individual experimental [treated] to their control [untreated] group), relative metabolic activity, and cell viability (Figure 5.2B). In undifferentiated ATDC5 cells, ZA drove concentration-dependent reductions in cell viability, but only at ~10-fold higher ZA concentrations (IC_{50} = 45.39µM) than those that drove reductions in cell number

expansion and relative metabolic activity (IC_{50} = 3.673μM & 6.497μM, for 'proliferation' and metabolic activity, respectively).

In ATDC5 cells differentiated for 3-weeks, ZA did not markedly affect cell number, metabolic activity, or cell viability at any of the ZA concentrations we tested (up to 100μM in all cells). However, in cells that only underwent 2-weeks of differentiation, we observed reductions in cell number, metabolic activity, and most appreciably, cell viability at high ZA concentrations (≥50μM). In a subset of undifferentiated ATDC5 cells and cells differentiated for 3-weeks, we evaluated the effect of supraphysiologic ZA concentrations (500 and 1000μM) on cell number, viability, and metabolic activity and found comparable findings on these cells to those driven by ZA at concentrations of 50 and 100μM. Thus, for the remainder of the study, we restricted our investigations to the use of a maximal ZA concentration of 100μM.

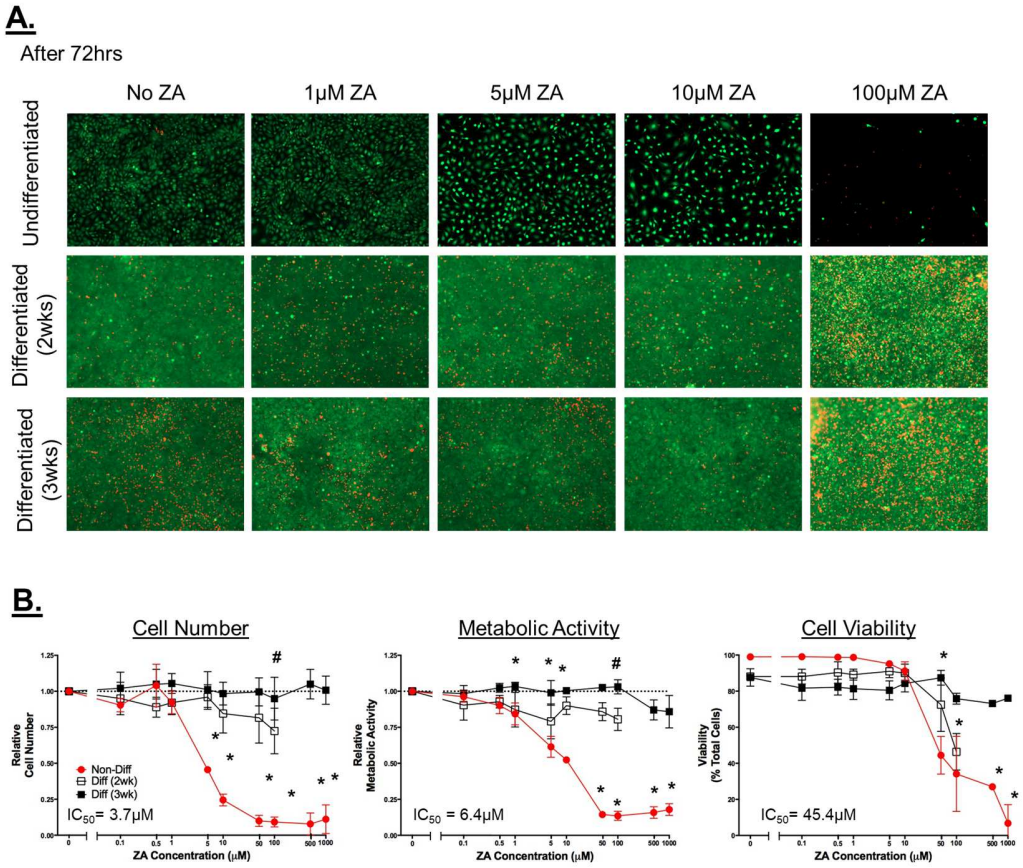

Figure 5.2: Continuous Administration of ZA Concentration-Dependently Decreased Cell Number Expansion, Viability, and Metabolic Activity in Undifferentiated ATDC5 Cells. (A.) Representative images of live/dead staining in undifferentiated and differentiated (2 and 3-week) ATDC5 cells after 72-hours of continuous ZA highlight concentrations ≥5μM decrease cell number and viability in undifferentiated cells; differentiated cells were only susceptible to ZA at concentrations 100μM. (B.) Quantitative analysis confirms the reduction in cell number expansion, viability, and metabolic activity. Differentiated cells at 3-weeks were mostly unaffected by any concentration, except at the supraphysiological levels of ≥500μM. Results are presented as mean ± STD (n=3/concentration/cell type/timepoint) where $p < 0.05$ and significance between the respective cell and concentration relative to no ZA denoted with * and # for undifferentiated and 2-week differentiation, respectively.

5.4.2 Influence of Length of Continuous ZA Exposure on ATDC5 Cell Number Expansion, Viability, and Metabolic Activity

Next, we explored the time-course of the observed concentration-dependent changes in cellular outcomes by evaluating the effect of continuous ZA (concentrations ≥5μM) after 12, 24, 48, and 72-hours of ZA exposure in a separate set of undifferentiated and differentiated (2wk) ATDC5 cells (0-hour, and untreated cells served controls). Findings from the 72-hour ZA exposure assessments in this data set confirmed the observed reductions in cell number, metabolic activity, and viability established in our preceding experiment (Figure 5.3A and 5.3B). Next, we observed that the minimal ZA exposure time required to drive specific cellular outcomes, i.e., reduced relative cell number, metabolism, or viability, was dependent upon the concentration of ZA. For example, at higher concentrations (≥50μM), only 24-hours of ZA exposure was required before significant suppression of cell number, metabolic activity, and viability could be observed in undifferentiated cells, while at lower concentrations (5 and 10μM) a full 72-hours of ZA exposure was required to drive statistically-meaningful reductions in outcomes in undifferentiated ATDC5 cells. In ATDC5 cells differentiated for 2-weeks, we saw that the only ZA concentration and exposure to explicit a meaningful effect was 100μM for 72-hours; which again only drove a significant reduction in cell viability (Figure 5.3B).

From this experiment, we also extracted information regarding ATDC5 proliferation in the presence of ZA by tracking relative changes in cell numbers (i.e. fold-change) amongst our groups over 72-hours. In undifferentiated ATDC5 in the absence of ZA, the population doubling time, based upon assessment over 72-hours, was ~12-16 hours (consistent with previously reported results[402]). In the presence of ZA concentrations ≤1μM, the extent, and thus rate, of population doubling

(proliferation) over 72-hours, was similar to that of untreated cells. However, cell number expansion and proliferation were significantly suppressed at 5 and 10μM and completely abolished at higher concentrations (≥50μM) (Figure 5.3B). In cells that had undergone the 2-week differentiation, cell number expansion (proliferation) is almost absent in untreated cells, and thus ZA had no appreciable effect on this index (Figure 5.3B).

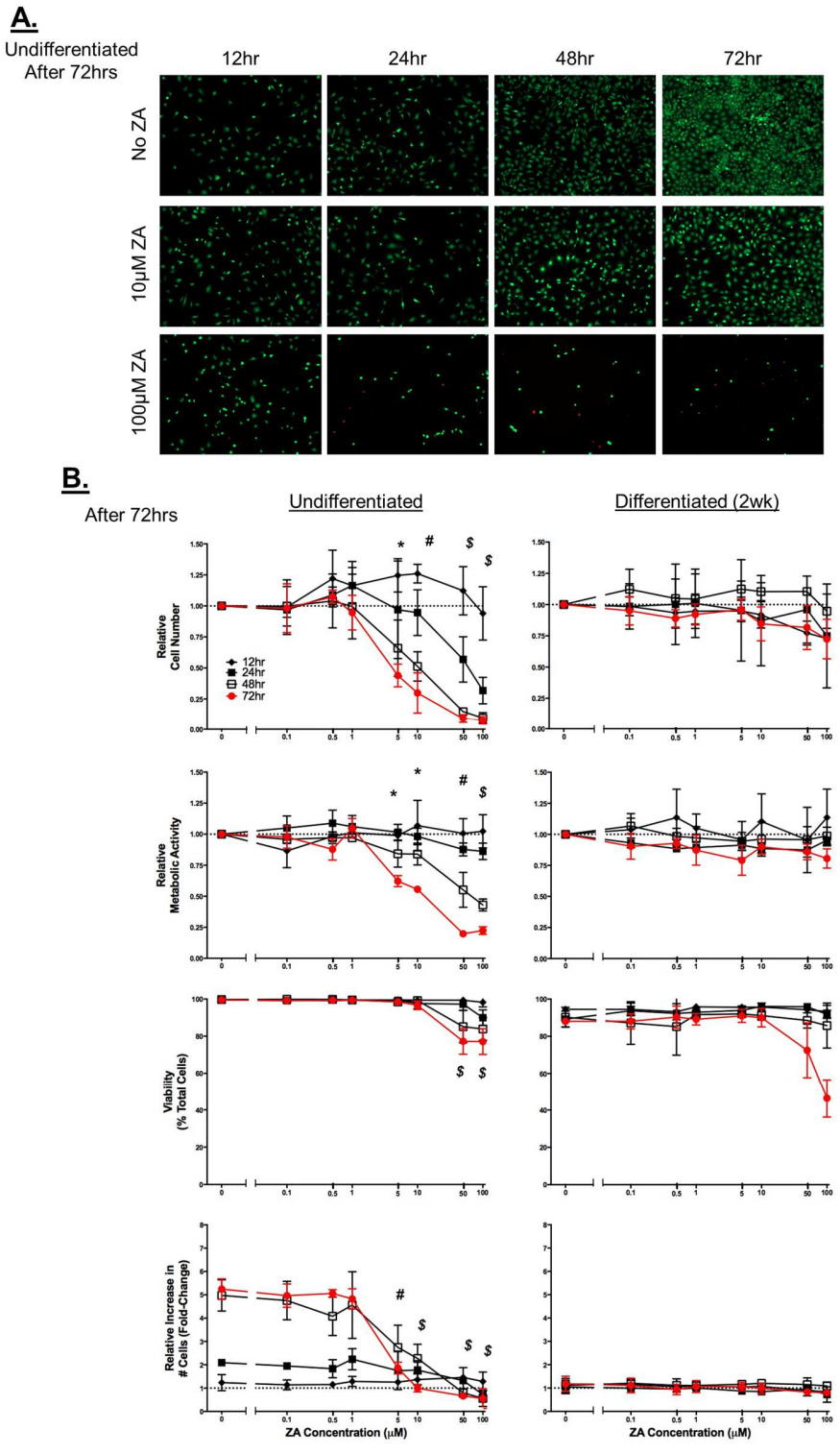
A.
Undifferentiated
After 72hrs
12hr
24hr
48hr
72hr
No ZA
10μM ZA
100μM ZA
B.
After 72hrs
Undifferentiated
Differentiated (2wk)
Relative Cell Number
Relative Metabolic Activity
Viability (% Total Cells)
Relative Increase in # Cells (Fold-Change)
12hr
24hr
48hr
72hr
ZA Concentration (μM)
ZA Concentration (μM)

Figure 5.3: Continuous Administration of ZA Exerted an Exposure-Dependent Decrease in Cell Number Expansion, Viability, and Metabolic Activity in Undifferentiated ATDC5 Cells. (A.) Representative live/dead images of undifferentiated ATDC5 cells demonstrate that 10μM of ZA can affect cell heath and function as early as 48-hours, whereas effects at 100μM are seen as early as 24-hours. (B.) Quantitative analysis highlights that by 48-hours lower concentration of ZA (5 and 10μM) effects on cell proliferation, viability, metabolic activity, and fold increase, while higher concentrations (≥50μM) have observable effects by 24-hour. Differentiated (2wk) cells were confirmed to require the full 72-hours to observe minimal effects with 100μM. Results are presented as mean ± STD (n=3/concentration/cell type/timepoint) where significance of $p < 0.05$ between respective concentration vs no ZA is indicated by * for only at 72-hour; $ for all time ≥24-hour; and # for all time ≥48-hour.

5.4.3 Long-term Effects of Short-term ZA Exposure on Cell Number Expansion, Viability, and Metabolic Activity in Undifferentiated ATDC5 Cells

To further explore ZA's ability to modulate the health and function of undifferentiated ATDC5, we performed pulse-chase experiments (consisting of a short ZA exposure followed by washout and continued culture out to 72-hours) to study the effect of short-term ZA exposure on long-term cellular outcomes. In this third set of data, we again confirmed a consistent, concentration-dependent effect of 72-hours of continuous exposure to ZA on cell number expansion and cell viability in undifferentiated ATDC5 cells (Figure 5.4A and 5.4B). Visually, we saw that ZA concentrations ≥10μM caused marked long-term (at 72-hours) changes in cell number and shape with as little as 2-hours of exposure (Figure 5.4A). These qualitative impressions were confirmed by significant reductions in cell numbers at 72-hours following early and brief exposure of the cells to ≥10μM ZA for 2-hour. For ZA concentrations ≥50μM significant long-term effects were observed with as little as 1-hour of exposure; while at 5μM concentration, only 72-hours of exposure drove

statistically significant changes in cell number outcomes. Regarding cell viability, only exposure to ZA concentrations ≥50μM demonstrated the ability to significantly reduce long-term cell viability; at 50μM a minimum of 12-hours exposure was required, while for 100μM 6-hours was needed.

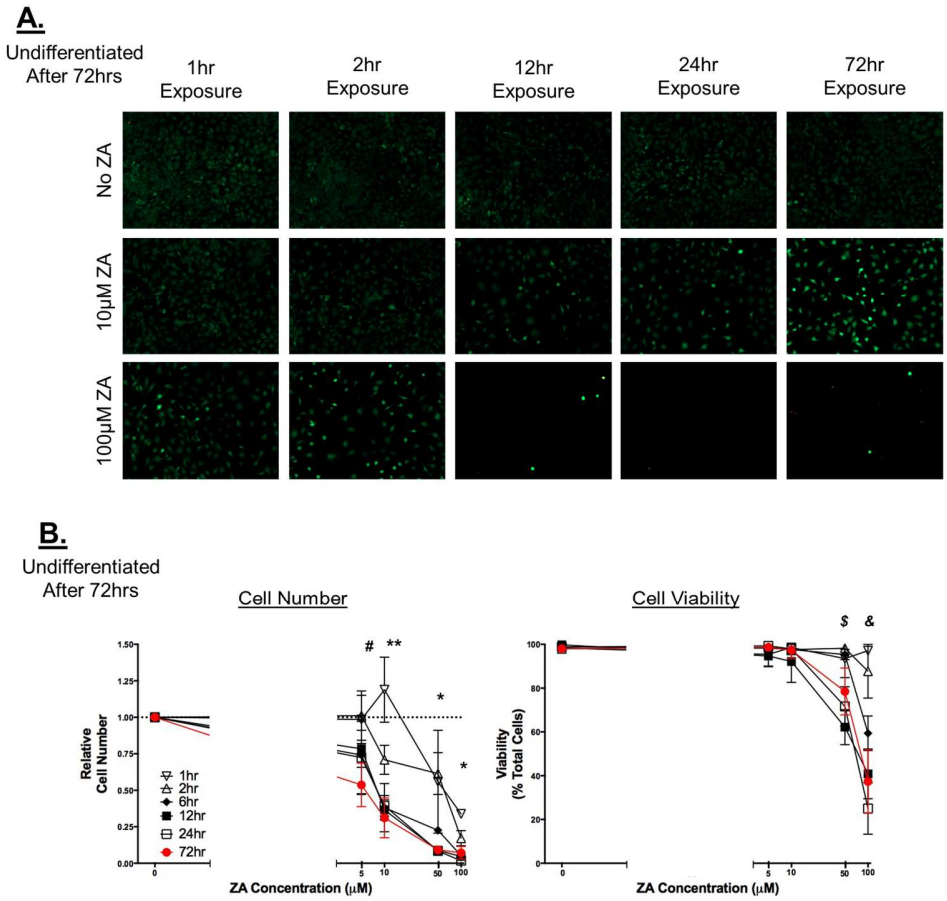

Figure 5.4: Short and Long-Term ZA Administration Exerted an Exposure-Dependent Decrease in Cell Number Expansion and Viability in Undifferentiated ATDC5 Cells. (A.) Representative live/dead images of undifferentiated ATDC5 cells demonstrate that 10µM of ZA can affect cell health and function as early as 48-hours, while effects at 100µM occur as early as 24-hours. (B.) Quantitative analysis highlights confirm these observations and show that 5µM requires the entire 72-hours of application to have effects, whereas the concentration of ≥10µM only needs to be present for a minimum of 2-hours and only 1-hour for ZA ≥50µM. Results are presented as mean ± STD (n=3/concentration/cell type/timepoint) where significance of $p < 0.05$ between respective concentration vs no ZA is indicated by # for only at 72-hours; $ for all time ≥12-hour; & for all time ≥6-hour; ** for all time ≥2-hour; and * for all time ≥1-hour.

5.4.4 ZA Induces S-Phase Cell Cycle Arrest in ATDC5 Cells

Cell cycle progression in undifferentiated ATDC5 cells subjected to 72-hours of ZA administration was assessed next using both flow cytometry and image-based approaches. Flow-based cell cycle analysis of undifferentiated ATDC5 cultured in the absence of ZA for 72-hours revealed that ATDC5 cells were predominately found in the G1/G0 phase of the cell cycle; the population-level phase breakdown was: ~60% G1/G0, ~30% S-phase, and ~5% each in G2/M, subG1, and superG2 (Figure 5.5). Exposure of undifferentiated ATDC5 cells to ZA concentrations ≥10µM lead to a marked increase (shift) in the percentage of cells arrested in S-phase (~50-60%), and a significant reduction of those in G1/G0 (~20%) (Figure 5.5A and 5.5B). An image-based approach using adhered ATDC5 cells confirmed our flow cytometry results regarding ZA exposure- and concentration-dependent S-phase arrest in undifferentiated ATDC5; this allowed us to rule out possible interaction between ZA administration and flow-cytometry preparation procedures on cell cycle outcomes in undifferentiated ATDC5 (Appendix D Figure D.1).

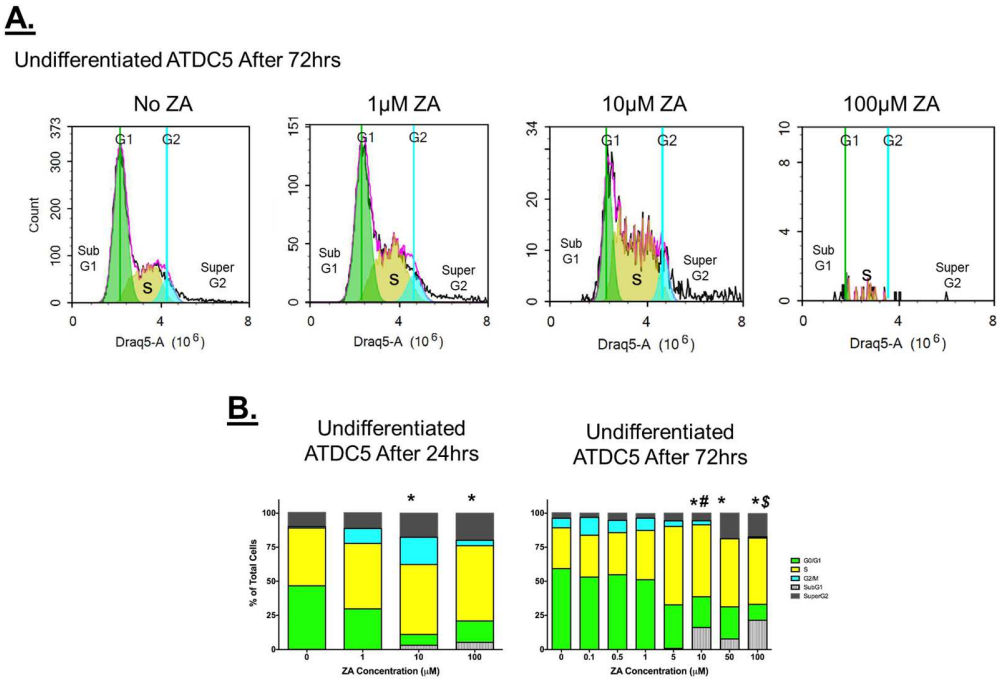

Figure 5.5: Continuous ZA Administration Concentration-Dependently Arrested Undifferentiated ATDC5 Cells in S-Phase of the Cell Cycle. (A.) Representative Draq5 area intensity histogram and resulting curve-fit for cell cycle stage at 72-hours in undifferentiated ATDC5 cells is shown and was used to extract the percentages of cells in either G1/G0 (green), S (yellow), G2/M (blue); subG1 (left of G1) and superG2 (right of G2) are not color coded. As highlighted, with increasing ZA concentration cells arrest in S-phase (increase in yellow), and a minimal number of cells/events is detectable in 100μM due to being washed away during sample preparation. (B.) Quantitative analysis of the resulting histogram and curve fits for each concentration at 24 and 72-hour confirms our qualitative observation S-phase arrest with increasing ZA and provides additional measurement on the increased percentage of cells in subG1 (apoptotic) and superG2 (polyploid) with increase ZA concentration. Results are presented as mean ± STD (n=3/concentration/cell type/timepoint) where * indicates $p < 0.05$ between respective concentration vs no ZA at G1/G0; # indicates S-phase; % indicates G2/M; $ indicates subG1; and & superG2.

5.4.5 Effect of ZA Exposure on ATDC5 Apoptosis

To investigate whether activation of apoptosis is associated with the apparent cell death seen as ZA concentration and exposure increase, we used a fluorescent caspase-3/7-activity probe (green) and propidium iodide (PI; a red-fluorescent probe of dead/dying cells with compromised plasma membranes) to assess apoptosis and generalizable death, respectively. Visually, 72-hours of ZA administration caused a concentration-dependent increase in the presence of dead cells (PI^+; red), those actively undergoing apoptosis (caspase-$3/7^+$; green; circled), and dual-stained cells (PI^+ and caspase-$3/7^+$) that we suspect are in the late-stages of apoptosis (Figure 5.6A). These impressions were confirmed via quantitative image analysis (Figure 5.6B and 5.6C). However, we again observed that only ZA concentrations ≥50µM were able to drive significant increases in cell death over the 72-hour timeframe investigated. Looking at the time-dependent evolution of this cell-death, we observed that following 24-hours of continuous ZA administration, changes in cell death (increased PI^+ and dual-stained [PI^+ & caspase-$3/7^+$] cell presence) were only observed under 100µM ZA. As ZA-exposure time increased out to 48-hours the percent of PI^+ (dead cells) and dual-stained cells increased significantly under both 50 and 100µM ZA, while a slight, non-significant increase in caspase-$3/7^+$ (apoptotic) cell-staining was seen under 100uM ZA. Following 72-continuous-hours of ZA exposure, the PI^+ (dead) cell percentage continued to increase at 50 and 100µM ZA, while percentage of caspase-$3/7^+$ (apoptotic) cells increased slightly and the percent of dual-labeled cells subsided; ultimately resulting in 70 to 90% of ATDC5 cells exposed to 50- and 100µM for 72-hours exhibiting a marker of one form or another for cell death.

We also investigated the effect that short-term ZA exposure (1, 2, 6, 12, 24, and 72-hours) could have on cell death and caspase-3/7-mediated apoptosis in a

separate set of 72-hour-long pulse-chase experiments. Again, we confirmed that ZA could induce cell apoptosis and death when present at 50 and 100μM for 72 continuous hours (Figure 5.6C). At ZA concentrations ≤10μM, ZA had no meaningful influence on ATDC5 cell death or apoptosis under any of the conditions tested. However, at ZA concentrations of 50 and 100μM very-brief exposure of cells to ZA could have a drastic impact on apoptosis and cell death. Exposure of cells to 50μM ZA for as little as 6-hours could drive markedly, albeit not statistically significant, elevated apoptosis and cell death; processes that increase to achieve statistically significant levels following ≥24-hours of exposure. In the presence of 100μM ZA, marked, but again, not statistically significant, increases in apoptosis and cell death were seen with as brief as a 1-hour exposure.

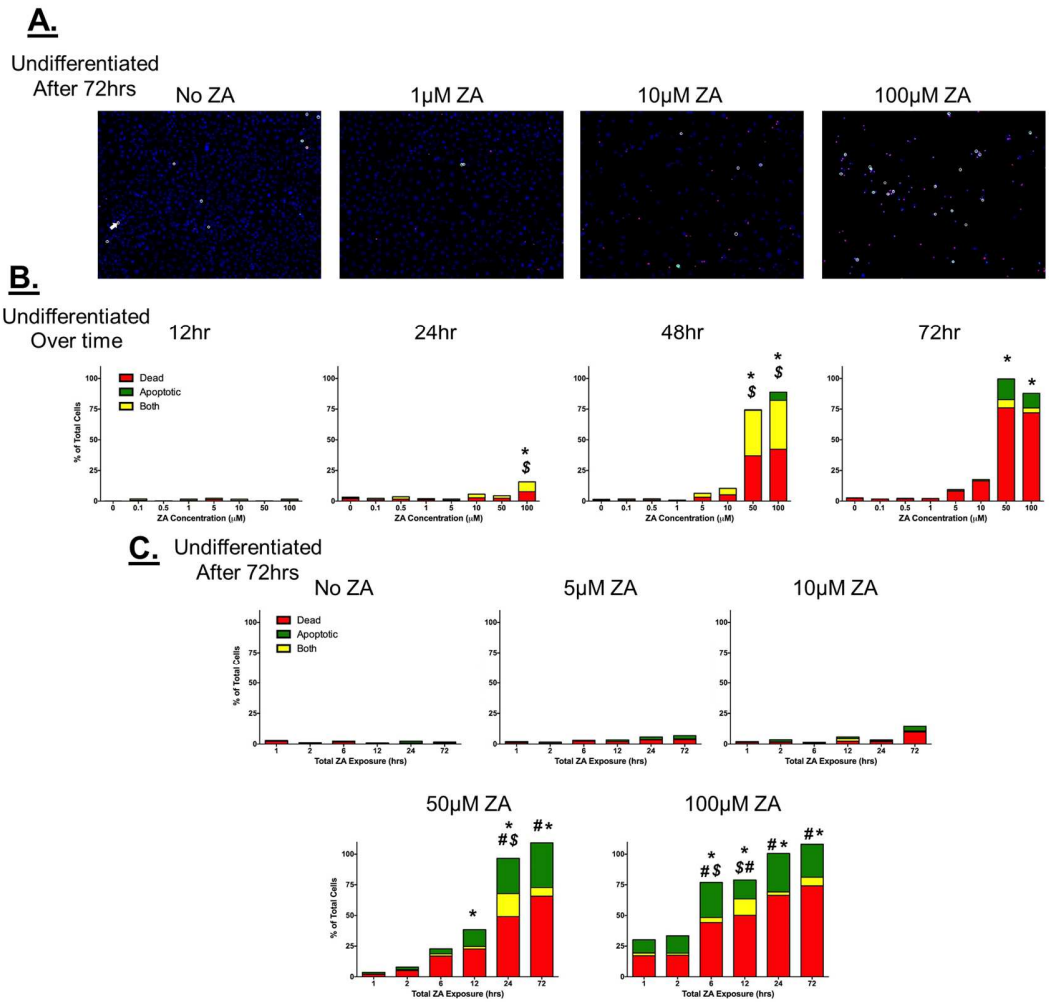
A.
Undifferentiated
After 72hrs
No ZA
1μM ZA
10μM ZA
100μM ZA
B.
Undifferentiated
Over time
12hr
24hr
48hr
72hr
Dead
Apoptotic
Both
% of Total Cells
ZA Concentration (μM)
C.
Undifferentiated
After 72hrs
No ZA
5μM ZA
10μM ZA
50μM ZA
100μM ZA
Total ZA Exposure (hrs)

Figure 5.6: ZA Exerted a Concentration- and Exposure-Dependent Increase in Caspase 3/7-Mediated Apoptosis in Undifferentiated ATDC5 Cells. (A.) Representative 10x magnification images at 72-hours highlighting the total cells (Hoechst+) and a general concentration-dependent increase of dead (PI+ only; red), undergoing apoptosis (caspase-3/7+; green; circled) or late-stage apoptosis (PI+ and caspase-3/7+; red+green; circled), after continuous ZA administration demonstrate that cells undergo death over time. (B.) Quantitative analysis confirms these qualitative observations and provides additional information regarding the time-dependent effects of this caspase-3/7 activation and death that occur as early as 24-hours with ZA concentrations ≥50µM. Further, late-stage apoptosis is observed largely at 48-hours and then diminishes by 72-hours with the highest concentrations. (C.) Quantitative analysis highlights activation of caspase-3/7-mediated cell death occurring at high concentrations after 72-hours with a minimum of 24-hour exposure time. Similar outcomes are observed if ZA at concentrations ≥50µM Results are presented as mean ± STD (n=3/concentration/timepoint/exposure) where * indicates $p < 0.05$ between concentration vs no ZA for dead cells; # for apoptotic; and $ for dual staining (late-stage apoptosis).

5.4.6 ZA Induces Mitochondria Depolarization in Undifferentiated ATDC5

The JC-1 mitochondria probe was used to assess the influence of ZA on mitochondria potential in undifferentiated ATDC5 cells at 12, 24, and 48-hours following ZA administration. In the present study, mitochondria dysfunction (MD) was defined experimentally, based upon the response of JC-1 loaded cells to exposure to the mitochondrial protonophore CCCP (positive control). Under normal conditions, undifferentiated ATDC5 cells with normal mitochondrial function exhibit very-low basal-levels of green JC-1 (monomer) fluorescent intensity and punctate, highly-intense red JC-1 (aggregate) intensity, as seen visually and via flow cytometry (Figure 5.7A, 5.7B, and 5.7C). With CCCP addition to healthy cells, a drastic decrease in red channel ‘punctate mitochondrial staining’ occurs and an increase in diffuse green monomer presence and fluorescent intensity can be seen throughout the cytosol. This

results in a shift in the overall green-channel fluorescence of individual toward values $\geq 1x10^5$ when assessed via cytometry. Thus, we choose to define mitochondria depolarization/dysfunction (MD) as the condition when the green JC-1 fluorescent values of an individual cell are $\geq 1x10^5$. In this study, it was clearly observable that ZA causes mitochondria depolarization in a concentration and exposure-dependent manner in undifferentiated ATDC5 cells (Figure 5.7B-5.7D); as little as 48-hours of exposure to 10µM ZA was able to induce statistically significant increases in mitochondria depolarization (Figure 5.7D), and as little as 24-hours of exposure to 100µM marked drove mitochondria dysfunction (Figure 5.7A-5.7C).

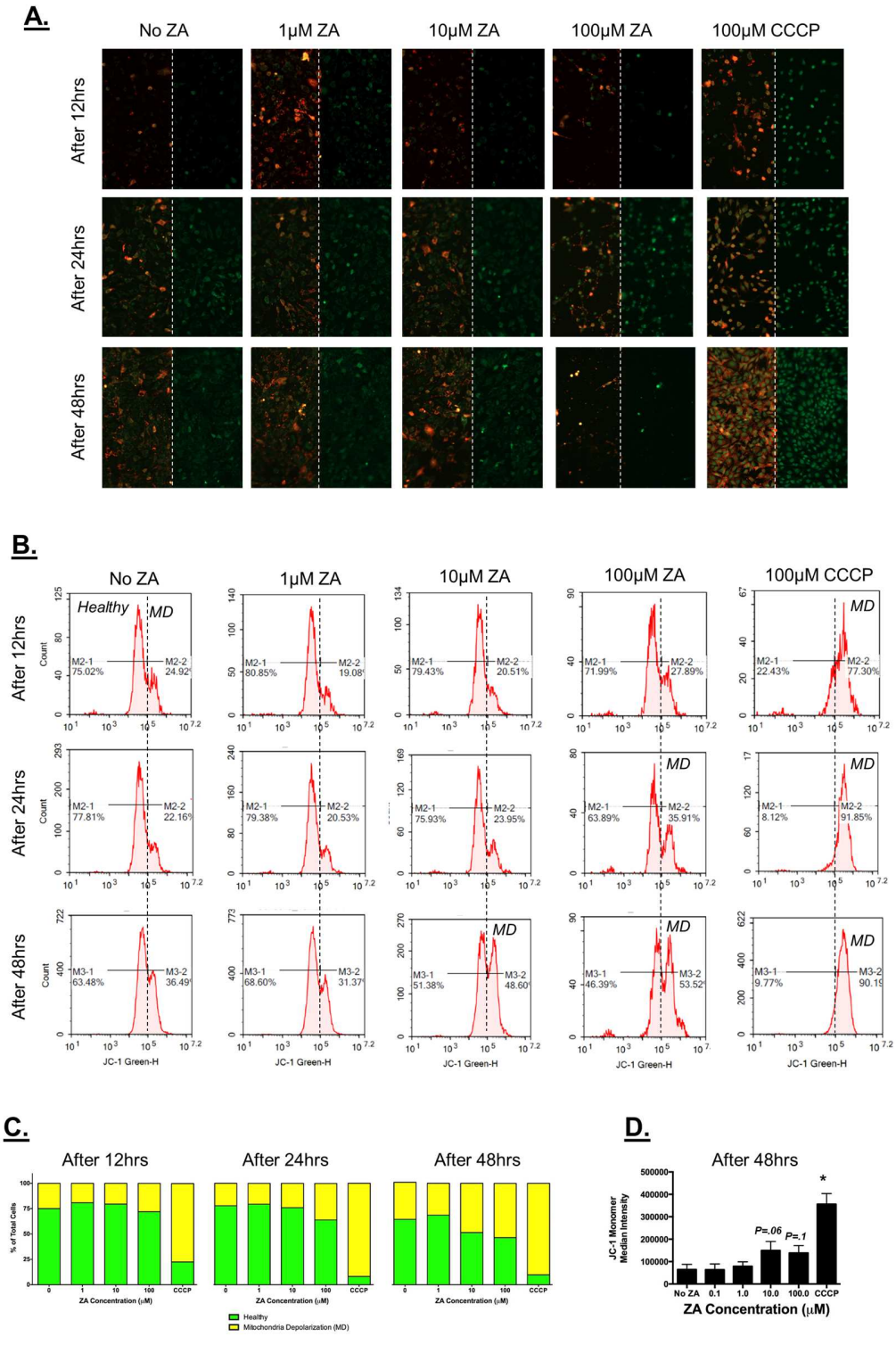
A.
No ZA
1μM ZA
10μM ZA
100μM ZA
100μM CCCP
After 12hrs
After 24hrs
After 48hrs
B.
No ZA
1μM ZA
10μM ZA
100μM ZA
100μM CCCP
Healthy
MD
Count
JC-1 Green-H
M2-1 75.02%
M2-2 24.92%
M2-1 80.85%
M2-2 19.08%
M2-1 79.43%
M2-2 20.51%
M2-1 71.99%
M2-2 27.89%
M2-1 22.43%
M2-2 77.30%
M2-1 77.81%
M2-2 22.16%
M2-1 79.38%
M2-2 20.53%
M2-1 75.93%
M2-2 23.95%
M2-1 63.89%
M2-2 35.91%
M2-1 8.12%
M2-2 91.85%
M3-1 63.48%
M3-2 36.49%
M3-1 68.60%
M3-2 31.37%
M3-1 51.38%
M3-2 48.60%
M3-1 46.39%
M3-2 53.52%
M3-1 9.77%
M3-2 90.19%
C.
After 12hrs
After 24hrs
After 48hrs
% of Total Cells
ZA Concentration (μM)
Healthy
Mitochondria Depolarization (MD)
D.
After 48hrs
JC-1 Monomer Median Intensity
P=.06
P=.1
*
No ZA
0.1
1.0
10.0
100.0
CCCP
ZA Concentration (μM)

Figure 5.7: ZA Caused a Concentration- and Exposure-Dependent Mitochondria Depolarization in Undifferentiated ATDC5 Cells. (A.) Representative 20x magnification images of JC-1 monomer+aggregate (left of white dotted line) and JC-1 monomer only (right of the white dotted line) over time demonstrating depolarization of mitochondria (increase in green monomer cytoplasmic and decrease in punctate red aggregates) in all CCCP treated groups. Mitochondria depolarization tended to occur after continuous ZA administration of 100µM as early as 24-hours, and by 48-hours with concentrations as low as 10µM caused MD. (B.) Representative JC-1 monomer intensity histogram confirms these qualitative observations and provides additional information regarding an overall shift in JC-1 green monomer intensity and the percentage of cells with values ≥1x105, which define the experimental cut-off for mitochondria dysfunction/depolarization (MD). Further representation of (C.) percentages of cells with JC-1 green monomer intensity values $\geq 1x10^5$ over time and (D.) overall JC-1 monomer histogram median intensity at 48-hours support these impressions. Results are presented as mean ± STD (n=3/concentration) where * indicates $p < 0.05$ between concentration vs no ZA.

5.4.7 ZA Administration Alters Cytoskeletal Architecture/Remodeling and Nuclear Morphology in ATDC5 Cells

To determine whether ZA can influence the cytoskeletal architecture and nuclear morphology, we performed immunocytochemical staining for F-actin, microtubules, and DNA content. in undifferentiated ATDC5 cells after 12, 24, 48, and 72-hours in the presence of ZA. Undifferenced cells cultured in the absence of ZA displayed highly aligned F-actin stress fibers and a well-organized microtubule network surrounding the nucleus and radiating outward. The presence of well-defined centrosomes was also noted. However, with increasing ZA concentration and exposure, the intricate F-actin and microtubule networks appeared visibly disrupted. After as little as 12-hours of ZA-exposure (Figure 5.8A), an apparent and sustained reduction in F-actin fiber staining and alignment and microtubule-network structure could be identified (Figure 5.8B). However, upon closer inspection, cells treated with

both 1 and 5µM ZA for 72-hours appear to exhibit a slight increase in microtubule presence, possibly as an adaptation to the loss of F-actin network integrity. In general, ZA treated cells also appeared to enlarge with increasing ZA concentration and exposure and exhibited a phenotype consistent with decreased surface-attachment or 'balling up'; which is clear at the highest ZA concentration (100µM).

Peering at the nucleus, undifferentiated ATDC5 cells cultured in the absence of ZA displayed a healthy, rounded nuclear morphology, with no indication of abnormal nuclear structure or signs of apoptosis. On the contrary, with increasing ZA concentration and exposure, cell nuclei exhibited extensive morphological changes: first, a marked enlargement in size was typically seen, followed by signs of nuclear blebbing and fragmenting, and ultimately nuclear shrinkage/collapse. Additionally, we often observed disrupted and bean-shaped nuclei in the presence of ZA, suggesting alterations in nuclear homeostasis and morphology.

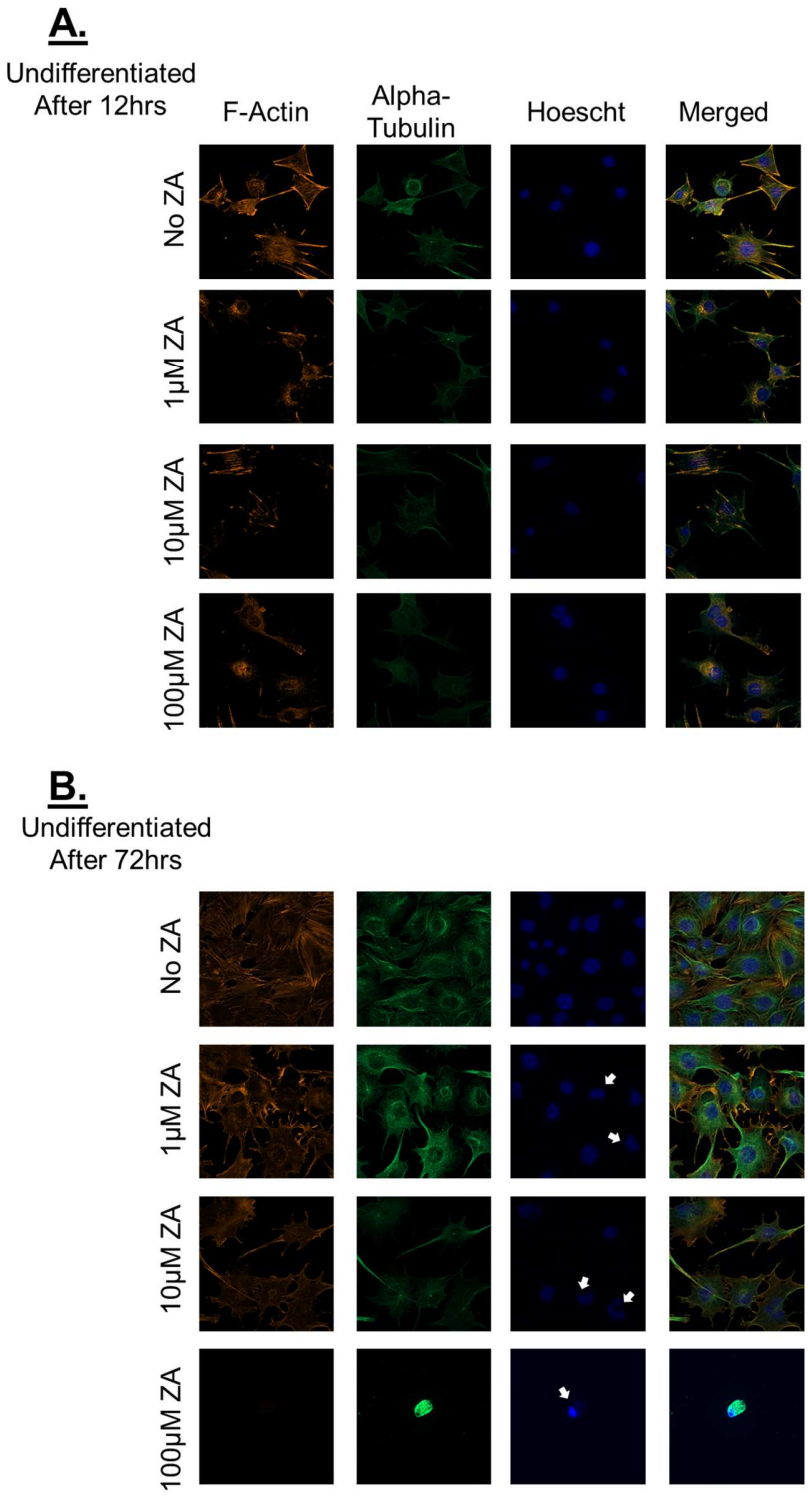
A.
Undifferentiated
After 12hrs
F-Actin
Alpha-
Tubulin
Hoescht
Merged
No ZA
1μM ZA
10μM ZA
100μM ZA
B.
Undifferentiated
After 72hrs
No ZA
1μM ZA
10μM ZA
100μM ZA

Figure 5.8: Continuous ZA Exerted a Concentration- and Exposure-Dependent Effects on Cytoskeleton Architecture and Nucleus Morphology in Undifferentiated ATDC5 Cells. (A.) Representative images at 63x magnification at 12-hours of actin (orange), microtubule (green), and nucleus (blue) highlight abundant actin stress fibers, an intricate microtubule network surrounding the nucleus radiating outwards, and rounded nucleus with no ZA treatment; on the other hand, increasing ZA concentration there is a reduction in actin intensity but similar nuclear morphology. (B.) Representative 63x magnification images of cytoskeleton and nucleus at 72-hour show similar observations made at 12-hour for all conditions; however, the effects on F-actin and microtubule are enhanced, and the nucleus appears fragmented and takes on a bean-shaped nucleus (white arrows).

5.5 Discussion

Recently, our team demonstrated the feasibility of four, weekly-repeated (4q7) intra-articularly administered zoledronic acid (ZA) to modulate chondrocyte death and proliferation, suppress cartilage erosions, and influence a number of non-cartilaginous tissues of the joint following the surgical destabilization of the medial meniscus (DMM) in the mouse. ZA's anti-resorptive, anti-neoplastic, anti-proliferative, anti-inflammatory, and pro-apoptotic mechanisms of action have been well-documented in numerous cell types (e.g. osteoclasts, osteoblasts, macrophages, cancerous cells) and disease states (e.g. bone loss and cancer). While studies in joint disease models have established that ZA can influence cartilage-level outcomes[239,376,410,411], knowledge of whether ZA could directly modulate chondrocyte health and function in isolation from other joint tissues remained limited[254]. Herein, we demonstrate that chondrocyte-like ATDC5 cells in monolayer culture respond to ZA in much the same way that other mammalian cells respond to nBPs. We observed that ZA could mediate the following effects in ATDC5 cells: anti-proliferative activity; cell cycle arrest (in S-phase); mitochondrial depolarization; pro-apoptotic activity and cell death; and alteration to

cytoskeletal architecture, and cell and nuclear morphology. Moreover, we have confirmed that ZA exhibits pleiotropic effects on chondrocyte-like ATDC5 cells, with the induction of the effects above being dependent upon ZA concentration, time of exposure, and the differentiation state of the cells (i.e. undifferentiated vs. differentiated).

In the present study, we utilized the immortalized murine chondrogenic ATDC5 cell line, a well-accepted cell line for the study of the differentiation and behavior of 'chondrocyte-like' cells[402–404], to investigate the influence of ZA on chondrocyte health and fate *in vitro*. While we did not directly evaluate the ability of ZA to influence the genetic program and differentiation processes themselves in ATDC5 cells, our ability to maintain these cells in two different states of differentiation, undifferentiated vs. differentiated, permitted us to isolate the effects of ZA on chondrocyte-like cells at different stages of cell-maturation and proliferative capacity[402,404,412]. At the time of ZA administration, undifferentiated cells are more proliferative in nature, and can mimic cells that have been 'activated' *in vivo* and induced to re-enter the cell cycle and proliferate following an acute injury; these may include resident progenitor cells in cartilage or otherwise quiescent chondrocytes coaxed into reentering the cell cycle to aid in injury repair/remodeling (Chapter 3)[100]. Conversely, differentiated ATDC5 cells are more representative of post-mitotic, quiescent chondrocytes in cartilage, as they exhibit a marked reduction in their proliferative potential, presumably due to both differentiation and contact inhibition. These cells can be considered to reflect both healthy chondrocytes and those not immediately 'activated' following injury/disease. Further, our use of the ATDC5 cell-line, as opposed to primary chondrocytes, allowed us to limit the phenotypic drift

often associated with primary chondrocyte culture[413,414], while retaining control over cell differentiation status.

By exploiting the ability to study cell health outcomes in both non-differentiated and differentiated ATDC5 cells, we identified that ZA's effects on cell proliferation, metabolic activity, and viability were concentration- and exposure-dependent, and heavily dependent on the ATDC5 cells' differentiation stage. Undifferentiated cells were far more susceptible to ZA than differentiated cells; and as ATDC5 cells spent progressively more time under differentiating conditions (e.g. three- versus two-weeks in culture media supplemented with 1% ITS^{+}) they became increasingly less susceptible to the chondromodulatory and pleiotropic effects of ZA. More specifically, when undifferentiated ATDC5 cells were cultured continuously in the presence of ZA for 72-hours, a minimal concentration of ≥5μM was required to drive significant reductions in cell number expansion (IC_{50} = 3.7μM), and thus proliferation, population-level metabolic activity (IC_{50} = 6.4μM). Above 5μM, the effects on cell number and metabolic activity increased in a concentration-dependent manner up to 100μM, at which point cell number expansion and metabolism were almost entirely suppressed. In these same cells, a nearly 10-fold higher concentration of ZA (IC_{50} = 45.4μM) was required to drive a similar degree of suppression of viability. In contrast, within differentiated ATDC5 cells, ZA has a far more attenuated effect on cell number, metabolism, and cell viability; in cells that underwent 2-weeks of differentiation only ≥50μM ZA could suppress cell number, metabolic activity, and cell viability, while ZA had no appreciable effect on the health and metabolism of cells that underwent 3-weeks of differentiation. Unfortunately, IC_{50} values could not be established for differentiated ATDC5 cells, as the conditions tested did not provide

sufficient inhibition of the requisite cell processes to model the inhibitory response. These results suggest that the susceptibility of ATDC5 to ZA depends on the proliferative capacity of ATDC5 cells at the time of ZA application. Subsequently, we focused the remainder of the study on undifferentiated ATDC5 cells in order to continue to dissect the effects of ZA on chondrocyte-like cells.

Next, we investigated the time-course over which proliferation, metabolism, and cell viability were suppressed in undifferentiated ATDC5 cells under conditions of i) continuous versus ii) brief, initial exposure to ZA. In undifferentiated cells continuously exposed to ZA, the minimal length of time that ZA needed to be present before significant changes (reductions) in cell proliferation, metabolic activity, and viability became apparent was, as expected, concentration dependent. At ZA concentrations ≥50μM cell number expansion (proliferation) and viability were suppressed after as little as 24-hours in continuous culture, while metabolic activity was significantly suppressed by 48hrs. Intermediate ZA concentrations (5 and 10μM) required longer continuous exposure times to drive significant suppression of cellular outcomes, and the lowest ZA concentrations (0.1 to 1μM), again, had no significant influence on cell numbers (proliferation), metabolic activity and cell viability in undifferentiated ATDC5. Pulse-chase experiments further demonstrated that one could achieve significant, if not extreme, suppression of cell proliferation and cell viability at our 72-hour endpoint, with very-brief, early exposure of undifferentiated ATDC5 cells to high concentration ZA. For instance, at 50 and 100μM, cell number expansion (proliferation) could be suppressed with as short as a 1-hour of ZA exposure, and cell viability suppressed with an initial exposure of 6- to 12-hours. At 10μM, suppression of proliferation appeared after just 2-hours of exposure. Moreover, consistent with the

results described above, 72-hours of ZA exposure remained insufficient to drive significant reductions in cell viability at ZA concentrations below 50µM.

Based upon these three experiments, ZA appears to exert pleiotropic, and concentration-and exposure-dependent effects on chondrocyte-like ATDC5 cells *in vitro,* and these effects are further modified by the differentiation status and proliferative capacity of the cells. Low- to moderate ZA concentrations (1 to 10µM) did not affect differentiated/post-mitotic ATDC5 cells and only exerted anti-proliferative and metabolic activity suppressing influences on undifferentiated/proliferating ATDC5 cells. Higher ZA concentrations (≥50µM) entirely suppress proliferation, drastically reduce metabolic activity, and drive cell death in undifferentiated ATDC5 cells. In differentiated ATDC5 cells, the effect of high-concentration ZA was restricted to suppressing cell viability in only the cells differentiated for 2-weeks. Overall, these experiments suggest the presence of two potential ZA therapeutic 'dosing' windows based upon the observed regulation of chondrocyte cell health: in the range of 5-10µM, ZA seems to predominately act as an anti-proliferative, while above ≥50µM ZA drives reductions in cell viability and cell death.

Given that ZA could inhibit cell proliferation and drive cell death in undifferentiated ATDC5 cells, we investigated the effect of ZA on a number of cellular processes that influence these outcomes; including, apoptosis, cell cycle arrest, cytoskeletal dysregulation, and mitochondrial dysfunction; which allowed us to begin to establish the cell-level mode-of-action of ZA in chondrocyte-like cells. Using an intracellular probe for caspase-3 and 7 activity, which are executioner proteases, our pulse-chase experiments demonstrated that high concentration ZA (≥50µM) could

rapidly and effectively drive cell death through apoptotic mechanisms. As little as 1 to 2-hours of exposure to high-concentration ZA could drive substantial increases in apoptosis compared to both control (no ZA) and low concentration ZA exposure; and as the length of ZA exposure increased, the number of dead cells (PI^+), apoptotic cells (caspase-$3/7^+$), and dual-labeled cells (PI^+- caspase-$3/7^+$) increased in lock-step till nearly all cells present were either dead or undergoing apoptosis. In the presence of 5-10µM ZA apoptotic ATDC5 cells were largely absent, even following 72-hours of continuous exposure. These findings are entirely consistent with outcomes observed across a number of different cell types treated with ZA[147,174,192,193].

Give the observation that ZA could drive concentration- and exposure-dependent ATDC5 programmed cell death, an important question arises: what mechanism might be driving these cells towards the activation and execution of apoptosis? Possible initiators of programmed cell death, and ones that have previously implicated in ZA-mediated cell-death include cell-cycle arrest-induced apoptosis, and activation of intrinsic apoptotic pathways as a result of mitochondrial dysfunction and/or cellular stress. Through the use of flow-cytometry and image-based cell cycle analysis we observed that exposure of ATDC5 cells to ZA could drive the arrest of undifferentiated ATDC5 cells in the S-phase of the cell cycle at concentrations ≥5µM; which is similar to outcomes in studies investigating the effect of ZA on cancer cells[191–194,202,415]. This cell-cycle arrest could also explain the concentration-dependent inhibition of proliferation and cell-number expansion (IC_{50} = 3.7µM), as S-phase arrest prevents progression into G2 and the subsequent cell division associated with mitosis. Such S-phase arrest or cytostasis, potentially mediated by the tumor suppressor protein p53[416–419]. This knowledge, combined with the observation that S-phase arrest could

be driven at ZA concentrations ~10-fold lower than those that promote apoptosis suggested that it is unlikely that S-phase arrest is a primary driver of ZA-mediated apoptosis; however, if S-phase arrest potentiated other apoptosis-inducing pathways in ATDC5 cells is presently unclear.

Cytoskeleton architecture and nucleus integrity/morphology play important roles in cell health and cell cycle progression and are associated with downstream products of the mevalonate pathway that ZA influences. For instance, ZA's inhibition of the mevalonate pathway reduces the prenylation of small GTPase critical for cytoskeleton architecture[136]. In various cancerous cells, ZA's is known to alter the F-actin cytoskeleton architecture[202,203,420]. Agreeing with this established knowledge, in our study we observed ZA's ability to alter the cytoskeleton architecture and remodeling of F-actin and microtubule network in undifferentiated ATDC5 cells. Specifically, we observed drastic changes in cytoskeleton infrastructure of undifferentiated ATDC5 cells as evident with decreased aligned actin stress fibers and altered microtubule network with 100µM ZA as early as 12hrs, and in all concentrations by 72-hours. Unfortunately, the role and implications of this altered cytoskeleton in cell death and cell cycle arrest remain unknown. Interestingly, recent work in breast cancer cells has identified a kinetochore protein, as a novel target of ZA[421]. These proteins are prenylated through the mevalonate pathway, associated with microtubule assembly, and required for proper chromosome separation during mitosis. Although it remains to be seen in our study, disruption of the kinetochore or other similar proteins could be associated with disrupted microtubule network, S-phase arrest, and cell death. Moreover, other cellular changes, such as nucleus integrity and morphology could also be affected and involved. Indeed, when peering closer at the

nucleus itself, we observed drastic changes in overall nucleus morphology and size that varied with ZA exposure time and concentration. Initially, the nucleus appears normal and rounded in all concentrations, however, by 72-hours the nucleus in intermediate concentrations (5 and 10µM), and in even the lower (1µM) concentration, appears abnormal; namely, enlargement of the nucleus, signs of blebbing, bean-shaped morphology, and fragmentation. These findings align well with other studies[196,202] and the fact that cells are unable to progress through the cell cycle and those that show signs of apoptosis at higher concentrations. While the causes of such nuclear changes are unknown, other aspects of the nucleus not studied herein, such as nuclear laminins, may provide insight. Mevalonate pathway plays a role in the posttranslational modification prenylation of GTPases required for the production of nuclear lamins[422,423]. While not addressed in our study, future studies should continue to investigate the role of ZA's influence on cytoskeleton and nuclear morphology in chondrocytes.

Mitochondria health is essential for normal mammalian cell function and could be associated with the other general cellular outcomes in our study, particularly cell death and apoptosis, affected by ZA administration in this study. For instance, blockade of the mevalonate pathway with ZA has been linked to mitochondria dysfunction and lowered mitochondria potential[424], as seen in kidney[174] and cancerous cells[147,195,196,198,202,425]. In agreement with these findings, in our undifferentiated ATDC5 cells, we found mitochondria tended to be depolarized as early as 24hrs with 100µM and by 48hrs with 10µM ZA. At the time points evaluated, the intermediate concentrations displayed a minimal caspase-3/7 activation yet significant mitochondrial dysfunction, unlike the 100µM where mitochondria depolarization

coincided with caspase-3/7 activation. These results suggest that other cellular mechanisms could underpin our current study findings. For instance, mitochondria dysfunction is associated with oxidative stress and autophagy-related processes requiring prenylation steps in the mevalonate pathway[424]. Indeed, autophagy and oxidative stress are involved with ZA's modulate of the mevalonate pathway in part because of the modifications necessary[426–430]. Future studies should continue to investigate the role of mitochondria health in ZA influence on chondrocytes and the aforementioned cellular outcomes.

While the present study starts to unravel potential modes-of-action of ZA in chondrocyte-like cells, several limitations to the study should be noted. These experiments presented herein were conducted in a cross-section manner, which while technically facile, limited our ability to study the longitudinal response of ATDC5 cells to different ZA administration strategies and concentrations. In the future longitudinal, live-cell-based studies will be needed to study the short-to long-term effect of ZA exposure on chondrocyte cells; including its effects on cell differentiation and the production of inflammatory cytokines, matrix-degrading enzymes (i.e., aggrecanases and collagenases), and matrix constituents (i.e., type II collagen and proteoglycan). While the concentration and exposure-dependent effects of ZA ATDC5-cells observed were profound, it is unclear if these cellular alterations are permanent or reversible in nature, or if they can be recovered/rescued by supplementing the cells with mevalonate pathway intermediates. It is also unclear if one would observe similar ZA-mediated outcomes in ATDC5 that were challenged with PTOA-like stressors, such a serum or inflammatory cytokines exposure. Lastly, the effects demonstrated here are on the immortalized chondrocyte-like ATDC5 cell

line. As a result, this requires confirmation in primary cells *in vitro*, including in chondrocyte-precursors, immature and mature chondrocytes, and hypertrophic chondrocytes, as well as *in situ* in chondrocytes residing within their native extracellular matrix.

In conclusion, this study is the first to demonstrate and establish the concentration- and exposure-dependent pleiotropic effects of ZA on cell proliferation, viability, mitochondria polarization, cell cycle progression, and cytoskeleton architecture in undifferentiated and differentiated cells from the chondrocyte-like ATDC5 cell line. The findings presented herein confirm ZA's ability to directly affect chondrocytes and align well with ZA's known ability to inhibit the mevalonate pathway and influence its downstream molecular and cellular targets (e.g., prenylated proteins) in almost all mammalian cells. Collectively, our data set the stage for the further study of the effect of ZA on chondrocytes *in vitro*, *in situ*, and *in vivo*, with the goal of leveraging locally (i.e., intra-articularly) administered nBPs for disease-modification of PTOA and other cartilage-related diseases.

Chapter 6

DISCUSSION

6.1 Major Findings

Currently, there is a significant unmet clinical need for disease-modifying therapies that can slow or stop PTOA progression. Lack of such therapies for PTOA is in part due to our lack of mechanistic understanding of how acute joint injury leads to loss of cartilage and joint function long-term. Thus, the first part of this dissertation investigated the immediate-to-early changes in cartilage cellularity and structure in hopes of uncovering potential biological targets for PTOA prevention. Since PTOA progression is a whole-joint disease, an ideal therapy would prevent both accelerated cartilage degeneration and modulate non-cartilaginous tissues changes (i.e. subchondral bone, meniscus, osteophyte, and joint synovitis). One therapeutic gaining significant attention in the field that was tested in this dissertation for its PTOA disease-modifying potential was zoledronic acid (ZA). ZA belongs to an FDA-approved class of drugs called bisphosphonates (BPs). BPs have historically been used for bone-related diseases because of anti-resorptive and bone remodeling properties. Given the anti-resorptive properties of BPs and the general belief that aberrant subchondral bone remodeling is involved in PTOA disease progression, ZA was used previously at high doses systemically to provide disease-modifying benefits in animal models of PTOA. While efficacious, systemic administration poses clinical concerns because of the increased risk for adverse skeletal and non-skeletal side effects. Therefore, alternative, locally-targeted routes of administration, such as intra-articular

(i.a.) injections are warranted to minimize the adverse side-effects. However, the use of i.a. injection of ZA (i.a.ZA) for PTOA prevention has received limited attention, and ZA's mode of action on chondrocytes and cartilage health remained largely unknown.

Overall, Aim #1 (Chapter 2) of this dissertation identified a focal population of chondrocytes linked in a spatiotemporal manner to the traumatic injury (i.e. loss of meniscus coverage due to extrusion) and the initiation and progression of cartilage degeneration in PTOA. In Aims #2 and #3 (Chapters 3-5), we determined that i.a.ZA could modulate these dysfunctional chondrocytes and other knee joint tissues leading to cartilage protection following a joint injury *in vivo*, and we began to uncover ZA's modes of action on chondrocytes *in vitro*.

In Aim #1 (Chapter 2), the primary objective was to characterize the spatiotemporal progression of cellular and tissue-level changes to cartilage post-injury *in vivo* using the murine destabilization of medial meniscus (DMM) model of PTOA. Our histological and immunohistochemical assessments from early (3d) through late (112d) stage identified an early, focal loss of chondrocytes in regions of the articular cartilage that ultimately developed overt tissue erosions. Importantly, these cellular and structural changes in cartilage localize to cartilage regions that experienced a drastic reduction in meniscal coverage due to DMM-induced medial meniscal extrusion. To the best of our knowledge, the results from Aim #1 were the first published to quantitatively relate the spatial aspect of DMM-induced meniscal extrusion to chondrocyte loss and cartilage damage. These findings further suggest that the meniscus plays a pivotal role in cartilage health and disease progression and we speculate the meniscus could be the unspoken guardian of articular cartilage.

Together, findings in Aim #1 suggest that a focal population of chondrocytes exists that may initiate biologically- or cell-driven cartilage degeneration. We then used this knowledge to focus our attention on specific regions of cartilage to evaluate the efficacy of i.a.ZA for cartilage prevention in PTOA and ZA's potential modes of action in chondrocytes.

In Aim #2 (Chapters 3 and 4), our objective was to determine the disease-modifying efficacy of local, intra-articular injection of ZA (i.a.ZA) to prevent cartilage degeneration and modify non-cartilaginous joint tissues post-injury in the murine DMM model of PTOA used in Aim #1. Specifically, the disease-modifying potential of repeated versus single i.a.ZA strategies on intra- and extra-capsular tissues, including cartilaginous and non-cartilaginous tissues, were investigated from early (7d) through late (84d) disease stages post-DMM. Using histological, immunohistochemical, and micro-computed tomography analyses, we focused on potential ZA's mode of action on chondrocyte (i.e. proliferation, death, and proteoglycan production) and cartilage (i.e. structural and proteoglycan content) changes post-DMM. Additionally, we were interested to see if i.a.ZA would minimize adverse skeletal side effects associated with systemic administration of ZA. To do so, we evaluated if i.a.ZA could influence more 'distant' bone compartments of the injured joint. In Aim #2 (Chapter 3), we found that weekly-repeated, but not single, i.a.ZA administration could suppress late-disease stage cartilage erosions; however, no strategy was able to mitigate early-stage fibrillation and clefting-damage to the superficial cartilage surface. Upon further dissection, repeated i.a.ZA appears to maintain and enhance proteoglycan content in articular cartilage, as well as modulate chondrocyte proliferation and death in a spatiotemporal manner. In Aim #2 (Chapter

4), we found that all i.a.ZA strategies could influence intra-capsular, mineralized joint tissues (meniscus, osteophytes, ectopically-formed bone) following injury, but not injury-induced joint synovitis. In addition, all i.a.ZA strategies had minimal influence on extra-capsular bone compartments (subchondral bone and 'distant' bone compartments of the epiphyseal and metaphyseal). Collectively, findings from Aim #2 (Chapters 3 and 4) suggest that repeated i.a.ZA administration can suppress cartilage erosions long-term by modulating the underlying chondrocyte biology and proteoglycan content in articular cartilage. Furthermore, findings from Aim #2 suggest that repeated i.a.ZA effects are localized to intra-capsular calcified tissues and have minimal effects on off-target bone compartments in the injured joint.

In Aim #3 (Chapter 5), our objective was to explore ZA's cellular mode(s) of action on chondrocytes *in vitro*. To do so, we evaluated the effects of ZA concentrations ranging from 0.1 to 1000μM given at different continuous and pulsed drug exposure times in chondrocyte-like ATDC5 cells, a well-established immortalized cell line for studying chondrocyte biology *in vitro*. ATDC5 cells enabled us to evaluate the effects of ZA on two sub-populations of chondrocytes expected to be seen *in vivo* following injury: those that are mitotic (undifferentiated), mimicking proliferating chondrocytes, and those are post-mitotic (differentiated) and mimic mature, quiescent, and non-proliferative chondrocytes. We found that increasing ZA concentration and exposure time had pleiotropic effects predominately in undifferentiated ATDC5 cells. Specifically, low ZA concentrations had no influence on undifferentiated ATDC5 cell health. However, moderate ZA concentrations (5μM and 10μM) decreased cell proliferation, viability, and metabolic activity, as well as arrests cell-cycle progression in S-phase, depolarized mitochondria, and diminished

cytoskeleton (i.e. actin and microtubules) architecture. Undifferentiated ATDC5 cells exposed to higher ZA concentrations (50 and 100μM) experienced the same effects as moderate concentrations, except there was additional reduction in cell-viability due to caspase 3/7-mediated apoptosis. While the effects of ZA in undifferentiated ATDC5 cells were quite astonishing, ZA's effects in differentiation ATDC5 cells were drastically reduced, if not completely abolished; with only the highest, supraphysiologic ZA concentrations (50μM through 1000μM) capable of driving cell death. Collectively, findings from Aim #3 (Chapter 5) suggest that ZA's effects in the chondrocyte-like ATDC5 cells are heavily dependent on the proliferative capacity of chondrocytes, hinting at the importance/involvement of the mevalonate pathway among ATDC5 cells that are actively proliferating versus those that are more quiescent in nature. Lastly, findings from Aim #3 align with the established effects of ZA on different mammalian cell types and identified critical concentrations and exposure times of ZA that could directly influence chondrocyte health.

In summary, findings from this dissertation have enabled us to put forth a working hypothesis on the natural progression of cartilage dysfunction following joint injury, as well as a theory regarding how ZA can modulate these processes for beneficial disease-modification. We call this theory the 'activated versus bystander chondrocyte hypothesis.' We speculate that naturally progressing PTOA is a function of an acute, focal mechanical insult (due to immediate uncovering of a portion of the medial tibial plateau and femoral condyle in our DMM-model) that causes both an initial wave of chondrocyte death (necrosis or apoptosis, it is unclear) and mechanically-induced superficial damage. This is followed by what we term the 'activation,' by either mechanical or molecular signals, of an immediately-adjacent

and spatially-distinct population of chondrocytes (‘activated’ chondrocytes). We posit that these activated cells undergo a phenotypic-shift to initiate the attempted repair of this locally ‘damaged’ tissue. We suspect that this phenotypic shift includes the production of soluble factors by these activated cells allowing for communication with neighboring chondrocytes, as well as the recruitment of these ‘activated’ chondrocytes, which were previously quiescent, back into the cell cycle to expand the local pool of chondrogenic precursors (proliferation). However, chondrocyte proliferation requires local ECM remolding (catabolism and anabolism) to allow for the cell volume expansion and division that accompanies mitosis. Consequentially, this may compromise of local matrix quality and mechanical integrity priming the tissue for degeneration. Subsequently, we hypothesize that these local changes in the mechanical and biochemical environment, driven by an initial population of activated cells, induce ‘dysfunction’ in normally quiescent but adjacent ‘bystander’ chondrocyte population: this leads to their activation, inducing cell-cycle recruitment, proliferation, matrix remodeling, and what we suggest is a self-reinforcing vicious cycle, ad infinitum, of cell-activation and cell-mediated matrix degradation.

Our *in vivo* (Chapters 3 and 4) and *in vitro* (Chapter 5) results have led us to suspect that the disease-modifying efficacy of ZA in PTOA development is rooted in the ability of intra-articularly administered ZA to differentially modulate the response of these activated and bystander chondrocytes populations. Our working hypothesis is that the repeated i.a. injection of ZA to the joint following acute injury can accelerate the death of the initial wave of acutely activated and spatially-localized chondrocyte cells following joint injury; the acute displacement of the medial meniscus across the medial tibial plateau due to DMM-induced meniscal extrusion in our case. Our *in vitro*

data and historical literature suggest that this occurs through ZA's ability to drive cytostasis and induce/exacerbate mitochondrial dysfunction and apoptosis in cells that may already be experiencing cellular stress. By suppressing the proliferation and enhancing the apoptosis/death of these initially activated cells, i.a.ZA may dampen their ability to 'activate' pro-catabolic pro-inflammatory phenotypes and interrupt the self-reinforcing vicious cycle of cell-activation, proliferation, and cell-mediated ECM catabolism/degradation.

On the other hand, our *in vivo* and *in vitro* data suggest that quiescent, non-proliferative 'bystander' chondrocytes respond differently to ZA. *In vitro*, the health and viability of post-mitotic chondrocyte-like cells were largely unaffected by the ZA concentrations that were delivered *in vivo*, reinforcing the idea that our i.a.ZA administration did not adversely influence the homeostasis of healthy chondrocytes. In contrast, instead of leading to chondrocyte dysfunction, i.a.ZA appeared to enhance proteoglycan production by 'bystander' chondrocytes *in vivo*, especially in the cartilage regions peripheral to those that would typically develop cartilage erosions if left untreated. These findings align with *in situ* findings from our collaborators, who have found that the biomechanical properties of healthy cartilage explants stimulated by mechanical loading can be enhanced by the introduction of ZA (1µM).

Collectively, our data suggest that both ZA concentration and exposure time have the ability to regulate the cellular outcomes of chondrocytes *in vivo*. It is important to note that, within the joint, changes in ZA concentration can change rapidly due to clearance from the synovial fluid. This would undoubtedly have the ability to alter the response of chondrocytes *in vivo* to different i.a.ZA administration strategies. Moreover, this fact, coupled with our 'activated versus bystander'

hypothesis could help to explain why the administration of single i.a.ZA injection was unable to provide disease-modifying beneficial outcomes (and in the case of the 0d injection actual worsen outcomes) following injury. Our single injection strategy may have been unable to mediate the cell-level influences needed to realize beneficial disease modification outcomes due to rapid drug clearance or the differential nature of the effect of ZA on chondrocytes, necessitating repeated dosing to achieve efficacy. However, given this dissertation's findings, and the injection constraints we could work under (limited to 4 weekly injections due to initial animal care concerns by our IACUC committee, and at one concentration), there is a strong possibility that we serendipitously stumbled upon a 'sweet spot' regarding both the timing and necessary concentration administered to the joint. This appears to be the ultimate Goldilocks paradigm: not too much, not too little, just right.

Overall, this dissertation provided new knowledge regarding the spatiotemporal evolution of cartilage degeneration and chondrocyte dysfunction following joint injury, which helps to establish a baseline from the application of novel disease-modifying therapeutics leads can be evaluated from. In addition, we demonstrated the preclinical promise of i.a.ZA as a potentially cheap, easy administered, and efficacious disease-modifying therapeutic for PTOA. Future studies should continue to explore the use of i.a.ZA and uncover the full disease-modifying potential of i.a.ZA for PTOA and other forms of arthritis.

6.2 Future Directions

While this dissertation has provided a great deal of insight into the general pathioetiology of PTOA and the potential mechanisms- and modes-of-action lending to i.a.ZA disease-modifying effects for PTOA therapy, a number of additional

questions and avenues for future researcher has arisen from these findings; some of those that have already been 'piloted' in conjunction with this dissertation and are highlighted. By expanding upon the findings describe briefly here, future studies can hopefully fully unlock the potential of i.a.ZA as a clinical therapeutic option for PTOA (and OA).

6.2.1 Deeper Mechanistic Understanding of ZA's Mechanisms of Action in PTOA In Vivo

In this dissertation, we began to uncover ZA mode of action in chondrocytes and PTOA progression, however, chondrocyte biology is far more complex than the few cellular processes we evaluated. To this end, it remains unclear if i.a.ZA was able to influence other cellular processes *in vivo* that could have led to our results. For instance, i.a.ZA could have modulated chondrocyte processes such as senescence, mitochondrial dysfunction, proinflammatory cytokines, and matrix constituents or degrading enzymes. Given that ZA is known to affect such processes in other cells and that our *in vitro* work suggests that ZA can directly affect chondrocytes, it is reasonable to believe ZA would regulate such processes in chondrocytes *in vivo*. Dissecting ZA's full mechanisms of action may explain why repeated, but not single, i.a.ZA suppressed the development of cartilage erosions. Addressing these deeper mechanistic questions could also lead to the discovery of new potential therapeutic leads for PTOA prevention.

Another aspect of disease progression that could be worth evaluating is the biomechanical and tribological properties of cartilage post-injury and i.a.ZA administration. It is generally accepted that the mechanical properties of cartilage are compromised by joint injury and cartilage degeneration, and perhaps ZA can mitigate

these changes or improve these mechanical properties. Preliminary studies by our collaborators suggest that ZA can enhance the mechanical properties of cartilage subjected to mechanical stimulation *in situ*. In support of this, we saw an increase in proteoglycan content with repeated i.a.ZA in Aim #2 (Chapter 3) that could be indicative of enhanced cartilage tissue biomechanical and tribological properties. Along these lines, it would also be worthwhile to confirm ZA's ability to modulate proteoglycan synthesis in other assays. Additionally, studies should investigate other matrix macromolecules constituents critical to cartilage biomechanical and tribological properties that could have been affected by ZA, such as type II collagen[63]. Alterations to these molecules could influence the underlying chondrocyte mechanotransduction and injury response. Beyond matrix-level constituents and mechanical properties, the properties of the local pericellular matrix (PCM) can also be investigated, especially since we saw injury- and ZA-induced changes in proteoglycan staining within the territory immediately surrounding articular cartilage chondrocytes (chondrons) in this dissertation. Given that the PCM is intricately linked with the extracellular matrix and to chondrocyte mechanotransduction machinery, ZA may hold the ability also to influence chondrocyte-PCM-ECM interaction and mechanotransduction post-injury.

Beyond cartilage, it is important to further address i.a.ZA influence on the cellular response in non-cartilaginous knee joint tissues following injury. While we assessed the gross structural changes associated with changes in osteophytes, meniscus, subchondral bone, and synovium, i.a.ZA could have influenced the underlying cellular responses. It also remains unknown from our studies whether non-cartilaginous joint tissue changes had direct or indirect roles in the cartilage

degeneration and chondrocyte biology observed with and without i.a.ZA. For instance, pro-inflammatory cytokines and matrix-degrading enzymes are known to be produced by both meniscal and synovium cells, which may influence the intrinsic cartilage repair mechanisms leading to degeneration. There is the possibility that ZA altered these tissues' cellular responses, suppressing chondrocyte injury response and cartilage degeneration.

While this dissertation focused on ZA, it remains unknown if the same cartilage structural, compositional, and cellular changes would be observed with other nBPs or other mevalonate pathway modulators (i.e. statins[431,432] or HMG-CoA reductase and GTPase inhibitors[136,148,433–435]). It would be interesting to see if other modulators of the mevalonate pathway could influence the evolution of joint changes following injury. If this is the case, it would suggest that the mevalonate pathway itself, whether through nBPs or other means, could be a primary therapeutic target and pathway for control of chondrocytes in PTOA.

In general, one way to potentially get *in situ* mechanistic data from intact injured joints other than histology would be to utilize a technique called staining and clearing of tissues, which minimizes the time, labor, and cost of standard histological techniques used while producing a three-dimensional spatiotemporal picture. Previously, in our lab we demonstrated within naïve mouse knees that this technique is feasible[436], setting the stage for this technique in future studies. Using this technique would be interesting for cellular markers and pathways of chondrocyte biology that are challenging to visualized due to the depth within cartilage or lost due to histological processing.

6.2.2 Establishing a Proper Local, ZA Delivery Dosage, Frequency, and Timing

To properly inform and design the next set of experiments in hopes of leveraging i.a. ZA into the clinic, *in situ* and *in vitro* experiments should be performed to optimize the concentration and treatment strategy. By using this dissertation's *in vivo* and *in vitro* findings as a baseline, the first step would be to recapitulate these findings, particularly chondrocyte proliferation, death, and proteoglycan production, using an *in situ* injury model. Currently, other laboratories have used various means of creating impact-induced cartilage damage and have found evidence of chondrocyte death and cartilage damage associated with impact[55]; however, investigations into the spatial aspect of chondrocyte proliferation and proteoglycan production in these studies have been minimal. Translating these findings into our laboratory, and as a pilot aspect of this dissertation, we developed an instrumented drop-tower to drive impact-induced degenerative changes in cartilage plugs isolated from bovine and equine. We have optimized and piloted an in-house system to isolate osteochondral plugs from live equine tissue. In addition, we have isolated live equine synovium and performed co-culture experiments with and without cartilage. Co-culture allows us to begin to tease out the potential cross-talk between the synovium and cartilage occurring *in vivo* that could be altered with i.a.ZA. Collectively, the preliminary studies performed as an extension demonstrated the feasibility of our in-house system and techniques for studying ZA influence on impacted osteochondral plugs post-impact. Also, future studies could be performed on primary chondrocytes (from rat, bovine, equine, or human sources) to confirm our findings on ATDC5 cells. Overall, the combination of both *in situ* and *in vitro* models will properly define a reasonable concentration and delivery strategy to implement into the next wave of preclinical model and clinical trials.

6.2.3 Clinical Translatability

To translate i.a.ZA into the clinic, it is essential to begin to study i.a.ZA influence in more clinically-relevant models and markers of disease progression. Ideally, the findings from this should be confirmed in human tissues, but again, the access to such samples is limited. In order to overcome this clinical translatability limitation, future preclinical studies utilizing i.a.ZA could determine clinically-relevant biomarkers of joint destruction in the circulatory system and synovial fluid[93] as well as incorporate other assessment techniques used in humans such as MRI or arthroscopic-based assessments. Other clinically-relevant markers could include functional outcomes such as gait/loading and pain following injury and i.a.ZA administration[93]. Gait and pain are altered in the murine DMM[266,298,437] and other animals models[93,438,439]. We cannot rule out the possibility that i.a.ZA could have influenced pain and gait in our animals, especially since recent studies have found that ZA can influence pain in a variety of animal[215] and human[220,233] conditions. Also, it would be of interests to see if these findings hold in other joints of the musculoskeletal system in man typically afflicted by PTOA (and OA), such as the ankle or hip.

While the murine DMM model has provided valuable information into PTOA disease progression and demonstrated preclinical efficacy of i.a.ZA for cartilage prevention, it's still limited in that it is an invasive, surgically-induced model of PTOA[93]. Surgically-induced models, like the DMM and anterior crucial ligament transection, do not truly mimic human PTOA because there is no surgical incision in humans during a traumatic joint injury. To overcome the invasive surgery required in these models, recent progress has been made to develop non-invasive preclinical models. Non-invasive models have been shown to mimic cartilage cellular and structural changes presented here from the murine DMM model[355]. Thus, it would be

reasonable to suspect that i.a.ZA administered in those animal models would prevent similar processes presented in this dissertation. However, the time course and spatial progression observed in the murine DMM with and without ZA could be different from non-invasive models; especially since disease severity and speed of progression of each model is different. Additionally, more clinically-relevant animals such as the horse could be used to confirm the translatability of i.a.ZA in the mouse.

6.2.4 Drug Delivery Depots and Encapsulation of ZA for Enhanced Therapeutic Benefits for PTOA

Although i.a.ZA may overcome concerns regarding high-dose, systemic administration, its efficacy may diminish because of the rapid clearance from the joint space, which is mediated through the synovium's capillary and lymphatic systems[246,248]. For instance, intra-articularly injected small molecules[246,248,440], including ZA as we have shown in naïve mice (Appendix C.6), are rapidly cleared from the joint over the timecourse of minutes to hours. As a result, patients may require repeated i.a. injections to achieve efficacious results with ZA, as we have demonstrated with i.a.ZA injection in this dissertation. While i.a.ZA holds preclinical promise; this may not be clinically feasible due to the time, costs, and risks of infection with each i.a. injection procedure, as well and concerns over patient compliance[246,249,441].

To overcome the rapid clearance of drugs from the joint space, an alternative delivery strategy was piloted in this dissertation: encapsulation of ZA within liposomes, an FDA-approved drug delivery platform[246,248,442]. Historically, liposomes have been used for a variety of applications[443]: i) to targeting monocyte/macrophages in cancer and other inflammatory diseases, ii) as carriers of protein peptides, and iii)

for gene delivery. In the context of arthritis, liposomes have been used to encapsulate steroids[444,445], and the first-generation bisphosphonate, clodronate (CLO)[446], to increase drug retention time within the joint and to target macrophages in the synovium. Towards this end, liposomes for PTOA treatment may provide multi-functional benefits as they are biocompatible, biodegradable, able to decrease friction at the cartilage surface[447], and directly target phagocytic macrophages[446] and fibroblast-like synoviocytes[448,449] within the synovium while simultaneously generating long-lasting intracapsular drug-depots. To further motivate liposomes usage for PTOA therapy, CLO encapsulated in liposomes has anti-inflammatory and anti-osteoarthritic benefits in inflammatory arthritis[450–455] and prevented osteophyte formation and cartilage destruction in preclinical models of OA[456–458]. However, to date, no study has investigated the use of ZA-encapsulating liposomes (ZA-lipo) for targeting the tissues/cells relevant to injured-knees and the modification of PTOA progression. Thus, as an extension of this dissertation, we investigated the effects of ZA-lipo on cells relevant to the injured-knee *in vitro* and *in situ*. To date, we have generated consistently sized liposomes (~100-300 nm) and encapsulation of ZA in liposomes (~40% encapsulation efficiency). We have conducted preliminary experiments using ZA-lipo with ATDC5 cells, fibroblasts (NIH3T3), and macrophages *in vitro*, as well as with cartilage and synovium explants *in situ*. In these preliminary studies, we confirmed the ability of these cells to internalize liposomes using high-resolution imaging and flow cytometry.

In addition to liposomes, other drug delivery formulations of nanoparticles or tissue engineered constructs may help facilitate drugs of interests to chondrocytes. For instance, we investigated the ability of ELP-CLP nanoparticles to bind to collagen

matrixes without causing chondrocyte cytotoxicity[459]. These vesicles could be useful in targeting focal populations of cartilage near damaged cartilage as well as providing a drug depot. Beyond ELP-CLP particles, other microparticles alone or in combination with polymer matrices such as PLGA, gelatin and hyaluronic acid[460] could be used in combination with ZA to enhanced ZA benefits and retention within the injured joint.

6.3 Closing Remarks

In conclusion, this dissertation has provided fundamental information regarding the cellular and tissue level efficacy of intra-articular injection of ZA as a disease-modifying therapy for PTOA. These findings provide a baseline from which to launch future studies aimed at optimally designing intra-articular ZA treatment strategy for PTOA, and for dissecting the mechanisms- and modes-of-action of intra-articular ZA on cells implicated in PTOA. I hope that this dissertation serves as a springboard for a future generation of scientists in the field of arthritis and musculoskeletal biology to develop better ways to treat PTOA (and OA), a debilitating and burdensome disease that is currently without a cure.

REFERENCES

1. Hootman JM, Helmick CG, Barbour KE, et al. 2016. Updated Projected Prevalence of Self-Reported Doctor-Diagnosed Arthritis and Arthritis-Attributable Activity Limitation Among US Adults, 2015–2040. Arthritis Rheumatol. 68(7):1582–1587.

2. Barbour K. 2017. Prevalence of doctor-diagnosed arthritis and arthritis-attributable activity limitation--United States, 2013-2015. MMWR. Morb. Mortal. Wkly. Rep. 66(9):869–73.

3. Hootman JM, Helmick CG. 2006. Projections of US prevalence of arthritis and associated activity limitations. Arthritis Rheum. 54(1):226–229.

4. Buckwalter J a., Martin J a. 2006. Osteoarthritis. Adv. Drug Deliv. Rev. 58:150–167.

5. Lawrence RC, Felson DT, Helmick CG, et al. 2008. Estimates of the prevalence of arthritis and other rheumatic conditions in the United States. Part II. Arthritis Rheum. 58(1):26–35.

6. Cross M, Smith E, Hoy D, et al. 2014. The global burden of hip and knee osteoarthritis: Estimates from the Global Burden of Disease 2010 study. Ann. Rheum. Dis. 73(7):1323–1330.

7. Mobasheri A, Batt M. 2016. An update on the pathophysiology of osteoarthritis. Ann. Phys. Rehabil. Med. 59(5–6):333–339.

8. Deshpande BR, Katz JN, Solomon DH, et al. 2016. Number of Persons With Symptomatic Knee Osteoarthritis in the US: Impact of Race and Ethnicity, Age, Sex, and Obesity. Arthritis Care Res. 68(12):1743–1750.

9. Theis KA, Murphy L, Hootman JM, et al. 2007. Prevalence and correlates of arthritis-attributable work limitation in the US population among persons ages 18-64: 2002 National health interview survey data. Arthritis Care Res. 57(3):355–363.

10. Woolf AD, Pfleger B. 2003. Burden of major musculoskeletal conditions. Bull. World Health Organ. 81(03):646–656.

11. Johnson VL, Hunter DJ. 2014. The epidemiology of osteoarthritis. Best Pract. Res. Clin. Rheumatol. 28(1):5–15.

12. Bortoluzzi A, Furini F, Scirè CA. 2018. Osteoarthritis and its management - Epidemiology, nutritional aspects and environmental factors. Autoimmun. Rev. 17(11):1097–1104.

13. Palazzo C, Nguyen C, Lefevre-Colau MM, et al. 2016. Risk factors and burden of osteoarthritis. Ann. Phys. Rehabil. Med. 59(3):134–138.

14. Murphy L, Helmick CG. 2012. The Impact of Osteoarthritis in the United States. Orthop. Nurs. 31(3):85–91.

15. Murphy L, Schwartz T a., Helmick CG, et al. 2008. Lifetime risk of symptomatic knee osteoarthritis. Arthritis Care Res. 59(9):1207–1213.

16. Stubbs B, Aluko Y, Myint PK, Smith TO. 2016. Prevalence of depressive symptoms and anxiety in osteoarthritis: A systematic review and meta-analysis. Age Ageing 45(2):228–235.

17. Brown TD, Johnston RC, Saltzman CL, et al. 2006. Posttraumatic osteoarthritis: a first estimate of incidence, prevalence, and burden of disease. J. Orthop. Trauma 20(10):739–744.

18. Nuki G. 1999. Osteoarthritis: A problem of joint failure. Z. Rheumatol. 58(3):142–147.

19. Poole AR. 2012. Osteoarthritis as a Whole Joint Disease. HSS J. 8(1):4–6.

20. Loeser RF, Goldring SR, Scanzello CR, Goldring MB. 2012. Osteoarthritis: A disease of the joint as an organ. Arthritis Rheum. 64(6):1697–1707.

21. Man GS, Mologhianu G. 2014. Osteoarthritis pathogenesis - a complex process that involves the entire joint. J. Med. Life 7(1):37–41.

22. Chen D, Shen J, Zhao W, et al. 2017. Osteoarthritis: Toward a comprehensive understanding of pathological mechanism. Bone Res. 5(August 2016).

23. Hunter DJ. 2011. Pharmacologic therapy for osteoarthritis—the era of disease modification. Nat. Rev. Rheumatol. 7(1):13–22.

24. Hunter DJ. 2008. Are there promising biologic therapies for osteoarthritis?

Curr. Rheumatol. Rep. .

25. Felson DT, Neogi T. 2018. Emerging Treatment Models in Rheumatology: Challenges for Osteoarthritis Trials. Arthritis Rheumatol. 70(8):1175–1181.

26. Silverwood V, Blagojevic-Bucknall M, Jinks C, et al. 2015. Current evidence on risk factors for knee osteoarthritis in older adults: A systematic review and meta-analysis. Osteoarthr. Cartil. 23(4):507–515.

27. Blagojevic M, Jinks C, Jeffery A, Jordan KP. 2010. Risk factors for onset of osteoarthritis of the knee in older adults: a systematic review and meta-analysis. Osteoarthr. Cartil. 18(1):24–33.

28. Coggon D, Croft P, Kellingray S, et al. 2000. Occupational Physical Activities and the Knee. Arthritis Rheum. 43(7):1443–9.

29. Wilder F V., Hall BJ, Barrett JP, Lemrow NB. 2002. History of acute knee injury and osteoarthritis of the knee: A prospective epidemiological assessment. The Clearwater Osteoarthritis Study. Osteoarthr. Cartil. 10(8):611–616.

30. Weatherall JM, Mroczek K, McLaurin T, et al. 2013. Post-traumatic ankle arthritis. Bull. Hosp. Jt. Dis. 71(1):104–112.

31. Carbone A, Rodeo S. 2017. Review of Current Understanding of Post-Traumatic Osteoarthritis Resulting From Sports Injuries.

32. Roos H, Adalberth T, Dahlberg L, Lohmander LS. 1995. Osteoarthritis of the knee after injury to the anterior cruciate ligament or meniscus: the influence of time and age. Osteoarthritis Cartilage 3:261–267.

33. Roos EM. 2005. Joint injury causes knee osteoarthritis in young adults. Curr. Opin. Rheumatol. 17(2):195–200.

34. Kujala UM, Taimela S, Antti-poika I, et al. 1995. Acute Injuries In Soccer , Ice Hockey , Volleyball , Basketball , Judo , And Karate : Analysis Of National Registry Data Author (s): Urho M . Kujala , Simo Taimela , Ilkka Antti-Poika , Sakari Orava , Risto Tuominen and Pertti Myllynen Published by : BM.311(7018):1465–1468.

35. Majewski M, Susanne H, Klaus S. 2006. Epidemiology of athletic knee injuries: A 10-year study. Knee 13(3):184–188.

36. Thelin N, Holmberg S, Thelin A. 2006. Knee injuries account for the sports-related increased risk of knee osteoarthritis. Scand. J. Med. Sci. Sport.

16(5):329–333.

37. Shankar PR, Fields SK, Collins CL, et al. 2007. Epidemiology of High School and Collegiate Football Injuries in the United States, 2005 2006. Am. J. Sports Med. 35(8):1295–1303.

38. Gage BE, McIlvain NM, Collins CL, et al. 2012. Epidemiology of 6.6 million knee injuries presenting to United States emergency departments from 1999 through 2008. Acad. Emerg. Med. 19(4):378–385.

39. Clifton DR, Onate JA, Schussler E, et al. 2017. Epidemiology of Knee Sprains in Youth, High School, and Collegiate American Football Players. J. Athl. Train. 52(5):464–473.

40. Buckwalter JA, Lane NE. 1997. Current Concepts: Athletics and Osteoarthritis. Am. J. Sports Med. 25(6):873–881.

41. Roemer FW, Jarraya M, Niu J, et al. 2015. Increased risk for radiographic osteoarthritis features in young active athletes: A cross-sectional matched case-control study. Osteoarthr. Cartil. 23(2):239–243.

42. Madaleno FO, Santos BA, Araújo VL, et al. 2018. Prevalence of knee osteoarthritis in former athletes: a systematic review with meta-analysis. Brazilian J. Phys. Ther. 22(6):437–451.

43. Amoako AO, Pujalte GGA. 2014. Osteoarthritis in young, active, and athletic individuals. Clin. Med. Insights Arthritis Musculoskelet. Disord. 7:27–32.

44. Cameron KL, Hsiao MS, Owens BD, et al. 2011. Incidence of physician-diagnosed osteoarthritis among active duty United States military service members. Arthritis Rheum. 63(10):2974–2982.

45. Rivera CPTJD, Wenke JC, Buckwalter J a, et al. 2013. Posttraumatic Osteoarthritis Caused by Battlefield Injuries: The Primary Source of Disability in Warrior.20(0 1):1–12.

46. Showery JE, Kusnezov NA, Dunn JC, et al. 2016. The Rising Incidence of Degenerative and Posttraumatic Osteoarthritis of the Knee in the United States Military. J. Arthroplasty 31(10):2108–2114.

47. Rhon D, Perez K, Eskridge S. 2018. Risk of post traumatic knee osteoarthritis after traumatic knee injury in deployed military service members. Osteoarthr. Cartil. 26(2018):S218.

48. Lauder TD, Baker SP, Smith GS, Lincoln AE. 2000. Sports and physical training injury hospitalizations in the Army. Am. J. Prev. Med. 18(3 SUPPL.):118–128.

49. Jones JC, Burks R, Owens BD, et al. 2012. Incidence and risk factors associated with meniscal injuries among active-duty US military service members. J. Athl. Train. 47(1):67–73.

50. Songer TJ, LaPorte RE. 2000. Disabilities due to injury in the military. Am. J. Prev. Med. 18(00):33–40.

51. Murtha AS, Johnson AE, Buckwalter JA, Rivera JC. 2016. Total knee arthroplasty for posttraumatic osteoarthritis in military personnel under age 50. J. Orthop. Res. .

52. Jones BH, Tomlinson JP, Robinson JR, et al. 1993. Epidemiology of injuries associatea with physical training among young men in the army. Off. J. Am. Coll. Sport. Med. 25(2):197–203.

53. Gwinn DE, Wilckens JH, McDevitt ER, et al. 2000. The relative incidence of anterior cruciate ligament injury in men and women at the United States Naval Academy. Am. J. Sports Med. 28(1):98–102.

54. Lohmander LS, Englund PM, Dahl LL, Roos EM. 2007. The long-term consequence of anterior cruciate ligament and meniscus injuries: osteoarthritis. Am. J. Sports Med. 35:1756–1769.

55. Anderson DD, Chubinskaya S, Guilak F, et al. 2011. Post-traumatic osteoarthritis: Improved understanding and opportunities for early intervention. J. Orthop. Res. 29(June):802–809.

56. Segawa H, Omori G, Koga Y. 2001. Long-term results of non-operative treatment of anterior cruciate ligament injury. Knee 8(1):5–11.

57. Oiestad BE, Holm I, Engebretsen L, Risberg M a. 2011. The association between radiographic knee osteoarthritis and knee symptoms, function and quality of life 10-15 years after anterior cruciate ligament reconstruction. Br. J. Sports Med. 45(7):583–588.

58. von Porat a, Roos EM, Roos H. 2004. High prevalence of osteoarthritis 14 years after an anterior cruciate ligament tear in male soccer players: a study of radiographic and patient relevant outcomes. Ann. Rheum. Dis. 63:269–273.

59. Osteoarthritis H, Gelber AC, Hochberg MC, et al. 2000. Joint injury in young

adults and risk for subsequent knee and hip osteoarthritis.(16).

60. Oeppen J, Vaupel JW. 2002. Broken Limits to Life Expectancy. Science (80-.). 296(10 May):2002.

61. Reimers CD, Knapp G, Reimers AK. 2012. Does physical activity increase life expectancy? A review of the literature. J. Aging Res. 2012.

62. Kontis V, Bennett JE, Mathers CD, et al. 2017. Future life expectancy in 35 industrialised countries: projections with a Bayesian model ensemble. Lancet 389(10076):1323–1335.

63. Sophia Fox a. J, Bedi A, Rodeo S a. 2009. The Basic Science of Articular Cartilage: Structure, Composition, and Function. Sport. Heal. A Multidiscip. Approach 1(6):461–468.

64. Hunziker EB, Quinn TM, Häuselmann HJ. 2002. Quantitative structural organization of normal adult human articular cartilage. Osteoarthr. Cartil. 10(7):564–572.

65. Mow VC, Ratcliffe a, Poole a R. 1992. Cartilage and diarthrodial joints as paradigms for hierarchical materials and structures. Biomaterials 13(2):67–97.

66. Frisbie DD, Cross MW, Mcllwraith CW. 2006. A comparative study of articular cartilage thickness in the stifle of animal species used in human pre-clinical studies compared to articular cartilage thickness in the human knee. Vet. Comp. Orthop. Traumatol. J. 19:142–146.

67. Mow VC, Wang CC, Hung CT. 1999. The extracellular matrix, interstitial fluid and ions as a mechanical signal transducer in articular cartilage. Osteoarthr. Cartil. 7:41–58.

68. Moore AC, Burris DL. 2017. Tribological rehydration of cartilage and its potential role in preserving joint health. Osteoarthr. Cartil. 25(1):99–107.

69. Buckwalter JA, Mow VC, Ratcliffe A. 1994. Restoration of Injured or Degenerated Articular Cartilage. J. Am. Acad. Orthop. Surg. 2(4):192–201.

70. Sanchez-Adams J, Leddy HA, McNulty AL, et al. 2014. The Mechanobiology of Articular Cartilage: Bearing the Burden of Osteoarthritis. Curr. Rheumatol. Rep. .

71. Wu QQ, Chen Q. 2000. Mechanoregulation of chondrocyte proliferation, maturation, and hypertrophy: ion-channel dependent transduction of matrix

deformation signals. Exp. Cell Res. 256:383–391.

72. Lee W, Leddy H a., Chen Y, et al. 2014. Synergy between Piezo1 and Piezo2 channels confers high-strain mechanosensitivity to articular cartilage. Proc. Natl. Acad. Sci. 111:E5114–E5122.

73. Goldring MB, Marcu KB. 2009. Cartilage homeostasis in health and rheumatic diseases. Arthritis Res. Ther. 11(3):224.

74. Riordan EA, Little C, Hunter D. 2014. Pathogenesis of post-traumatic OA with a view to intervention. Best Pract. Res. Clin. Rheumatol. 28(1):17–30.

75. Lotz MK, Kraus VB. 2010. Posttraumatic osteoarthritis: pathogenesis and pharmacological treatment options. Arthritis Res. Ther. 12:211.

76. Chaudhari AMW, Briant PL, Bevill SL, et al. 2008. Knee kinematics, cartilage morphology, and osteoarthritis after ACL injury. Med. Sci. Sports Exerc. 40(2):215–222.

77. Jonh T, Stahel PF, Morgan SJ, Schulze-Tanzil G. 2007. Impact of the complement cascade on posttraumatic cartilage inflammation and degradation. Histol. Histopathol. 22:781–790.

78. Lieberthal J, Sambamurthy N, Scanzello CR. 2015. Inflammation in joint injury and post-traumatic osteoarthritis. Osteoarthr. Cartil. 23(11):1825–1834.

79. Punzi L, Galozzi P, Luisetto R, et al. 2016. Post-traumatic arthritis: overview on pathogenic mechanisms and role of inflammation. RMD Open 2(2):e000279.

80. Swärd P, Kostogiannis I, Neuman P, et al. 2010. Differences in the radiological characteristics between post-traumatic and non-traumatic knee osteoarthritis. Scand. J. Med. Sci. Sport. 20:731–739.

81. Buckland-Wright JC, Lynch J a, Dave B. 2000. Early radiographic features in patients with anterior cruciate ligament rupture. Ann. Rheum. Dis. 59:641–646.

82. van der Kraan PM, van den Berg WB. 2007. Osteophytes: relevance and biology. Osteoarthr. Cartil. 15:237–244.

83. Meyer EG. 2009. Biomechanical Response of the Knee To Injury.

84. Dare D, Rodeo S. 2014. Mechanisms of post-traumatic osteoarthritis after ACL injury. Curr. Rheumatol. Rep. 16(10):448.

85. Lerer DB, Umans HR, Xu MX, Jones MH. 2004. The role of meniscal root

pathology and radial meniscal tear in medial meniscal extrusion. Skeletal Radiol. 33(10):569–574.

86. Hunter DJ, Zhang YQ, Niu JB, et al. 2006. The association of meniscal pathologic changes with cartilage loss in symptomatic knee osteoarthritis. Arthritis Rheum. 54(3):795–801.

87. Bin S Il, Jeong TW, Kim SJ, Lee DH. 2016. A new arthroscopic classification of degenerative medial meniscus root tear that correlates with meniscus extrusion on magnetic resonance imaging. Knee 23(2):246–250.

88. Badlani JT, Borrero C, Golla S, et al. 2013. The effects of meniscus injury on the development of knee osteoarthritis: data from the osteoarthritis initiative. Am. J. Sports Med. 41(6):1238–44.

89. Little CB, Zaki S. 2012. What constitutes an “animal model of osteoarthritis” - the need for consensus? Osteoarthr. Cartil. 20(4):261–267.

90. Malfait AM, Little CB. 2015. On the predictive utility of animal models of osteoarthritis. Arthritis Res. Ther. 17(1).

91. Goetz JE, Fredericks D, Petersen E, et al. 2015. A clinically realistic large animal model of intra-articular fracture that progresses to post-traumatic osteoarthritis. Osteoarthr. Cartil. 23(10):1797–1805.

92. Christiansen BA, Guilak F, Lockwood KA, et al. 2015. Non-invasive mouse models of post-traumatic osteoarthritis. Osteoarthr. Cartil. 23(10):1627–1638.

93. Blaker CL, Clarke EC, Little CB. 2017. Using mouse models to investigate the pathophysiology, treatment, and prevention of post-traumatic osteoarthritis. J. Orthop. Res. 35(3):424–439.

94. Poulet B. 2017. Models to define the stages of articular cartilage degradation in osteoarthritis development. Int. J. Exp. Pathol. 98(3):120–126.

95. Anderson DD, Marsh JL, Brown TD. 2011. OREF 2011 Clinical Research Award Paper: The pathomechanical etiology of post-traumatic osteoarthritis following intraarticular fractures. Iowa Orthop. J. 31:1–20.

96. Cope PJ, Ourradi K, Li Y, Sharif M. 2018. Models of osteoarthritis: the good, the bad and the promising. Osteoarthr. Cartil. 27:230–239.

97. Johnson CI, Argyle DJ, Clements DN. 2016. In vitro models for the study of osteoarthritis. Vet. J. 209:40–49.

98. Little CB, Hunter DJ. 2013. Post-traumatic osteoarthritis: From mouse models to clinical trials. Nat. Rev. Rheumatol. .

99. Glasson SS, Blanchet TJ, Morris E a. 2007. The surgical destabilization of the medial meniscus (DMM) model of osteoarthritis in the 129/SvEv mouse. Osteoarthr. Cartil. 15:1061–1069.

100. Lotz MK, Otsuki S, Grogan SP, et al. 2010. Cartilage cell clusters. Arthritis Rheum. 62(8):2206–2218.

101. Papathanasiou I, Michalitsis S, Hantes ME, et al. 2016. Molecular changes indicative of cartilage degeneration and osteoarthritis development in patients with anterior cruciate ligament injury. BMC Musculoskelet. Disord. 17(1):21.

102. Goggs R, Carter SD, Schulze-Tanzil G, et al. 2003. Apoptosis and the loss of chondrocyte survival signals contribute to articular cartilage degradation in osteoarthritis. Vet. J. 166:140–158.

103. Appleton CTG, Pitelka V, Henry J, Beier F. 2007. Global analyses of gene expression in early experimental osteoarthritis. Arthritis Rheum. 56(6):1854–1868.

104. Kramer WC, Hendricks KJ, Wang J. 2011. Pathogenetic mechanisms of posttraumatic osteoarthritis: Opportunities for early intervention. Int. J. Clin. Exp. Med. 4(4):285–298.

105. Buckwalter JA, Brown TD. 2004. Joint Injury, Repair, and Remodeling. Clin. Orthop. Relat. Res. 423(423):7–16.

106. Lotz M. 2001. Cytokines in cartilage injury and repair. In: Clinical Orthopaedics and Related Research. .

107. Adams D. 2012. Current Concepts for Anterior Cruciate Ligament Reconstruction: A Criterion-Based Rehabilitation Progression. J. Orthop. Sports Phys. Ther. .

108. Gineyts E, Mo JA, Ko A, et al. 2004. Effects of ibuprofen on molecular markers of cartilage and synovium turnover in patients with knee osteoarthritis. Ann Rheum Dis 63(7):857–861.

109. Fleming BC, Hulstyn MJ, Oksendahl HL, Fadale PD. 2005. Ligament Injury, Reconstruction and Osteoarthritis. Curr. Opin. Orthop. 16(5):354–362.

110. Hunziker EB. 2002. Articular cartilage repair: Basic science and clinical

progress. A review of the current status and prospects. Osteoarthr. Cartil. 10(2001):432–463.

111. Kurtz S, Ong K, Lau E, et al. 2007. Projections of primary and revision hip and knee arthroplasty in the United States from 2005 to 2030. J. Bone Jt. Surg. - Ser. A 89(4):780–785.

112. Old AB, Long WJ, Scott WN. 2017. Revision of Total Knee Arthroplasties Performed in Young, Active Patients with Posttraumatic Arthritis and Osteoarthritis. J. Knee Surg. 30(9):905–908.

113. Bala A, Penrose CT, Seyler TM, et al. 2015. Outcomes after Total Knee Arthroplasty for post-traumatic arthritis. Knee 22(6):630–639.

114. Konopka JF, Gomoll AH, Thornhill TS, et al. 2014. The cost-effectiveness of surgical treatment of medial unicompartmental knee osteoarthritis in younger patients a computer model-based evaluation. J. Bone Jt. Surg. - Am. Vol. 97(10):807–817.

115. Watt FE, Corp N, Kingsbury SR, et al. 2018. Towards prevention of post-traumatic osteoarthritis: report from an international expert working group on considerations for the design and conduct of interventional studies following acute knee injury. Osteoarthr. Cartil. 27(1):23–33.

116. Sellam J, Berenbaum F. 2010. The role of synovitis in pathophysiology and clinical symptoms of osteoarthritis. Nat. Rev. Rheumatol. 6:625–635.

117. Furman BD, Mangiapani DS, Zeitler E, et al. 2014. Targeting pro-inflammatory cytokines following joint injury: Acute intra-articular inhibition of interleukin-1 following knee injury prevents post-traumatic arthritis. Arthritis Res. Ther. 16(3):1–15.

118. Kraus VB, Birmingham J, Stabler T V., et al. 2012. Effects of intraarticular IL1-Ra for acute anterior cruciate ligament knee injury: A randomized controlled pilot trial (NCT00332254). Osteoarthr. Cartil. 20(4):271–278.

119. Caron JP, Fernandes JC, Martel-Pelletier J, et al. 1996. Chondroprotective effect of intraarticular injections of interleukin-1 receptor antagonist in experimental osteoarthritis. Suppression of collagenase-1 expression. Arthritis Rheum. 39(9):1535–1544.

120. Coughlin TR, Kennedy OD. 2016. The role of subchondral bone damage in post-traumatic osteoarthritis. Ann. N. Y. Acad. Sci. 1383:58–66.

121. Findlay DM, Kuliwaba JS. 2016. Bone – cartilage crosstalk : a conversation for understanding osteoarthritis.(July).

122. Kwan Tat S, Lajeunesse D, Pelletier JP, Martel-Pelletier J. 2010. Targeting subchondral bone for treating osteoarthritis: what is the evidence? Best Pract. Res. Clin. Rheumatol. 24(1):51–70.

123. Castañeda S, Roman-Blas J a., Largo R, Herrero-Beaumont G. 2012. Subchondral bone as a key target for osteoarthritis treatment. Biochem. Pharmacol. 83:315–323.

124. Mahjoub M, Berenbaum F, Houard X. 2012. Why subchondral bone in osteoarthritis? the importance of the cartilage bone interface in osteoarthritis. Osteoporos. Int. 23(8 SUPPL).

125. Zhang LZ, Zheng HA, Jiang Y, et al. 2012. Mechanical and biologic link between cartilage and subchondral bone in osteoarthritis. Arthritis Care Res. 64(7):960–967.

126. Pan J, Wang B, Li W, et al. 2012. Elevated cross-talk between subchondral bone and cartilage in osteoarthritic joints. Bone 51(2):212–217.

127. Fleisch HA. 1997. Bisphosphonates: Preclinical aspects and use in osteoporosis. Ann. Med. 29(1):55–62.

128. Russell RGG. 2011. Bisphosphonates : The first 40 years. Bone 49:2–19.

129. Fleisch H, Maerki J, Russell RG. 1966. Effect of pyrophosphate on dissolution of hydroxyapatite and its possible importance in calcium homeostasis. Proc. Soc. Exp. Biol. Med. Soc. Exp. Biol. Med. 122(2):317–320.

130. Goldring SR, Gravallese EM. 2004. Bisphosphonates: Environmental protection for the joint? Arthritis Rheum. 50(7):2044–2047.

131. Roelofs AJ, Thompson K, Gordon S, et al. 2006. Molecular mechanisms of action of bisphosphonates: Current status. Clin. Cancer Res. 12.

132. Russell RG, Rogers MJ, Frith JC, et al. 1999. The pharmacology of bisphosphonates and new insights into their mechanisms of action. J. Bone Miner. Res. 14 Suppl 2:53–65.

133. Graham R, Russell G. 2007. Bisphosphonates : Mode of Action and Pharmacology. Pediatrics 119:S150–S162.

134. Green JR, Rogers MJ. 2002. Pharmacologic profile of zoledronic acid: A highly

potent inhibitor of bone resorption. Drug Dev. Res. 55(October 2001):210–224.

135. Reszka A a, Rodan G a. 2004. Nitrogen-containing bisphosphonate mechanism of action. Mini Rev. Med. Chem. 4:711–719.

136. Buhaescu I, Izzedine H. 2007. Mevalonate pathway: A review of clinical and therapeutical implications. Clin. Biochem. 40:575–584.

137. Ebetino FH, Hogan AML, Sun S, et al. 2011. The relationship between the chemistry and biological activity of the bisphosphonates. Bone 49(1):20–33.

138. Rogers MJ, Watts DJ, Russell RG. 1997. Overview of bisphosphonates. Cancer 80:1652–1660.

139. Widler L, Jaeggi KA, Glatt M, et al. 2002. Highly potent geminal bisphosphonates. From pamidronate disodium (Aredia) to zoledronic acid (Zometa). J. Med. Chem. 45(17):3721–3738.

140. Reszka A a, Rodan G a. 2003. Bisphosphonate mechanism of action. Curr. Rheumatol. Rep. 5:65–74.

141. Luckman S., Hughes D., Coxon F., et al. 1998. Nitrogen-Containing Bisphosphonates Inhibit the Prenylation of GTP-Binding Proteins , Including Ras. J. Bone Miner. Res. 13(4):581–590.

142. Rogers MJ, Crockett JC, Coxon FP, Mönkkönen J. 2011. Biochemical and molecular mechanisms of action of bisphosphonates. Bone 49(1):34–41.

143. Halasy-Nagy JM, Rodan GA, Reszka AA. 2001. Inhibition of bone resorption by alendronate and risedronate does not require osteoclast apoptosis. Bone 29(6):553–559.

144. Kellinsalmi M, Mönkkönen H, Mönkkönen J, et al. 2005. In vitro comparison of clodronate, pamidronate and zoledronic acid effects on rat osteoclasts and human stem cell-derived osteoblasts. Basic Clin. Pharmacol. Toxicol. 97(6):382–391.

145. Nagaoka Y, Kajiya H, Ozeki S, et al. 2015. Mevalonates restore zoledronic acid-induced osteoclastogenesis inhibition. J. Dent. Res. 94(4):594–601.

146. Brien O. 2012. Zoledronic Acid not only Inhibits Osteoclast Activity but also Enhances Mineralisation. English J. 28(0505):2012.

147. Tai T-W, Chen C-Y, Su F-C, et al. 2017. Reactive oxygen species are required for zoledronic acid-induced apoptosis in osteoclast precursors and mature

osteoclast-like cells. Sci. Rep. 7(November 2016):44245.

148. Goldstein JL, Brown MS. 1990. Regulation of the mevalonate pathway. Nature 343(6257):425–430.

149. Massy ZA, Keane WF, Kasiske BL. 1996. Inhibition of the mevalonate pathway: benefits beyond cholesterol reduction? Lancet 347(8994):102–103.

150. Miziorko HM. 2011. Enzymes of the mevalonate pathway of isoprenoid biosynthesis. Arch. Biochem. Biophys. 505(2):131–143.

151. Hinson DD, Chambliss KL, Toth MJ, et al. 1997. Post-translational regulation of mevalonate kinase by intermediates of the cholesterol and nonsterol isoprene biosynthetic pathways. J. Lipid Res. 38(11):2216–23.

152. Ridley AJ, Paterson HF, Johnston CL, et al. 1992. The small GTP-binding protein rac regulates growth factor-induced membrane ruffling. Cell 70(3):401–410.

153. Ridley AJ, Hall A. 1992. The small GTP-binding protein rho regulates the assembly of focal adhesions and actin stress fibers in response to growth factors. Cell 70(3):389–399.

154. Doughman RL, Firestone AJ, Wojtasiak ML, et al. 2003. Membrane Ruffling Requires Coordination between Type Iα Phosphatidylinositol Phosphate Kinase and Rac Signaling. J. Biol. Chem. 278(25):23036–23045.

155. Pasapera AM, Plotnikov S V., Fischer RS, et al. 2015. Rac1-dependent phosphorylation and focal adhesion recruitment of myosin IIA regulates migration and mechanosensing. Curr. Biol. 25(2):175–186.

156. Rogers TL, Holen I. 2011. Tumour macrophages as potential targets of bisphosphonates. J. Transl. Med. 9(1):177.

157. Orriss IR, Key ML, Colston KW, Arnett TR. 2009. Inhibition of osteoblast function in vitro by aminobisphosphonates. J. Cell. Biochem. 106(November 2008):109–118.

158. Huang X, Huang S, Guo F, et al. 2016. Dose-dependent inhibitory effects of zoledronic acid on osteoblast viability and function in vitro. Mol. Med. Rep. 13(1):613–622.

159. Bellido T, Plotkin LI. 2011. Novel actions of bisphosphonates in bone: Preservation of osteoblast and osteocyte viability. Bone 49(1):50–55.

160. Reinholz GG, Getz B, Pederson L, et al. 2000. Bisphosphonates directly regulate cell proliferation, differentiation, and gene expression in human osteoblasts. Cancer Res. 60(21):6001–6007.

161. Maruotti N, Corrado A, Neve A, Cantatore FP. 2012. Bisphosphonates: Effects on osteoblast. Eur. J. Clin. Pharmacol. 68(7):1013–1018.

162. Reinholz GG, Getz B, Sanders ES, et al. 2002. Distinct mechanisms of bisphosphonate action between osteoblasts and breast cancer cells: Identity of a potent new bisphosphonate analogue. Breast Cancer Res. Treat. 71(3):257–268.

163. Zafar S, Coates DE, Cullinan MP, et al. 2016. Effects of zoledronic acid and geranylgeraniol on the cellular behaviour and gene expression of primary human alveolar osteoblasts. Clin. Oral Investig. 20(8):2023–2035.

164. Albadawi H, Haurani MJ, Oklu R, et al. 2013. Differential effect of zoledronic acid on human vascular smooth muscle cells. J. Surg. Res. 182(2):339–346.

165. Wu L, Zhu L, Shi WH, et al. 2009. Zoledronate inhibits the proliferation, adhesion and migration of vascular smooth muscle cells. Eur. J. Pharmacol. 602(1):124–131.

166. Lang M, Zhou Z, Shi L, et al. 2016. Influence of zoledronic acid on proliferation , migration , and apoptosis of vascular endothelial cells.54:889–893.

167. Ziebart T, Pabst A, Klein MO, et al. 2011. Bisphosphonates: Restrictions for vasculogenesis and angiogenesis: Inhibition of cell function of endothelial progenitor cells and mature endothelial cells in vitro. Clin. Oral Investig. 15(1):105–111.

168. Yang JX, Chen B, Pan YY, et al. 2012. Zoledronate Attenuates Angiogenic Effects of Angiotensin II-Stimulated Endothelial Progenitor Cells via RhoA and MAPK Signaling. PLoS One 7(10):1–10.

169. Tsai SH, Huang PH, Chang WC, et al. 2012. Zoledronate inhibits ischemia-induced neovascularization by impairing the mobilization and function of endothelial progenitor cells. PLoS One 7(7).

170. Yamada J, Tsuno NH, Kitayama J, et al. 2009. Anti-Angiogenic Property of Zoledronic Acid by Inhibition of Endothelial Progenitor Cell Differentiation. J. Surg. Res. 151(1):115–120.

171. Wood J, Bonjean K, Ruetz S, et al. 2002. Novel antiangiogenic effects of the

bisphosphonate compound zoledronic acid. J. Pharmacol. Exp. Ther. 302(3):1055–61.

172. Scheper MA, Badros A, Chaisuparat R, et al. 2009. Effect of zoledronic acid on oral fibroblasts and epithelial cells: A potential mechanism of bisphosphonate-associated osteonecrosis. Br. J. Haematol. 144(5):667–676.

173. F.G. B, T.N. P, C.F. de O, et al. 2013. Cytotoxic effects of zoledronic acid on human epithelial cells and gingival fibroblasts. Braz. Dent. J. 24(6):551–558.

174. Singireesu SSNR, Mondal SK, Yerramsetty S, Misra S. 2018. Zoledronic acid induces micronuclei formation, mitochondrial-mediated apoptosis and cytostasis in kidney cells. Life Sci. 203(March):305–314.

175. Heino TJ, Alm JJ, Halkosaari HJ, Välimäki V-V. 2016. Zoledronic acid in vivo increases in vitro proliferation of rat mesenchymal stromal cells. Acta Orthop. 87(4):412–417.

176. Zafar S, Coates DE, Cullinan MP, et al. 2014. Zoledronic acid and geranylgeraniol regulate cellular behaviour and angiogenic gene expression in human gingival fibroblasts. J. Oral Pathol. Med. 43(9):711–721.

177. Ohlrich EJ, Coates DE, Cullinan MP, et al. 2016. The bisphosphonate zoledronic acid regulates key angiogenesis-related genes in primary human gingival fibroblasts. Arch. Oral Biol. 63:7–14.

178. Liu H, Wang S-H, Chen S-C, et al. 2016. Immune modulation of CD4+CD25+ regulatory T cells by zoledronic acid. BMC Immunol. 17(1):45.

179. Orsini G, Failli A, Legitimo A, et al. 2011. Zoledronic acid modulates maturation of human monocyte-derived dendritic cells. Exp Biol Med 236(12):1420–1426.

180. Bringmann a, Schmidt SM, Weck MM, et al. 2007. Zoledronic acid inhibits the function of Toll-like receptor 4 ligand activated monocyte-derived dendritic cells. Leukemia :732–738.

181. Wolf AM, Rumpold H, Tilg H, et al. 2006. The effect of zoledronic acid on the function and differentiation of myeloid cells. Haematologica 91(9):1165–1171.

182. Moreau MF, Guillet C, Massin P, et al. 2007. Comparative effects of five bisphosphonates on apoptosis of macrophage cells in vitro. Biochem. Pharmacol. 73(5):718–723.

183. Sabatino R, Antonelli A, Battistelli S, et al. 2014. Macrophage Depletion by Free Bisphosphonates and Zoledronate-Loaded Red Blood Cells. PLoS One 9(6):e101260.

184. Cecchini MG, Felix R, Fleisch H, Cooper PH. 1987. Effect of bisphosphonates on proliferation and viability of mouse bone marrow-derived macrophages. J. Bone Miner. Res. 2(2):135–42.

185. Rogers MJ, Chilton KM, Coxon FP, et al. 1996. Bisphosphonates induce apoptosis in mouse macrophage-like cells in vitro by a nitric oxide-independent mechanism. J. Bone Miner. Res. 11(10):1482–1491.

186. Muratsu D, Yoshiga D, Taketomi T, et al. 2013. Zoledronic Acid Enhances Lipopolysaccharide-Stimulated Proinflammatory Reactions through Controlled Expression of SOCS1 in Macrophages. PLoS One 8(7):3–9.

187. Van Offel JF, Schuerwegh a J, Bridts CH, et al. 2002. Effect of bisphosphonates on viability, proliferation, and dexamethasone-induced apoptosis of articular chondrocytes. Ann. Rheum. Dis. 61(10):925–8.

188. Green JR, Guenther A. 2011. The backbone of progress - preclinical studies and innovations with zoledronic acid. Crit. Rev. Oncol. Hematol. 77(SUPPL.1):S3–S12.

189. Costa L, Harper P, Coleman RE, Lipton A. 2011. Anticancer evidence for zoledronic acid across the cancer continuum. Crit. Rev. Oncol. Hematol. 77(SUPPL.1):S31–S37.

190. Schech AJ, Kazi AA, Gilani RA, Brodie AH. 2013. Zoledronic Acid Reverses the Epithelial-Mesenchymal Transition and Inhibits Self-Renewal of Breast Cancer Cells through Inactivation of NF- B. Mol. Cancer Ther. 12(7):1356–1366.

191. Romani AA, Desenzani S, Morganti MM, et al. 2009. Zoledronic acid determines S-phase arrest but fails to induce apoptosis in cholangiocarcinoma cells. Biochem. Pharmacol. 78(2):133–141.

192. Okamoto S, Kawamura K, Li Q, et al. 2012. Zoledronic acid produces antitumor effects on mesothelioma through apoptosis and S-Phase arrest in p53-Independent and ras prenylation-independent manners. J. Thorac. Oncol. 7(5):873–882.

193. Liu S-S, Wang X-P, Li X-B, et al. 2014. Zoledronic acid exerts antitumor effects in NB4 acute promyelocytic leukemia cells by inducing apoptosis and S

phase arrest. Biomed. Pharmacother. = Biomédecine pharmacothérapie 68(8):1031–6.

194. Li X-Y, Lin Y-C, Huang W-L, et al. 2012. Zoledronic acid inhibits human nasopharyngeal carcinoma cell proliferation by activating mitochondrial apoptotic pathway. Med. Oncol. 29(5):3374–3380.

195. You Y, Li H, Chen J, et al. 2017. Zoledronic acid reverses cisplatin resistance in nasopharyngeal carcinoma cells by activating the mitochondrial apoptotic pathway. Oncol. Lett. :1840–1846.

196. Ma YG, Liu WC, Dong S, et al. 2012. Activation of BKca channels in zoledronic acid-induced apoptosis of MDA-MB-231 breast cancer cells. PLoS One 7(5).

197. Coscia M, Quaglino E, Iezzi M, et al. 2010. Zoledronic acid repolarizes tumour-associated macrophages and inhibits mammary carcinogenesis by targeting the mevalonate pathway. J. Cell. Mol. Med. 14(12):2803–2815.

198. Han FS, Lin M Bin, Zhu HY, et al. 2016. Anti-proliferation effect of zoledronic acid on human colon cancer line SW480. Asian Pac. J. Trop. Med. 9(2):168–171.

199. Fujita M, Tohi M, Sawada K, et al. 2012. Involvement of the mevalonate pathway in the antiproliferative effect of zoledronate on ACHN renal cell carcinoma cells. Oncol. Rep. 27(5):1371–1376.

200. Gao X, Jiang B, Zou S, et al. 2015. Zoledronate can promote apoptosis and inhibit the proliferation of colorectal cancer cells. Tumor Biol. 36(7):5315–5322.

201. Taran F, Hartkopf A, Seeger H, et al. 2011. Antitumor activity of zoledronic acid in primary breast cancer cells determined by the ATP tumor chemosensitivity assay. Geburtshilfe Frauenheilkd. 71(08):1.

202. Ory B, Blanchard F, Battaglia S, et al. 2007. Zoledronic acid activates the DNA S-phase checkpoint and induces osteosarcoma cell death characterized by apoptosis-inducing factor and endonuclease-G translocation independently of p53 and retinoblastoma status. Mol. Pharmacol. 71(1):333–343.

203. Denoyelle C, Hong L, Vannier JP, et al. 2003. New insights into the actions of bisphosphonate zoledronic acid in breast cancer cells by dual RhoA-dependent and -independent effects. Br. J. Cancer 88(10):1631–1640.

204. Zekria J, Mansour M, Karim SM. 2014. The anti-tumour effects of zoledronic acid. J. Bone Oncol. 3(1):25–35.

205. Levin-Gromiko U, Koshelev V, Kushnir P, et al. 2014. Amplified lipid rafts of malignant cells constitute a target for inhibition of aberrantly active NFAT and melanoma tumor growth by the aminobisphosphonate zoledronic acid. Carcinogenesis 35(11):2555–2566.

206. Li YY, Chang JWC, Chou WC, et al. 2008. Zoledronic acid is unable to induce apoptosis, but slows tumor growth and prolongs survival for non-small-cell lung cancers. Lung Cancer 59(2):180–191.

207. Croucher P, Jagdev S, Coleman R. 2003. The anti-tumor potential of zoledronic acid. Breast 12 Suppl 2:S30-6.

208. Yuasa T, Kimura S, Ashihara E, et al. 2007. Zoledronic acid - a multiplicity of anti-cancer action. Curr. Med. Chem. 14:2126–2135.

209. Podworny N V., Kandel RA, Renlund RC, Grynpas MD. 1999. Partial chondroprotective effect of zoledronate in a rabbit model of inflammatory arthritis. J. Rheumatol. 26(9):1972–1982.

210. Herrak P, Görtz B, Hayer S, et al. 2004. Zoledronic acid protects against local and systemic bone loss in tumor necrosis factor-mediated arthritis. Arthritis Rheum. 50(7):2327–2337.

211. Keller KK., Thomsen JS., Stengaard-Pedersen K., Hauge E-M. 2014. Systemic but no local effects of combined zoledronate and parathyroid hormone treatment in experimental autoimmune arthritis. PLoS One 9(3):1–8.

212. Le Goff B, Soltner E, Charrier C, et al. 2009. A combination of methotrexate and zoledronic acid prevents bone erosions and systemic bone mass loss in collagen induced arthritis. Arthritis Res. Ther. 11(6):R185.

213. Pysklywec MW, Moran EL, Bogoch ER. 2000. Changes in cross-sectional geometry of the distal femoral metaphysis associated with inflammatory arthritis are reduced by a bisphosphonate (zoledronate). J. Orthop. Res. 18(5):734–738.

214. Sims N a., Green JR, Glatt M, et al. 2004. Targeting osteoclasts with zoledronic acid prevents bone destruction in collagen-induced arthritis. Arthritis Rheum. 50(7):2338–2346.

215. Morado-Urbina CE, Alvarado-Vázquez PA, Montiel-Ruiz RM, et al. 2014.

Early, middle, or late administration of zoledronate alleviates spontaneous nociceptive behavior and restores functional outcomes in a mouse model of CFA-induced arthritis. Drug Dev. Res. 75(7):438–448.

216. Harada H, Nakayama T, Tanaka T, Katsumata T. 2004. Effects of bisphosphonates on joint damage and bone loss in rat adjuvant-induced arthritis. Inflamm. Res. 53(2):45–52.

217. Muehleman C, Green J, Williams JM, et al. 2002. The effect of bone remodeling inhibition by zoledronic acid in an animal model of cartilage matrix damage. Osteoarthr. Cartil. 10:226–233.

218. Strassle BW, Mark L, Leventhal L, et al. 2010. Inhibition of osteoclasts prevents cartilage loss and pain in a rat model of degenerative joint disease. Osteoarthr. Cartil. 18(10):1319–1328.

219. Yu D, Liu F, Liu M, et al. 2013. The inhibition of subchondral bone lesions significantly reversed the weight-bearing deficit and the overexpression of CGRP in DRG neurons, GFAP and Iba-1 in the spinal dorsal horn in the monosodium iodoacetate induced model of osteoarthritis pain. PLoS One 8(10):e77824.

220. Laslett LL, Doré DA, Quinn SJ, et al. 2012. Zoledronic acid reduces knee pain and bone marrow lesions over 1 year: a randomised controlled trial. Ann. Rheum. Dis. 71(8):1322–8.

221. Aitken D, Laslett LL, Cai G, et al. 2018. A protocol for a multicentre, randomised, double-blind, placebo-controlled trial to compare the effect of annual infusions of zoledronic acid to placebo on knee structural change and knee pain over 24 months in knee osteoarthritis patients - ZAP2. BMC Musculoskelet. Disord. 19(1):1–12.

222. Rossini M, Viapiana O, Ramonda R, et al. 2009. Intra-articular clodronate for the treatment of knee osteoarthritis: Dose ranging study vs hyaluronic acid. Rheumatology 48(7):773–778.

223. Rossini M, Adami S, Fracassi E, et al. 2014. Effects of intra-articular clodronate in the treatment of knee osteoarthritis: results of a double-blind, randomized placebo-controlled trial. Rheumatol. Int. :255–263.

224. Varenna M, Zucchi F, Failoni S, et al. 2015. Intravenous neridronate in the treatment of acute painful knee osteoarthritis: a randomized controlled study. Rheumatology (Oxford). 54(10):1826–1832.

225. Jokar M, Mirfeizi Z, Keyvanpajoh K. 2010. The effect of alendronate on symptoms of knee osteoarthritis: A randomized controlled trial. Iran. J. Med. Sci. 35(1):9–15.

226. S. S, S.A. K, H.M. J. 2017. Alendronate sodium in osteoarthritis: Effects on anabolic, cartilage degredative markers, circulating leptin and the clinical activity. Osteoporos. Int. 28(03):S317.

227. Bingham CO, Buckland-Wright JC, Garnero P, et al. 2006. Risedronate decreases biochemical markers of cartilage degradation but does not decrease symptoms or slow radiographic progression in patients with medial compartment osteoarthritis of the knee: Results of the two-year multinational knee osteoarthritis st. Arthritis Rheum. 54(11):3494–3507.

228. Buckland-Wright CJ, Messent EA, Bingham CO, et al. 2007. A 2 yr longitudinal radiographic study examining the effect of a bisphosphonate (risedronate) upon subchondral bone loss in osteoarthritic knee patients. Rheumatology 46(2):257–264.

229. Spector TD, Conaghan PG, Buckland-Wright JC, et al. 2005. Effect of risedronate on joint structure and symptoms of knee osteoarthritis: results of the BRISK randomized, controlled trial [ISRCTN01928173]. Arthritis Res. Ther. 7(3):R625.

230. Iwamoto J, Takeda T, Sato Y, Matsumoto H. 2010. Effects of Risedronate on Osteoarthritis of the Knee.51(2):164–170.

231. Fujita T, Ohue M, Fujii Y, et al. 2008. Analgesic and chondroprotective effects of risedronate in osteoarthritis assessed by electroalgometry and measurement of collagen type II fragments in urine. J. Int. Med. Res. 36(5):932–941.

232. Laslett LL, Kingsbury SR, Hensor EMA, et al. 2014. Effect of bisphosphonate use in patients with symptomatic and radiographic knee osteoarthritis: data from the Osteoarthritis Initiative. Ann. Rheum. Dis. 73(5):824–30.

233. Davis AJ, Smith TO, Hing CB, Sofat N. 2013. Are Bisphosphonates Effective in the Treatment of Osteoarthritis Pain? A Meta-Analysis and Systematic Review. PLoS One 8(9).

234. Saag KG. 2008. Bisphosphonates for osteoarthritis prevention: Holy Grail or not? Ann. Rheum. Dis. 67(10):1358–9.

235. Lems WF. 2018. Bisphosphonates: A therapeutic option for knee osteoarthritis? Ann. Rheum. Dis. 77(9):1247–1248.

236. Xing RL, Zhao LR, Wang PM. 2016. Bisphosphonates therapy for osteoarthritis: a meta-analysis of randomized controlled trials. Springerplus 5(1):1704.

237. Deveza LA, Bierma-Zeinstra SMA, van Spil WE, et al. 2018. Efficacy of bisphosphonates in specific knee osteoarthritis subpopulations: protocol for an OA Trial Bank systematic review and individual patient data meta-analysis. BMJ Open 8(12):e023889.

238. Yu D, Yu B, Mao Y, et al. 2012. Efficacy of zoledronic acid in treatment of teoarthritis is dependent on the disease progression stage in rat medial meniscal tear model. Acta Pharmacol. Sin. 33:924–934.

239. Lampropoulou-Adamidou K, Dontas I, Stathopoulos IP, et al. 2014. Chondroprotective effect of high-dose zoledronic acid: An experimental study in a rabbit model of osteoarthritis. J. Orthop. Res. 32(12):1646–1651.

240. Dearmin MG, Trumble TN, García A, et al. 2014. Chondroprotective effects of zoledronic acid on articular cartilage in dogs with experimentally induced osteoarthritis. Am. J. Vet. Res. 75(4):329–337.

241. Price C, Li B, Quabili TR, et al. 2011. Early interventions in Post-Trauma OA with zoledronic acid. Trans. Annu. Meet. Orthop. Res. Soc. 3(128):821236.

242. Black DM, Kelly MP, Genant HK, et al. 2010. Bisphosphonates and Fractures of the Subtrochanteric or Diaphyseal Femur. N. Engl. J. Med. 362(19):1761–1771.

243. Giusti A, Hamdy NAT, Papapoulos SE. 2010. Atypical fractures of the femur and bisphosphonate therapy. A systematic review of case/case series studies. Bone 47(2):169–180.

244. Khosla S, Burr D, Cauley J, et al. 2007. Bisphosphonate-associated osteonecrosis of the jaw: report of a task force of the American Society for Bone and Mineral Research. J. Bone Miner. Res. 22(10):1479–91.

245. Carbonare LD, Zanatta M, Gasparetto A, Valenti MT. 2010. Safety and tolerability of zoledronic acid and other bisphosphonates in osteoporosis management. Drug. Healthc. Patient Saf. 2(1):121–137.

246. Evans CH, Kraus VB, Setton L a. 2013. Progress in intra-articular therapy. Nat. Rev. Rheumatol. 10(1):11–22.

247. Wehling P, Evans C, Wehling J, Maixner W. 2017. Effectiveness of intra-

articular therapies in osteoarthritis: a literature review. Ther. Adv. Musculoskelet. Dis. 9(8):183–196.

248. Larsen C, Østergaard J, Larsen SW, et al. 2008. Intra-articular depot formulation principles: Role in the management of postoperative pain and arthritic disorders. J. Pharm. Sci. 97(11):4622–4654.

249. Edwards SHR. 2011. Intra-articular drug delivery: The challenge to extend drug residence time within the joint. Vet. J. 190(1):15–21.

250. Rai MF, Pham CT. 2018. Intra-articular drug delivery systems for joint diseases. Curr. Opin. Pharmacol. 40:67–73.

251. Evans CH. 2018. Catering to chondrocytes. Sci. Transl. Med. 10(469):eaav7043.

252. Maudens P, Jordan O, Allémann E. 2018. Recent advances in intra-articular drug delivery systems for osteoarthritis therapy. Drug Discov. Today 23(10):1761–1775.

253. de Lange-Brokaar BJE, Ioan-Facsinay a., van Osch GJVM, et al. 2012. Synovial inflammation, immune cells and their cytokines in osteoarthritis: A review. Osteoarthr. Cartil. 20(12):1484–1499.

254. Sulochana K, Srinivasan V. 2014. Effect of Zoledronate on expression of vascular endothelial growth factor and pigment epithelium-derived factor: An in vitro study. J Bone Metab 21(1):249–255.

255. Zhou Y, Resutek L, Wang L, Lu XL. 2013. Effects of Bisphosphonate on long-term culture of cartilage allografts. ASME Summer Bioeng. Conf. :26–27.

256. Zhou J, Zhou Y, Park M, et al. 2015. Chondro-protective Effects of Bisphosphonate for PTOA Could Attribute to the Inhibition of Chondrocyte Mevalonate Pathway. Trans. Annu. Meet. Orthop. Res. Soc. (1):1–4.

257. Zhou Y, Park M, Wang L, Lu X. 2014. Bisphosphonate rescues cartilage from trauma damage by promoting mechanical sensitivity and calcium signaling in chondrocytes. Osteoarthr. Cartil. 22(2014):S307–S308.

258. Li W, Park M, Kirn-safran C, et al. 2012. Calcium Signaling of Chondrocytes under Osmotic Stress and Mechanical Stimulation. ASME Summer Bioeng. Conf. :5–6.

259. Cınar BM, Ozkoc G, Bolat F, et al. 2015. Intra-articular zoledronic acid in a rat

osteoarthritis model: significant reduced synovitis may indicate chondroprotective effect. Knee Surgery, Sport. Traumatol. Arthrosc. 23(5):1410–1418.

260. Uysal M, Ozkoc G, Bolat F, et al. 2016. Zoledronic acid effect on chondrocyte apoptosis in degenerative osteoarthritis model. Int. Surg. 101(5–6):291–296.

261. Leahy A a., Esfahani S a., Foote AT, et al. 2015. Analysis of the Trajectory of Osteoarthritis Development in a Mouse Model by Serial Near-Infrared Fluorescence Imaging of Matrix Metalloproteinase Activities. Arthritis Rheumatol. 67(2):442–453.

262. Kim BJ, Choi BH, Jin LH, et al. 2013. Comparison between subchondral bone change and cartilage degeneration in collagenase-and DMM-induced osteoarthritis (OA) models in mice. Tissue Eng. Regen. Med. 10(4):211–217.

263. Loeser RF, Olex AL, McNulty M a., et al. 2013. Disease Progression and Phasic Changes in Gene Expression in a Mouse Model of Osteoarthritis. PLoS One 8(1).

264. Kim BJ, Kim DW, Kim SH, et al. 2013. Establishment of a reliable and reproducible murine osteoarthritis model. Osteoarthr. Cartil. 21(12):2013–2020.

265. Gardiner MD, Vincent TL, Driscoll C, et al. 2015. Transcriptional analysis of micro-dissected articular cartilage in post-traumatic murine osteoarthritis. Osteoarthr. Cartil. 23(4):616–628.

266. Inglis JJ, McNamee KE, Chia SL, et al. 2008. Regulation of pain sensitivity in experimental osteoarthritis by the endogenous peripheral opioid system. Arthritis Rheum. 58(10):3110–3119.

267. Das Neves Borges P, Forte a. E, Vincent TL, et al. 2014. Rapid, automated imaging of mouse articular cartilage by microCT for early detection of osteoarthritis and finite element modelling of joint mechanics. Osteoarthr. Cartil. 22(10):1419–1428.

268. Burleigh A, Chanalaris A, Gardiner MD, et al. 2012. Joint immobilization prevents murine osteoarthritis and reveals the highly mechanosensitive nature of protease expression in vivo. Arthritis Rheum. 64(7):2278–2288.

269. Takayama K, Kawakami Y, Kobayashi M, et al. 2014. Local intra-articular injection of rapamycin delays articular cartilage degeneration in a murine model of osteoarthritis. Arthritis Res. Ther. 16(6):1–10.

270. Botter SM, Glasson SS, Hopkins B, et al. 2009. ADAMTS5-/- mice have less subchondral bone changes after induction of osteoarthritis through surgical instability: implications for a link between cartilage and subchondral bone changes. Osteoarthr. Cartil. 17(5):636–645.

271. Muramatsu Y, Sasho T, Saito M, et al. 2014. Preventive effects of hyaluronan from deterioration of gait parameters in surgically induced mice osteoarthritic knee model. Osteoarthr. Cartil. 22(6):831–835.

272. Xu L, Servais J, Polur I, et al. 2010. Attenuation of osteoarthritis progression by reduction of discoidin domain receptor 2 in mice. Arthritis Rheum. 62(9):2736–2744.

273. Van Lent PLEM, Blom AB, Schelbergen RFP, et al. 2012. Active involvement of alarmins S100A8 and S100A9 in the regulation of synovial activation and joint destruction during mouse and human osteoarthritis. Arthritis Rheum. 64(5):1466–1476.

274. Akagi R, Sasho T, Saito M, et al. 2014. Effective knock down of matrix metalloproteinase-13 by an intra-articular injection of small interfering RNA (siRNA) in a murine surgically-induced osteoarthritis model. J. Orthop. Res. 32(9):1175–1180.

275. Glasson SS, Askew R, Sheppard B, et al. 2004. Characterization of and osteoarthritis susceptibility in ADAMTS-4-knockout mice. Arthritis Rheum. 50(8):2547–2558.

276. Glasson SS, Askew R, Sheppard B, et al. 2005. Deletion of active ADAMTS5 prevents cartilage degradation in a murine model of osteoarthritis. Nature 434(7033):644–648.

277. Li W, Cai L, Zhang Y, et al. 2015. Intra-articular resveratrol injection prevents osteoarthritis progression in a mouse model by activating SIRT1 and thereby silencing HIF-2?? J. Orthop. Res. 1(July):1061–1070.

278. Sophocleous a., Börjesson a. E, Salter DM, Ralston SH. 2015. The type 2 cannabinoid receptor regulates susceptibility to osteoarthritis in mice. Osteoarthr. Cartil. :1–9.

279. Ma HL, Blanchet TJ, Peluso D, et al. 2007. Osteoarthritis severity is sex dependent in a surgical mouse model. Osteoarthr. Cartil. 15(6):695–700.

280. Little CB, Barai A, Burkhardt D, et al. 2009. Matrix metalloproteinase 13-deficient mice are resistant to osteoarthritic cartilage erosion but not

chondrocyte hypertrophy or osteophyte development. Arthritis Rheum. 60(12):3723–3733.

281. Sondergaard BC, Catala-Lehnen P, Huebner a. K, et al. 2012. Mice over-expressing salmon calcitonin have strongly attenuated osteoarthritic histopathological changes after destabilization of the medial meniscus. Osteoarthr. Cartil. 20(2):136–143.

282. Chambers MG, Bayliss MT, Mason RM. 1997. Chondrocyte cytokine and growth factor expression in murine osteoarthritis. Osteoarthr. Cartil. 5:301–308.

283. McNulty M a., Loeser RF, Davey C, et al. 2011. A Comprehensive Histological Assessment of Osteoarthritis Lesions in Mice. Cartilage 2(4):354–363.

284. Glasson SS, Chambers MG, Berg WB van den, Little CB. 2010. The OARSI histopathology initiative - recommendations for histological assessments of osteoarthritis in the mouse. Elsevier Ltd; p S17-23.

285. Moodie JP, Stok KS, Müller R, et al. 2011. Multimodal imaging demonstrates concomitant changes in bone and cartilage after destabilisation of the medial meniscus and increased joint laxity. Osteoarthr. Cartil. 19(2):163–170.

286. Arunakul M, Tochigi Y, Goetz JE, et al. 2013. Replication of chronic abnormal cartilage loading by medial meniscus destabilization for modeling osteoarthritis in the rabbit knee in vivo. J. Orthop. Res. 31(10):1555–1560.

287. Iijima H, Aoyama T, Ito a., et al. 2014. Destabilization of the medial meniscus leads to subchondral bone defects and site-specific cartilage degeneration in an experimental rat model. Osteoarthr. Cartil. 22(7):1036–1043.

288. Wu P, Holguin N, Silva MJ, et al. 2014. Early response of mouse joint tissue to noninvasive knee injury suggests treatment targets. Arthritis Rheumatol. 66(5):1256–1265.

289. McNulty MA, Loeser RF, Davey C, et al. 2012. Histopathology of naturally occurring and surgically induced osteoarthritis in mice. Osteoarthr. Cartil. 20(8):949–956.

290. Nelson F, Billinghurst RC, Pidoux RT, et al. 2006. Early post-traumatic osteoarthritis-like changes in human articular cartilage following rupture of the anterior cruciate ligament. Osteoarthr. Cartil. 14:114–119.

291. Kawamura S, Lotito K, Rodeo S a. 2003. Biomechanics and healing response of the meniscus. Oper. Tech. Sports Med. 11(2):68–76.

292. Thambyah A, Nather A, Goh J. 2006. Mechanical properties of articular cartilage covered by the meniscus. Osteoarthr. Cartil. 14(6):580–588.

293. Iijima H, Aoyama T, Ito A, et al. 2014. Immature articular cartilage and subchondral bone covered by menisci are potentially susceptive to mechanical load. BMC Musculoskelet. Disord. 15(1):101.

294. Moore AC, Burris DL. 2015. Tribological and material properties for cartilage of and throughout the bovine stifle: Support for the altered joint kinematics hypothesis of osteoarthritis. Osteoarthr. Cartil. 23(1):161–169.

295. Stolberg-Stolberg JA, Furman BD, William Garrigues N, et al. 2013. Effects of cartilage impact with and without fracture on chondrocyte viability and the release of inflammatory markers. J. Orthop. Res. 31(8):1283–1292.

296. Chen CT, Burton-Wurster N, Borden C, et al. 2001. Chondrocyte necrosis and apoptosis in impact damaged articular cartilage. J. Orthop. Res. 19(4):703–711.

297. Miller RE, Tran PB, Das R, et al. 2012. CCR2 chemokine receptor signaling mediates pain in experimental osteoarthritis. Pnas 109(50):2–7.

298. Malfait AM, Ritchie J, Gil AS, et al. 2010. ADAMTS-5 deficient mice do not develop mechanical allodynia associated with osteoarthritis following medial meniscal destabilization. Osteoarthr. Cartil. 18(4):572–580.

299. Kamekura S, Hoshi K, Shimoaka T, et al. 2005. Osteoarthritis development in novel experimental mouse models induced by knee joint instability. Osteoarthr. Cartil. 13:632–641.

300. Furman BD, Strand J, Hembree WC, et al. 2007. Joint degeneration following closed intraarticular fracture in the mouse knee: A model of posttraumatic arthritis. J. Orthop. Res. 25(5):578–592.

301. Felson DT, Kim YJ. 2007. The futility of current approaches to chondroprotection. Arthritis Rheum. 56(5):1378–1383.

302. Buckwalter JA, Felson DT. 2015. Post-traumatic arthritis: Definitions and burden of disease. In: Post-Traumatic Arthritis: Pathogenesis, Diagnosis and Management. p 7–15.

303. Thomas AC, Hubbard-Turner T, Wikstrom EA, Palmieri-Smith RM. 2017. Epidemiology of Posttraumatic Osteoarthritis. J. Athl. Train. 52(6):491–496.

304. Gillquist J, Messner K. 1999. Anterior cruciate ligament reconstruction and the

long-term incidence of gonarthrosis. Sports Med. 27(3):143–156.

305. Takeda H, Nakagawa T, Nakamura K, Engebretsen L. 2011. Prevention and management of knee osteoarthritis and knee cartilage injury in sports. Br. J. Sports Med. 45:304–309.

306. Dhinsa BS, Adesida AB. 2012. Current clinical therapies for cartilage repair, their limitation and the role of stem cells. Curr. Stem Cell Res. Ther. 7(2):143–148.

307. Lipton A. 2005. New therapeutic agents for the treatment of bone diseases. Expert Opin. Biol. Ther. 2598.

308. Corrado A, Santoro N, Cantatore FP. 2007. Extra-skeletal effects of bisphosphonates. Jt. Bone Spine 74(1):32–38.

309. Agnello K a, Trumble TN, Chambers JN, et al. 2005. Effects of zoledronate on markers of bone metabolism and subchondral bone mineral. Am. J. Vet. Res. 66(9):1487–1495.

310. David MA, Smith MK, Pilachowski RN, et al. 2017. Early, focal changes in cartilage cellularity and structure following surgically induced meniscal destabilization in the mouse. J. Orthop. Res. 35(3):537–547.

311. Scholzen T, Gerdes J. 2000. The Ki-67 protein: From the known and the unknown. J. Cell. Physiol. 182(3):311–322.

312. Bavle R. 2014. Eosinophilic Nucleoli. J. Oral Maxillofac. Pathol. 18(2):152.

313. Zuscik MJ, Hilton MJ, Zhang X, et al. 2008. Regulation of chondrogenesis and chondrocyte differentiation by stress. J. Clin. Invest. 118(2):429–438.

314. Mackie EJ, Ahmed Y a., Tatarczuch L, et al. 2008. Endochondral ossification: How cartilage is converted into bone in the developing skeleton. Int. J. Biochem. Cell Biol. 40:46–62.

315. Han SK, Ronkainen AP, Saarakkala S, et al. 2018. Alterations in structural macromolecules and chondrocyte deformations in lapine retropatellar cartilage 9 weeks after anterior cruciate ligament transection. J. Orthop. Res. 36(1):342–350.

316. Bi X, Yang X, Bostrom MPG, et al. 2007. Fourier transform infrared imaging and MR microscopy studies detect compositional and structural changes in cartilage in a rabbit model of osteoarthritis. Anal. Bioanal. Chem. 387(5):1601–

1612.

317. Majumdar MK, Askew R, Schelling S, et al. 2007. Double-knockout of ADAMTS-4 and ADAMTS-5 in mice results in physiologically normal animals and prevents the progression of osteoarthritis. Arthritis Rheum. 56(11):3670–3674.

318. Little CB, Meeker CT, Golub SB, et al. 2007. Blocking aggrecanase cleavage in the aggrecan interglobular domain abrogates cartilage erosion and promotes cartilage repair. J. Clin. Invest. 117(6):1627–1636.

319. Bian L, Lima EG, Angione SL, et al. 2008. Mechanical and biochemical characterization of cartilage explants in serum-free culture. J. Biomech. 41(6):1153–1159.

320. Goldring MB. 2012. Chondrogenesis, chondrocyte differentiation, and articular cartilage metabolism in health and osteoarthritis. Ther. Adv. Musculoskelet. Dis. 4(4):269–85.

321. Roach HI, Aigner T, Kouri JB. 2004. Chondroptosis: A variant of apoptotic cell death in chondrocytes? Apoptosis 9(3):265–277.

322. Goldring MB, Tsuchimochi K, Ijiri K. 2006. The control of chondrogenesis. J. Cell. Biochem. 97:33–44.

323. Decker RS. 2017. Articular cartilage and joint development from embryogenesis to adulthood. Semin. Cell Dev. Biol. 62:50–56.

324. Seol D, McCabe DJ, Choe H, et al. 2012. Chondrogenic progenitor cells respond to cartilage injury. Arthritis Rheum. 64(11):3626–3637.

325. Redman SN, Dowthwaite GP, Thomson BM, Archer CW. 2004. The cellular responses of articular cartilage to sharp and blunt trauma. Osteoarthr. Cartil. 12(2):106–116.

326. Lee CM, Kisiday JD, McIlwraith CW, et al. 2013. Development of an in vitro model of injuryinduced osteoarthritis in cartilage explants from adult horses through application of single-impact compressive overload. Am. J. Vet. Res. 74(1):40–47.

327. Jeon OH, Kim C, Laberge R-M, et al. 2017. Local clearance of senescent cells attenuates the development of post-traumatic osteoarthritis and creates a pro-regenerative environment. Nat. Med. (April):1–9.

328. Wang C-J, Cheng J-H, Chou W-Y, et al. 2017. Changes of articular cartilage and subchondral bone after extracorporeal shockwave therapy in osteoarthritis of the knee. Int. J. Med. Sci. 14(3):213–223.

329. Zhang M, Mani SB, He Y, et al. 2016. Induced superficial chondrocyte death reduces catabolic cartilage damage in murine posttraumatic osteoarthritis. J. Clin. Invest. 126(8):2893–2902.

330. Boyce MK, Trumble TN, Carlson CS, et al. 2013. Non-terminal animal model of post-traumatic osteoarthritis induced by acute joint injury. Osteoarthr. Cartil. 21(5):746–755.

331. Jia H, Ma X, Tong W, et al. 2016. EGFR signaling is critical for maintaining the superficial layer of articular cartilage and preventing osteoarthritis initiation. Proc. Natl. Acad. Sci. U. S. A. 113(50):201608938.

332. Eyre DR, Mcdevitt CA, Billinghamii MEJ, Muiri H. 1980. Biosynthesis of Collagen and other Matrix Proteins by Articular Cartilage in Experimental Osteoarthrosis. Biochem. J 188:823–837.

333. Sandy JD, Adams ME, Billingham MEJ, et al. 1984. In Vivo and in Vitro Stimulation of Chondrocyte Biosynthetic Activity in Early Experimental Osteoarthritis. Arthritis Rheum. 27(4):388–397.

334. Venn G. 1995. Increased Proteoglycan Synthesis in Cartilage in experimental canine osteoarthritis does not reflect a permanent change in chondrocyte phenotype. Arthritis Rheum. 38(4):525–532.

335. Altman RD, Tenenbaum J, Latta L, et al. 1984. Biomechanical and biochemical properties of dog cartilage in experimentally induced osteoarthritis. Ann. Rheum. Dis. 43(1):83–90.

336. Palmoski MJ, Colyer RA, Brandt KD. 1980. Marked suppression by salicylate of the augmented proteoglycan synthesis in osteoarthritic cartilage. Arthritis Rheum. 23(1):83–91.

337. Carney SL, Billingham MEJ, Muir H, Sandy JD. 1984. Demonstration of increased proteoglycan turnover in cartilage explants from dogs with experimental osteoarthritis. J. Orthop. Res. .

338. Duan X, Rai MF, Holguin N, et al. 2017. Early changes in the knee of healer and non-healer mice following non-invasive mechanical injury. J. Orthop. Res. 35(3):524–536.

339. Dar Q, Schott EM, Catheline SE, et al. 2017. Daily oral consumption of hydrolyzed type 1 collagen is chondroprotective and anti- inflammatory in murine posttraumatic osteoarthritis.:1–24.

340. Schott EM, Farnsworth CW, Grier A, et al. 2018. Targeting the gut microbiome to treat the osteoarthritis of obesity. JCI Insight 3(8):1–18.

341. Lv, Mengxi, Zhou Y, Fan S, et al. 2017. Inhibition of Mevalonate Pathway in Chondrocytes Attenuates IL-1 Induced Cartilage Degeneration. ORS 2017 Annu. Meet. Poster No . 1529 (1529):2017.

342. Jotanovic Z, Mihelic R, Sestan B, Dembic Z. 2014. Emerging Pathways and Promising Agents with Possible Disease Modifying Effect in Osteoarthritis Treatment. Curr. Drug Targets 15(6):635–661.

343. Park DY, Min BH, Choi BH, et al. 2015. The degeneration of meniscus roots is accompanied by fibrocartilage formation, which may precede meniscus root tears in osteoarthritic knees. Am. J. Sports Med. 43(12):3034–3044.

344. Reszka A. 2012. Nitrogen-Containing Bisphosphonate Mechanism of Action. Mini Rev. Med. Chem. 4(7):711–719.

345. Wood J, Bonjean K, Ruetz S, et al. 2002. Novel antiangiogenic effects of the bisphosphonate compound zoledronic acid. J. Pharmacol. Exp. Ther. 302(3):1055–1061.

346. Otsu N. 1979. A Threshold Selection Method from Gray-Level Histograms. IEEE Trans. Syst. Man. Cybern. 9(1):62–66.

347. Glasson SS, Kraus VB, Huebner JL, et al. 2010. The OARSI histopathology initiative - recommendations for histological assessments of osteoarthritis in the mouse. Osteoarthr. Cartil. 18(SUPPL. 3):S17–S23.

348. Kwok J, Onuma H, Olmer M, et al. 2016. Histopathological analyses of murine menisci: Implications for joint aging and osteoarthritis. Osteoarthr. Cartil. 24(4):709–718.

349. López-Franco M, Gómez-Barrena E. 2018. Cellular and molecular meniscal changes in the degenerative knee: a review. J. Exp. Orthop. 5(1):11.

350. Levillain A, Boulocher C, Kaderli S, et al. 2015. Meniscal biomechanical alterations in an ACLT rabbit model of early osteoarthritis. Osteoarthr. Cartil. 23(7):1186–1193.

351. Svensson F, Felson DT, Zhang F, et al. 2019. Meniscal body extrusion and cartilage coverage in middle-aged and elderly without radiographic knee osteoarthritis. Eur. Radiol. 29(4):1848–1854.

352. Hada S, Ishijima M, Kaneko H, et al. 2017. Association of medial meniscal extrusion with medial tibial osteophyte distance detected by T2 mapping MRI in patients with early-stage knee osteoarthritis. Arthritis Res. Ther. 19(1):1–12.

353. Wenger A, Wirth W, Hudelmaier M, et al. 2013. Meniscus body position, size, and shape in persons with and persons without radiographic knee osteoarthritis: Quantitative analyses of knee magnetic resonance images from the osteoarthritis initiative. Arthritis Rheum. 65(7):1804–1811.

354. Jung KA, Lee SC, Hwang SH, et al. 2010. High frequency of meniscal hypertrophy in persons with advanced varus knee osteoarthritis. Rheumatol. Int. 30(10):1325–1333.

355. Wu P, Holguin N, Silva MJ, et al. 2014. Early response of mouse joint tissue to noninvasive knee injury suggests treatment targets. Arthritis Rheumatol. 66(5):1256–1265.

356. Christiansen B a., Anderson MJ, Lee C a., et al. 2012. Musculoskeletal changes following non-invasive knee injury using a novel mouse model of post-traumatic osteoarthritis. Osteoarthr. Cartil. 20(7):773–782.

357. Rai MF, Duan X, Quirk JD, et al. 2017. Post-Traumatic Osteoarthritis in Mice Following Mechanical Injury to the Synovial Joint. Sci. Rep. 7(1):45223.

358. Duan X, Sandell LJ, Chinzei N, et al. 2017. Therapeutic efficacy of intra-articular hyaluronan derivative and platelet-rich plasma in mice following axial tibial loading. PLoS One 12(4):e0175682.

359. Sampson ER, Beck CA, Ketz J, et al. 2011. Establishment of an index with increased sensitivity for assessing murine arthritis. J. Orthop. Res. 29(8):1145–1151.

360. O'Conor CJ, Ramalingam S, Zelenski NA, et al. 2016. Cartilage-Specific Knockout of the Mechanosensory Ion Channel TRPV4 Decreases Age-Related Osteoarthritis. Sci. Rep. 6(July):29053.

361. Louer CR, Furman BD, Huebner JL, et al. 2012. Diet-induced obesity significantly increases the severity of posttraumatic arthritis in mice. Arthritis Rheum. 64(10):3220–3230.

362. Nauth A, Giles E, Potter BK, et al. 2013. Heterotopic Ossification in Orthopaedic Trauma. J Orthop Trauma 26(12):684–688.

363. Kraft CT, Student M, Arbor A, et al. 2017. Trauama induced heterotopic bone formation and the role of the immune system: A review.80(1):156–165.

364. Pottenger LA, Phillips FM, Draganich LF. 1990. The effect of marginal osteophytes on reduction of varus-valgus instability in osteoarthritic knees. Arthritis Rheum. 33(6):853–858.

365. Zhou S, Wang Z, Tang J, et al. 2016. Exogenous fibroblast growth factor 9 attenuates cartilage degradation and aggravates osteophyte formation in post-traumatic osteoarthritis. Osteoarthr. Cartil. 24(12):2181–2192.

366. Huang H, Skelly JD, Ayers DC, Song J. 2017. Age-dependent Changes in the Articular Cartilage and Subchondral Bone of C57BL/6 Mice after Surgical Destabilization of Medial Meniscus. Sci. Rep. 7(January):42294.

367. Oh H, Chun CH, Chun JS. 2012. Dkk-1 expression in chondrocytes inhibits experimental osteoarthritic cartilage destruction in mice. Arthritis Rheum. 64(8):2568–2578.

368. Panahifar a., Maksymowych WP, Doschak MR. 2012. Potential mechanism of alendronate inhibition of osteophyte formation in the rat model of post-traumatic osteoarthritis: Evaluation of elemental strontium as a molecular tracer of bone formation. Osteoarthr. Cartil. 20(7):694–702.

369. Hayami T, Pickarski M, Wesolowski G a., et al. 2004. The Role of Subchondral Bone Remodeling in Osteoarthritis: Reduction of Cartilage Degeneration and Prevention of Osteophyte Formation by Alendronate in the Rat Anterior Cruciate Ligament Transection Model. Arthritis Rheum. 50(4):1193–1206.

370. Aho O-M, Finnilä M, Thevenot J, et al. 2017. Subchondral bone histology and grading in osteoarthritis. PLoS One 12(3):e0173726.

371. Pickarski M, Hayami T, Zhuo Y, Duong LT. 2011. Molecular changes in articular cartilage and subchondral bone in the rat anterior cruciate ligament transection and meniscectomized models of osteoarthritis. BMC Musculoskelet. Disord. 12(1):197.

372. Boyd SK, Müller R, Leonard T, Herzog W. 2005. Long-term periarticular bone adaptation in a feline knee injury model for post-traumatic experimental osteoarthritis. Osteoarthr. Cartil. 13:235–242.

373. Dong Y, Liu H, Zhang X, et al. 2016. Inhibition of SDF-1α/CXCR4 signaling in subchondral bone attenuates post-traumatic osteoarthritis. Int. J. Mol. Sci. 17(6):1–12.

374. Maerz T, Kurdziel M, Newton MD, et al. 2016. Subchondral and epiphyseal bone remodeling following surgical transection and noninvasive rupture of the anterior cruciate ligament as models of post-traumatic osteoarthritis. Osteoarthr. Cartil. 24(4):698–708.

375. Doyran B, Tong W, Li Q, et al. 2016. Nanoindentation modulus of murine cartilage: A sensitive indicator of the initiation and progression of post-traumatic osteoarthritis. Osteoarthr. Cartil. 25:108–117.

376. She G, Zhou Z, Zha Z, et al. 2017. Protective effect of zoledronic acid on articular cartilage and subchondral bone of rabbits with experimental knee osteoarthritis. Exp. Ther. Med. :4901–4909.

377. Mohan G, Perilli E, Parkinson IH, et al. 2013. Pre-emptive, early, and delayed alendronate treatment in a rat model of knee osteoarthritis: Effect on subchondral trabecular bone microarchitecture and cartilage degradation of the tibia, bone/cartilage turnover, and joint discomfort. Osteoarthr. Cartil. 21:1595–1604.

378. Chen H, Dong Q, Jiang W. 2016. 3-D Structural Changes in Subchondral Bone and the Effect of Bisphosphonate Intervention in Early Osteoarthritis. Int. J. Morphol. 34(1):291–297.

379. Shirai T, Kobayashi M, Nishitani K, et al. 2011. Chondroprotective effect of alendronate in a rabbit model of osteoarthritis. J. Orthop. Res. 29(October):1572–1577.

380. Zhang L, Hu H, Tian F, et al. 2011. Enhancement of subchondral bone quality by alendronate administration for the reduction of cartilage degeneration in the early phase of experimental osteoarthritis. Clin. Exp. Med. 11:235–243.

381. Nishitani K, Shirai T, Kobayashi M, et al. 2009. Positive Effect of Alendronate on Subchondral Bone Healing and Subsequent Cartilage Repair in a Rabbit Osteochondral Defect Model. Am. J. Sports Med. 37(1_suppl):139S–147S.

382. Khorasani MS, Diko S, Hsia AW, et al. 2015. Effect of alendronate on post-traumatic osteoarthritis induced by anterior cruciate ligament rupture in mice. Arthritis Res. Ther. 17(1):1–11.

383. Jackson MT, Moradi B, Zaki S, et al. 2014. Depletion of protease-activated

receptor 2 but not protease-activated receptor 1 may confer protection against osteoarthritis in mice through extracartilaginous mechanisms. Arthritis Rheumatol. 66(12):3337–3348.

384. Sambamurthy N, Zhou C, Nguyen V, et al. 2018. Deficiency of the pattern-recognition receptor CD14 protects against joint pathology and functional decline in a murine model of osteoarthritis. PLoS One 13(11):e0206217.

385. Khatab S, van Buul GM, Kops N, et al. 2018. Intra-articular Injections of Platelet-Rich Plasma Releasate Reduce Pain and Synovial Inflammation in a Mouse Model of Osteoarthritis. Am. J. Sports Med. 46(4):977–986.

386. Gilbert SJ, Bonnet CS, Stadnik P, et al. 2018. Inflammatory and degenerative phases resulting from anterior cruciate rupture in a non-invasive murine model of post-traumatic osteoarthritis. J. Orthop. Res. 36(8):2118–2127.

387. Lewis JS, Hembree WC, Furman BD, et al. 2011. Acute joint pathology and synovial inflammation is associated with increased intra-articular fracture severity in the mouse knee. Osteoarthr. Cartil. 19(7):864–873.

388. Shi J, Liang Q, Zuscik M, et al. 2014. Distribution and alteration of lymphatic vessels in knee joints of normal and osteoarthritic mice. Arthritis Rheumatol. (Hoboken, N.J.) 66(3):657–66.

389. Yu YY, Lieu S, Hu D, et al. 2012. Site specific effects of zoledronic acid during tibial and mandibular fracture repair. PLoS One 7(2).

390. Green JR. 2005. Zoledronic acid: Pharmacologic profile of a potent bisphosphonate. J. Organomet. Chem. 690:2439–2448.

391. Carbone LD, Nevitt MC, Wildy K, et al. 2004. The relationship of antiresorptive drug use to structural findings and symptoms of knee osteoarthritis. Arthritis Rheum. 50(11):3516–3525.

392. Haudenschild DR, Nguyen B, Chen J, et al. 2008. Rho kinase-dependent CCL20 induced by dynamic compression of human chondrocytes. Arthritis Rheum. 58(9):2735–2742.

393. Haudenschild DR, D'Lima DD, Lotz MK. 2008. Dynamic compression of chondrocytes induces a Rho kinase-dependent reorganization of the actin cytoskeleton. In: Biorheology. .

394. Wan Q, Kim SJ, Yokota H, Na S. 2013. Differential activation and inhibition of RhoA by fluid flow induced shear stress in chondrocytes. Cell Biol. Int.

37(6):568–576.

395. Zignego DL, Hilmer JK, June RK. 2015. Mechanotransduction in primary human osteoarthritic chondrocytes is mediated by metabolism of energy, lipids, and amino acids. J. Biomech. 48(16):4253–4261.

396. Novakofski K, Boehm A, Fortier L. 2009. The small GTPase Rho mediates articular chondrocyte phenotype and morphology in response to interleukin-1?? and insulin-like growth factor-1. J. Orthop. Res. 27(1):58–64.

397. Fortier LA, Miller BJ. 2006. Signaling through the small G-protein Cdc42 is involved in insulin-like growth factor-I resistance in aging articular chondrocytes. J. Orthop. Res. 24(8):1765–1772.

398. Dombrecht EJ, Schuerwegh AJ, Bridts CH, et al. 2007. Effect of bisphosphonates on nitric oxide production by inflammatory activated chondrocytes. Clin. Exp. Rheumatol. 25:817–822.

399. Dombrecht EJ, De Tollenaere CB, Aerts K, et al. 2006. Antioxidant effect of bisphosphonates and simvastatin on chondrocyte lipid peroxidation. Biochem. Biophys. Res. Commun. 348(2):459–464.

400. Evans KD, Oberbauer a M. 2009. Alendronate inhibits VEGF expression in growth plate chondrocytes by acting on the mevalonate pathway. Open Orthop. J. 3:83–88.

401. Rosa RG, Collavino K, Lakhani A, et al. 2014. Clodronate exerts an anabolic effect on articular chondrocytes mediated through the purinergic receptor pathway. Osteoarthritis Cartilage 22(9):1327–1336.

402. Atsumi T, Miwa Y, Kimata K, Ikawa Y. 1990. A chondrogenic cell line derived from a differentiating culture of ATDC5 teratocarcinoma cells. Cell Differ. Dev. 30:109–116.

403. Shukunami C, Shigeno C, Atsumi T, et al. 1996. Chondrogenic Differentiation of Clonal Mouse Embryonic Cell Line ATDC5 In Vitro. J. Cell Biol. 133(2):457–468.

404. C. S, C. S, T. A, et al. 1996. Chondrogenic differentiation of clonal mouse embryonic cell line ATDC5 in vitro: Differentiation-dependent gene expression of parathyroid hormone (PTH)/PTH-related peptide receptor. J. Cell Biol. 133(2):457–468.

405. Watson J V., Chambers SH, Smith PJ. 1987. A pragmatic approach to the

analysis of DNA histograms with a definable G1 peak. Cytometry 8(1):1–8.

406. Sun J, Zhang J, Yang H, et al. 2017. Microfluidic cell cycle analysis of spread cells by DAPI staining. Micromachines 8(2):1–8.

407. Roukos V, Pegoraro G, Voss TC, Misteli T. 2015. Cell cycle staging of individual cells by fluorescence microscopy. Nat. Protoc. 10(2):334–348.

408. Ferro A, Mestre T, Carneiro P, et al. 2017. Blue intensity matters for cell cycle profiling in fluorescence DAPI-stained images. Lab. Investig. 97(5):615–625.

409. Perelman A, Wachtel C, Cohen M, et al. 2012. JC-1: Alternative excitation wavelengths facilitate mitochondrial membrane potential cytometry. Cell Death Dis. 3(11):e430-7.

410. Muehleman C, Green J, Williams JM, et al. 2002. The effect of bone remodeling inhibition by zoledronic acid in an animal model of cartilage matrix damage. Osteoarthr. Cartil. 10(3):226–233.

411. Özenc AM, Aslan T, Zeliha N, et al. 2013. Protective effect of zoledronic acid on corticosteroid-induced chondrocyte apoptosis in rat articular cartilage.47(6):430–435.

412. Yao Y, Zhai Z, Wang Y. 2014. Evaluation of insulin medium or chondrogenic medium on proliferation and chondrogenesis of ATDC5 cells. Biomed Res. Int. 2014(July).

413. van Beuningen HM, Stoop R, Buma P, et al. 2002. Phenotypic differences in murine chondrocyte cell lines derived from mature articular cartilage. Osteoarthr. Cartil. 10(12):977–986.

414. Dehne T, Schenk R, Perka C, et al. 2010. Gene expression profiling of primary human articular chondrocytes in high-density micromasses reveals patterns of recovery, maintenance, re- and dedifferentiation. Gene 462(1–2):8–17.

415. Du C, Wang Y, Li H, et al. 2017. Zoledronic acid augments the radiosensitivity of cancer cells through perturbing S- and M-phase cyclins and p21CIP1 expression. Oncol. Lett. .

416. Agarwal ML, Agarwal A, Taylor WR, et al. 1998. A p53-dependent S-phase checkpoint helps to protect cells from DNA damage in response to starvation for pyrimidine nucleotides. Proc. Natl. Acad. Sci. U. S. A. 95(December):14775–14780.

417. Reinhardt HC, Schumacher B. 2012. The p53 network: Cellular and systemic DNA damage responses in aging and cancer Cologne Excellence Cluster on Cellular Stress Response in Aging-Associated Diseases p53 at the crossroad of cancer and aging. Trends Genet. 28(3):128–136.

418. Pfister NT, Yoh KE, Prives C. 2014. p53, DNA damage, and NAD+ homeostasis. Cell Cycle 13(11):1661–1662.

419. Pan LZ, Ahn DG, Sharif T, et al. 2014. The NAD+synthesizing enzyme nicotinamide mononucleotide adenylyltransferase 2 (NMNAT-2) is a p53 downstream target. Cell Cycle 13(6):1041–1048.

420. Tassone P, Tagliaferri P, Viscomi C, et al. 2003. Zoledronic acid induces antiproliferative and apoptotic effects in human pancreatic cancer cells in vitro. Br. J. Cancer 88(12):1971–1978.

421. Brown HK, Ottewell PD, Coleman RE, Holen I. 2011. The kinetochore protein Cenp-F is a potential novel target for zoledronic acid in breast cancer cells. J. Cell. Mol. Med. 15(3):501–513.

422. Paschal BM, Kelley JB. 2013. Nuclear Lamina. In: Encyclopedia of Biological Chemistry. Elsevier; p 310–313.

423. Maltese WA. 1990. Posttranslational modification of proteins by isoprenoids in mammalian cells. FASEB J. 4(15):3319–28.

424. Tricarico PM, Crovella S, Celsi F. 2015. Mevalonate pathway blockade, mitochondrial dysfunction and autophagy: A possible link. Int. J. Mol. Sci. 16(7):16067–16084.

425. Mitrofan LM, Castells FB, Pelkonen J, Mönkkönen J. 2010. Lysosomal-mitochondrial axis in zoledronic acid-induced apoptosis in human follicular lymphoma cells. J. Biol. Chem. 285(3):1967–1979.

426. Khandelwal VKM, Mitrofan LM, Hyttinen JMT, et al. 2014. Oxidative stress plays an important role in zoledronic acid-induced autophagy. Physiol. Res. 63:S601–S612.

427. Ge XY, Yang LQ, Jiang Y, et al. 2014. Reactive oxygen species and autophagy associated apoptosis and limitation of clonogenic survival induced by zoledronic acid in salivary adenoid cystic carcinoma cell line SACC-83. PLoS One 9(6):1–10.

428. Wang I-T, Chou S-C, Lin Y-C. 2014. Zoledronic acid induces apoptosis and

autophagy in cervical cancer cells. Tumour Biol. 35(12):11913–20.

429. Wu C-C, Huang Y-F, Hsieh C-P, et al. 2016. Combined Use of Zoledronic Acid Augments Ursolic Acid-Induced Apoptosis in Human Osteosarcoma Cells through Enhanced Oxidative Stress and Autophagy. Molecules 21(12):1640.

430. Jiang P, Zhang P, Mukthavaram R, et al. 2016. Anti-cancer effects of nitrogen-containing bisphosphonates on human cancer cells. Oncotarget 7(36).

431. Simopoulou T, Malizos KN, Poultsides L, Tsezou A. 2010. Protective effect of atorvastatin in cultured osteoarthritic chondrocytes. J. Orthop. Res. 28(January):110–115.

432. Dombrecht EJ, Van Offel JF, Bridts CH, et al. [date unknown]. Influence of simvastatin on the production of pro-inflammatory cytokines and nitric oxide by activated human chondrocytes. Clin. Exp. Rheumatol. 25:534–539.

433. Wang C, Min S, Zhang H, et al. 2017. Downregulation of GGPPS in chondrocytes accelerates osteoarthritis progression.10(2):1084–1093.

434. Kim JG, Islam R, Cho JY, et al. 2018. Regulation of RhoA GTPase and various transcription factors in the RhoA pathway. J. Cell. Physiol. 233(9):6381–6392.

435. Luckman SP, Hughes DE, Coxon FP, et al. 1998. Nitrogen-containing bisphosphonates inhibit the mevalonate pathway and prevent post-translational prenylation of GTP-binding proteins, including Ras. J. Bone Miner. Res. 13(4):581–589.

436. Berke IM, Miola JP, David MA, et al. 2016. Seeing through musculoskeletal tissues: Improving in situ imaging of bone and the lacunar canalicular system through optical clearing. PLoS One 11(3):1–29.

437. Miller RE, Ishihara S, Bhattacharyya B, et al. 2017. Chemogenetic Inhibition of Pain Neurons in a Mouse Model of Osteoarthritis. Arthritis Rheumatol. 69(7):1429–1439.

438. ter Heegde F, Luiz AP, Santana-Varela S, et al. 2019. Non-invasive mechanical joint loading as an alternative model for osteoarthritic pain. Arthritis Rheumatol. .

439. Zhang R-X, Ren K, Dubner R. 2013. Osteoarthritis pain mechanisms: basic studies in animal models. Osteoarthritis Cartilage 21(9):1308–15.

440. Owen S, Francis H, Roberts M. 1994. Disappearance kinetics of solutes from

synovial fluid after intra- articular injection. Br. J. Clin. Pharmacol. 38(4):349–355.

441. Butoescu N, Jordan O, Doelker E. 2009. Intra-articular drug delivery systems for the treatment of rheumatic diseases: A review of the factors influencing their performance. Eur. J. Pharm. Biopharm. 73(2):205–218.

442. Gerwin N, Hops C, Lucke A. 2006. Intraarticular drug delivery in osteoarthritis. Adv. Drug Deliv. Rev. 58:226–242.

443. Torchilin VP. 2005. Recent advances with liposomes as pharmaceutical carriers. Nat. Rev. Drug Discov. 4(2):145–160.

444. Shaw IH, Knight CG, Dingle JT. 1976. Liposomal Retention of a Modified anti-inflammatory steroid. Biochem. J. 158:473–476.

445. Bonanomi MH, Velvart M, Stimpel M, et al. 1987. Studies of pharmacokinetics and therapeutic effects of glucocorticoids entrapped in liposomes after intraarticular application in healthy rabbits and in rabbits with antigen-induced arthritis. Rheumatol. Int. 7(5):203–212.

446. Rooijen N Van, Sanders A. 1994. Liposome mediated depletion of macrophages: mechanism of action, preparation of liposomes and applications. J. Immunol. Methods 174(1–2):83–93.

447. Sivan S, Schroeder A, Verberne G, et al. 2010. Liposomes act as effective biolubricants for friction reduction in human synovial joints. Langmuir 26(2):1107–1116.

448. Vanniasinghe a. S, Manolios N, Schibeci S, et al. 2014. Targeting fibroblast-like synovial cells at sites of inflammation with peptide targeted liposomes results in inhibition of experimental arthritis. Clin. Immunol. 151(1):43–54.

449. Harigai T, Hagiwara H, Ogawa Y, et al. 2007. Prednisolone phosphate-containing TRX-20 liposomes inhibit cytokine and chemokine production in human fibroblast-like synovial cells: A novel approach to rheumatoid arthritis therapy. J. Pharm. Pharmacol. 59(1):137–143.

450. Čeponis A, Waris E, Mönkkönen J, et al. 2001. Effects of low-dose, noncytotoxic, intraarticular liposomal clodronate on development of erosions and proteoglycan loss in established antigen-induced arthritis in rabbits. Arthritis Rheum. 44(8):1908–1916.

451. Gomez-Barrena E, Lindroos L, Čeponis A, et al. 2006. Cartilage oligomeric

matrix protein (COMP) is modified by intra-articular liposomal clodronate in an experimental model of arthritis. Clin. Exp. Rheumatol. 24:622–628.

452. Kinne RW, Schmidt-Weber CB, Hoppe R, et al. 1995. Long-term amelioration of rat adjuvant arthritis following systemic elimination of macrophages by clodronate-containing liposomes. Arthritis Rheum. 38(12):1777–1790.

453. Van Lent PL, Holthuysen a E, Van Rooijen N, et al. 1998. Local removal of phagocytic synovial lining cells by clodronate-liposomes decreases cartilage destruction during collagen type II arthritis. Ann. Rheum. Dis. 57:408–413.

454. Richards PJ, Williams a. S, Goodfellow RM, Williams BD. 1999. Liposomal clodronate eliminates synovial macrophages, reduces inflammation and ameliorates joint destruction in antigen-induced arthritis. Rheumatology 38:818–825.

455. Barrera P, Blom A, Van Lent PLEM, et al. 2000. Synovial macrophage depletion with clodronate-containing liposomes in rheumatoid arthritis. Arthritis Rheum. 43(9):1951–1959.

456. Van Lent PLEM, Blom a. B, Van Der Kraan P, et al. 2004. Crucial Role of Synovial Lining Macrophages in the Promotion of Transforming Growth Factor Beta-Mediated Osteophyte Formation. Arthritis Rheum. 50(1):103–111.

457. Blom AB, Van Lent PL, Libregts S, et al. 2007. Crucial role of macrophages in matrix metalloproteinase-mediated cartilage destruction during experimental osteoarthritis: Involvement of matrix metalloproteinase 3. Arthritis Rheum. 56(1):147–157.

458. Bakker AC, van de Loo FAJ, van Beuningen HM, et al. 2001. Overexpression of active TGF-beta-1 in the murine knee joint: Evidence for synovial-layer-dependent chondro-osteophyte formation. Osteoarthr. Cartil. 9(2):128–136.

459. Luo T, David MA, Dunshee LC, et al. 2017. Thermoresponsive Elastin-b-Collagen-Like Peptide Bioconjugate Nanovesicles for Targeted Drug Delivery to Collagen-Containing Matrices. Biomacromolecules 18(8):2539–2551.

460. Janssen M, Mihov G, Welting T, et al. 2014. Drugs and polymers for delivery systems in OA joints: Clinical needs and opportunities. Polymers (Basel). 6(3):799–819.

461. Singh S AI. 2013. A Comparison of the Histochemical and Image-Derived Proteoglycan Content of Articular Cartilage. Anat. Physiol. 03(2):2–7.

462. Moussavi-Harami SF, Pedersen DR, Martin JA, et al. 2009. Automated objective scoring of histologically apparent cartilage degeneration using a custom image analysis program. J. Orthop. Res. 27(4):522–528.

Appendix A

SUPPLEMENTAL METHODS AND RESULTS FOR CHAPTER 2

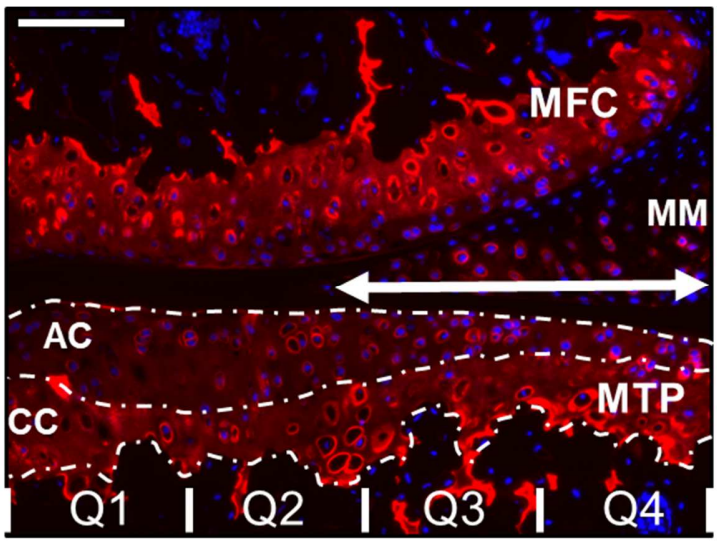

Figure A.1: Quantification of meniscal coverage, chondrocyte cellularity, and cartilage thickness. Immunohistochemical staining for type II collagen (an indicator of cartilage composition) and DAPI-nuclear staining (indicating chondrocytes presence) was performed on sections spanning the central cartilage contact (level 2-4) of the medial joint. The articular cartilage (AC) and calcified cartilage (CC) of the medial tibial plateau (MTP; dotted white lines), and medial meniscus (MM) were manually traced, and the total number of DAPI-positive cells were counted in the AC and CC. Cartilage thickness and chondrocyte number was quantified for each of four separate regions, quadrants 1 (Q1) through quadrant 4 (Q4), representing the innermost through outermost regions of the MTP AC, respectively. The degree of meniscal coverage (MM width/AC width; white arrows) was quantified with respect to the MTP joint margin. Lastly, manual tracing of the extent of linear cartilage damage (including histological values of ≥1) across the width of the MTP was performed (not shown in image). All analysis was performed in MATLAB. A representative image of a control joint, oriented with the medial joint margin to the right is shown. Image captured at 20x magnification, scale bar = 100µm.

Table A.1: Temporal quantification of cartilage damage scoring in DMM, Contralateral, Sham and Age-Matched Joints.

	Medial Femoral Condyle (Width-Wise Score)				Lateral Femoral Condyle (Width-Wise Score)			
Days Post-Surgery	DMM	DMM Contralateral	Sham	Age-Matched ‡	DMM	DMM Contralateral	Sham	Age-Matched ‡
3	0.67 ± 0.34	0.33+ 0.07	0.47 ± 0.20	0.42 ± 0.14	0.55 ± 0.14	0.65 ± 0.28	0.47 ± 0.15	0.39 ± 0.18
7	1.48 ± 1.09	0.46 ± 0.14	0.52 ± 0.11	"	0.71 ± 0.30	0.51 ± 0.27	0.70 ± 0.17	"
14	1.31 ± 0.35	0.77 ± 0.46	0.51 ± 0.08	"	0.63 ± 0.14	0.69 ± 0.36	0.44 ± 0.19	"
56	1.58 ± 0.46***	0.55 ± 0.12	0.41 ± 0.08	0.49 ± 0.27	0.66 ± 0.30	0.70 ± 0.24	0.50 ± 0.05	0.55 ± 0.34
84	2.16 ± 0.80***	0.52 ± 0.19	0.56 ± 0.22	0.47 ± 0.06	0.81 ± 0.35	0.71 ± 0.21	0.83 ± 0.20	0.67 ± 0.19
112	3.27 ± 1.32***	0.49 ± 0.07	0.38 ± 0.02	0.40 ± 0.14	1.34 ± 0.49	1.20 ± 0.46	0.73 ± 0.15	1.16 ± 0.65

	Medial Femoral Condyle (Depth-Wise Score)				Lateral Femoral Condyle (Depth-Wise Score)			
Days Post-Surgery	DMM	DMM Contralateral	Sham	Age-Matched ‡	DMM	DMM Contralateral	Sham	Age-Matched ‡
3	0.67 ± 0.32	0.32 ± 0.07	0.47 ± 0.20	0.42 ± 0.14	0.55 ± 0.14	0.65 ± 0.28	0.47 ± 0.15	0.39 ± 0.18
7	1.41 ± 0.98	0.47 ± 0.13	0.52 ± 0.11	"	0.71 ± 0.30	0.53 ± 0.32	0.70 ± 0.17	"
14	1.30 ± 0.33	0.79 ± 0.43	0.51 ± 0.08	"	0.63 ± 0.14	0.68 ± 0.35	0.44 ± 0.19	"

56	1.57 ± 0.45***	0.55 ± 0.12	0.41 ± 0.08	0.49 ± 0.27	0.64 ± 0.25	0.69 ± 0.21	0.43 ± 0.12	0.55 ± 0.34
84	2.14 ± 0.83***	0.52 ± 0.19	0.56 ± 0.22	0.47 ± 0.06	0.79 ± 0.31	0.71 ± 0.21	0.83 ± 0.20	0.67 ± 0.19
112	2.95 ± 1.18***	0.49 ± 0.08	0.38 ± 0.02	0.41 ± 0.15	1.38 ± 0.55	1.18 ± 0.43	0.73 ± 0.15	1.04 ± 0.51

	Medial Tibia Plateau (Width-Wise Score)				Lateral Tibia Plateau (Width-Wise Score)			
Days Post-Surgery	DMM	DMM Contralateral	Sham	Age-Matched ‡	DMM	DMM Contralateral	Sham	Age-Matched ‡
3	0.70 ± 0.16*	0.47 ± 0.06S	0.73 ± 0.03C, AM	0.42 ± 0.18S	0.70 ± 0.13	0.69 ± 0.19	0.83 ± 0.22	0.51 ± 0.24
7	1.16 ± 0.30*	0.52 ± 0.14	0.59 ± 0.05	"	0.88 ± 0.29	0.77 ± 0.25	0.92 ± 0.21	"
14	1.19 ± 0.42*	0.61 ± 0.16	0.65 ± 0.06	"	0.78 ± 0.20	0.75 ± 0.16	0.57 ± 0.04	"
56	1.64 ± 0.58***	0.55 ± 0.10	0.63 ± 0.17	0.56 ± 0.31	0.93 ± 0.22	0.76 ± 0.23	0.77 ± 0.12	0.68 ± 0.26
84	2.59 ± 0.98***	0.60 ± 0.24	0.61 ± 0.15	0.63 ± 0.15	0.98 ± 0.34	1.01 ± 0.34	1.10 ± 0.31	0.80 ± 0.11
112	3.33 ± 1.35***	0.63 ± 0.18	0.86 ± 0.01	0.74 ± 0.37	1.07 ± 0.34	1.03 ± 0.37	0.96 ± 0.12	0.74 ± 0.21

	Medial Tibia Plateau (Depth-Wise Score)				Lateral Tibia Plateau (Depth-Wise Score)			
Days Post-Surgery	DMM	DMM Contralateral	Sham	Age-Matched ‡	DMM	DMM Contralateral	Sham	Age-Matched ‡
3	0.70 ± 0.16*	0.47 ± 0.06S	0.73 ± 0.03C, AM	0.42 ± 0.18S	0.70 ± 0.13	0.69 ± 0.19	0.83 ± 0.22	0.51 ± 0.24
7	1.16 ± 0.30*	0.52 ± 0.14	0.59 ± 0.05	"	0.88 ± 0.29	0.73 ± 0.23	0.92 ± 0.21	"
14	1.19 ± 0.42*	0.61 ± 0.16	0.65 ± 0.06	"	0.78 ± 0.20	0.75 ± 0.16	0.58 ± 0.04	"
56	1.77 ± 0.80**	0.55 ± 0.10	0.63 ± 0.17	0.56 ± 0.31	0.93 ± 0.22	0.76 ± 0.23	0.77 ± 0.12	0.68 ± 0.26
84	2.80 ± 1.16***	0.60 ± 0.24	0.61 ± 0.15	0.63 ± 0.15	0.97 ± 0.33	1.00 ± 0.32	1.12 ± 0.33	0.80 ± 0.11
112	3.39 ± 1.17***	0.63 ± 0.18	0.86 ± 0.01	0.74 ± 0.37	1.10 ± 0.36	1.03 ± 0.40	0.96 ± 0.12	0.72 ± 0.21

* = Significantly different from respective contralateral joint, $p<0.05$; ** = $p<0.01$; *** = $p<0.001$; **** = $p<0.0001$; paired t-test, GraphPad Prism

C = Significantly different from respective contralateral joint, $p<0.05$; One-way ANOVA, Tukey's post hoc test, GraphPad Prism

S = Significantly different from respective Sham joint, $p<0.05$; One-way ANOVA, Tukey's post hoc test, GraphPad Prism

AM = Significantly different from respective age-matched joint, $p<0.05$; One-way ANOVA, Tukey's post hoc test, GraphPad Prism

‡ = Baseline (0d) values used for statistical comparison at 3, 7, and 14-days post-DMM

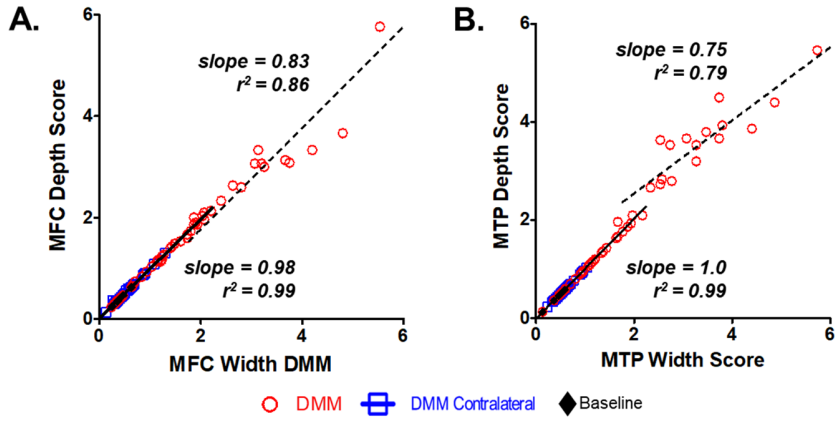

Figure A.2: Pair-wise comparison of width- vs. depth-wise semi-quantitative cartilage damage scoring in the medial joint compartment. To determine if a preferences for overall width- vs. depth-wise erosional damage could be observed following DMM, linear regression was performed on paired semi-quantitative MTP and MFC cartilage damage scores. Since damages scores ≤2 are identical in both scoring systems, an expected linear regression slope of ~1.0 for damage scores ≤2 was observed. However, for damage scores >2 we observed a slight preference towards increased width-wise erosion compared to depth-wise in the MTP, and no preference in the MFC. Linear regression r2- and p-values are shown for values ≤2 and values >2; data for all groups are included.

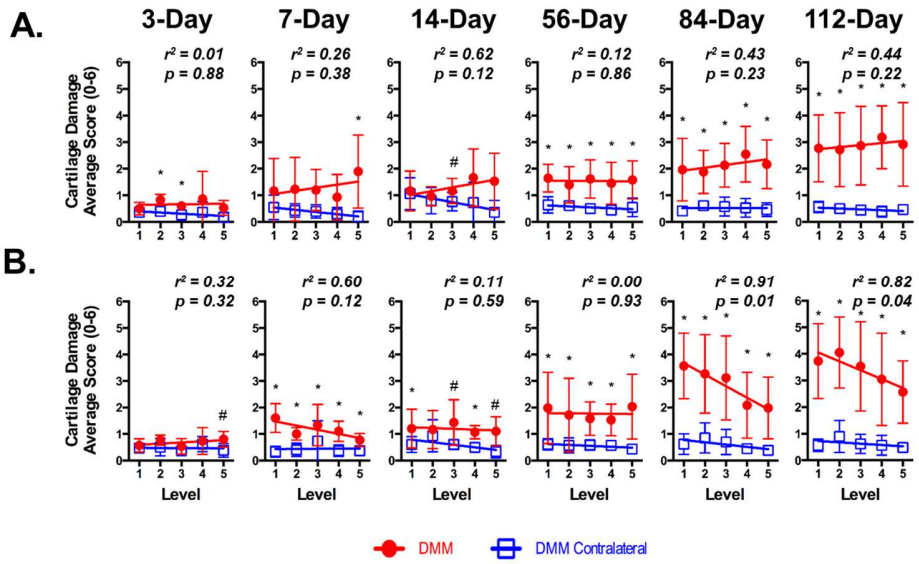

Figure A.3: Anterior-to-posterior distribution of depth-wise damage within medial joint post-DMM. The distribution of semi-quantitative depth-wise cartilage damage scores in the medial femoral condyle (MFC; A.) and tibial plateau (MTP; B.), from the anterior (level 1) to posterior (level 5) of the central cartilage contact of the joint. Similar to the damage distribution in the width-wise analysis, no spatial preference for damage was observed in the MFC; again, the MTP demonstrated significantly increased damage anteriorly compared to posteriorly at late time-points (84- and 112-days). Results are presented as mean ± STD (n = 5-10/time point/group) where * = $p<0.05$ and # = $p<0.10$ (trend) for paired t-test between DMM and DMM contralateral joints at a given level. Linear regression r2- and p-values are shown for DMM joints only.

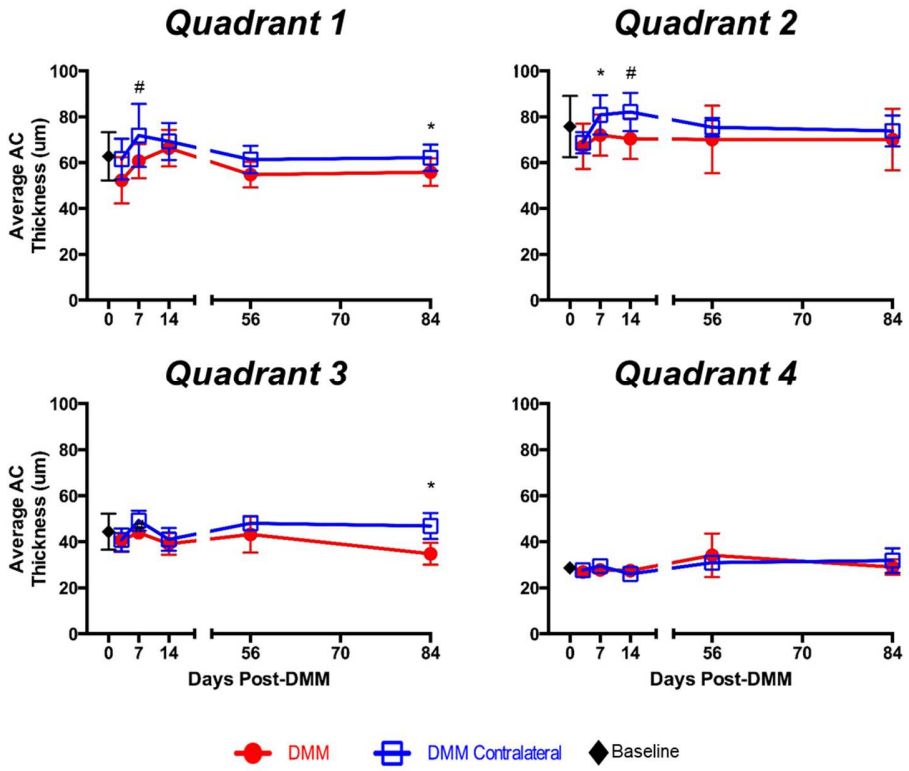

Figure A.4: Quantification of changes in cartilage thickness across the medial tibial plateau post-DMM. The articular cartilage (AC) thickness in each quadrant of the medial tibia plateau (MTP) was quantified, in MATLAB, from traces of the AC in type II collagen stained sections (level 2-4) using a Euclidian distance transform. A statistically significant decrease in AC thickness was only observed within MTP quadrant 3 at 84-days, which confirms the observed cartilage erosions in this quadrant. Results are presented as mean ± STD (n = 5/timepoint/group) where * = $p<0.05$ and # = $p<0.1$ (trend) for paired t-test between DMM and contralateral joints.

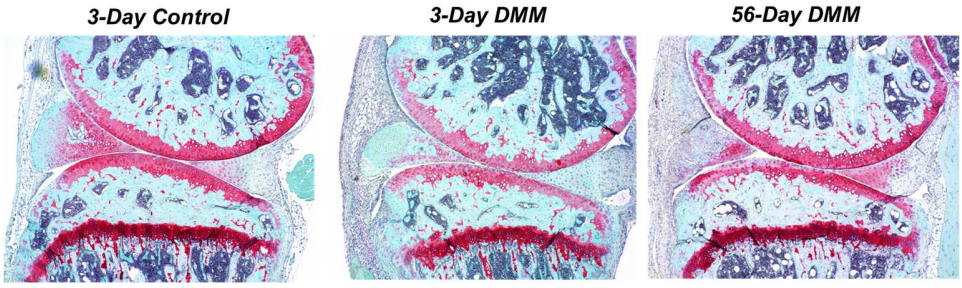

Figure A.5: Histological sections demonstrating the anterior-to-posterior distribution of cartilage damage post-DMM. Representative Safranin-O/fast green stained sagittal sections taken from approximately quadrant 3 of DMM injured and contralateral (control) joints. For orientation, the femur is located on the top, the tibia the bottom, the anterior of the joint to the left and posterior to the right. At 56-days post-DMM there is clear anteriorly-localized cartilage damage in the medial tibia plateau and to a lesser extent in the medial femoral condyle. No apparent localization at 3-days is observed in either the condyle or tibial plateau. Additionally, sections at 3-day post-DMM highlight the lack of blunt surgical trauma to the articular cartilage during the DMM procedure. While inadvertent damage could cofound our findings, we are confident that such damage is minimal. Lastly, these images show the consistency of our embedding technique to fix all our joints at approximately the same natural flexed position. Images were acquired at 5x magnification.

Appendix B

SUPPLEMENTAL METHODS AND RESULTS FOR CHAPTER 3

Quantification of Proteoglycan Content

To provide additional information regarding proteoglycan amount (area) and composition (intensity), we exploited the metachromatic and stoichiometric binding properties of Safranin-O (Saf-O) dye to proteoglycan molecules[461,462]. After staining slides with Safranin-O/Fast-Green/Hematoxylin, images were captured at 5x magnification under consistent settings and processed in 8-bit RGB color space via a custom image processing algorithm in MATLAB. All sections were normalized to the slide background (using complement values and subtraction) and then thresholded using a built-in MATLAB color thresholding application. Next, the articular cartilage was manually traced, and then the Saf-O^+ articular cartilage area and total articular cartilage area was extracted to determine the relative amount (area) of proteoglycan. Additional analysis was performed on thresholded images to determine the concentration of proteoglycans (indicated by the intensity of Saf-O^+ tissue). To do so, all RGB pixels were converted into grayscale values and then averaged among all the grayscale values of each pixel on a quadrant-by-quadrant basis; lower grayscale pixel values indicate an increased proteoglycan concentration. As an internal staining control for each slide, the region with maximum tibial growth plate Saf-O^+ staining was traced, and then the average grayscale pixel value was determined. For the final representative Saf-O^+ intensity in each quadrant, the following equation was used:

$$SafO\ Intensity = \frac{SafOgp - SafOac}{SafOgp}$$

Where: SafOgp = growth plate Saf-O^+ average grayscale pixel value; and SafOac = articular cartilage Saf-O^+ average grayscale pixel value.

Immunohistochemical Staining

For immunohistochemical staining of Ki-67, all slides underwent the following procedure: i) antigen retrieval with 0.1% Citrate Buffer (pH 7.0) overnight at 60°C; ii) blocking with 1% bovine serum albumin in PBS; iii) staining with a primary goat anti-mouse Ki-67 antibody (1:200 dilution; SC-7846, Santa Cruz Biotechnology) overnight at 4°C; and iv) detection with a donkey anti-goat AlexaFlour 555 secondary antibody (1:400 dilution; A21432, Thermo Fisher Scientific) for 1 hour at room temperature. For TUNEL staining, the manufacturer's (Molecular Probes) recommended procedure was followed. For all immunohistochemical staining, autofluorescence was suppressed via 0.1% w/v Sudan Black (FisherBioReagents) in 70% ethanol for 30 mins and then mounted with a DAPI-containing mounting media (ThermoFisher). Within 72 hours of staining, overlapping images of the stained sections were captured at 20x magnification using an epifluorescent microscope (Axio.Observer.Z1, Carl Zeiss, Thornwood, NY) and a digital camera (AxioCam MrC, Zeiss) under consistent settings, and then combined (tiled) using Zen software (Zeiss).

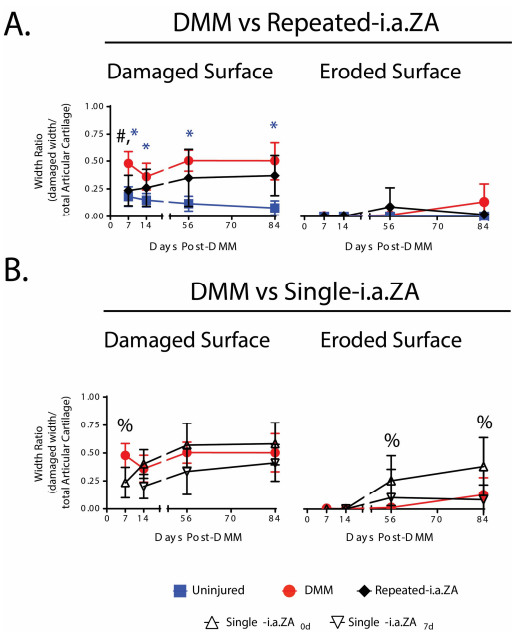

Figure B.1: Assessment Tissue Damage Across the Width of the Articular Cartilage Following DMM-Injury and i.a.ZA Injection. (A.) Analysis of the fraction of the medial tibial plateau articular cartilage width exhibiting damage (either surface damage or tissue erosions, respectively). Uninjured joints exhibited a limited degree of cartilage surface damage and no overt erosions. DMM-injury lead to a rapid accumulation of surface damage (surface fibrillations and clefts) over ~50% of the medial tibial plateau by 7d, followed by the long-term accumulation of cartilage erosions over ~25% of the cartilage. In joints treated with repeated-i.a.ZA, the appearance of superficial damage was somewhat delayed, being significantly reduced at 7d compared to intreated DMM-joints, then catching up to the untreated DMM-joints by 14d. Repeated-i.a.ZA suppressed the appearance of DMM-mediated erosions to the medial tibial plateau cartilage at 84d. (B.) Width-wise cartilage surface damage analysis for the single-i.a.ZA treated groups. Joints receiving a single i.a. ZA injection immediately after surgery (0d) exhibited damaged surface outcomes that were similar to untreated DMM-joints from 7d onward, while experiencing far worse surface erosions than untreated DMM-joints. Joints receiving a single i.a. ZA injection 7d after DMM-injury exhibited slightly suppressed cartilage surface damage progression, but no difference in the long-term size of DMM-mediated cartilage erosions. Results are presented as mean ± STD (n=5-10/timepoint/group) where: # indicates $p < 0.05$ when comparing repeated-.i.a.ZA to untreated DMM; * - $p < .05$ when comparing uninjured to untreated DMM-joints; and % - $p < .05$ when comparing single-i.a.ZA_{0d} to untreated DMM-joints.

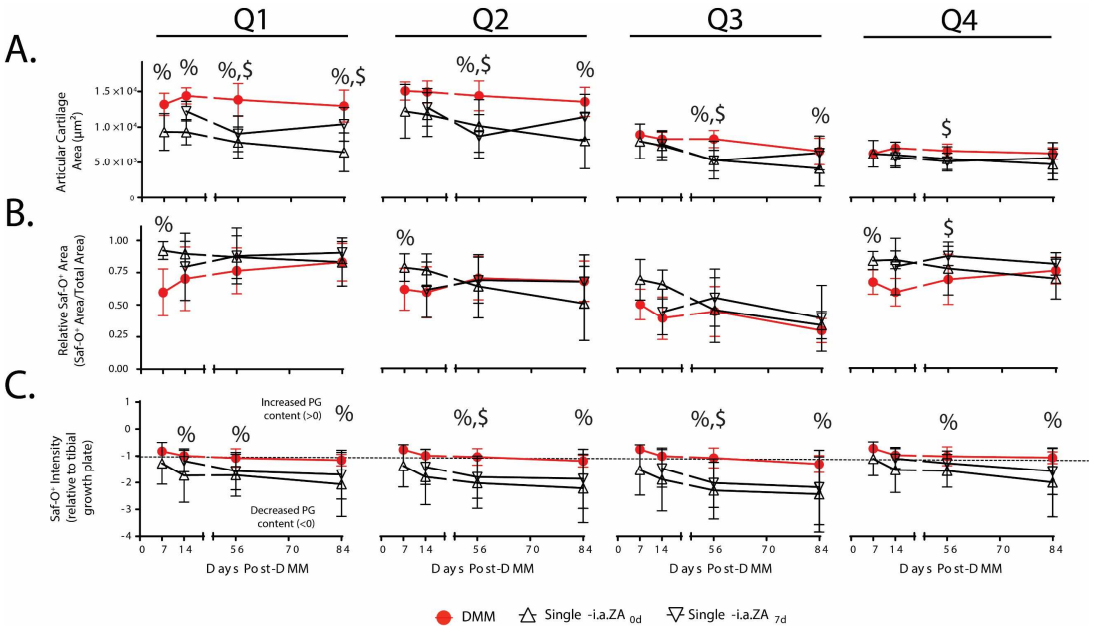

Figure B.2: Single-i.a.ZA Treatment Altered Articular Cartilage Area and Proteoglycan-Rich Cartilage post-DMM**.** (A.) Both single-i.a.ZA treatments led to decreases in the area of the articular cartilage in Q1, Q2, and Q3; Q4 cartilage area remained unaffected. The cartilage thinning associated with single-i.a.ZA joints was attributable to loss of articular cartilage height and the development of erosions. (B.) Assessment of Safranin-O positive (Saf-O^+) cartilage tissue areas across the medial tibial plateau suggested that neither single-i.a.ZA injection altered the evolution of proteoglycan (PG)-rich cartilage tissue following DMM. (C.) Furthermore, in the PG-containing areas, the PG concentration (i.e. Saf-O^+ staining intensity relative to the Saf-O^+ intensity of the growth plate) was consistently reduced in both single-i.a.ZA treatment groups. Results are presented as mean ± STD (n=5-10/timepoint/group) where: # indicates $p< 0.05$ when comparing repeated-.i.a.ZA to untreated DMM; * - $p<.05$ when comparing uninjured to untreated DMM-joints; and % - $p<.05$ when comparing single-i.a.ZA_{0d} to untreated DMM-joints.

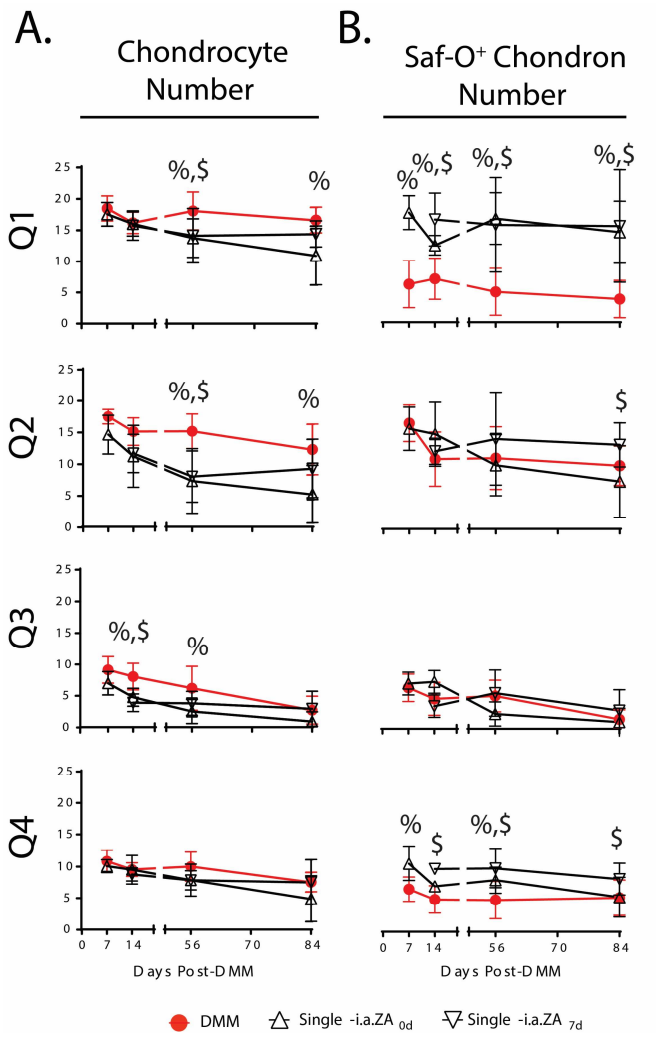

Figure B.3: Single-i.a.ZA Administrations Drove Location-Dependent Changes in Articular Cartilage Chondrocyte Presence and the number of Proteoglycan-Rich Chondrons Post-DMM. (A.) Counting, on a quadrant-by-quadrant basis, the number of hematoxylin-positive chondrocytes in H&E stained sections indicated that single i.a.ZA injections at both 0d or 7d drove consistently larger loses in chondrocyte number than in untreated DMM-joints, especially in Q1, 2, and 3. (B.) The number of chondrons exhibiting PG-rich (Saf-O^+) peri-cellular halos was elevated in the peripheral quadrants (Q1 and Q4) of all of the singly-injected joints when compared to untreated DMM-joints. Results are presented as mean ± STD (n=5-10/timepoint/group) where: % indicates $p<.05$ when comparing single-i.a.ZA_{0d} to untreated DMM-joints; and $ - when comparing single-i.a.ZA_{7d} to untreated DMM-joints.

Appendix C

SUPPLEMENTAL RESULTS FOR CHAPTER 4

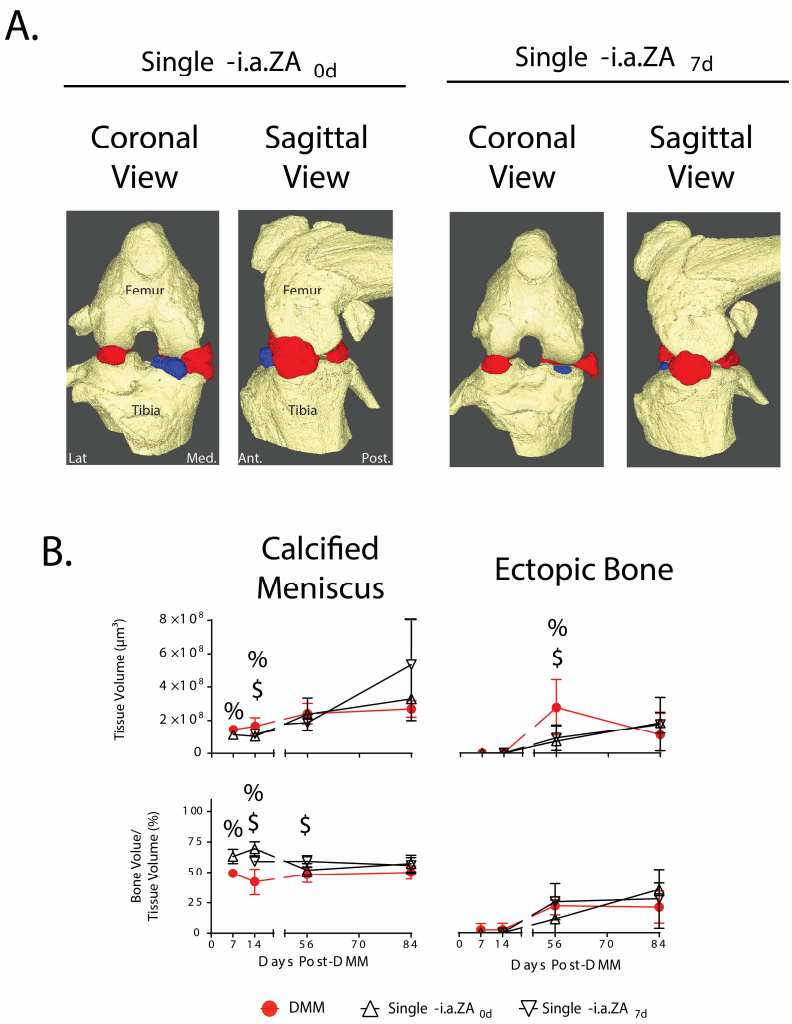

Figure C.1: Assessment of Periarticular Calcified Tissue Changes in the Tibiofemoral Joint Following DMM and Single-i.a.ZA Treatments. (A.) 3D µ-CT renderings of representative knee joints following both DMM and single-i.a.ZA treatments illustrated the extrusion and volumetric increase of the medial meniscus (red), and the spontaneous formation of ectopic bone (blue) in all joints. (B.) Quantitative analysis indicated similar increases in meniscal tissue volume relative to untreated DMM-joints and increased bone volume fractions at earlier time points. In addition, the development of ectopic bone and its structure (tissue volume & bone volume fraction) was similar among both single-i.a.ZA groups and untreated-DMM joints. Results are presented as mean ± STD (n=3-5/timepoint/group) where: % indicates $p<0.05$ comparing single-i.a.ZA$_{0d}$ to the untreated DMM-joints at that timepoint; and $ comparing single-i.a.ZA$_{7d}$ to the untreated DMM-joints at that timepoint.

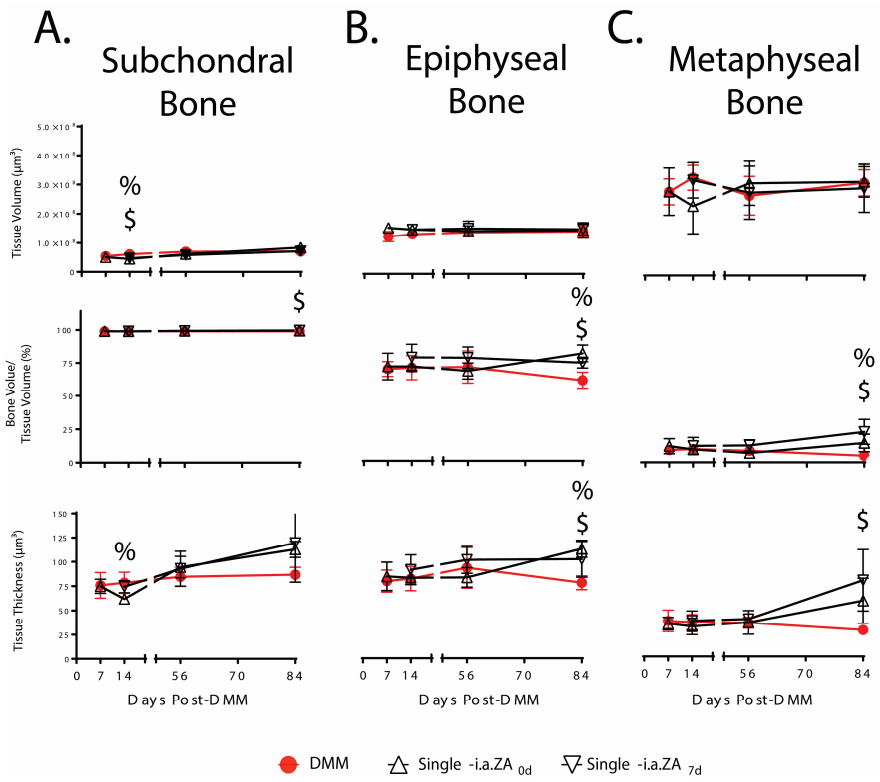

Figure C.2: Assessment of Periarticular Calcified Tissue Changes in the Tibiofemoral Joint Following DMM and Single-i.a.ZA Treatments. (A.) 3D *m*-CT renderings of representative knee joints following both DMM and single-i.a.ZA treatments illustrated the extrusion and volumetric increase of the medial meniscus (red), and the spontaneous formation of ectopic bone (blue) in all joints. (B.) Quantitative analysis indicated similar increases in meniscal tissue volume relative to untreated DMM-joints and increased bone volume fractions at earlier time points. In addition, the development of ectopic bone and its structure (tissue volume & bone volume fraction) was similar among both single-i.a.ZA groups and untreated-DMM joints. Results are presented as mean ± STD (n=3-5/timepoint/group) where: % indicates $p<0.05$ comparing single-i.a.ZA$_{0d}$ to the untreated DMM-joints at that timepoint; and $ comparing single-i.a.ZA$_{7d}$ to the untreated DMM-joints at that timepoint.

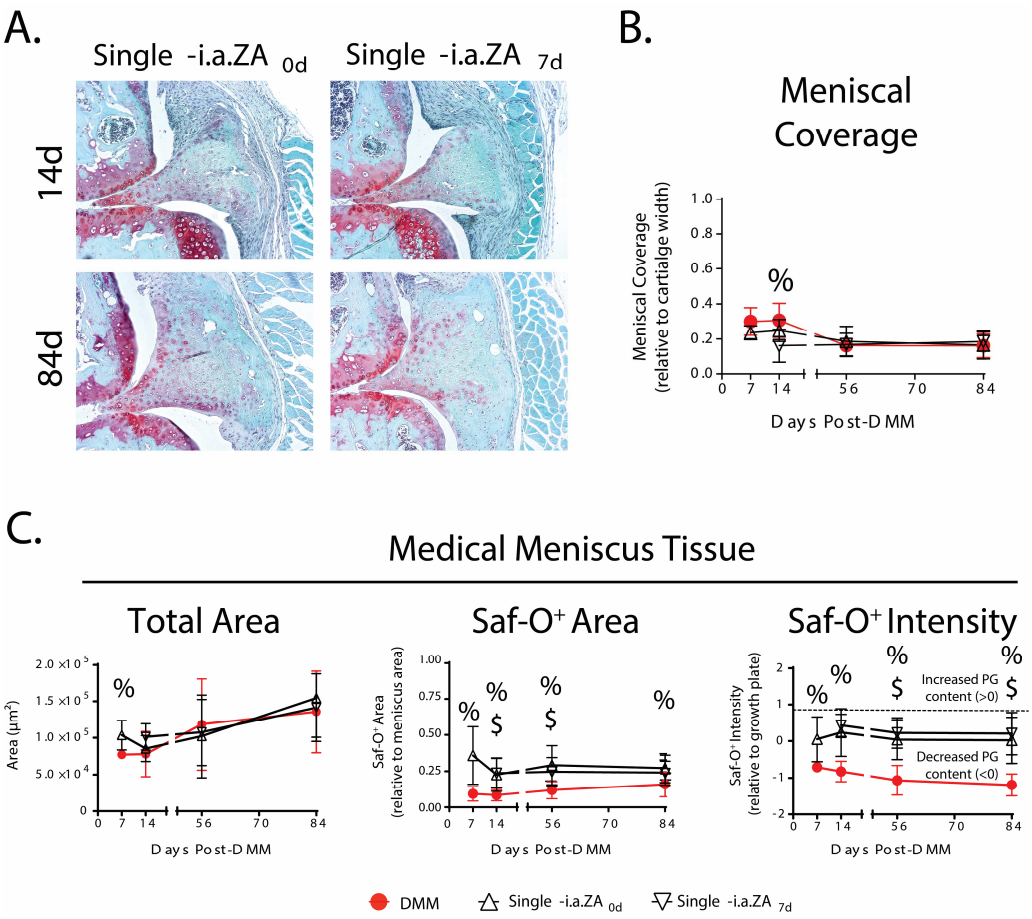

Figure C.3: Meniscal Changes Associated with Single-i.a.ZA Treatments Post-DMM. (A.) Safranin-O stained sections qualitatively highlighted the meniscal extrusion and changes in meniscus size and proteoglycan distribution and intensity that accompany DMM injury in the untreated, and single-i.a.ZA treated joints. These representative images were acquired from the anterior region (level 2) of the joint at 10x magnification. Quantitative histological analyses highlighted that neither immediate- or delayed-single-i.a.ZA administration markedly influenced (B.) meniscal coverage or (C.) meniscal size (area) post-DMM, but single-i.a.ZA injections did drive increases in the relative proportion of Saf-O$^+$ area (proteoglycan-rich tissue) present and the relative staining intensity of these Saf-O$^+$ areas. Results are presented as mean ± STD (n=3-5/timepoint/group) where: % indicates $p<0.05$ comparing single-i.a.ZA$_{0d}$ to the untreated DMM-group at that timepoint; and $ comparing single-i.a.ZA$_{7d}$ to the untreated DMM-group at that timepoint.

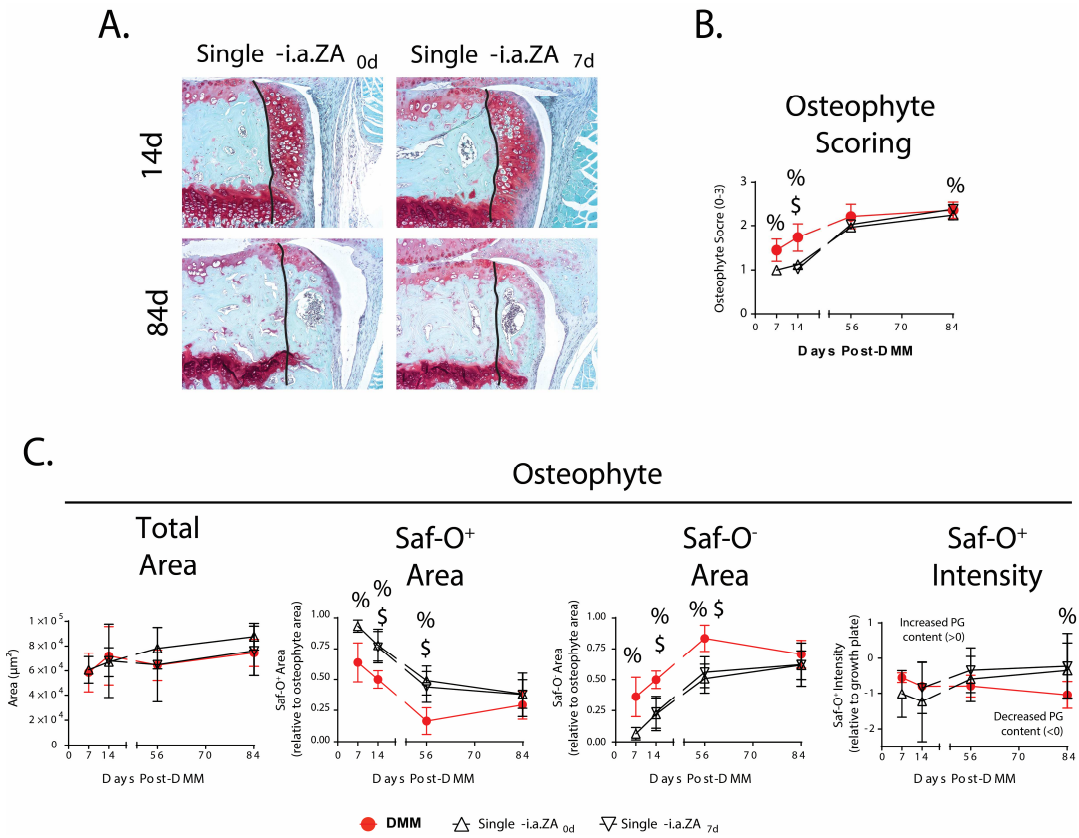

Figure C.4: Osteophyte Maturation is Delayed Following Single-i.a.ZA Treatment Post-DMM. (A.) Safranin-O stained sections demonstrated the formation and transition of osteophytes from a cartilage-like template into bone along the medial tibial plateau joint margin (right of black lines) of singly-i.a.ZA injected DMM-joints. These representative images were acquired from the anterior region (level 2) of the joint at 10x magnification. (B.) Semi-quantitative osteophyte scoring indicated a significant delay in osteophyte maturation following either single-i.a.ZA. treatment when compared to untreated DMM-joints. (C.) Quantitative analysis revealed that single-i.a.ZA treatments did not affect the size of the osteophytes that formed post-DMM but did increase the retention of Saf-O^+ area (proteoglycan-rich tissue) and a delayed accumulation of Saf-O^- area (bone tissue) post-DMM. Within these Saf-O^+ areas, neither of the single-i.a.ZA treatments influence the tissue-level staining intensity of these Saf-O^+ (proteoglycan rich) tissue regions. Results are presented as mean ± STD (n=3-5/timepoint/group) where: % indicates $p<0.05$ comparing single-i.a.ZA_{0d} to the untreated DMM-groups at that timepoint; and $ comparing single-i.a.ZA_{7d} to the untreated DMM-groups at that timepoint.

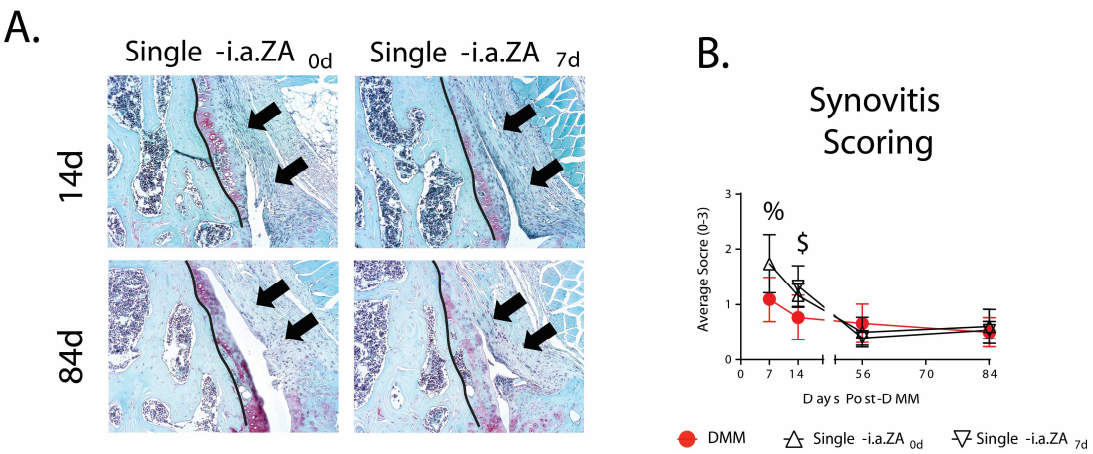

Figure C.5: Joint Synovitis is Not Altered by Single-i.a.ZA Treatment Post-DMM. (A.) Safranin-O stained sections demonstrate the presence of joint synovitis (black arrows) within the medial compartment following DMM, which was not suppressed by either single-i.a. ZA injection. These representative images were acquired from the anterior region (level 2) of the joint at 10x magnification. Osteophytes forming along the medial femur are indicated by the tissue to the right of black lines. (B.) Semi-quantitative synovitis scores confirmed the qualitative impressions. Results are presented as mean ± STD (n=3-5/timepoint/group) where: % indicates $p<0.05$ comparing single-i.a.ZA_{0d} to the untreated DMM-group at that timepoint; and $ comparing single-i.a.ZA_{7d} to the untreated DMM-group at that timepoint.

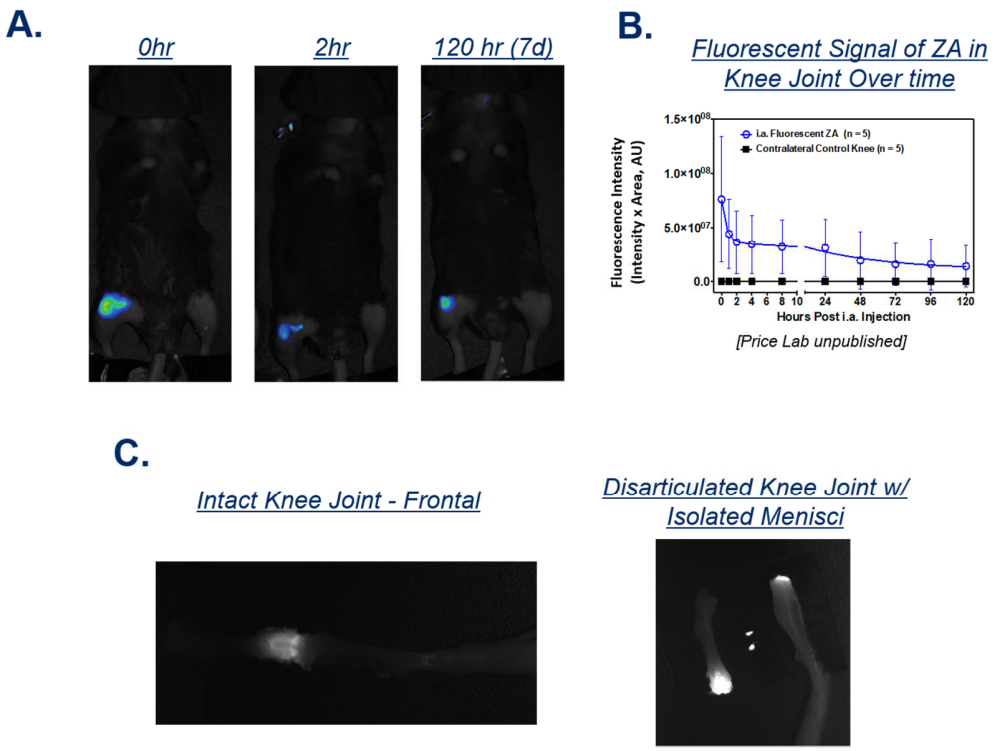

Figure C.6: Zoledronic Acid Clearance in Uninured Mouse Knee. Fluorescently-tagged zoledronic acid (ZA) was injected into naïve, uninjured murine knees to determine the clearance of ZA from the joint space over 7 days (120-hours) using IVIS imaging. (A.) Images of ZA fluorescent signal from 0, 2, and 120-hours (7-days) post-injection highlight the loss of ZA from the joint over time (pseudo colored; yellow/green indicates more ZA while blue is less). (B.) Quantification of the fluorescent-ZA signal in the injected and non-injected knee confirmed ZA's clearance from the joint. Note the rapid clearance of ZA from the joint by 4-hours, but ZA still persists in the joint by 120-hours. (C.) The intact and disarticulated knee highlight the presence of ZA (non-pseudo colored) after 120-hour within the joint space, cartilage, and isolated menisci (small white tissue).

Appendix D

SUPPLEMENTAL RESULTS FOR CHAPTER 5

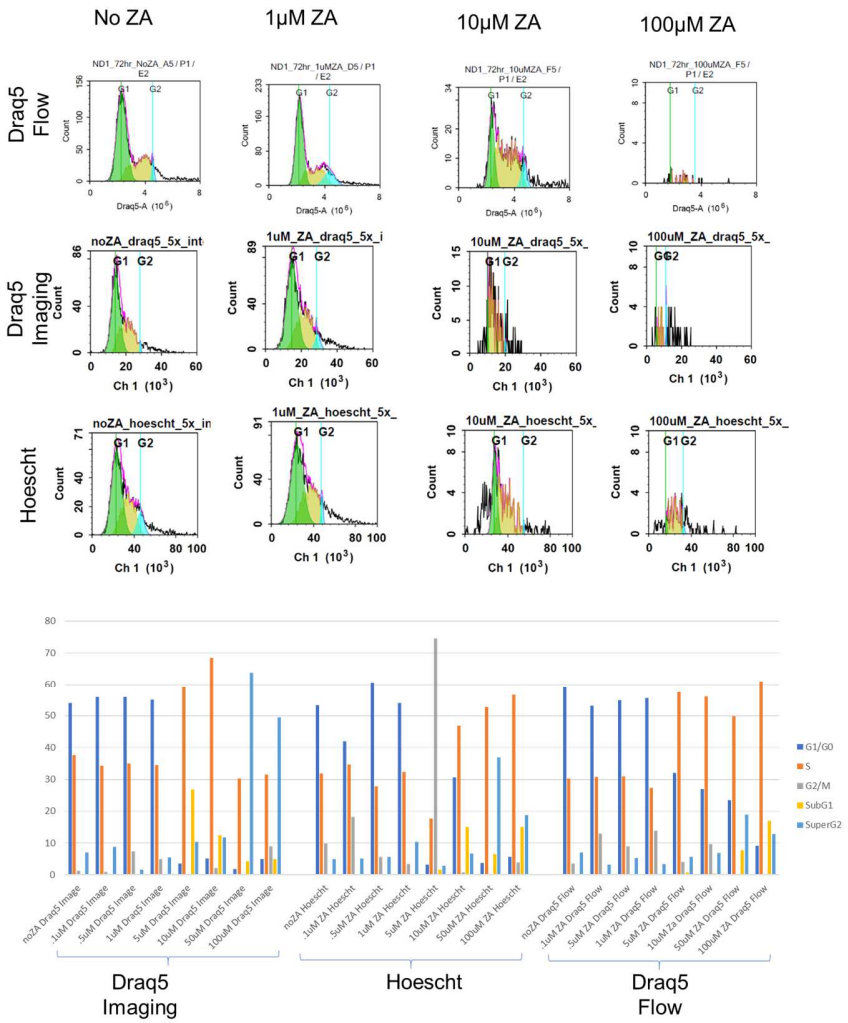

Figure D.1: Demonstration of Cell Cycle performed via Flow Cytometry and Image-Based. The top portion of figure highlights the DNA staining (Draq5 and Hoescht) histograms obtained via flow and image-based. While slightly different in the overall shapes, the general pattern and trends still hold true. The bottom demonstrates the resulting cell cycle percentages as a function of technique and ZA concentrations.

Appendix E

PERMISSIONS AND RIGHTS

At the time of submitting this dissertation, the work in Chapter 2 was published in the Journal of Orthopaedic Research. The Journal of Orthoapedic Research allows manuscripts to be published in academics dissertations without permission from the journal.

Journal of Orthopaedic Research:
https://www.elsevier.com/journals/journal-of-orthopaedics/0972-978X/guide-for-authors

Submission declaration

Submission of an article implies that the work described has not been published previously (except in the form of an abstract, a published lecture or academic thesis, see 'Multiple, redundant or concurrent publication' for more information), that it is not under consideration for publication elsewhere, that its publication is approved by all authors and tacitly or explicitly by the responsible authorities where the work was carried out, and that, if accepted, it will not be published elsewhere in the same form, in English or in any other language, including electronically without the written consent of the copyright-holder.

Multiple, redundant or concurrent publication: An author should not in general publish manuscripts describing essentially the same research in more than one journal or primary publication. Elsevier does not view the following uses of a work as prior publication: publication in the form of an abstract; publication as an academic thesis; publication as an electronic preprint. Note: some society-owned titles and journals that operate double-blind review have different policies on prior publication. Information on prior publication is included within each Elsevier journal's guide for authors.

Appendix F

IACUC ANIMAL APPROVAL

RECEIVED
JUN 21 2013
IACUC

University of Delaware
Institutional Animal Care and Use Committee
Application to Use Animals in Research and Teaching

(Please complete below using Arial, size 12 Font.)

Title of Protocol: Bisphosphonates in the prevention of post-traumatic osteoarthritis.

AUP Number: 1252-2013-0 | **← (4 digits only — if new, leave blank)**

Principal Investigator: Dr. Christopher Price

Common Name: Mice

Genus Species: Mus musculus

Pain Category: ***(please mark one)***

USDA PAIN CATEGORY: ***(Note change of categories from previous form)***

Category	Description
☐ B	Breeding or holding where NO research is conducted
☐ C	Procedure involving momentary or no pain or distress
X D	Procedure where pain or distress is alleviated by appropriate means (analgesics, tranquilizers, euthanasia etc.)
☐ E	Procedure where pain or distress cannot be alleviated, as this would adversely affect the procedures, results or interpretation

Official Use Only

IACUC Approval Signature: Steve Talkington, DVM

Date of Approval: 6/24/13

RECEIVED
APR – 7 2014
IACUC

University of Delaware
Institutional Animal Care and Use Committee
Annual Review

Title of Protocol: Bisphosphonates in the prevention of post-traumatic osteoarthritis

AUP Number: 1252-2014-1 ← **(4 digits only)**

Principal Investigator: Dr. Christopher Price

Common Name: Common Mouse

Genus Species: Mus musculus

Pain Category: ***(please mark one)***

USDA PAIN CATEGORY: ***(Note change of categories from previous form)***

Category	Description
☐ B	Breeding or holding where NO research is conducted
☐ C	Procedure involving momentary or no pain or distress
☐ X D	Procedure where pain or distress is alleviated by appropriate means (analgesics, tranquilizers, euthanasia etc.)
☐ E	Procedure where pain or distress cannot be alleviated, as this would adversely affect the procedures, results or interpretation

Official Use Only

IACUC Approval Signature: Steven Talken, DVM

Date of Approval: 6/1/14

University of Delaware
Institutional Animal Care and Use Committee
Annual Review

RECEIVED
APR 7 2015
IACUC JH

Title of Protocol: Bisphosphonates in the prevention of post-traumatic osteoarthritis.

AUP Number: 1252-2015-2 ← **(4 digits only)**

Principal Investigator: Dr. Christopher Price

Common Name: Mice

Genus Species: Mus musculus

Pain Category: ***(please mark one)***

USDA PAIN CATEGORY: ***(Note change of categories from previous form)***

Category	Description
☐ B	Breeding or holding where NO research is conducted
☐ C	Procedure involving momentary or no pain or distress
☐ X D	Procedure where pain or distress is alleviated by appropriate means (analgesics, tranquilizers, euthanasia etc.)
☐ E	Procedure where pain or distress cannot be alleviated, as this would adversely affect the procedures, results or interpretation

Official Use Only

IACUC Approval Signature: _____

Date of Approval: 6/1/2015

University of Delaware
Institutional Animal Care and Use Committee
Application to Use Animals in Application to use animals in Research
(New and 3-Yr submission)

Title of Protocol: **Bisphosphonates in the prevention of post-traumatic osteoarthritis.**	
AUP Number: 1252-2016-0	**← (4 digits only — if new, leave blank)**
Principal Investigator: Dr. Christopher Price	
Common Name (Strain/Breed if Appropriate): Mice; C57BL/6J **Genus Species:** Mus musculus	
Date of Submission: 04/12/2106	

Official Use Only

IACUC Approval Signature: Jim Talbert, DVM

Date of Approval: 6/1/16

University of Delaware
Institutional Animal Care and Use Committee

Annual Review

RECEIVED
MAY 11 2017
IACUC

*When entering data, text boxes that allow multiple lines will have a scroll bar. After completing entry, click anywhere outside the text box to see the expanded field.

Title of Protocol:	Bisphosphonates in the prevention of post-traumatic osteoarthritis
AUP Number *(4 digits only)*:	1252-2017-1
Principal Investigator:	Christopher Price

Common Name:	Mouse; C57BL/6J
Genus Species:	Mus musculus

Pain Category

USDA PAIN CATEGORY *(Note change of categories from previous form)*

- ○ Category B: Breeding or holding where NO research is conducted
- ○ Category C: Procedure involving momentary or no pain or distress
- ◉ Category D: Procedure where pain or distress is alleviated by appropriate means (analgesics, tranquilizers, euthanasia, etc.)
- ○ Category E: Procedure where pain or distress cannot be alleviated, as this would adversely affect the procedures, results, or interpretation

IACUC approval of major changes to an animal protocol must be reviewed and approved prior to initiating the work.

Official Use Only

IACUC Approval Signature: [signature], DVM

Date of Approval: 6/1/17

University of Delaware
Institutional Animal Care and Use Committee
Annual Review

RECEIVED
APR 2 3 2018
IACUC

Title of Protocol: **Bisphosphonates in the prevention of post-traumatic osteoarthritis.**	
AUP Number: 1252-2018-2	**← (4 digits only)**
Principal Investigator: Dr. Christopher Price	
Common Name: Mouse; C57BL/6J **Genus Species:** Mus musculus	

Pain Category: ***(please mark one)***

USDA PAIN CATEGORY: *(Note change of categories from previous form)*	
Category	**Description**
☐ **B**	Breeding or holding where NO research is conducted
☐ **C**	Procedure involving momentary or no pain or distress
☒ **D**	Procedure where pain or distress is alleviated by appropriate means (analgesics tranquilizers, euthanasia etc.)
☐ **E**	Procedure where pain or distress cannot be alleviated, as this would adversely affect the procedures, results or interpretation

Official Use Only

IACUC Approval Signature: [signature], DVM

Date of Approval: 6.1.18